

Université de Paris

Ecole doctorale:

Bio Sorbonne Paris Cité (BioSPC) ED 562

Laboratoire / Equipe de recherche :

INSERM U1141 Hôpital Robert Debré, Paris, France

Conditional inactivation of EIF2B5 gene in oligodendrocytes' or astrocytes' cell lineages in adult mice

Par Abed El Rahim BARK

Thèse de doctorat de Neurobiologie

Dirigée par Pr Odile BOESPFLUG-TANGUY

Présentée et soutenue publiquement à l'hôpital Robert Debré le 18 Décembre 2019

Rapporteurs : Mr DEIVA Kumaran / MD, PhD, HDR / UMR1184 Université Paris-Sud

Mme SARRET Catherine / MD, PhD, HDR / CNRS UMR6602 Institut Pascal

Examineurs : Mme HUYGHE, Aurélia / PhD / Centre de Recherche en Cancérologie de LYON (CRCL)

Mr AYRIGNAC, Xavier / MD, PhD, PH / CHU DE Montpellier Hopital GUI DE CHAULIAC

Directeur de thèse : Pr BOESPFLUG-TANGUY Odile / PU-PH / INSERM U1141 Hôpital Robert Debré

Titre :

Inactivation conditionnelle du gène EIF2B5 dans les lignées oligodendrocytaires ou astrocytaires chez les souris adultes.

Résumé :

Vanishing white matter disease (VWMD) ou childhood ataxia with central nervous system hypomyelination (CACH) est une maladie démyélinisante autosomale récessive qui présente un spectre phénotypique hétérogène et qui est causée par des mutations autosomales récessives touchant les gènes qui codent pour les cinq sous-unités du facteur d'initiation de la traduction EIF2B. Cette maladie provoque des dévastations et raréfactions de la substance blanche cérébrale avec une morphologie atypique des astrocytes et des oligodendrocytes d'aspect spumeux. Plusieurs modèles ont été développés pour comprendre la pathophysiologie de la maladie et pour essayer de trouver des stratégies thérapeutiques. Dans notre étude, nous avons établi deux nouveaux modèles murins. Dans le premier, nous avons ciblé le gène *eif2b5* dans les oligodendrocytes en utilisant la forme inductible par Tamoxifène de la Cre (CreERT2) exprimée dans un locus de la protéine oligodendrocyte-spécifique protéolipoprotéine (PLP) ce qui permet la délétion du gène au moment précis dans les oligodendrocytes (Plp-Cre-ERT2/*Eif2b5*^{fl/fl}). (i) Dans les souris femelles adultes, nous avons observé, neuf semaines après induction, une perte significative du poids accompagnée d'une paralysie aiguë ; (ii) Les tests de comportement ont montré une déficience de la coordination motrice et de l'activité locomotrice avec une perte de la force musculaire ; (iii) Au niveau histologique, nous avons observé une baisse du nombre des oligodendrocytes matures olig2+/CC1+ avec persistance voire augmentation du pool des immatures. D'autre part, nous avons observé une augmentation des astrocytes GFAP+ et des microglies Iba1+ dans le cortex avec un aspect réactif des deux types cellulaires, en plus d'une perte neuronale. (iv) La microscopie électronique a montré une tendance qui reste non significative à la baisse du nombre des axones myélinisés ; (v) L'analyse en RNAseq des cellules triées (MACS) sur des cerveaux de souris adultes a révélé l'activation des voies du stress chronique exclusivement dans les oligodendrocytes immatures (O4+) et la reprogrammation de l'expression des gènes favorisant le maintien des cellules immatures et l'activation des voies de la neuroinflammation lors de l'entrée dans la phase symptomatique. Dans le deuxième modèle, nous avons ciblé le gène *eif2b5* dans les astrocytes en utilisant le même système avec la Cre exprimée dans un locus de la protéine Glutamate-Aspartate Transporter (Glast) ce qui permet la délétion du gène au moment précis dans les astrocytes (Glast-Cre-ERT2/*Eif2b5*^{fl/fl}) ce qui a permis d'avoir deux phénotypes distincts résultant de la présence ou non d'une copie de Glast dans les souris (Glast-Cre-ERT2^{+/-}/*Eif2b5*^{fl/fl} avec une copie de Glast présente et Glast-Cre-ERT2^{-/-}/*Eif2b5*^{fl/fl} avec absence totale de Glast). (i) Chez les femelles Glast-Cre-ERT2^{+/-}/*Eif2b5*^{fl/fl} traitées au Tamoxifène, nous n'avons observé ni perte de poids ni paralysie ; (ii) au niveau histologique, nous avons observé une augmentation des astrocytes GFAP+ et des microglies Iba1+ avec un aspect réactif des deux types cellulaires, alors que les oligodendrocytes et les neurones n'ont pas été affectés, ceci contrastant avec les souris Glast-Cre-ERT2^{-/-}/*Eif2b5*^{fl/fl} chez lesquelles nous avons observé (iii) une perte significative du poids accompagnée d'une paralysie spastique à six semaines après induction ; (iv) une augmentation des astrocytes GFAP+ et des microglies Iba1+ dans le cortex avec un aspect réactif des deux types cellulaires, en plus d'une baisse du nombre des oligodendrocytes matures olig2+/CC1+ et d'une perte neuronale. L'ensemble de ces travaux souligne la susceptibilité des cellules oligodendrocytes en particulier immatures au stress du RE chronique induit par un déficit d'EIF2B. Les astrocytes nécessitent plusieurs facteurs associés pour entraîner une souffrance neurologique aiguë. Ils sont peut-être plus impliqués dans la phase développementale et chronique.

Mots clefs :

EIF2B5, Syndrome CACH/VWM, Oligodendrocytes, Myéline, Astrocytes, Microglies, Stress du réticulum endoplasmique, Maturation cellulaire

Title :

Conditional inactivation of EIF2B5 gene in oligodendrocytes' or astrocytes' cell lineages in adult mice.

Abstract :

Vanishing white matter disease (VWMD) or childhood ataxia with central nervous system hypomyelination (CACH) is an autosomal recessive demyelinating disorder with wide phenotypic heterogeneity caused by autosomal recessive mutations in the genes encoding the five subunits of the translation-initiation factor eIF2B. It causes cerebral white matter devastations and rarefactions with an atypical morphology of astrocytes and a “foamy” morphology of oligodendrocytes. Several animal models were developed to understand the pathophysiology of the disease and to investigate therapeutic strategies. In our studies, we established two new mouse models. In the first, we targeted the *eif2b5* gene in oligodendrocytes in the tamoxifen inducible form of Cre (CreERT2) expressed in the locus of the oligodendrocyte-specific proteolipid protein (PLP) that allows precisely timed gene deletion in adult oligodendrocytes (Plp-Cre-ERT2/*Eif2b5*^{fl/fl}). (i) In adult female mice, we observed after nine weeks of induction a significant loss of weight and acute paralysis; (ii) Behavioral tests, showed a deficiency in motor coordination and locomotor activity, and a loss of muscular strength; (iii) At the histological level, we observed a decrease of olig2/CC1 mature oligodendrocytes with persistence and even an increase in the pool of immature cells. On the other hand, an increase of number of GFAP+ astrocytes and Iba1+ microglia has been observed in cortex with an activated aspect of both cell types in addition to a neuronal loss; (iv) Electronic microscopy showed a non-significant but obvious tendency to decrease in the number of myelinated axons; (v) RNAseq analysis on cells sorted (MACS) from brains of adult mice showed the activation of pathways related to chronic stress, especially in the immature (O4+) oligodendrocytes and the reprogramming of the expression of genes favoring the maintaining of the immature cells and the activation of neuroinflammation pathways when going into the symptomatic phase. In the second model, we targeted the *eif2b5* gene in astrocytes using the same system with the Cre expressed in the locus of the Glutamate-Aspartate Transporter (Glast) protein that allows precisely timed gene deletion in adult astrocytes (Glast-Cre-ERT2/*Eif2b5*^{fl/fl}) which resulted in two distinct phenotypes related to the presence or not of a copy of the Glast locus in the resulting mice (Glast-Cre-ERT2^{+/-}/*Eif2b5*^{fl/fl} where one copy of Glast exists and Glast-Cre-ERT2^{-/-}/*Eif2b5*^{fl/fl} where no copy of Glast exists). (i) In the Glast-Cre-ERT2^{+/-}/*Eif2b5*^{fl/fl} TMX treated female mice, no weight loss nor paraplegia were observed; (ii) At the histological level, we observed an increase of number of GFAP+ astrocytes and Iba1+ microglia with an activated aspect of both cell types while no oligodendrocyte nor neuronal loss were seen in contrast to the Glast-Cre-ERT2^{-/-}/*Eif2b5*^{fl/fl} where (iii) significant loss of weight and paraplegia were observed at six weeks after induction; (iv) an increase of number of GFAP+ astrocytes and Iba1+ microglia has been observed with an activated aspect of both cell types in addition to mature oligodendrocyte and neuronal loss. This whole work underlines the susceptibility of oligodendrocyte cells, particularly the immature ones, to chronic ER stress induced by EIF2B deficit. The astrocytes require the association of many factors in order to cause acute neurologic distress. They might be more involved in the developmental and chronic phase.

Keywords :

EIF2B5, CACH/VWM syndrome, Oligodendrocytes, Myelin, Astrocytes, Microglia, ER Stress, Cell maturation

*In loving memory of my late grandfather whom I lost during my period of research. May his
soul rest in peace*

ACKNOWLEDGMENT

First of all, I wish to express my gratitude and warmly thank Professor Odile BOESPFLUG-TANGUY for welcoming me into her team, guiding and supporting me all the time during these years of research. I would never have embarked on this scientific adventure without her guide on my work.

Then I would like to thank Doctor Kumaran DEIVA and Doctor Catherine SARRET for agreeing to be rapporteurs of my thesis, and also other members of jury Doctor Aurélia HUYGHE and Doctor Xavier AYRIGNAC who accepted to judge my work.

I would also like to thank Doctor Ronza ABDEL RASSOUL and Doctor Imen DORBOZ, precious mentors, collaborators and friends for being nearby, supporting me and showing me the small tricks and the proper way of doing things.

Thank you Professor Diana RODRIGUEZ for the moments of discussions (scientific and casual) in the lab.

Special thanks to Mutaz AMIN, Karima BOUSSAID, Adnan KARKAR, Mouhamad ABUAWAD and Florence RENALDO, dear friends and fellow PhD students with whom I shared the best of moments.

I won't forget to thank Jeanette NARDELLI for helpful discussions and Zsolt CSABA for always being there whenever a problem occurred with confocal microscope.

Finally, my deepest gratitude to my father Dib, mother Zeinab, brother Ramzi and sisters Yasmine and Roula for always supporting me, being there for me, pushing me forward and believing in me unconditionally. Your mere presence brightens my world and my life. I love you all.

I acknowledge grant support of association RHAGENE.

Table of contents

Table of contents

ACKNOWLEDGMENT	7
TABLE OF CONTENTS	10
LIST OF FIGURES.....	13
LIST OF ABBREVIATIONS.....	16
I. INTRODUCTION	21
II. BIBLIOGRAPHY	22
1. GLIAL CELLS IN THE CNS.....	22
1.1. PROGENITORS (NSCs).....	22
1.2 OLIGODENDROCYTES.....	23
1.3 ASTROCYTES.....	26
1.4 MICROGLIA.....	29
1.5 NEURONS.....	31
1.6 CNS CELLS INTERACTIONS.....	33
2. LEUKODYSTROPHIES	36
2.1 CLASSIFICATION OF LEUKODYSTROPHIES.....	36
2.1.1 HYPOMYELINATING LEUKODYSTROPHIES.....	37
2.1.2 DEMYELINATING LEUKODYSTROPHIES.....	40
2.2 VACUOLATING LEUKODYSTROPHIES.....	41
2.2.1 ALEXANDER DISEASE	41
2.2.2 MEGALENCEPHALIC LEUKOENCEPHALOPATHY WITH SUBCORTICAL CYSTS (MLC).....	42
2.2.3 CYSTIC LEUKOENCEPHALOPATHY WITHOUT MEGALENCEPHALY	43
2.2.4 CACH/VWM SYNDROME.....	43
3. CACH/VWM SYNDROME	43
3.1 HISTORY OF THE DISEASE RECOGNITION.....	43
3.2 CACH/VWM AND EIF2B MUTATIONS.....	44
3.4 BRAIN MRI AND VWM.....	47
3.5 NEUROPATHOLOGICAL ASPECTS OF CACH/ VWMD.....	49
3.6 BIOCHEMICAL MARKERS	50
3.7 GENOTYPE-PHENOTYPE CORRELATION	51
4. TRANSLATION INITIATION FACTOR AND CELLULAR STRESS REGULATION	53
4.1 RIBOSOMES	53
4.2 STEPS OF TRANSLATION.....	54
4.2.1 TRANSLATION INITIATION	54
4.2.1.1 CAP-DEPENDENT TRANSLATION INITIATION.....	54
4.2.1.2 ALTERNATIVE CAP-INDEPENDENT TRANSLATION INITIATION	57
4.2.2 TRANSLATION ELONGATION	58
4.2.3 TRANSLATION TERMINATION	59
4.3 ROLE OF EIF2B IN TRANSLATION INITIATION	60
4.3.1 EIF2B, ACTIVATOR OF EIF2	60

4.3.2 STRUCTURE AND FUNCTIONAL DOMAINS OF EIF2B.....	61
4.4 REGULATION OF TRANSLATION INITIATION IN RESPONSE TO STRESS.....	64
4.4.1 DIRECT REGULATION OF EIF2B	65
4.4.1.1 ALLOSTERIC REGULATION	65
4.4.1.2 REGULATION BY PHOSPHORYLATION.....	65
4.4.1.3 ROLE OF HEAT SHOCK PROTEINS (HSP)	66
4.4.2 REGULATION BY EIF2A PHOSPHORYLATION IN RESPONSE TO STRESS	66
4.4.3 ER STRESS AND UPR	70
5. EIF2B MUTANTS MODELS	72
5.1 THE YEAST MODEL	72
5.2 MOUSE MODELS.....	73
5.2.1 THE G2723A MUTATION KI MOUSE MODEL	73
5.2.2 THE 572G>A AND THE 1450C>T MUTATIONS KI MOUSE MODELS	74
5.2.3 THE <i>PLP/FV2E-PERK</i> MOUSE MODEL	77
5.3 CELLULAR MODELS:.....	78
5.3.1 LYMPHOCYTES / LYMPHOBLASTS	78
5.3.2 FIBROBLASTS	79
5.3.3 EMBRYONIC STEM CELLS.....	79
5.3.4 INDUCED PLURIPOTENT STEM CELLS (iPSCs).....	80
II. OBJECTIVES.....	82
III- MATERIALS AND METHODS (SUMMARY).....	83
1. MOUSE MODELS: INDUCIBLE EIF2B5 CONDITIONAL KNOCK-OUT	83
2. IMMUNOHISTOCHEMISTRY MARKERS OF ASTROCYTES, MICROGLIAL CELLS, NEURONS AND OLIGODENDROCYTES..	85
3. BEHAVIOURAL TESTS: MOTOR AND COGNITIVE FUNCTIONS	86
4. TRANSCRIPTOMIC ANALYSIS OF ISOLATED GLIA CELLS	87
4-1 MACS ISOLATION OF GLIAL CELLS.....	87
4-2. TRANSCRIPTOMIC ANALYSIS: RNAseq	88
IV: RESULTS AND DISCUSSION OF THE CONSEQUENCES OF EIF2B5 INACTIVATION IN OLIGODENDROCYTES (SUMMARY)	89
1. SEVERE DECREASE OF EIF2B5 TRANSCRIPTS IN THE PREMYELINATING OLIGODENDROCYTES O4+ SORTED CELLS ...	89
3. TMX TREATED PLP-CRE-ERT2/EIF2B5 ^{FL/FL} MICE HAVE A DECREASE IN MATURE OLIGODENDROCYTES AT THE TIME OF THE ACUTE NEUROLOGICAL DISTRESS (W8 PI)	92
4. EIF2B5 INACTIVATION INDUCED A CHRONIC INTEGRATED STRESS RESPONSE IN THE O4+ SORTED CELLS.....	93
5. EIF2B5 INACTIVATION INDUCED SEVERE CHANGES IN THE GENE PROFILE EXPRESSION OF THE O4+ SORTED CELLS BETWEEN D10 AND W8 PI TOWARD MICROGLIAL GENE EXPRESSION AND CYTOKINES PRODUCTION.....	95
ARTICLE 1	100
IMPAIRED <i>EIF2B5</i> SPECIFICALLY IN ADULT OLIGODENDROCYTES INDUCED, WITH DELAY, AN ACUTE NEUROLOGICAL DEGRADATION RELATED TO CHRONIC STRESS RESPONSE AND INFLAMMATION ACTIVATION OF THE OPC	100
V. RESULTS AND DISCUSSION OF THE CONSEQUENCES OF EIF2B5 INACTIVATION IN ASTROCYTES.	144
ARTICLE 2 (IN PREPARATION)	147
CONDITIONAL INACTIVATION OF THE TRANSLATION INITIATION FACTOR <i>EIF2B5</i> GENE IN ASTROCYTES INDUCED A DELAYED ACUTE NEUROLOGICAL DISTRESS ONLY IN THE GLAST NULL MOUSE BUT NOT IN THE GLAST-CRE-ERT2 ^{+/-} /EIF2B5 ^{FL/FL}	
VI. GENERAL DISCUSSION AND PERSPECTIVES	169
VII. CONCLUSION.....	172

VIII. REFERENCES	173
-------------------------------	------------

List of Figures

FIGURE 1 : NEUROEPITHELIAL CELLS AND RADIAL GLIA ARE NEURAL STEM CELLS.	23
FIGURE 2 : SCHEMATIC REPRESENTATION OF OLIGODENDROCYTE (OL) DEVELOPMENT	24
FIGURE 3 : SCHEMATIC REPRESENTATIONS THAT SUMMARIZE, ASTROCYTES FUNCTIONS... ..	28
FIGURE 4: BRAIN DEVELOPMENT AND MICROGLIAL ONTOGENY..	29
FIGURE 5: MORPHOLOGY AND MARKERS OF EMBRYONIC AND ADULT MICROGLIA IN THE MOUSE.	30
FIGURE 6: SCHEMATIC REPRESENTATION OF A PYRAMIDAL NEURON WITH AN ASTROCYTE AND OLIGODENDROCYTE IN CLOSE PROXIMITY..	32
FIGURE 7: SCHEMATIC REPRESENTATION OF A CHEMICAL SYNAPSE.....	33
FIGURE 8: SCHEMATIC DIAGRAM DEPICTING SOME OF THE METABOLIC TRAFFICKING BETWEEN NEURONS, OLIGODENDROCYTES, AND ASTROCYTES.	35
FIGURE 9: EIF2B-PATHIES CLINICAL SPECTRUM: CORRELATION BETWEEN AGE AT DISEASE ONSET AND CLINICAL SEVERITY..	45
FIGURE 10: MRI ASPECTS OF THE WHITE MATTER FROM A CACH/ VWM PATIENT.	48
FIGURE 11: LIGHT MICROSCOPIC PICTURE OF OLIGODENDROCYTES.	49
FIGURE 12: ELEMENTS INFLUENCING MRNA TRANSLATION.....	53
FIGURE 13: OVERVIEW OF THE GENERAL EUKARYOTIC TRANSLATION INITIATION PATHWAY.	56
FIGURE 14: ALTERNATIVE MECHANISMS OF TRANSLATION INITIATION.....	58
FIGURE 15: A SCHEMATIC DIAGRAM OF THE ELONGATION PHASE OF THE RIBOSOME- CATALYZED TRANSLATION.....	59
FIGURE 16: ROLE OF EIF2B.	61
FIGURE 17: LAYOUT OF INDIVIDUAL EIF2B SUBUNITS (DOMAINS) AND THE CATALYTIC AND REGULATORY SUBCOMPLEXES OF EIF2B.	63
FIGURE 18: THE STRUCTURE OF EIF2B.	64
FIGURE 19: MECHANISM OF EIF2B INHIBITION BY MEANS OF EIF2 PHOSPHORYLATION.	67
FIGURE 20: INTEGRATED STRESS RESPONSE SIGNALING.....	68

FIGURE 21: DEPICTION OF THE ATF4 MECHANISM OF PREFERENTIAL TRANSLATION.	69
FIGURE 22: DEPICTION OF THE PREFERENTIALLY TRANSLATED MRNAS AND THEIR FUNCTION IN STRESS REMEDIATION	70
FIGURE 23: THE UNFOLDED PROTEIN RESPONSE.	71
FIGURE 24: GENERATION OF PLP-CRE-ERT2/EIF2B5 ^{FL/FL} AND GLAST-CRE-ERT2/EIF2B5 ^{FL/FL} MICE.....	84
FIGURE 25: ENRICHMENT ANALYSIS AT D10 PI.....	89
FIGURE 26: GENE EXPRESSION PROFILES AT D10 DISSECTED BY EPIDISH.....	90
FIGURE 27: MRNA EXPRESSION LEVELS FOR EACH OF THE FIVE GENES (EIF2B1-5) CODING FOR THE FIVE SUBUNITS OF THE EIF2B COMPLEX AT D10	91
FIGURE 28: TRANSCRIPTOMIC ANALYSIS: DIFFERENTIALLY EXPRESSED GENES IN TMX VERSUS VEHICLE INJECTED MICE	94
FIGURE 29: ACTIVATED GENES.....	95
FIGURE 30: CELL TYPE SPECIFIC ENRICHMENT	95
FIGURE 31: TRANSCRIPTOMIC ANALYSIS: PROPORTION OF DIFFERENT CELLULAR TYPES	96
FIGURE 32: CONSTRUCTIO , WEIGHT PLOT AND SURVIVAL PLOT OF GLAST-CRE- ERT2/EIF2B5 ^{FL/FL} MICE	152
FIGURE 33: ALTERATIONS IN ASTROCYTE CELL MARKER'S EXPRESSION IN TAMOXIFEN INJECTED GLAST-CRE-ERT2 ^{+/-} /EIF2B5 ^{FL/FL} MICE.....	154
FIGURE 34: ALTERATIONS IN PERCENTAGE OF MATURE AND IMMATURE OLIGODENDROCYTES IN TAMOXIFEN INJECTED GLAST-CRE-ERT2 ^{+/-} /EIF2B5 ^{FL/FL} MICE.	156
FIGURE 35: ALTERATIONS IN PERCENTAGE OF MICROGLIAL CELL NUMBERS IN TAMOXIFEN INJECTED GLAST-CRE-ERT2 ^{+/-} /EIF2B5 ^{FL/FL} MICE.....	158
FIGURE 36: ALTERATIONS IN PERCENTAGE OF MICROGLIAL CELL NUMBERS IN TAMOXIFEN INJECTED GLAST-CRE-ERT2 ^{+/-} /EIF2B5 ^{FL/FL} MICE.....	160
FIGURE 37: ALTERATIONS IN ASTROCYTE CELL MARKER'S EXPRESSION IN TAMOXIFEN INJECTED GLAST-CRE-ERT2 ^{+/-} /EIF2B5 ^{FL/FL} MICE.	162
FIGURE 38: ALTERATIONS IN PERCENTAGE OF MATURE AND IMMATURE OLIGODENDROCYTES IN TAMOXIFEN INJECTED GLAST-CRE-ERT2 ^{+/-} /EIF2B5 ^{FL/FL} MICE.....	164

FIGURE 39: ALTERATIONS IN PERCENTAGE OF MICROGLIAL CELL NUMBERS IN TAMOXIFEN INJECTED GLAST-CRE-ERT2 ^{-/-} /EIF2B5 ^{FL/FL} MICE.	166
FIGURE 40: ALTERATIONS IN PERCENTAGE OF NEURONES IN TAMOXIFEN INJECTED GLAST- CRE-ERT2 ^{-/-} /EIF2B5 ^{FL/FL} MICE.	168

List of abbreviations

ABCD1: ATP-binding cassette D1

AD : Autosomique Dominant

ADLD : Adult-onset autosomal Dominant Leukodystrophy

AGS : Aicardi-Goutieres Syndrome

ALD : Adrenoleucodystrophy

ALDH3A2 : Aldéhyde Déshydrogénase 3 A2

AMN : Adrenomyeloneuropathy

Aqp4: Aquaporin-4

AR: Autosomique Recessive

ATF: Activated Transcription Factor

ATP: Adenosine Triphosphate

AxD: alexander disease

BBB: Blood-Brain Barrier

BiP: Binding Protein

BM: Bone Marrow

BMP: Bone Morphogenic Protein

BTK: Bruton tyrosine kinase

CADASIL: Cerebral Autosomal Dominant Arteriopathy with Subcortical Infarcts and Leukoencephalopathy

CACH: Childhood Ataxia with Central Hypomyelination

CAT1: Cationic Amino acid Transporter 1

cDNA: complimentary Deoxyribonucleic acid

CHOP: C/EBP Homologous Protein

CK: Casein Kinase

cKO: conditional Knock-Out

CLE: Cree Leukoencephalopathy

CNS: Central Nervous System

CNTF: Ciliary Neurotrophic Factor

CSF: cerebrospinal fluid

CX3CR1: CX3C chemokine receptor 1

Cx: Connexin

DNA: deoxyribonucleic acid
 DRCTNNB1A: Down Regulated by CTNNB1 proteinA
 DYRK: Dual-specificity tyrosine-phosphorylation-Regulated Kinase
 eEF: eukaryotic Elongation Factors
 EGF: Epidermal Growth Factor
 EIF2: Eukaryotic Initiation Factor 2
 EIF2B: Eukaryotic Initiation Factor 2B
 EPRS: Glutamyl-prolyl tRNA synthetase
 ER: Endoplasmic Reticulum
 eRF: eukaryotic Release Factors
 FALDH: Fatty Aldehyde Dehydrogenase
 FGF: Fibroblast Growth Factor
 FGFR3: Fibroblast Growth Factor Receptor3
 FL: Fetal Liver
 FLAIR: Fluid Attenuation Inversion Recovery
 GADD34: Growth Arrest and DNA Damage induced gene 34
 GAP: GTPase activator protein
 GCN: General Control Non-derepressible
 GDP: GDI-dissociation factor
 GDI: GDP-dissociation inhibitor
 GDP: Guanosine Diphosphate
 GEF: Guanine nucleotide Exchange Factor
 GFAP: Glial Fibrillary Acidic Protein
 GJA12: Gap Junction Alpha-12
 GJC2: Gap Junction Gamma-2
 Glast: Glutamate Aspartate Transporter
 GM: Grey Matter
 GSK3: Glycogen Synthase Kinase 3
 GTP: Guanosine Triphosphate
 HCC: Hypomyelination and Congenital Cataract
 HLD: Hypomyelinating leukodystrophies
 HRI: Heme-Regulated Inhibitor of translation
 HSP: Heat Shock Protein
 Iba1: ionized calcium-binding adapter molecule 1

IBTK: inhibitor of Bruton tyrosine kinase

INF- α : interferon- α

IPC: Intermediate Progenitor Cells

iPSC: Induced Pluripotent Stem Cells

IRE1: Inositol-Requiring Enzyme 1

IRES: Internal Ribosome Entry Site

ISR: Integrated Stress Response

ITAF: IRES Trans Acting Factors

KI: Knock-In

KO: Knock-out

LBSL: Leukoencephalopathy with Brain Stem and spinal cord involvement and high Lactate

MAG: Myelin Associated Protein

MBP: Myelin Basic Protein

mESC: mouse Embryonic Stem Cells

Met-tRNA_i: Initiator tRNA

MLC: Megalencephalic Leukoencephalopathy with subcortical Cysts

MLD: Metachromatic Leukodystrophy

MOG: Myelin Oligodendrocyte Protein

mRNA: Messenger RNA

MRI: Magnetic Resonance Imaging

mRNA: messenger Ribonucleic Acid

MRS: Magnetic-Resonance Spectroscopy

mtAspRS: Mitochondrial Aspartyl-tRNA Synthetase

NAA: N-acetyl-aspartic acid

NAAG: N-acetyl-aspartyl glutamate

NG2: Neural/glial antigen 2

NRF: Nuclear respiratory factor

NSC: Neural Stem Cell

OL: Oligodendrocyte

Olig2: Oligodendrocyte Transcription Factor2

OPC: Oligodendrocyte progenitor cells

ORFs: Open reading Frames

PABP: Poly-A Binding Protein

PBS: Phosphate Buffered Saline
PCR: Polymerase Chain reaction
PDGF: Platelet Derived Growth Factor
PERK: PKR like ER Kinase
PIC: Preinitiation Complex
PKR: double-strandes RNA Activated Protein Kinase
PLP: Proteolipid Protein
PMD: Pelizaeus-Merzbacher Disease
PMLD: Pelizaeus-Merzbacher Like Disease
RF: Rosenthal fibers
RMS: rostral migratory stream
RNA: Ribonucleic Acid
RVCL: Retinal Vasculopathy and Cerebral Leukodystrophy
Shh: Sonic hedgehog
SPG: spastic paraplegia
SOX: SRY-related HMG-box gene
SVZ : Subventricular Zone
TC : ternary complex
TGF- β : Transforming Growth Factor Beta
TMX: Tamoxifen
tRNA: transfer Ribonucleic Acid
uORFs: upstream Open reading Frames
VWM: Vanishing White Matter
WM: White Matter
WT: Wild Type
XBP1: X-box Binding Protein 1

I. INTRODUCTION

Childhood Ataxia with Central Nervous System Hypomyelination/Vanishing White Matter disease (CACH/VWM) is a leukodystrophy caused by mutations affecting any of the five genes coding for the five subunits of the Eukaryotic Initiation Factor 2B (EIF2B) which plays an important role in regulating protein synthesis especially under stress conditions. Patients present a proliferation of immature oligodendrocytes and dysmorphic astrocytes. The life expectancy is variable following the variable clinical forms that range from the acute severe infantile forms to the milder adult forms.

Our lab generated two inducible conditional knock-out mouse models targeting the EIF2B gene specifically in oligodendrocytes in the first model and in astrocytes in the second.

My work consisted on characterizing these two mice models in order to better evaluate and understand the consequences of the loss of the EIF2B factor in glial cells by using different approaches such as immunohistochemical analysis, electron microscopy, behavior analysis and transcriptomic analysis.

The first part of this manuscript consists on a bibliography study including glial cells, leukodystrophies and CACH/VWM disease, translation initiation factor and stress regulation in addition to different studied models. Then I present my results in our models and finish with the discussion of this work.

II. Bibliography

1. Glial cells in the CNS

The central nervous system (CNS) takes its origins from the neural tube which is formed early during embryonic development, more specifically, following the neurulation phase which in turn is induced by signals from the mesoderm to the ectoderm (Delhay-Bouchaud., 2001).

Brain and spinal cord form the CNS but we will mainly be focusing on the brain.

The CNS is composed of grey matter (GM) and white matter (WM), and regroups mainly two types of cells, which are glial cells and neurons. While the GM is rich in neuron cell bodies and synapses, the white matter lacks those and is however rich in axon fibers. Glial cells are present in grey as well as white matter.

Glial cells are divided into four types: astrocytes, oligodendrocytes, microglia and ependymal cells.

Neurons, astrocytes, oligodendrocyte and ependymal cells share a common ancestor as they all originate from the neural stem cells (NSCs). In contrast, microglia cells are generated in the hematopoietic stem cells as monocytes and migrate to the brain.

1.1. Progenitors (NSCs)

By definition, neural stem cells are cells that are capable of auto-renewal while keeping their ability to differentiate into neurons, astrocytes and oligodendrocytes (for review, Bergstrom and Forsberg-Nilsson., 2012).

Neural stem cells have epithelial origins arising from the neural tube and they keep their epithelial characteristics like apico-basal polarity (which plays an important role in neuronal migration at later stages), symmetric and asymmetric cell divisions in proportions that

determine the size of the nervous system and modulate the neuro-glial balance (for reviews, Kameneva and Adameyko., 2019; Allen and Lyons., 2018; Götz., 2001).

Radial glial cells, arising from NSCs, form a niche of neuro-glial progenitors in the CNS and when they divide following the symmetric cell division, they give birth to identical daughter NSCs, greatly expanding the niche. This symmetric cell division is favored at an earlier stage than the asymmetric cell division which is favored during neurogenesis and where each cell gives rise to a radial glial progenitor daughter cell to replenish the niche and an immature neuron or an intermediate progenitor cell (IPC) (Figure 1) (for reviews, Kameneva and Adameyko., 2019; Bergstrom and Forsberg-Nilsson., 2012), which in turn differentiate into neurons, oligodendrocytes or astrocytes.

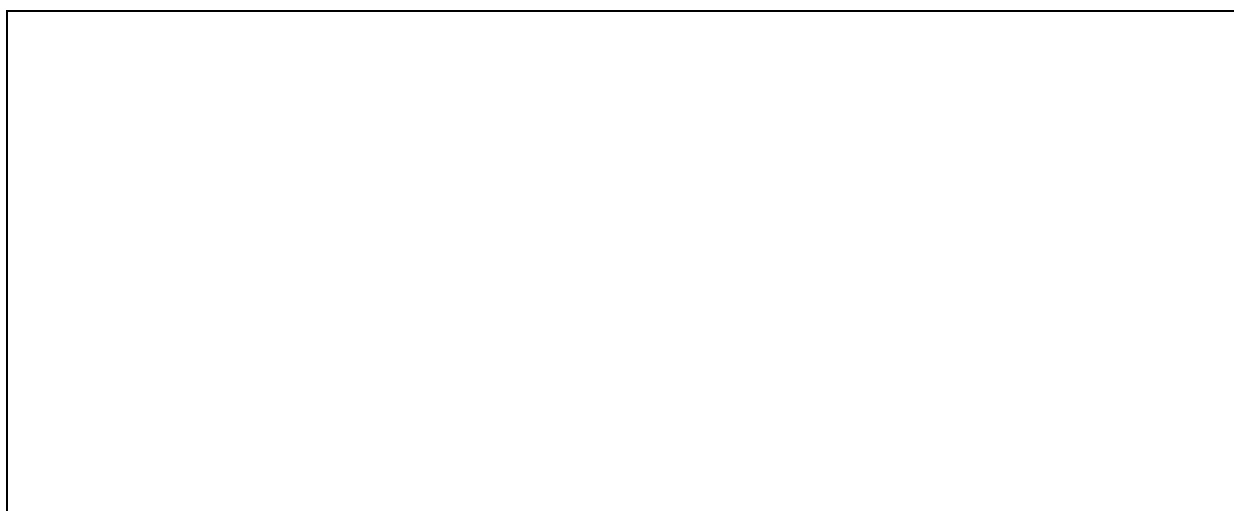


Figure 1 : Neuroepithelial cells and radial glia are neural stem cells. nIPC, aIPC and oIPC denote intermediate progenitor cells for neurons, astrocytes, and oligodendrocytes, respectively. (Bergstrom and Forsberg-Nilsson., 2012)

1.2 Oligodendrocytes

Oligodendrocytes are the myelin forming cells of the central nervous system. They arise from NSC-derived oligodendrocyte precursor cells (OPC or oIPC) that differentiate into immature non-myelinating oligodendrocytes (pre-OL) before finally going through the

maturation process and becoming a myelinating oligodendrocyte (mature OL) (for reviews, Van Tilborg et al., 2017; Bergles and Richardson., 2016).

This process follows several steps going from the proliferation of the OPCs, to migration and finally differentiation.

Each step is influenced by certain factors like the migration inducing PDGF (Platelet Derived Growth Factor) and the proliferation inhibiting TGF- β (Transforming Growth Factor Beta), which allows OPC differentiation. Adding to that, there is the differentiating role of the thyroid hormones and the extracellular matrix proteins (for reviews, Van Tilborg et al., 2017; Tritsch et al., 1999).

There are also several transcription factors that characterize the cells at each step such as NG2, Olig2, sox10, CC1 and others (Figure 2) (for reviews, Emery., 2010; Van Tilborg et al., 2018).

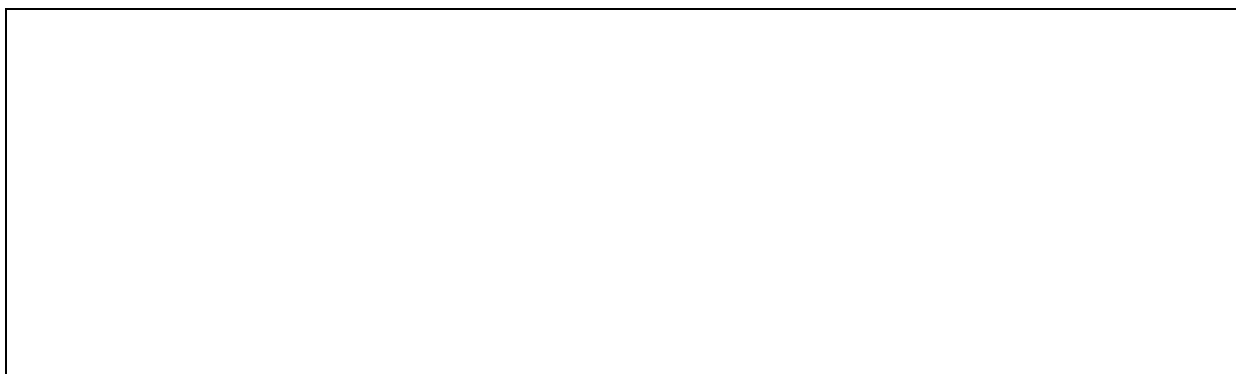


Figure 2 : Schematic representation of oligodendrocyte (OL) development and transcription factors that contribute to OL lineage progression at different developmental stages. OL precursor cells (OPCs) originate from neuroepithelial zones surrounding the ventricles, where neural stem cells (NSCs) differentiate into (OPCs) under the influence of OL-specific transcription factors Olig1/2, Nkx2.2, and Sox10. OPCs migrate toward an appropriate site via blood vessels, while at the same time promoting angiogenesis in a HIF1 α -dependent manner, in areas requiring more oxygen. At their final destination, OPCs proliferate to expand the pool of OPCs, under the regulation of transcription factors such as Id2, Id4, Tcf4, and Hes5. When proliferation is inhibited, OLs differentiate into premyelinating OLs (pre-OLs), and finally into mature OLs that enwrap neuronal axons with myelin sheaths, under the influence of, for example, Myrf (Van Tilborg et al., 2018)

Generation of OPC proceeds by waves. The first is a ventral wave, followed by a more dorsal origin consisting of a second wave and another ventral wave starting from the SVZ (Van Tilborg et al., 2018).

In addition, it has been shown that vascularization is very important for OPC migration through the fact that they crawl along blood vessels when migrating with the ability to also jump from one to another (Tsai et al., 2016; Van Tilborg et al., 2018).

As oligodendrocytes undergo the maturation process, they come into contact with axons and start heavily expressing myelin genes such as MAG (Myelin-Associated Glycoprotein), MOG (Myelin Oligodendrocyte Glycoprotein), MBP (Myelin Basic Protein) and PLP (Myelin Proteolipid Protein) in order to allow the ensheathment of axons by myelin (Nawaz et al., 2015), noting that a single axon is usually myelinated by several oligodendrocytes.

During the myelination process, oligodendrocytes might die by apoptosis. It has been shown that 50% of Oligodendrocytes die in rat optic nerve and 20% in the developing cerebral cortex, the reason possibly being the severe competition towards limited growth factors (For review, Miller., 2002).

Myelinating an optimal length of axon allows the increase in the conduction speed. In fact the action potential will go in a saltatory movement along the myelin sheaths and depolarize at specific non-myelinated regions on the axon called Nodes of Ranvier thus going from node to node (Knott and Molnar., 2001; Pritchard and Alloway., 2002).

More recently, an important metabolic role has been recognized to oligodendrocytes as providing lactates to neurons from glucose (glycolysis) and lipids (peroxysomal beta oxidation) (Saab et al., 2013; Morrison et al., 2013).

Myelination was also found to be adaptative to cope with learning environments such as motor skill learning in running wheels or Morris water maze where animals that went through a learning period of time showed increased white matter using MRI. This adaptive role of myelin was also noted for another type of learning in humans where neuroimaging showed increased white matter after learning a second language (Fields 2015; Monje 2018).

1.3 Astrocytes

Astrocytes, also called so because of their star shape, arise from NSC-derived astrocyte precursor cells (aIPC) and their differentiation occurs towards the end of gliogenesis throughout the CNS (Allen and Lyons., 2018).

Astrocytes are the most abundant and diverse type of glial cell in the CNS. They used to be regarded as supportive glial cells in neural tissue and astrogliosis was regarded as a reliable and sensitive marker of diseased tissue but it has changed into that of having a very important role in the CNS homeostasis (Sofroniew and vinters., 2010).

Morphologically, astrocytes are subclassified into protoplasmic and fibrous astrocytes. Protoplasmic astrocytes are mainly located in the gray matter and present several stem branches, giving rise to finely branching processes, in a uniform globoid distribution, which envelop synapses while fibrous astrocytes are located in the white matter and present long fiber-like processes that contact the nodes of Ranvier, noting that processes from both types are also in contact with blood vessels (Sofroniew and vinters., 2010).

Several signaling pathways play important roles in astrocyte proliferation, migration and maturation such as Notch, Hedgehog (Hh)/ Sonic Hedgehog (Shh), Fibroblast Growth Factor (FGFs) and Bone Morphogenetic Protein (BMP) (Yang and Jackson ., 2019).

Astrocytes are also subjected to apoptosis in order to regulate their numbers. Several growth factors affect the survival and differentiation of astrocytes such as EGF (Epidermal Growth Factor), le TGF- β (Transforming Growth Factor- β), LIF, CNTF (Ciliary Neurotrophic Factor), BMP (Bone Morphogenic Proteins), in addition to hormones, such as thyroid hormones, insuline and hydrocortisone (Tritsch et al., 1999).

Astrocyte lineage has been characterized with a number of markers such as the most commonly used GFAP (Glial Fibrillary Acidic Protein), Vimentin, Nestin S100 β , Glast (Glutamate Aspartate Transporter), Fgfr3 (Fibroblast growth factor receptor-3) and Aqp4 (Aquaporin-4) (Chen et al., 2017), however these markers are not always astrocyte-specific. For example, GFAP labels almost all reactive astrocytes but not necessarily all non-reactive

astrocytes especially in healthy CNS or far away from CNS lesions (Sofroniew and Vinters., 2010).

There exists many isoforms of GFAP (α , β , γ , δ and κ) and they can be heterogeneously expressed in both healthy and pathological CNS tissue (Kamphuis et al., 2012; Sofroniew and Vinters., 2010). At the transcript level in mouse brain, the expression of Gfap- α (set at 100%) is by far the most abundant followed by Gfap- δ (7.9%), Gfap- γ (4.5%), Gfap- κ (1.0%), Gfap- γ (0.3%), and Gfap- β (0.008%). The Gfap- δ is highly expressed in SVZ, RMS and olfactory bulb astrocytes and these Gfap- δ astrocytes also express neural stem cell marker Nestin and some other proliferation markers which classified them as neurogenic astrocytes (Kamphuis et al., 2012).

Astrocytes have several functions. They react, with microglia, to lesions by secretion of proinflammatory cytokines like INF- α (interferon- α). They secrete PDGF- α (Platelet Derived Growth Factor- α) which affects proliferation and migration of OPCs thus possibly affecting myelination. They are also very important for the formation and maintenance of the Blood-Brain Barrier (BBB) and in the control of the blood flow. That in addition to their role in keeping a healthy environment in the brain and modulating neuronal activity (Lindgaard et al., 2014). (Figure 3).

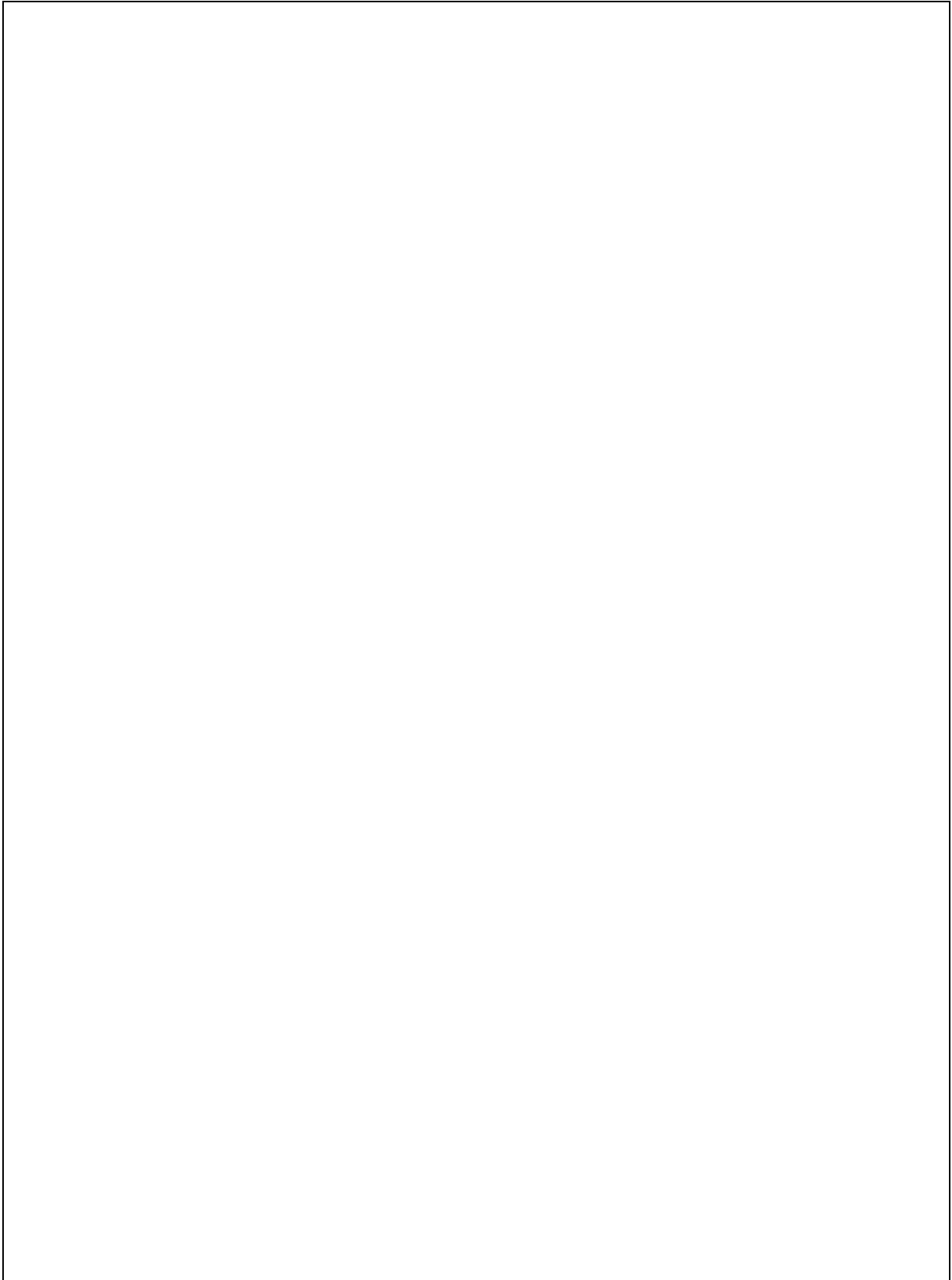


Figure 3 : Schematic representations that summarize, astrocytes functions in healthy CNS (a), and triggers and molecular regulators of reactive astrogliosis (b) (Sofroniew and Vinters., 2010).

1.4 Microglia

Microglia are the resident macrophages of the CNS where they represent almost 10% of the total number of cells (Knott and Molnar., 2001). They are present in Grey and White Matters. They derive from the extraembryonic yolk sac and then migrate to the CNS (Chen et al., 2017; Ginhoux, et al., 2010; Rigato, et al., 2011; Chan, et al., 2007; Saijo and Glass, 2011) via direct invasion (Figure 4).

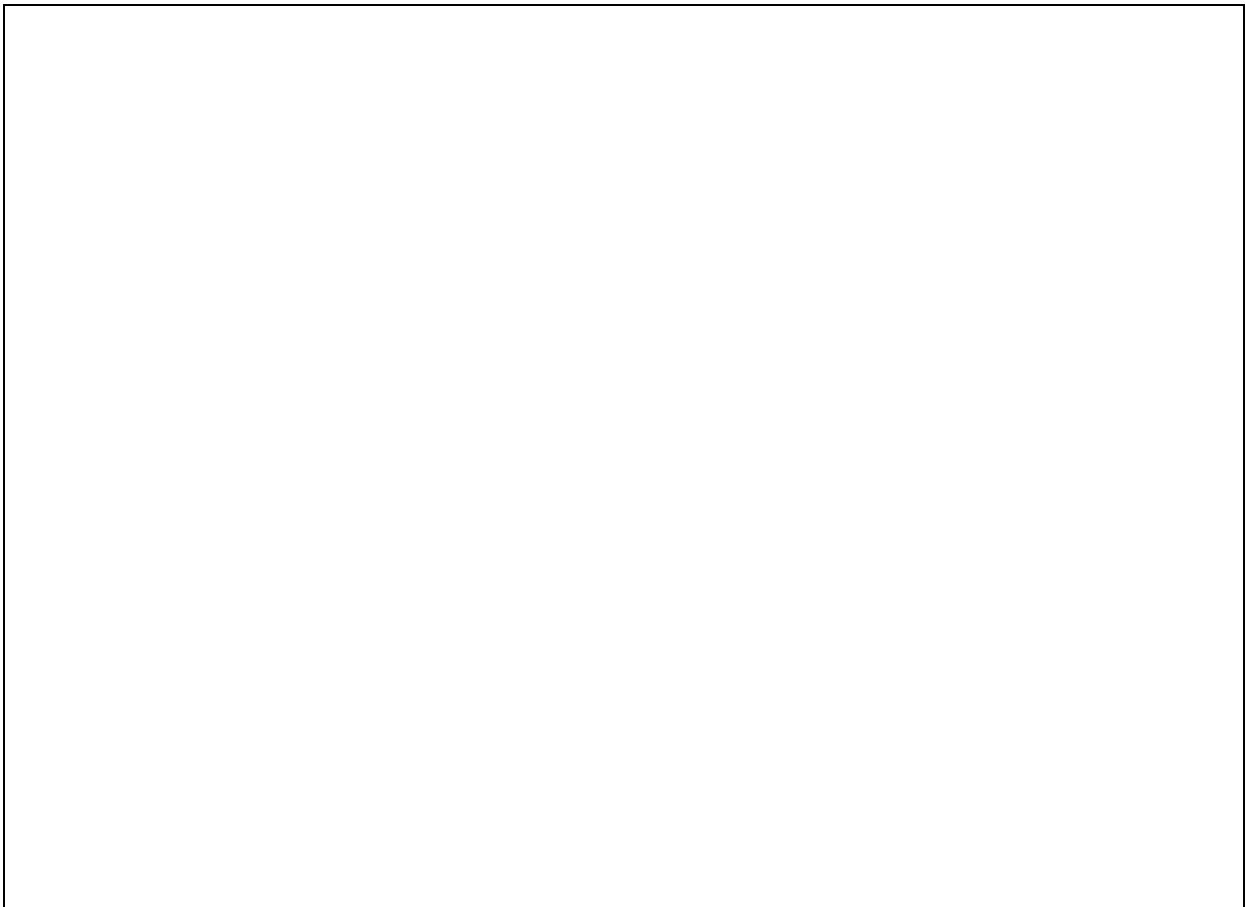


Figure 4: Brain development and microglial ontogeny. Primitive macrophages generated in the yolk sac (YS) blood islands around E8.0 spread into the embryos at the onset of blood circulation established around E8.5 and colonize the neuroepithelium from E9.0/E9.5, giving rise to embryonic microglia. In parallel, definitive hematopoiesis arises in the AGM and gives rise to progenitors that colonize the fetal liver (FL) from E10.5. The blood–brain barrier (BBB) starts to form from E13.5 and may isolate the developing brain from the contribution of FL and, later, of bone marrow (BM) hematopoiesis. Embryonic microglial cells expand, colonize the whole CNS, and will maintain themselves until adulthood via local proliferation during late gestation and postnatal development, as well as in the injured adult brain in reaction to

inflammation. Nevertheless, under certain inflammatory conditions found, for example, after BM transplantation, the recruitment of BM-derived progenitors can supplement the microglial population to some extent (Ginhoux and Prinz., 2015).

They are characterized by many markers such as CD11b, CD11c, CD68, and chemokine (C-X3-C) receptor 1 (Cx3cr1) as well as Iba-1 (Chen et al., 2017; Santos, et al., 2008; Chan, et al.; 2007; Ginhoux, et al., 2010; Rigato, et al., 2011; Dalmau, et al. 2003).

They are elongated and have small cell bodies with many short processes and are mobilized following lesion, infection or disease. Another important aspect is that they conserve their mitotic capacity all their life (Knott and Molnar., 2001) in addition to their role in phagocytosis of neuronal debris (Ginhoux and Prinz., 2015).

Microglial development is affected by several transcription factors and surface receptors (Figure 5).

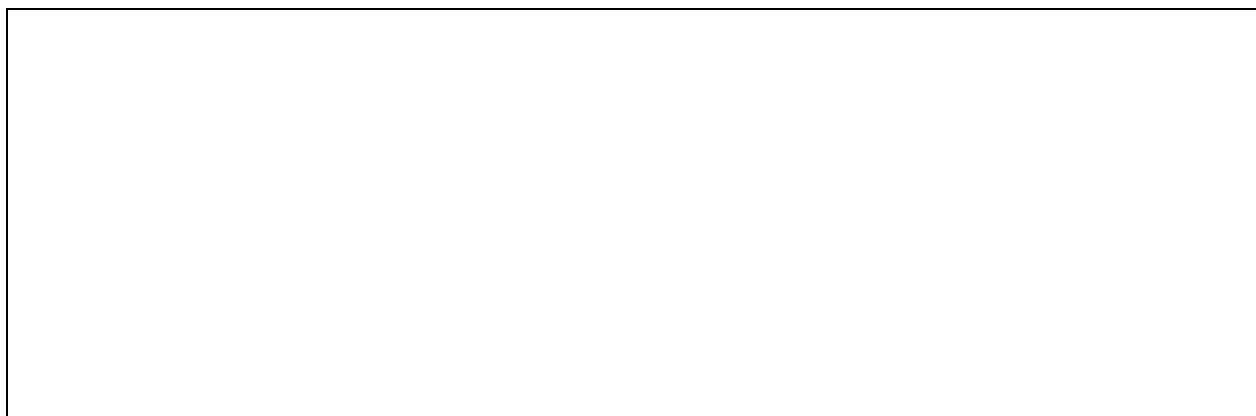


Figure 5: Morphology and markers of embryonic and adult microglia in the mouse. During embryogenesis (left), microglia show an activated and proliferating macrophage-like phenotype. Developing microglia with a round shape migrate throughout the maturing CNS phagocytizing neuronal debris. In adulthood (right), parenchymal microglia build a network of cells interacting with local neurons and display delineated small processes through which they actively survey the interneuronal space. The figure illustrates the precursors, transcription factors (black), and receptors (red) required for each developmental stage (Ginhoux and Prinz., 2015).

There are two forms of microglia activation, Classical activation (M1) or alternative activation (M2). M1 activation is characterized by a proinflammatory and neurotoxic state

where microglia secrete certain cytokines and chemokines like $\text{TNF-}\alpha$, IL-6, IL-1 β , IL-12, and CCL2 while producing reactive oxygen species. M2 activation is characterized by anti-inflammatory and healing activities of microglia by secreting anti-inflammatory cytokines (IL-10 and $\text{TGF-}\beta$), growth factors (IGF-1 and FGF), several neurotrophic factors (NGF, BDNF and GDNF) which help modulate synaptic strength and plasticity, and prosurvival factor progranulin (Colonna and Butovsky., 2017, Kabba et al., 2018).

1.5 Neurons

Neurons originate from NSC-derived Radial glia cells. They are composed of soma (of different shapes and sizes), dendrites and an axon. The soma surface and the dendrites represent the receiving surface while the axon represents the transmitting region (by transporting certain molecules such as neurotransmitters), which give neurons their functional polarity (Knott and Molnar., 2001).

Neurons are protected by oligodendrocytes through the formation of the lipid-rich myelin sheath around the axons, which also accelerates the speed of conduction of the action potential along the length of the axons, noting that the axon diameter also plays a role in that process (Knott and Molnar., 2001). (Figure 6)

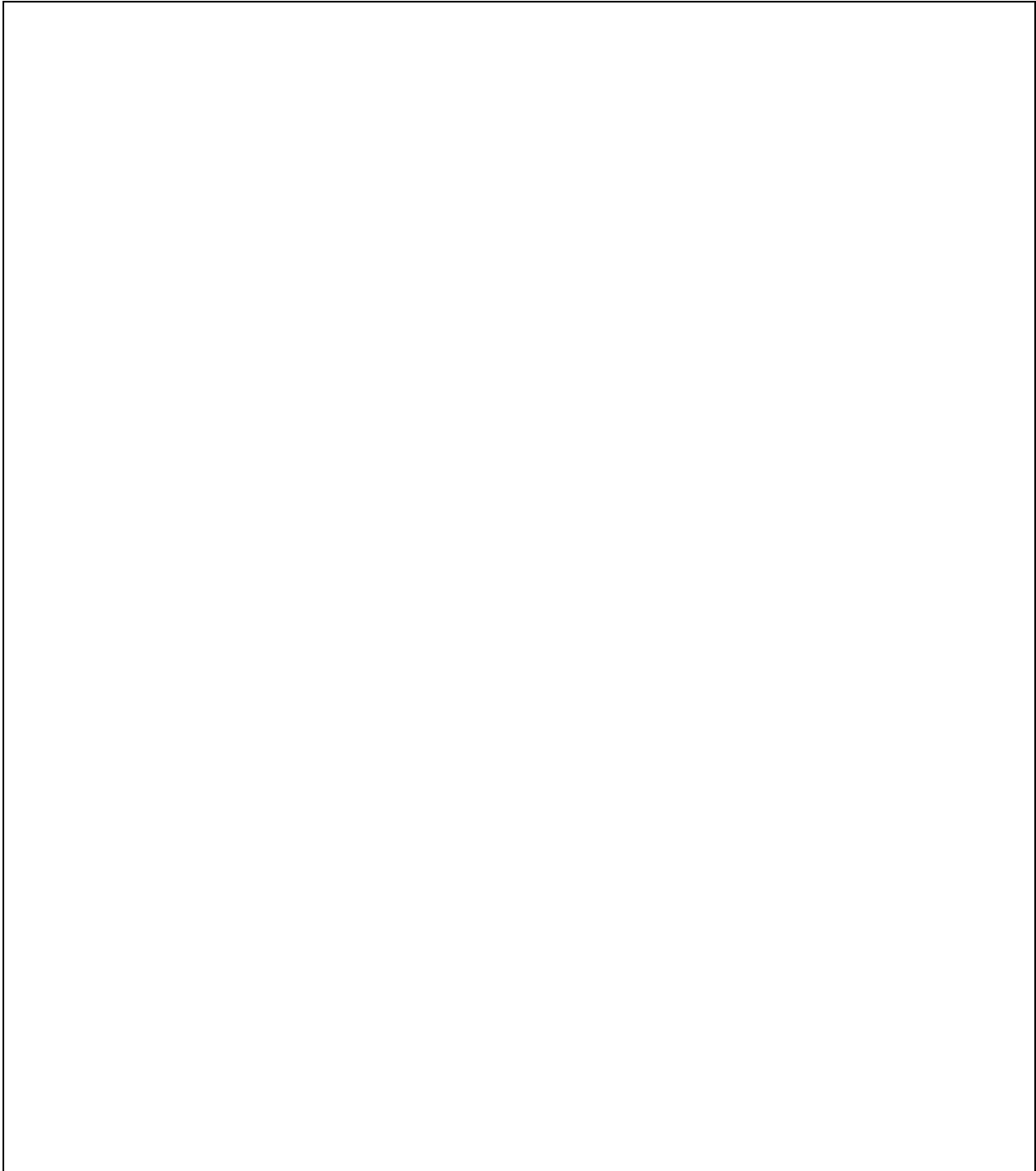


Figure 6: Schematic representation of a pyramidal neuron with an astrocyte and oligodendrocyte in close proximity. The astrocyte has an endfoot formed around the capillary endothelial cells and some of its other processes are in close association with the dendrites of the neuron. The oligodendrocyte is myelinating the axon immediately distal to the axon hillock. Axonal boutons are also shown synapsing on the apical dendrite (circled) (Knott and Molnar., 2001).



Figure 7: Schematic representation of a chemical synapse, showing the movement of calcium ions through voltage-gated calcium channels, causing neurotransmitter-containing vesicles to bind to the presynaptic membrane and releasing molecules into the synaptic cleft. These molecules are able to diffuse across the gap and bind to receptors in the postsynaptic membrane. Ligand-gated (fast) receptors are shown in which the movement of ions takes place across the receptor itself once the neurotransmitter attaches to its binding site (Knott and Molnar., 2001).

Synapses play an important role in neuron-neuron communication, noting that each neuron in the CNS has an average of 10^6 synapses.

1.6 CNS cells interactions

Neurons and astrocytes interact with each other using neurotransmitters and by regulating neuronal and synaptic function via the release of gliotransmitters (Araque et al., 2014; Eroglu and Barres., 2010; Perea et al., 2014). Another type of interaction is in the form of Glutamate/Glutamine cycle where glutamine synthesized in the astrocytes is used by neurons to form GABA and glutamate which is then up-taken by astrocytes to form glutamine through the TCA cycle (Danbolt., 2001; Schousboe et al., 1997).

Neurons interact with OPCs by forming synapses with NG2 cells. These synapses could be the classical ones or non-classical ones. The non-classical ones' mode of transmission could

be ectopic, spillover or diffuse transmission and are more widespread than the classical ones. Their importance stems from neurotransmitters affecting certain receptors expressed by NG2 cells such as AMPA, GABA, NMDA and glutamate receptors. Neurons-NG2 cell synapses play an important role in NG2 cell cycle control in addition to proliferation, migration and differentiation. NG2 cells are also affected by neuronal activity and respond accordingly such as promote differentiation and myelination when neurons are demyelinated. Finally, when cells begin differentiation, these synapses are decreased, in addition to a decrease in NG2 cells' glutamate receptors (Yang et al., 2013).

Neurons also interact with microglia through the microglia synaptic pruning role where they remove the excess of synapses formed during development (Tyler and Boulanger., 2012; Wu et al., 2015) and through their role in adult neurogenesis (Frick et al., 2016). Neurons in turn affect the microglia through the secretion of ligands for certain microglial receptors (Wu et al., 2015).

A tripartite metabolic function exists between neuron-astrocytes-OLG. In fact, another type of interaction is in the form of Glutamate/Glutamine cycle where glutamine synthesized in the astrocytes is used by neurons to form GABA and glutamate which is then up-taken by astrocytes to form glutamine through the TCA cycle (Danbolt., 2001; Schousboe et al., 1997). The other part of the tripartite metabolic function is represented by the NAA-NAAG cycle where NAA generated by the neuron passes to the oligodendrocyte. The ASPA in the oligodendrocyte then converts the NAA into free acetate which is then used for fatty acid synthesis and histone acetylation. The NAA-derived aspartate could also be recycled to the neuron once again (Figure 8) (Moffett et al., 2013).

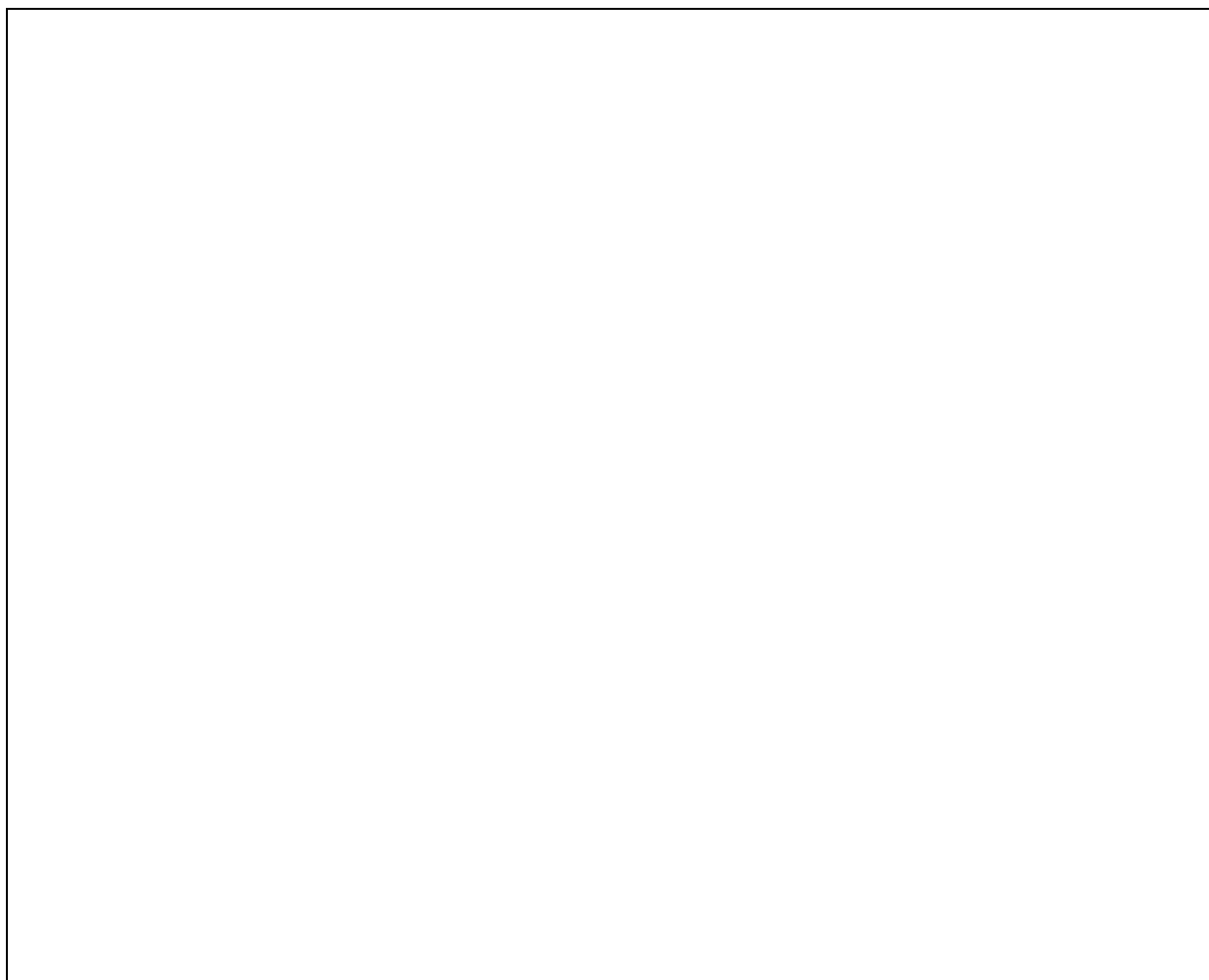


Figure 8: Schematic diagram depicting some of the metabolic trafficking between neurons, oligodendrocytes, and astrocytes. A major intercellular cycle between neurons and astrocytes is exemplified by the glutamate-glutamine cycle. A percentage of glutamate is not recycled however, and instead is oxidized for energy derivation in the TCA cycle of neurons and astrocytes. A major metabolite cycle also exists between neurons and oligodendrocytes via NAA that is transferred from axons to oligodendrocytes at axo-glial contact zones between the innermost oligodendrocyte plasma membrane in a myelin segment and the axonal membrane. ASPA in the oligodendrocytes generates free acetate which can then be converted to acetyl CoA by AceCS1, which can then go on to be utilized for fatty acid synthesis, cytoplasmic protein acetylation reactions, and nuclear histone acetylation (blue lines). It is possible that some acetate derived from NAA in oligodendrocytes is transferred to astrocytes for energy derivation though the enzyme AceCS2 present in mitochondria in astrocyte end feet and cellular contact zones. AceCS2 in astrocytes is also in a position to capture blood borne acetate for energy derivation. It is also possible that some NAA-derived aspartate in oligodendrocytes is recycled back to neurons. AAT, aspartate aminotransferase; AceCS1, acetyl CoA synthase-1; AceCS2, acetyl CoA synthase-2; AKG, α -ketoglutarate; ASP, aspartate; ASPA, aspartoacylase; aspNAT, aspartate N-acetyltransferase; CL, ATP citrate lyase; GLN, glutamine; GLU, glutamate; GS, glutamine synthase; NH₃, ammonia; PAG, phosphate activated glutaminase (adapted from Moffett et al., 2013).

2. Leukodystrophies

The term leukodystrophy technically refers to disorders with wasting (dystrophy) of the brain's white matter (leuko) and is traditionally reserved for heritable disorders, however there is lack of consensus on how this term should be applied.

“Heritable white matter disorders” is a general term to define inherited neurological disorders involving cerebral white matter, they includes leukodystrophies and genetic leukoencephalopathies.

More recently, an iterative consensus-building effort among a panel of leukodystrophy experts aimed at precisely defining the definition, descriptive terms, inclusion criteria and exclusion criteria that characterize leukodystrophies (vanderver 2015).

Leukodystrophies were defined as “heritable disorders affecting the white matter of the central nervous system with or without peripheral nervous system involvement. These disorders have in common glial cell or myelin sheath abnormalities. Where known, neuropathology is primarily characterized by the involvement of oligodendrocytes, astrocytes and other non-neuronal cell types, although in many disorders the mechanism of disease remains unknown, and in other cases is suspected to include significant axonal pathology”. Leukodystrophies do not include acquired CNS myelin disorders, such as multiple sclerosis and related acquired demyelinating processes, infectious and post-infectious white matter damage, toxic injuries and non-genetic vascular insults. In addition, CNS diseases in which neuropathology shows primary involvement of neurons in cerebral cortex or other gray matter structures should not be characterized as leukodystrophies”.

They represent a heterogeneous group of rare diseases touching childhood and, in some cases, adulthood.

2.1 Classification of Leukodystrophies

Classification of leukodystrophies evolved, over the years, following the evolution of CNS analysis technics. Initially based on neuropathological examination, myelin related pathologies were defined as “hypomyelinating” (reduced amount of myelin) or “demyelinating” (myelin destruction) pathologies (Labauge and Boespflug-Tanguy, 2010).

It is nowadays based on magnetic resonance imaging (MRI). In leukodystrophies, on magnetic resonance imaging (MRI), abnormal T2 hyperintensity in the affected white matter is present and T1 signal may be variable. Mildly hypo-, iso- or hyperintense T1 signal relative to the cortex may be consistent with a hypomyelinating leukodystrophy. Demyelinating leukodystrophy leads to significantly hypointense T1 signal.

An increasing number of genes causing leukodystrophies have been reported during the last decade suggestive distinct physiopathological pathways.

The main forms of leukodystrophies are reported on table 1 (Kohlschütter et al., 2010)

2.1.1 Hypomyelinating leukodystrophies

Hypomyelinating leukodystrophies (HLDs) are characterized by a lack of myelin quantity in the CNS, which can be seen in the MRI and recognized by an abnormal diffused WM aspect.

There is a clinical continuum between the severe forms caused by maturation problems of the myelinating oligodendrocytes in the early stages of life and the moderate forms caused by problems in myelin compaction and stability in the adult manifesting by motor problems affecting the lower limbs (spastic paraplegia SPG).

PLP-pathies are a major group of HLDs with X-linked transmission. They are caused by a mutation affecting the *PLP1* gene which codes for the PLP and DM20 proteins (major myelin proteins). Among this group are the Pelizaeus-Merzbacher disease (PMD) and

Type		Protein/gene	Phenotype	Transmission
Hypomyelinating leukodystrophies		Proteolipid proteins PLP DM20 / PLP1	Pelizaeus-Merzbacher disease (PMD) [MIM 3120800], spastic paraplegia type 2 (SPG2) [MIM 312920]	X-linked
		GJA12 (connexin 47) / GJA12	Pelizaeus-Merzbacher-like disease 1 (PMLD1) [MIM 608804]	AR
		SOX10 / SRY-related HMG-box gene 10 (SOX10)	Peripheral demyelinated neuropathy, central dysmyelinated leukodystrophy (PCWH) [MIM 609136]	AR
		Hyccin / Down Regulated by CTNNB1 protein A (DRCTNNB1A)	Hypomyelination and congenital cataract (HCC) [MIM 610532]	AR
		Monocarboxylate transporter 8 / MCT8	Allan-Herndon-Dudley Syndrome (MIM 300523)	X-linked
		Aldehyde dehydrogenase 3A2 / ALDH3A2	Sjögren-Larsson Syndrome (MIM 270200)	AR
Demyelinating leukodystrophies	Vacuolating leukodystrophies	Glial fibrillary acidic protein / GFAP	Alexander disease [MIM 203450]	AD
		MLC1 / Megalencephalic Leukoencephalopathy with subcortical Cysts 1 (MLC1)	Megalencephalic leukoencephalopathy with subcortical cysts (MLC) [MIM 604004]	AR
		Ribonuclease T2 / RNASET2	Cystic leukoencephalopathy without megalencephaly (MIM 612951)	AR
		Eukaryotic initiation factor 2B α to ϵ / EIF2B 1 to 5	Childhood ataxia with CNS hypomyelination or vanishing white matter (CACH/VWM) [MIM 603896], Cree leukoencephalopathy, ovarioleukodystrophy	AR
	Non vacuolating Demyelinating leukodystrophies	Mitochondrial aspartyl tRNA synthetase / DARS2	Leukoencephalopathy with brain stem and spinal cord involvement and high lactates (LBSL) [MIM 611105]	AR
		Lamin B1 / LMNB1	Adult AD leukodystrophy (ADLD) 5q31 [MIM 169500]	AD
	Vasculopathic leukoencephalopathies	Ribonuclease H2 A, B, or C / RNASEH2A,B,C	Aicardi Goutières syndrome (AGS) [MIM 225750]	AR
		TREX1 endonuclease / TREX1	Aicardi Goutières syndrome (AGS) [MIM 225750], Cree leukoencephalitis, retinal vasculopathy with cerebral leukodystrophy (RVCL) [MIM 192315]	AR (AGS), AD (RVCL)
		Notch 3 / Notch3	Cerebral AD arteriopathy with subcortical infarcts leukoencephalopathy (CADASIL) [MIM 125310]	AD
		Collagene IV A1 / COL4A1	Porencephaly familial [MIM 175780], brain small vessel disease [MIM 607595]	AD
	Lysosomal defects	Arylsulfatase A / ARSA	Metachromatic leukodystrophy type 1 (MLD1) [MIM 250100]	AR
		Prosaposin / PSAP	Metachromatic leukodystrophy type 2 (MLD2) related to saposin B deficiency [MIM 249900]	AR
		Galactocerebroside / GALC	Krabbe disease type 1 [MIM 245200]	AR
	Peroxisomal defects	ATP-binding cassette Transporter D1 / ABCD1	Adrenoleukodystrophy (ALD) [MIM 300100], adrenomyeloneuropathy (AMN)	X-linked
	AA metabolism defect	Aspartoacylase / ASPA	Canavan disease [MIM 271900]	AR

Table 1: Classification and genes identified in main leukodystrophies/leukoencephalopathies. AR : Autosomal Recessive, AD : Autosomal Dominant, aa : amino acids (Boespflug-Tanguy et al., 2008; Kohlschütter et al., 2010).

spastic Paraplegia type 2 (SPG2). The severe PMD forms are caused by point mutations in the *PLP1* gene, while the SPG2 forms are caused by less severe null mutations (Cailloux et al., 2000; Inoue, 2005).

Gap Junction Alpha-12 (GJA12), also known as Gap Junction Gamma-2 (GJC2) or Connexin-47 (Cx47), which is the oligodendrocyte-specific Cx that forms junctions with the astrocyte-specific Cx43, is encoded by the *GJC2* gene. Mutations to this gene are responsible for the Pelizaeus-Merzbacher-Like Disease 1 (PMLD1). Patients present PMD phenotype with an autosomal recessive transmission, followed by rapid neurological degradation possibly linked with a rapid axonal degeneration (Boespflug-Tanguy et al., 2008).

Mutations to *SOX10* gene (*SRY-related HMG-box gene 10*), which codes a transcription factor regulating cell migration from the neural crest and oligodendrocyte differentiation, are also responsible for a hypomyelinating phenotype of the SNC and SNP (Schiffmann and Boespflug-Tanguy, 2001).

Another gene involved in HLD is *DRCTNNB1A* (Down Regulated by CTNNB1 proteinA) which codes a ubiquitous cell membrane protein called hyccin. This protein is involved in the Hypomyelination and Congenital Cataract (HCC) syndrome (Zara et al., 2006).

Mutations affecting the *MCT8* (Monocarboxylate Transporter 8) gene, which codes a thyroid hormone transporter, are usually responsible for the Allan-Herndon-Dudley syndrome but might also cause PMLD. However, unlike PMD patients, these patients present disturbed thyroid balance in addition to a progressively recovering hypomyelination, giving rise to a delayed myelination phenotype (Vaurs-Barrière et al., 2009).

Recessive mutations affecting the lipids such as the fatty aldehyde dehydrogenase (FALDH) enzyme in the Sjögren-Larsson syndrome, (Gordon 2007) or the ceramides biosynthesis by loss of the sphingolipid desaturase DEGS1 (Pant D C et al., 2019) .

More recently mutations affecting genes implicated in the function of Polymerases 3 (PolR3A, PolR3B, PolR3F et PolR1C) (HLD 7, HLD8 et HLD11) were found to cause hypomyelinating leukodystrophies (Potic et al., 2012; Thiffault et al., 2015).

Other hypomyelinating leukodystrophies with basal ganglia and cerebellum atrophy (H-ABC) were found to be caused by dominant heterozygous mutations in *TUBB4A* (HLD6) (Duncan et al., 2017).

2.1.2 Demyelinating leukodystrophies

Demyelinating leukodystrophies are characterized by a normal myelin formation followed by loss or rearrangement of this myelin.

They can be divided into four groups:

- Vacuolating leukodystrophies: result from WM homeostasis disorder in association with macro or micro cystic changes. This group will be further discussed later on.
- Non vacuolating demyelinating leukodystrophies: among these, LBSL caused by mutations in the *DARS2* gene coding for the mitochondrial aspartyl-tRNA synthetase (mtAspRS) with high levels of lactate in the brain and the spinal cord, in addition to the ADLD, presenting multiple sclerosis-like phenotype, that is caused by lamin B1 over expression (Boespflug-Tanguy et al., 2008).
- Vasculopathic leukoencephalopathies: such as Aicardi-Goutières syndrome which is characterized by brain calcifications and high interferon level in the CSF and caused by mutations in *ADAR*, *RNASEH2A*, *RNASEH2B*, *RNASEH2C*, *SAMHD1*, *TREX1* IFIH. (Crow et al., 2014; Kaye, 2001). In this group we also find CADASIL, caused by mutations in the *NOTCH3* gene coding transmembrane receptor with an important role in cell differentiation, which is characterized by strokes, dementia and higher migraine frequency (Chabriat et al., 2009). Finally, mutations in the *COL4A1* gene coding for collagen type 4A1 cause microangiopathy.
- Metabolic diseases: are usually caused by metabolism deregulation of ubiquitous enzymes of peroxysomes, lysosomes and amino acids responsible for myelin biogenesis and maintenance. Among the diseases in this group are metachromatic leukodystrophies (MLD) and Krabbe diseases, both being lysosomal diseases with an autosomal recessive transmission. MLDs are caused by deficits in arylsulfatase A (MLD 1) and saposin B (MLD 2). Krabbe disease is caused by a deficit in galactocerebroside enzyme, and what affects the myelin is actually the excessive accumulation of a secondary metabolite called psychosine which is toxic to WM (Baumann and Turpin, 2000; Kaye, 2001). Adrenoleucodystrophies (ALD) and Canavan diseases are also part of this group. ALD is a peroxisome disease with an X-linked transmission, characterized by the accumulation of very long chain fatty amino

acids and caused by mutations to the *ABCD1* (ATP-binding cassette D1) gene. The classic early form with inflammation and adrenal insufficiency is more severe than the adult adrenomyeloneuropathy with slow and progressive spastic paraplegia (Baumann and Turpin, 2000; Kaye, 2001). Finally, the Canavan disease is caused by deficiency in aspartoacylase which hydrolyses N-acetyl-aspartic acid (NAA) into aspartate and acetate. NAA is necessary to the neurotransmitter N-acetyl-aspartyl glutamate (NAAG) synthesis, and so its deficiency leads to NAA accumulation, which has a high osmolarity and interferes with glutamatergic functions and promoting the disease (Baumann and Turpin, 2000).

2.2 Vacuolating leukodystrophies

This group of leukodystrophies presents a cavitating appearance detectable with MRI through the presence of micro/macro-cystic zones with a signal identical to that of the cerebrospinal fluid (CSF). Four major diseases have been identified in this group, which are the Alexander disease (AxD), the Megalencephalic leukoencephalopathy with subcortical cysts (MLC), the Cystic leukoencephalopathy without megalencephaly and the CACH/VWM syndrome. At the border between vasculopathic and vacuolating leukodystrophies, the leukoencephalopathy with calcifications and cysts (LCC) is due to heterozygote mutations of the *SNORD118* gene encoding a small nucleolar RNA important for ribosomal biogenesis and functions (Jenkinson et al., 2016).

2.2.1 Alexander disease

This is a fatal, progressive disease starting at childhood with an autosomal dominant transmission mode. It is the first disease to be directly and genetically associated with astrocyte dysfunction and is characterized by the formation of Rosenthal fibers (RF) which are clumps of proteins accumulating in astrocytes' cytoplasm. Clinically, three forms have been described. The first one is the most frequent infantile form, which is characterized by an early beginning (1 month to 2 years of age) and a severe evolution. Among other signs, it presents progressive megalencephaly, psychomotor development retardation, ataxia and

seizures, leading to death in the first 10 years of life. The second form is the juvenile form that begins between 2 and 12 years of life. It is associated with spastic paraplegia and progressive bulbar signs, but usually with preserved intellectual capacities. The third is the adult form with a more heterogeneous clinical spectrum with neurodegeneration resembling that of multiple sclerosis. AxD cases are mostly sporadic and *GFAP* gene has been determined to be a candidate gene after the discovery of RF, identical to those described in AxD but without demyelination, in brains of mice overexpressing human GFAP. The RF are mainly composed of GFAP, $\alpha\beta$ -crystalline chaperones and Heat Shock Protein 27 (HSP27). Both latter proteins are involved in ensuring good protein conformation including that of GFAP with their anti-apoptotic and anti-oxidant functions, and their retention in the RF keeps them from playing their role thus leading to neurodegeneration and astrocytic dysfunctions (Schiffmann and Boespflug-Tanguy, 2001; Mignot et al., 2004; Boespflug-Tanguy et al., 2008).

2.2.2 Megalencephalic leukoencephalopathy with subcortical cysts (MLC)

MLC is a spongiform disease with autosomal recessive transmission mode. It is an infantile disease (beginning before 10 years of age) caused by mutations in the *MLC1* (*Megalencephalic Leukoencephalopathy with subcortical Cysts 1*) gene which codes a transmembrane protein, of unknown function, found essentially in astrocytes and neurons. This protein interacts with the glycoprotein complex associated to the dystrophin, the potassium channels Kir4.1 and the aquaporin-4 channels. MLC is characterized by macrocephaly, slow and progressive deterioration of motor functions in association with ataxia and spasticity, epilepsy in 50% of the cases and variable mental retardation. MRI shows a diffuse WM with the presence of sub-cortical cysts in the temporal and/or fronto-parietal regions. The spongiform aspect of the WM reveals the presence of vacuoles between the outer membranes of the myelin sheets, without affecting the axons.

2.2.3 Cystic leukoencephalopathy without megalencephaly

It is a disease with an autosomal recessive transmission mode, caused by mutations of the *RNASET2* gene. Patients show no symptoms at birth and later develop an encephalopathy with microcephaly associated to a slow psychomotor development during the early years. MRI show sub-cortical cystic lesions with bilateral alterations of the WM that resemble cytomegalovirus congenital infections (Henneke et al., 2009).

2.2.4 CACH/VWM syndrome

CACH/VWM syndrome is a vacuolating leukodystrophy with an autosomal recessive transmission mode. It is associated with mutations in any of the 5 genes *Eukaryotic Initiation Factor 2B 1 to 5* coding for the 5 subunits of the ubiquitous eif2b factor necessary for the transcription initiation. This disease will be discussed more in detail in the next section.

3. CACH/VWM syndrome

3.1 History of the disease recognition

Eicke, in 1962, reported in a 36-years old female patient with a secondary amenorrhea (defined as abnormal cessation of menstrual cycles for at least 6 months) a slowly progressive disease with rapid neurological worsening-triggered by minor head trauma.

Neuropathological analysis of the postmortem brain, showed a diffuse cystic degeneration of the cerebral white matter surrounded by dense aggregations of oligodendrocytes.

In 1993 the disease was reinvestigated by Hanefeld (Hanefeld et al., 1993) as “Myelinopathia Centralis Diffusa” affecting young children with minor head trauma as a provoking factor. With a larger number of affected patients, Schiffmann and al 1994, described the disease as childhood ataxia with central nervous system hypomyelination (CACH) and confirmed the “cerebrospinal fluid (CSF) like” signal of the white matter on magnetic-resonance imaging (MRI) and spectroscopy (MRS) already mentioned by Hanefeld.

Subsequently, Van der Knaap and her collaborators(1997) suggested that magnetic resonance imaging (MRI) and MRS results of gradual devastating cystic degeneration of cerebral white matter and proposed to name of Vanishing White Matter Disease (VWD) (Van der Knaap et al., 2006).

3.2 CACH/VWM and EIF2B mutations

CACH/VWMD reported by Hanefeld Schiffmann and van der Knaap corresponds to the classical form and was identified as a progressive neurodegenerative disorder characterized by a cerebello-spastic syndrome, rapidly precipitated acute phases induced by stress leading to death in 2 to 5 years due to the complete lack of treatment. This rare disease (incidence around 1/7500 of living births), have an autosomal recessive-transmission.

In 1999, Leegwater and colleagues were able to identify a region of interest in 3q27 by studying 19 families with CACH/VWM syndrome (Leegwater et al., 1999). Following that, sequencing the exon regions of 25 genes in the 3q27 region allowed the identification of mutations in *EIF2B5* which codes the epsilon subunit of the eukaryotic transcription initiation factor 2B (Leegwater et al., 2001). Then, by homology of function, mutations were found in the other 4 genes, *EIF2B1* to *B4*, coding for the other 4 subunits of eIF2B, α , β , γ and δ (van der Knaap et al., 2002). There are at least 160 mutations, most of which are missense mutations (Abbink et al., 2018). The majority of these mutations affect *EIF2B5* (66.5%) while this proportion amounts to 1.7% for *EIF2B1*, 16.6% for *EIF2B2*, 7.8% for *EIF2B3* and 7.4% for *EIF2B4* (Van Der Knaap et al., 2019). These missense mutations can be homozygote or compound heterozygote, while frameshift mutations and nonsense mutations can only be heterozygous. eIF2B being essential to translation initiation, such mutations, should-they

exist at the homozygous state, would cause a total loss of function of this initiation factor, which is non-viable even at the embryonic stage of development.

3.3 The large clinical spectrum and concept of eIF2B related disorders

EIF2B genes analysis in a large group of patients with undetermined leukodystrophies allowed the extension of the disease's clinical spectrum ranging from congenital to adult-onset forms named EIF2B related disorders (Fogli et al., 2004a) (Figure 9).

The highest incidence was documented in children. It is more prevalent in females than in males. The symptoms appear directly after birth or during maturation, in which ataxia and spasticity are the major ones, seizures and cognitive decline are apparent but with less significance, however, neurological motor and behavioral abnormalities in addition to psychiatric problems are of the least significance in the disease's phenotypic heterogeneity.

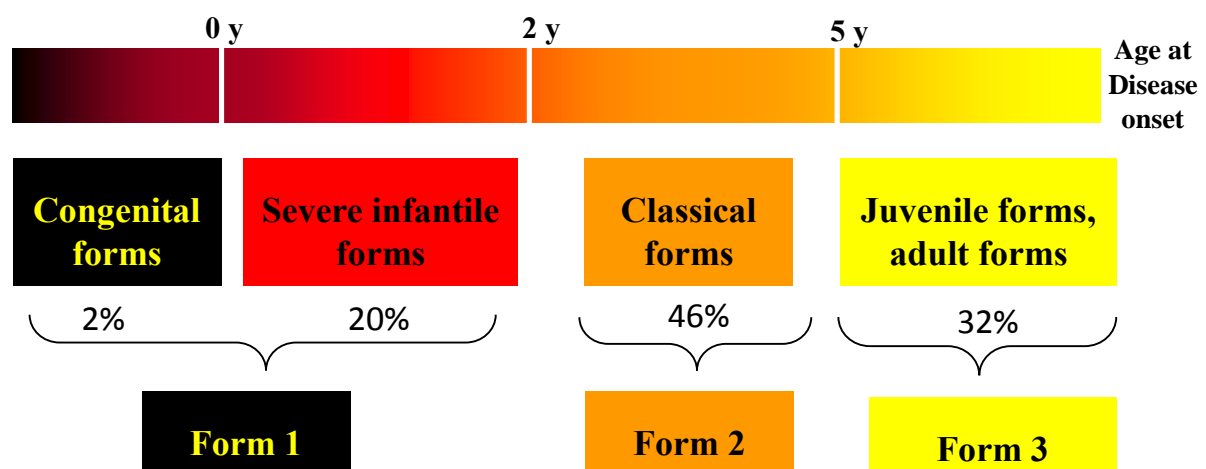


Figure 9: eIF2B-pathies clinical spectrum: Correlation between age at disease onset and clinical severity. Proportions have been calculated based on 219-patient cohort (adapted from Fogli et al., 2004a).

Early onset forms (<2 years of age)

These included the severe forms with onset before 1 year of age and death in several months only (Francalanci et al., 2001) and the congenital forms.

(1) Fatal infantile forms including Cree leukoencephalopathy described among the Canadian Cree Indians. This form is characterized by the appearance of symptoms at 3 to 6 months of age with death of 100% of patients occurring before 21 months of age (Black et al., 1988; Fogli et al., 2002a, Fogli et al., 2002b). Patients have hypotonia followed by the brutal apparition of neurologic distress, hyperventilation, vomiting and diarrhea. Psychomotor regression, lethargy, blindness and interruption of cranial perimeter are also observed. Neuropathological analysis showed a WM with cells having large vacuoles and expressing MOG protein, in addition to the presence of astrogliosis, detectable by GFAP staining (Fogli et al., 2002b). A peripheral neuropathy has also been detected (Huntsman et al., 2007) and the main cause for this Cree leukodystrophy has been shown to be the p.Arg195His homozygous mutation (Fogli et al., 2002b).

(2) Lethal Congenital forms associated to developmental anomalies (intrauterine growth retardation with oligohydramnios, renal hypoplasia, congenital cataract/glaucoma, facial dysmorphism and ovarian dystrophy), sometimes to hepatic and pancreatic lesions (van der Knaap et al., 2003) or even demyelinating peripheral neuropathy (Federico et al., 2006)

Juvenile / adult forms /Ovarioleukodystrophies

On the opposite, forms having onsets at adolescence and adult age (usually at the second decade and sometimes even later) have been later recognized (Fogli et al., 2003b; Ohtake et al., 2004). Onset is usually progressive with unrecognized cognitive or behavioral symptoms, until the appearance of cerebello-spastic signs or acute episodes of epileptic seizures. Same as infantile forms, environmental factors might trigger or exacerbate the disease (Fogli et al., 2004a). These environmental factors, (including infections, cranial trauma, fright, exposure to sun rays, pregnancy etc) act fast within few hours to few days (Vermeulen et al., 2005; Peter et al., 2008). A certain phenotypic heterogeneity has also been described in the adult forms leading to localized epilepsy (Jansen et al., 2008), localized dementia, without other symptoms of focalization, which suggests a senile dementia diagnostic (Ohtake et al., 2004) or even pure psychiatric disorders sometimes resembling schizophrenia (Denier et al., 2007). Other paucisymptomatic forms, asymptomatic forms or even forms with non-neurologic symptoms have been described (Fogli et al., 2003b). The disease of the adult-onset is always underestimated because it shows milder symptoms in addition to psychiatric and behavioral problems.

In 1997, Schiffmann and colleagues described for the first time, 4 female patients between 15 and 29 years of age, with a leukodystrophy associated to ovarian dysfunction called ovarioleukodystrophy (Schiffmann et al., 1997). These female patients presented symptoms at adolescence or adult age with walking disorders sometimes associated with cognitive dysfunction and a slow progressive evolution. Two of the patients had primary amenorrhea (absence of menstruation), the third had a secondary amenorrhea (early termination of menstruation before the age of 40) and the last had ovarian dysgenesis that began at the age of 13. All four patients had normal karyotype and a non-deregulated hypothalamic-pituitary axis. In addition, a correlation between age of neurological symptoms' onset and severity of ovarian deficit has been established suggesting a common physiopathological pathway for both tissues (Fogli et al., 2003b).

An association between the severity of disease and age of disease onset have been confirmed (Fogli et al., 2004a, Labauge et al., 2009; Bonkowsky et al., 2010; Klingelhoefer et al., 2014; Alamri et al., 2016; Dooves et al., 2018).

In conclusion, among the eIF2B-related disorders or EIF2opathies (Fogli et al., 2004a) three groups emerged according to severity degree: infantile form (form 1) with early onset and symptoms manifesting before the age of 2 years and a severe evolution, childhood form with late onset between 2 and 5 years of age (form 2) and the juvenile/adult form with an age of onset beyond 5 years of age (form 3). More recently, an even larger number of subgroup of patients' evolution have been proposed (Hamilton et al 2018).

3.4 Brain MRI and VWM

Brain MRI play a significant role in EIF2B related disorders diagnosis in the suspicion of clinical manifestation in which the aberrant cerebral white matter (WM) abnormalities is apparent even at pre-symptomatic disease stages. Herein, the typical findings are cystic degeneration in the cerebral WM, which continues to be vanished (Klingelhoefer et al., 2014). MRI assessment depends on imaging by T1, T2, and fluid attenuation inversion recovery (FLAIR) sequences and it shows the localization and spread of WM abnormalities, rarefactions, lateral ventricles and subarachnoid spaces extensiveness, and the atrophies at the level of cerebrum, cerebellum and corpus callosum (Labauge et al., 2009). In addition, it

shows the spreading vacuolization that gives spongiform morphology of the rarefactions (Marjo S van der Knaap et al., 2006). Moreover, this symmetric, progressive and diffuse degeneration of WM in both cerebral hemispheres was shown to be accompanied by standard CSF consistency (Song et al., 2017). The MRI of patients of adult-onset (Figure 10) shows the spread of abnormal WM signals using T2-weighted hyperintensity and T1-weighted hypointensity relative to cortical signs. In addition, FLAIR sequences show vast hyposignal zones that highlight the cavitation aspect of this leukodystrophy. The extensive WM cavitation in infantile forms explains the Vanishing White Matter name given to this syndrome (Labauge et al., 2007).

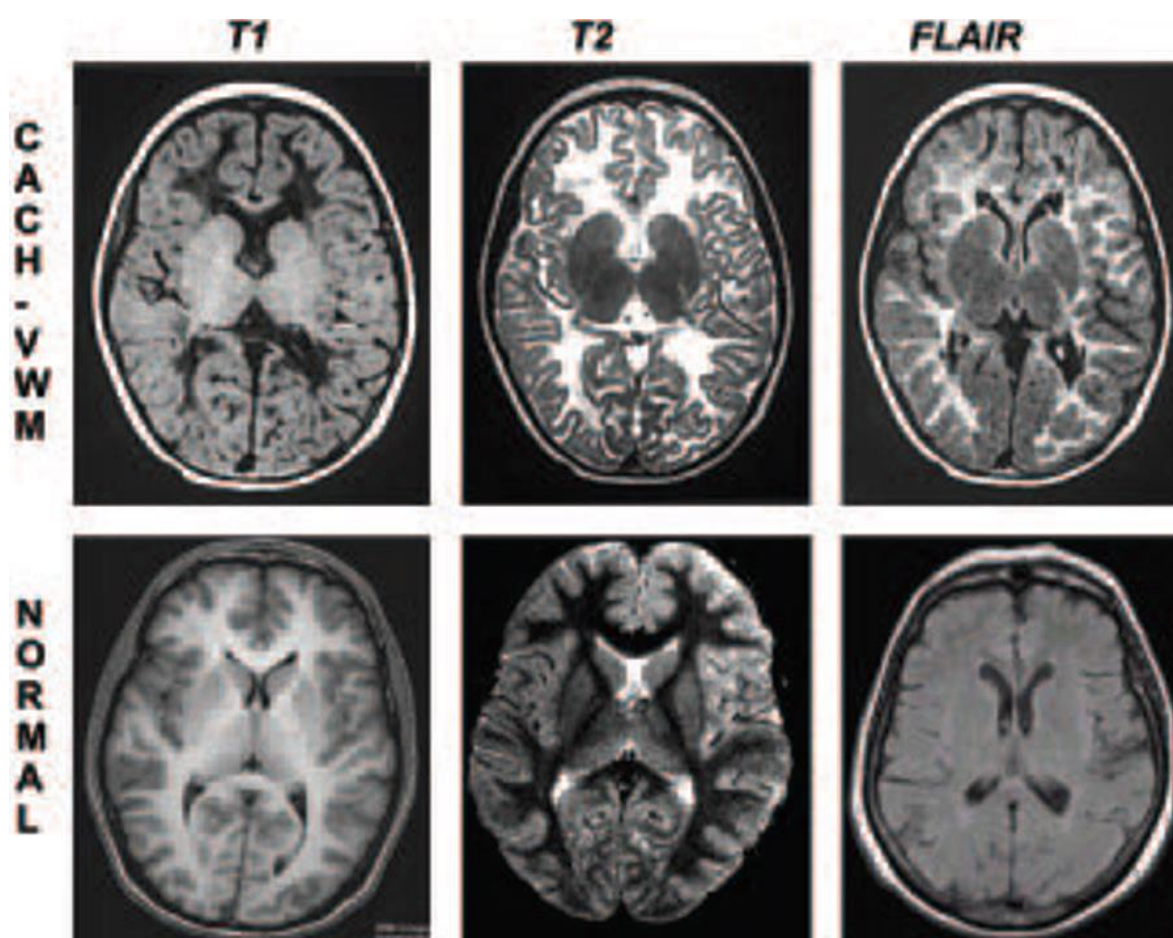


Figure 10: MRI aspects of the white matter from a CACH/ VWM patient of 5 years old in comparison to an age-matched healthy control. White matter presents a signal closed to CSF on T1- and T2- weighted images. Cavitating zones appear in the frontal white matter on FLAIR sequences (Labauge et al., 2007).

In conclusion, MRI is the good marker of EIF2B related disorders showing the symmetric, diffuse degeneration of the WM leading, in severe forms, to a CSF like aspect (vanishing). However the presence of this aspect, even in presymptomatic patients, suggests a developmental abnormal process in the white matter cohesivity more than the result of a degenerative process responsible for the neurological symptoms.

3.5 Neuropathological aspects of CACH/ VWMD

Neuropathological studies on infantile and adult forms showed the presence of orthochromatic cavitating leukodystrophy characterized by a demyelinating spongiform lesion limited only to cerebral WM, with axonal preservation and absence of microglial and macrophagic reaction indicating the absence of inflammation (Schiffmann et al., 1994; van der Knaap et al., 1997).

Another study showed an increase in the number of oligodendrocytes which had highly developed cytoplasm with lots of organelles (Rodriguez et al., 1999) (Figure 11).

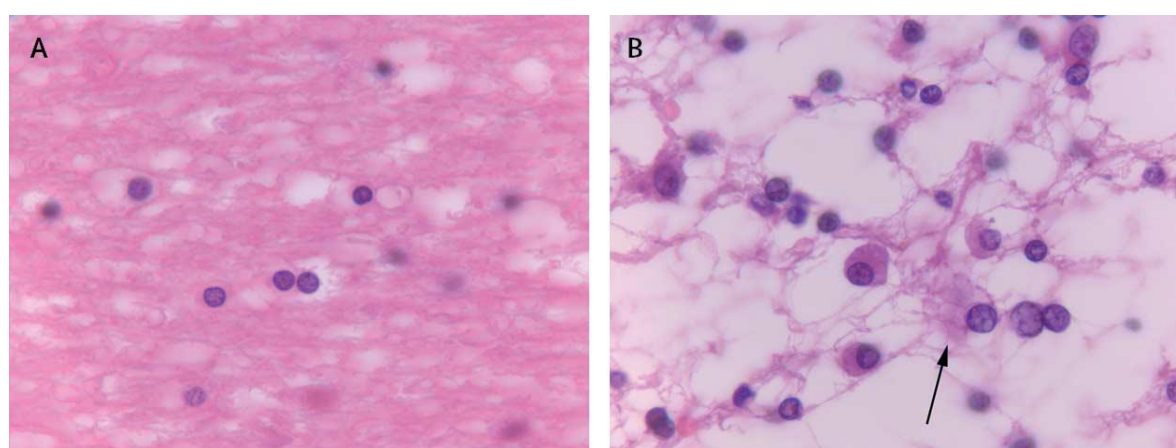


Figure 11: Light microscopic picture of oligodendrocytes. Normal oligodendrocytes (A) and oligodendrocytes in VWMD (B). The stain used is haematoxylin–eosin. Normal oligodendrocytes are small cells with little cytoplasm and uniform, round dense nuclei (A). In VWMD, oligodendrocytes usually have abundant, homogeneous or finely granular cytoplasm and the nuclei have an eccentric location. One oligodendrocyte with “foamy”, vacuolated cytoplasm is shown (B; arrow). Magnification $\times 400$ (Rodriguez et al 1999).

A study using electron microscopy showed the existence of foamy cells expressing MOG and PLP and which are considered as oligodendrocytes. This cellular accumulation was positive for sugar staining (PAS+) and related to abnormal glycoproteins. In addition a perivascular astrocytic gliosis was noticed (Wong et al., 2000).

However, analysis of the brain of a boy, with an early form, deceased at 2 years of age, revealed the loss of mature oligodendrocytes by apoptosis, followed by recruitment of PLP

expressing progenitor cells, suggesting a cellular dynamic implicated in the physiopathology of the disease (Brück et al., 2001).

Francalanci and his collaborators showed a decrease in astrocyte numbers in the affected brain areas of two 10 and 11-month-old sisters (Francalanci et al., 2001).

In addition, unfamiliar astrocyte morphology was found with abnormally long processes and no astrocyte feet (Dietrich et al., 2005).

These astrocytes were found to be immature proliferating cells with an increase of GFAP δ expression, which results from the alternative splicing of *GFAP* (Bugiani et al., 2011).

Finally, the cerebellar astrocytic subpopulation of Bergmann glia was found in this disease (human patients and mice) to translocate into the molecular layer. The more severe the disease, the more important the translocation (Dooves et al., 2016)

In conclusion, the neuropathological hallmarks of the diseases seem to be:

- **the cystic demyelinating degeneration of the white matter contrasting with an increased number of oligodendrocytes with an immature and sometimes foamy aspect.**
- **the limited astrogliosis compared to the other leukodystrophies with a dystrophic aspect of the astrocytes and aberrant localisation as observed with the bergmann glia which represented a high degree of specialized astrocytes.**

3.6 Biochemical markers

A decrease in the GEF activity of EIF2B in the eIF2B mutated cells particularly in the classical and severe forms have been demonstrated in the active dividing cells such as lymphoblastoids cells but not in the lymphocytes or fibroblasts (see cellular models). However, juvenile and adult forms of the disease as well as certain severe forms showed a

normal GEF activity (see genotype phenotype correlation). This finding suggests that the disease is not only related to a loss of enzymatic function.

Magnetic Resonance Spectroscopy (MRS) studies revealed a decrease in NAA (neuronal integrity marker), Choline (myelin membranes renewal marker) and creatine (cellular activity marker) strictly limited to WM, in addition to an increase in glucose and lactate levels (Hanefeld et al., 1993).

Analysis of phosphorus by MRS in 7 patients revealed a decrease of all high-energy phosphorylated metabolites in affected regions of the brain, suggesting an altered energetic state of the affected tissues (Blüml et al., 2003).

Vanderver and colleagues showed a decrease of the asialylated form of transferrin (asialotransferrin) in CACH/VWM patients' CSF (Vanderver et al., 2005; Vanderver et al., 2008). Fogli and colleagues who studied the glycomic profile in the CSF of eIF2B mutated patients and compared them to control patients found a global change in N-glycosylation of CSF proteins (Fogli et al., 2012). These results suggested an abnormal maturation profile of glycosylation in the CACH/VWM brains particularly in oligodendrocytes where abnormal "sugar like material" have been described.

3.7 Genotype-phenotype correlation

A correlation between age of onset and severity degree of the disease was established in a study involving 83 patients with eIF2B-pathies (Fogli et al., 2004a). The age of onset is correlated to survival and not to the mutated gene or the position of the mutation (due to inter-patients and inter-siblings phenotypic variations). This is especially the case for the juvenile/adult form, suggesting a possible role for environmental factors in the evolution and severity of the eIF2B-pathies. However, p.Arg195His mutation of the *EIF2B5* gene (described in Cree leukodystrophies) was associated with severe forms, while p.Arg113His and p.Glu213Gly mutations on *EIF2B5* and *EIF2B2* genes respectively were found in moderate adult forms or even ovarioleukodystrophies. In addition, a more recent study revealed that

patients homozygous for the p.Arg113His mutation had more moderate phenotype than patients who were compound heterozygous for the same mutation, suggesting that the combination of the p.Arg113His mutation with a more severe one allowed to moderate the phenotype with the conclusion that the clinical phenotype ins depends on both mutations and not only the more severe one (van der Lei et al., 2010).

Table 2: Overview of eIF2B Mutations, the Effects on eIF2B Structure and Activity and Disease Severity. (^a) eIF2B activity (relative to control) ↓70–90%; ↓↓50–70%; ↓↓↓<50%; ±indicates no significant difference from controls (Abbink et al., 2018).

Patient Information	
Full Name	
Date of Birth	
Gender	
Address	
City	
State	
Zip	
Phone	
Medical History	
Allergies	
Current Medications	
Past Medical History	
Family History	
Social History	
Physical Examination	
Vital Signs	
Laboratory Tests	
Imaging Studies	
Diagnosis	
Treatment Plan	
Follow-up	

4. Translation Initiation Factor and Cellular Stress Regulation

Translation is the mechanism by which proteins are made. It allows the assembly of amino acids into polypeptide chains. It is the messenger RNA (mRNA) that determines the nature and the specific order of these amino acids. The mRNA is the genetic information carrier between the DNA and the ribosome where translation takes place. Translation is optimized by adding a poly A tail to the 3'UTR extremity and a special 7-methylguanosine triphosphate residue (m^7GpppN , where N represents a nucleotide) at the 5'UTR extremity (Figure 12).

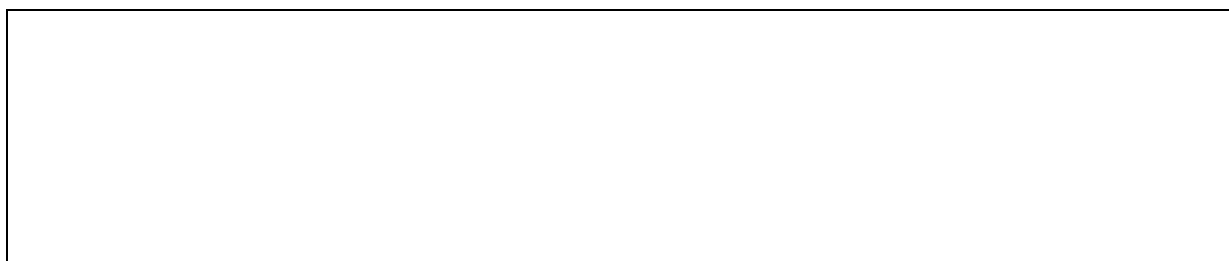


Figure 12: Elements influencing mRNA translation. m^7GpppN cap at the 5'UTR and the poly A tail $((A)_n)$ at the 3'UTR are canonical motifs allowing translation initiation. Hairpins and IRES (Internal Ribosome Entry Site) structures allow cap-independent translation. uORFs upstream (Open reading Frames) act as negative regulators for the ORFs (Open reading Frames) starting translation (Gebauer and Hentze., 2004).

4.1 Ribosomes

Eukaryotic ribosomes are formed by 2 subunits, a large 60S subunit and a smaller 40S subunit, which form the 80S ribosome. They are located in the cytoplasm or adhere to the Endoplasmic Reticulum (ER) membranes. A (aminoacyl), P (peptidyl) and E (exit) sites are 3 of the many important functional sites of a ribosome, which in turn is formed by 80 proteins and 4 RNAs. These ribosomal RNAs are in charge of most of the ribosomal functions, while ribosomal proteins are mainly in charge of subunit assembly (Schmeing and Ramakrishnan., 2009; Hoerter and Ellis., 2019).

There exists another type of ribosomes in the mitochondria with origins tracing back to bacteria and which synthesize certain proteins which are distinct from those in the cytoplasm (Hoerter and Ellis., 2019).

Interestingly, a mRNA can be translated by more than one ribosome, thus forming polysome complexes.

4.2 Steps of translation

Translation is a process consisting of three phases, namely initiation, elongation and termination. Each phase can be regulated and the differential regulation of translation plays an important role in the development, growth and cell proliferation.

4.2.1 Translation initiation

Eukaryotic translation initiation proceeds according to 2 distinct classes of main mechanisms: the cap-dependent initiation, where ribosomes scan mRNA starting from the 5' cap until recognizing the start codon AUG, and the alternative cap-independent mechanisms involving the recruitment of mRNA directly inside the ribosome at the IRES or the shunt process.

4.2.1.1 Cap-dependent translation initiation

The cap-dependent eukaryotic translation initiation (Figure 13) is a process involving many regulating factors called eukaryotic initiation factors (eIF).

It begins with the activation of the eukaryotic initiation factor eIF2 from its inactive eIF2-GDP form into its active eIF2-GTP form by eIF2b and its GEF (Guanine nucleotide Exchange Factor) activity. Met-tRNA is then recruited to the eIF2-GTP to form the ternary complex (TC) eIF2-GTP-Met-tRNA.

TC is recruited to the ribosomal subunit 40S-eIF1-eIF1A-eIF3 complex to form the 43S complex also known as the preinitiation complex (PIC). EIF3 helps stabilize this complex and keeps the 40S and 60S subunits from interacting again and forming the inactive 80S ribosome.

In parallel, mRNA is activated by interacting with eIF4E which recognizes the m⁷G cap, eIF4G which is a scaffold protein helps boost eIF4E affinity for the cap, eIF4A which is a RNA helicase helping with mRNA recognition and eIF4B which also recognizes mRNA. In addition, the poly-A binding protein (PABP) binds the 3'UTR poly-A tail while at the same time interacting with eIF4G (which bound the 5'UTR cap) to circularize the mRNA in a closed-loop model.

The 43S PIC and the activated mRNA complex interact together forming the 48S complex, where the first recognizes the 5'UTR cap and starts scanning the mRNA until detecting the AUG start codon. The scanning step is ATP-dependent and controlled by eIF1 and eIF1A both of which oversee the progression of the ribosome.

EIF5 hydrolyzes GTP causing the TC to dissociate and eIF2-GTP to revert back to its inactive eIF2-GDP form and separating from the complex. Then the 60S ribosomal subunit is recruited with help of eIFB5 which promotes 60S and 40S assembly to form the 80S ribosome.

EIF2 is recycled and the elongation step starts.

(Merrick and Pavitt., 2018; Shirokikh and Preiss,. 2018; Hinnebusch and Lorsch., 2012)

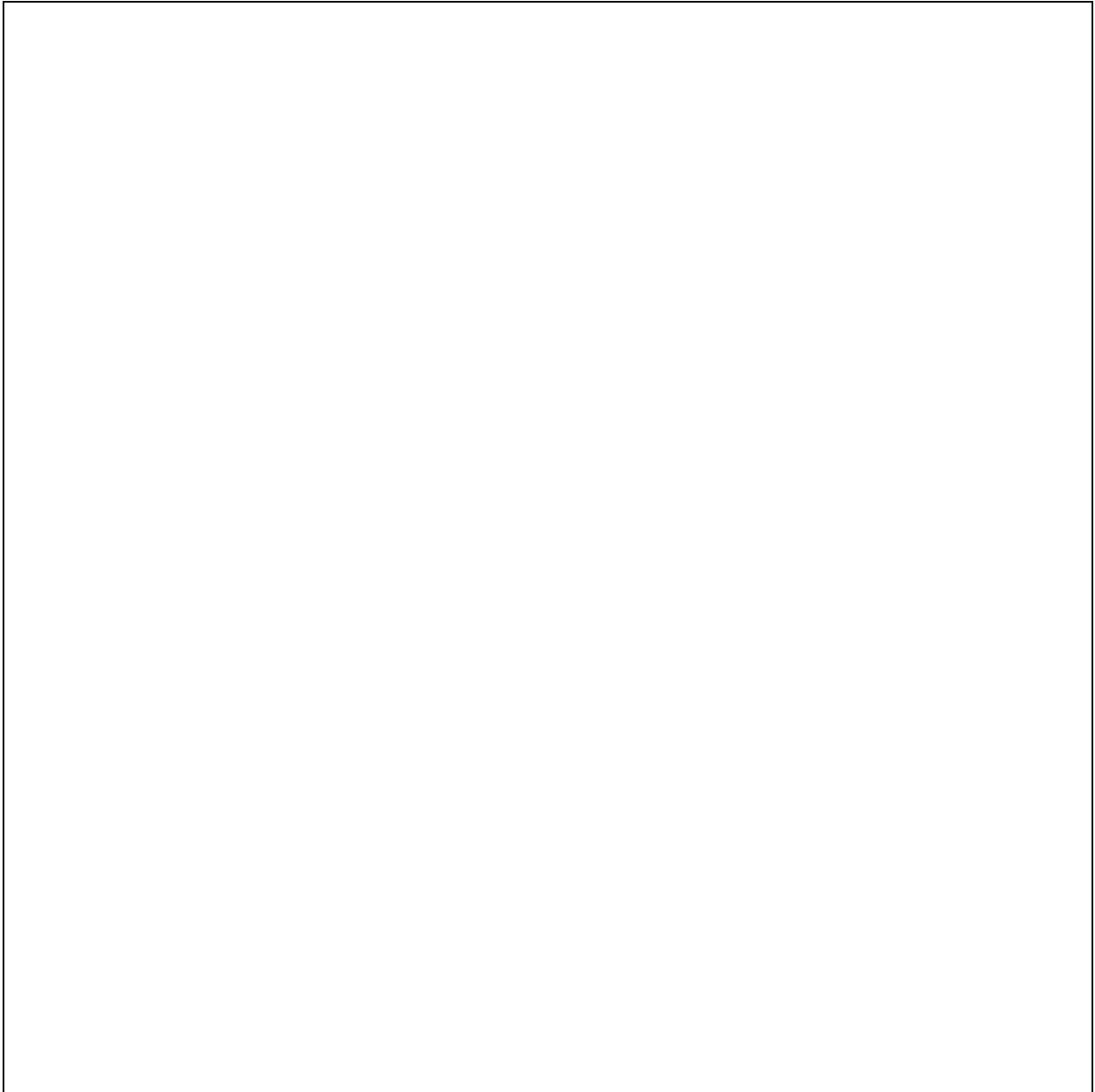


Figure 13: Overview of the general eukaryotic translation initiation pathway. The pathway for recruiting initiator transfer RNA (tRNA) to the messenger RNA (mRNA) AUG codon in the context of an 80S ribosome (bottom right) is depicted as a series of major steps, labeled with blue text, linked with black arrows. Individual eukaryotic initiation factor (eIF) cartoons and complexes are labeled with black text and nucleotide hydrolysis/inorganic phosphate release reactions are shown by blue arrows. The broad green arrow indicates the direction of scanning toward the AUG codon. The regulatory reactions leading to eIF2 and eIF4E inhibition are shown with plum and red arrows. The timing of release of some factors from initiating ribosomes/mRNA (eIF4F, eIF4B, or eIF3) is not yet clear, so this is not shown (Merrick and Pavitt., 2018).

4.2.1.2 Alternative cap-independent translation initiation

The cap-dependent translation initiation is considered as the most prominent mechanism, however it does not explain the fact that some proteins can still be translated even under conditions where it is impaired.

There exist alternative mechanisms that do not involve eIF4 such as IRES and Shunt mechanisms.

Some mRNAs present internal ribosomes entry sites (IRES), a GC rich region, at their 5'UTR end. IRES allow cap-independent 40S ribosomal subunit recruitment near the AUG start codon using the initiation machinery except for the eIF4E. Specific cellular proteins such as IRES Trans Acting Factors (ITAF) are necessary (Figure 14).

This mechanism allows bypassing the global translation inhibition following stress conditions such as ER stress or viral infections allowing stress regulation.

Another alternative is the shunt mechanism that is like a hybrid of the cap-dependent scanning and the IRES mechanisms. The PIC is formed at the cap by intermediary of eIF3d which is an eIF4E inhibitory and then scanning begins until reaching specific regions that allow its transfer forward towards the start codon while bypassing some stable RNA structures that could not be unfolded during scanning (Figure 14).

(James and Smyth., 2018; Merrick and Pavitt., 2018; Lacerda et al., 2016).

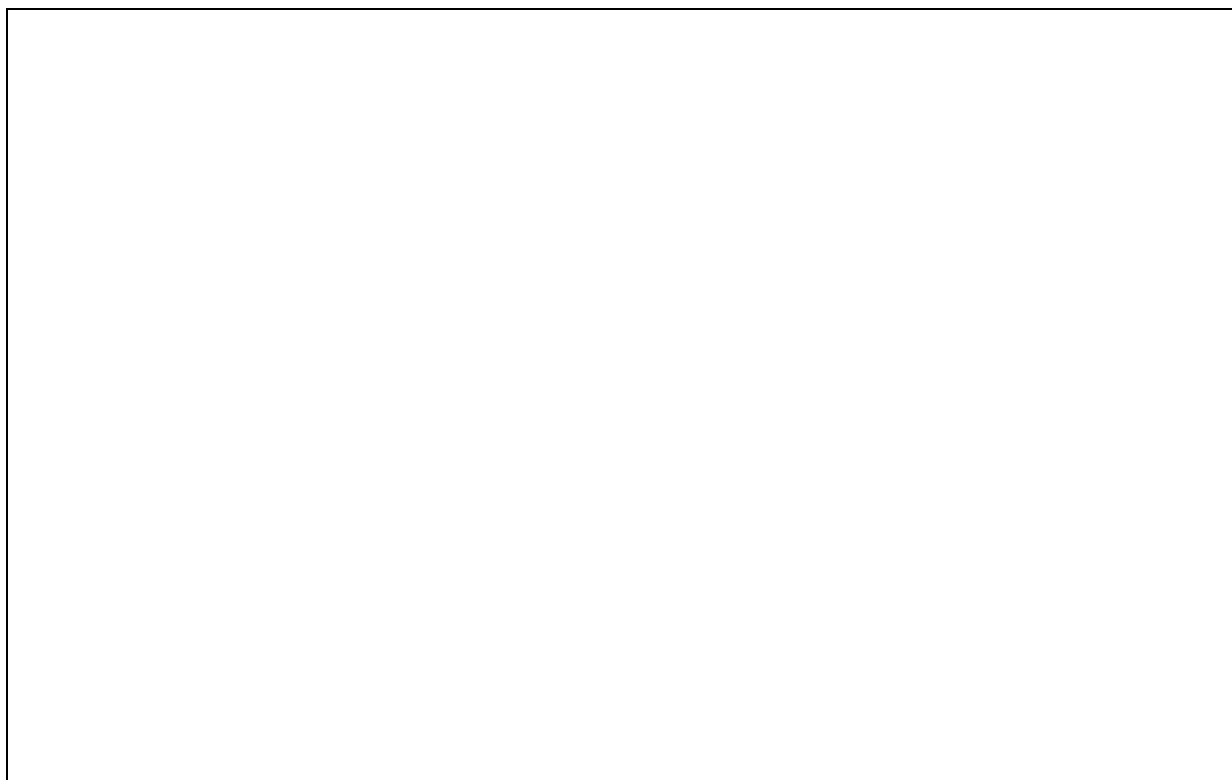


Figure 14: Alternative mechanisms of translation initiation. A) Highly structured mRNA elements, in many cases with the assistance of IRES trans acting factors (ITAF) recruit ribosomes to specific start codons in viral mRNAs, allowing cap-independent translation initiation. The requirement for mRNA structure, ITAFs, and other factors in eukaryotic IRES remains a subject of research. B) A subset of mRNAs are bound by the d subunit of the eIF3 complex. eIF3d cap recognition directs translation initiation allowing cap-dependent translation independent of eIF4E, the canonical cap recognition protein (adapted from James and Smyth., 2018).

4.2.2 Translation elongation

At the end of the initiation phase, the correctly formed 80S-Met-tRNA complex is ready to undergo the elongation phase by the sequential addition of amino acids according to correct reading of mRNA (Figure 15).

The elongation involves several specific proteins called eukaryotic elongation factors (eEF). eEF1A interacts with aminoacyl-tRNA and GTP to form ternary complexes which bind to the ribosome's A site through codon-anticodon recognition, at which point GTP is hydrolyzed

and eEF1A unbound. Then, peptide bonds are formed between the COO^- end of an amino acid and the NH_3^+ end of the following one, catalyzed by a peptidyl-transferase enzyme of the 60S ribosomal subunit. Finally, the peptidyl-tRNA moves from the A to the P site of the ribosome using the eEF2 protein and GTP, which leaves the A site available for the next elongation cycle (Simonovic and Steitz., 2009; Hoerter JE, Ellis SR. Biochemistry, Protein Synthesis. [Updated 2019 Aug 13]. In: StatPearls [Internet]. Treasure Island (FL): StatPearls Publishing; 2019 Jan-. Available from: <https://www.ncbi-nlm-nih-gov.gate2.inist.fr/books/NBK545161/>).

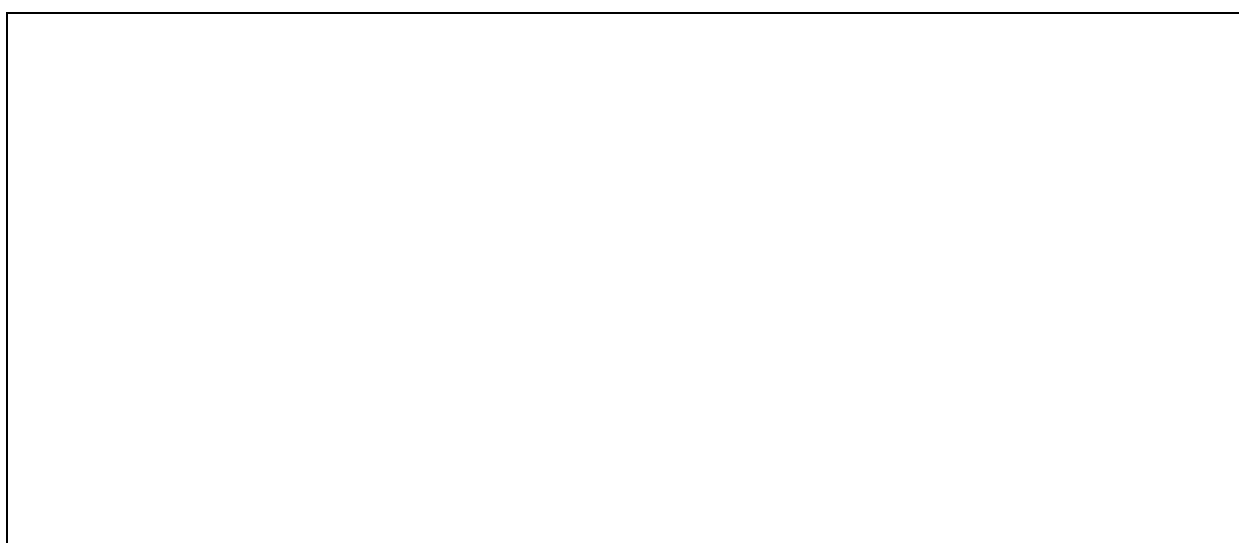


Figure 15: A schematic diagram of the elongation phase of the ribosome-catalyzed translation (Simonovic and Steitz., 2009).

4.2.3 Translation termination

After the polypeptide chain formation and the peptidyl-tRNA translocation to the P site, special proteins called eukaryotic release factors (eRF) go into action. eRF1 located at the A site recognizes stop codons (UAA, UAG or UGA) on the mRNA. Then it interacts with eRF3-GTP to cleave the peptidyl-tRNA and release the completed protein chain. The protein then undergoes conformational changes to reach its final form.

Finally, ribosomal subunits dissociate and can join another translation cycle (Hoerter and Ellis., 2019).

4.3 Role of eIF2B in Translation Initiation

EIF2B plays a critical role in translation initiation. Mainly, it activates eIF2 by its GEF activity through which GDP is exchanged by GTP.

4.3.1 EIF2B, activator of eIF2

As previously mentioned, eIF2B promotes the formation of ternary complex (eIF2-GTP-Met-tRNA) via its GEF activity and its interaction with eIF2. This latter is formed by 3 subunits (α , β , and γ). eIF2 α is phosphorylated at the Ser⁵¹ position and β has several phosphorylation sites, while eIF2 γ is a GTPase and has a role in the interaction with the Met-tRNA (Bogorad et al., 2018).

Originally, eIF2 is present as eIF2-GDP and needs to be converted, at the end of each cycle, into eIF2-GTP in order for the translation initiation to begin. This is due to the low affinity of eIF2-GDP to Met-tRNA which prevents their binding (Abbink et al., 2019; Bogorad et al., 2018). At the end of translation initiation, eIF2-GDP is released from the ribosome. eIF2 has a high affinity for GDP which leads to a slow dissociation of GDP from eIF2. This being the case, an external factor (eIF2B) is required to catalyze this process and allow the exchange of GDP by GTP in order to reform the active complex eIF2-GTP needed for the initiation (Abbink et al., 2019).

Another additional role for eIF2B has been shown in yeast. This role is that of dissociating eIF2 from eIF5. The latter usually prevents the dissociation of GDP from eIF2 playing a GDP-dissociation inhibitor (GDI) role in addition to being a GTPase activator protein (GAP) for the

eIF2-GTP complex, so eIF2B acting to dissociate eIF2 from eIF5 means that it is a GDI-dissociation factor (GDF) (Abbink et al., 2019; Wortham and Proud., 2015). (Figure 16)

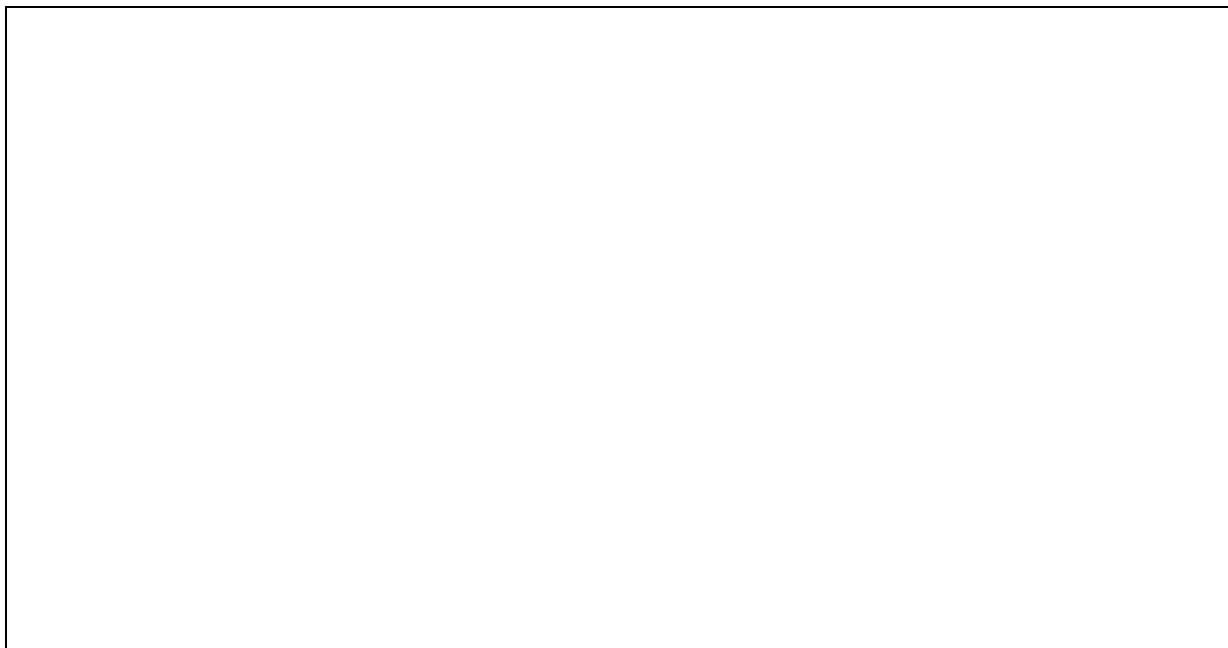


Figure 16: Role of eIF2B. eIF2B helps dissociate GDP from eIF2, which allows GTP binding and forming the active eIF2-GTP complex. This figure also illustrates the function of eIF2, to recruit – in its GTP-bound form – the initiator Met-tRNA to the 40S ribosomal subunit and the dual role of eIF5 as a GAP for eIF2-bound GTP and a GDI for the resulting eIF2-GDP complex. Red and green indicate, respectively, the inactive and active forms of eIF2 (Abbink et al., 2018).

4.3.2 Structure and functional domains of eIF2B

eIF2B is a decamer (dimer of pentamers) protein complex of 600 KDa, composed of 5 types of different subunits (α , β , γ , δ and ϵ) which are relatively conserved between humans and several other species (table 3). These subunits eIF2B α , eIF2B β , eIF2B γ , eIF2B δ and eIF2B ϵ are encoded by the genes *EIF2B1* (12q24), *EIF2B2* (14q24), *EIF2B3* (1p36.23), *EIF2B4* (2p23) and *EIF2B5* (3q27) respectively (Bogorad et al., 2018; Pavitt., 2018). In yeast, losing any of the eIF2B β , eIF2B γ , eIF2B δ or eIF2B ϵ subunits leads to death which indicates that losing eIF2B is lethal (Abbink et al., 2018).

Gene	EIF2B1	EIF2B2	EIF2B3	EIF2B4	EIF2B5
NCBI N° for RNA	NM001414	NM014239	NM020365	NM015636	NM003907
Number of exons	9	8	11	13	16
Corresponding protein subunit	eIF2B α	eIF2B β	eIF2B γ	eIF2B δ	eIF2B ϵ
NCBI N° for protein subunit	NP001405	NP055054	NP065098	NP751945	NP003898
Subunit length (in number of aa)	305	351	452	522	721
Human protein homology with: <i>Mus musculus</i>	86%	94%	89%	79%	83%
<i>Rattus norvegicus</i>	85%	92%	88%	79%	83%
<i>Drosophila melanogaster</i>	46%	48%	34%	48%	29%
<i>Saccharomyces cerevisiae</i>	39%	32%	22%	36%	28%

Table 3 : Data on the five human EIF2B genes: protein correspondence and inter-species sequence homology

The structure has regulatory and catalytic domains (Figure 17). The regulatory domain is the core composed of eIF2B α , β and δ where a $\beta\delta$ tetramer links with an α dimer to form 2 heterotrimers, each having the capacity to link eIF2 α . This regulatory core is widely linked to binding eIF2 α which is improved by Ser⁵¹ phosphorylation (Pavitt., 2018).

The catalytic domain consists of eIF2B γ and eIF2B ϵ . These two subunits bind together to form an arm-like structure, and two of such structures bind to the core regulatory domain. These arms are the main actors of the GEF and GDF activities of eIF2B by interacting with eIF2 $\beta\gamma$ (Figure 18).

It is the sequence homology between the different subunits that made it possible for the regulatory and the catalytic domains to form. Each of these two domains can bind to eIF2 with the catalytic domain being the only one possessing GEF activity.

This GEF activity is mainly realized by the largest subunit which is eIF2B ϵ , the latter being indispensable for the role while also being capable of that role on its own but is enhanced by the formation of the complex (Pavitt., 2018).



Figure 17: Layout of individual eIF2B subunits (domains) and the catalytic and regulatory subcomplexes of eIF2B. Homologous regions are shown in matching colours, and are labelled to show the nucleotidyltransferase and acyltransferase regions of eIF2B γ and eIF2B ϵ . The latter contain the so-called I-patch repeats. The catalytic (GEF) domain of eIF2B ϵ is shown, as are the mutually homologous C-terminal regions of eIF2B α , β and δ . eIF2B γ and eIF2B ϵ together form the catalytic subcomplex, which displays some GEF activity; full activity of mammalian eIF2B requires all five types of subunit. The other three subunits form the regulatory subcomplex (Abbink et al., 2018).

Studies in yeast showed that the C-terminal end of the eIF2B ϵ is the region responsible for the GEF activity and for binding eIF2 (Gomez et al., 2002) and that missense mutations in this region decrease GEF activity (Gomez and Pavitt, 2000). In addition, deletions at this region prevent the stable interaction between eIF2 and eIF2B and the GEF activity (Gomez et al., 2002). This region also presents a glutamate residue at the 569 position (human E577) (Pavitt 2018).

The N-terminal end of the eIF2B ϵ subunit is essential in the interaction with the other subunits and the subsequent activity since missense mutations in this region affect GEF activity but not the binding of eIF2 (Gomez et Pavitt, 2000).



Figure 18: The structure of eIF2B. (a) "Top view" of the eIF2B decamer from Schizosaccharomyces pombe (PDB file 5B04) (Kashiwagi et al., 2016) showing one half of the regulatory core and catalytic arm 1 as both transparent surface and secondary structure elements (SSE) and catalytic arm 2 as SSE only. One copy of the independent 2Bε^{GEF} domain from Saccharomyces cerevisiae (PDB file 1PAQ) (Boesen, Mohammad, Pavitt, & Andersen, 2004) is also shown with SSE and transparent surface. Residues discussed in the text are highlighted. (b) Rotated views of eIF2B decamer as in panel (a), with one half in SSE only view. "Front" view (left) showing the (2Bβδ)₂ core and "back" view (right) showing the 2Bα dimer. (c) Cartoons showing intersubunit interactions as lines connecting circles representing each subunit within the decamer (top) and eIF2 interaction regions (bottom) (Pavitt., 2018)

4.4 Regulation of translation initiation in response to Stress

eIF2B is a limiting factor in translation and is subjected to different regulation processes, especially under stress conditions. Hormones and growth factors promote translation while stress conditions such as amino acid deprivation, viral infection or ER stress inhibit global protein synthesis. These stress conditions induce an adaptive response called Integrated Stress Response (ISR), which allows the expression of certain genes and the activation of

specific pathways affecting the fate of the cell, and the global protein synthesis inhibition prevents the formation of defective proteins while at the same time promoting the expression of genes involved in cell survival.

4.4.1 Direct regulation of eIF2B

4.4.1.1 Allosteric regulation

NAD^+ and NADP^+ inhibit eIF2B activity in rats while NADH and NADPH promote it, the latter binding to eIF2B and being necessary to its function (Price and Proud, 1994). Another study in rats showed a decrease in eIF2B activity in skeletal muscles but not in the heart of diabetic rats when the $\text{NADPH}/\text{NADP}^+$ ratio increased only in the heart, thus showing that NADPH prevents eIF2B inhibition (Karin et al., 1993).

An ATP-binding site was found on eIF2B sequence, which had an inhibiting effect on its activity (Kimball et Jefferson, 1995).

Other studies revealed a role for polyamines and some other molecules such as glucose-6-phosphate, fructose-6-phosphate and fructose 1,6-bisphosphate in the activation of eIF2B in cell lysates (Price et Proud, 1994).

GTP also plays a role in promoting eIF2B activity. The GEF activity is energy dependent and a low GTP/GDP ratio inhibits regeneration of ternary complex and translation.

4.4.1.2 Regulation by phosphorylation

eIF2B presents several phosphorylation sites and can be directly phosphorylated in all subunits especially at the eIF2B ϵ subunit which is the only one affecting the GEF activity when phosphorylated (Wortham and Proud, 2015).

Several kinases act directly on eIF2B such as CK1, CK2 (Casein Kinase 1 and 2), DYRK (Dual-specificity tyrosine-phosphorylation-Regulated Kinase) and GSK3 (Glycogen Synthase Kinase 3).

CK1 and CK2 phosphorylate eIF2B ϵ and help increase its GEF activity. CK2 targets Ser⁷¹² and Ser⁷¹³ which are located at the C-terminal end of eIF2B ϵ thus allowing a 5-fold stronger eIF2B activation (Price and Proud, 1994). Mutations at these phosphorylation sites decrease eIF2B ϵ

affinity for eIF2 showing an important role for CK2 in the interaction between eIF2B and eIF2. CK1 phosphorylate Ser⁴⁶⁴ with no known consequences on the interaction between eIF2B and eIF2 (Wang et al., 2001).

DYRK phosphorylates Ser⁵³⁹ thus allowing the phosphorylation of Ser⁵³⁵ by GSK. The latter acts under insulin deficiency conditions and inhibits eIF2B GEF activity (Wortham and Proud, 2015).

4.4.1.3 Role of heat shock proteins (HSP)

A study on rats showed the aggregation of eIF2B complexes from rat hepatic complexes following exposure to moderate temperatures (<44°C). The results proposed two mechanisms for eIF2B inactivation, one being a direct inactivation by heat (denaturation) and the other being the aggregation with thermoprotective molecules, which might prevent eIF2B denaturation, suggesting a role for Heat Shock Proteins (HSP) in eIF2B activity (Scheper et al., 1998). HSP synthesis is promoted by several stress conditions such as heat shocks, hormones, growth factors, infections or oxygen deprivation and act as chaperons while also having protective and anti-apoptotic characteristics.

4.4.2 Regulation by eIF2 α phosphorylation in response to stress

A widely studied mechanism for eIF2B activity regulation is the eIF2 α subunit phosphorylation at Ser⁵¹ under stress conditions (Figure 19).

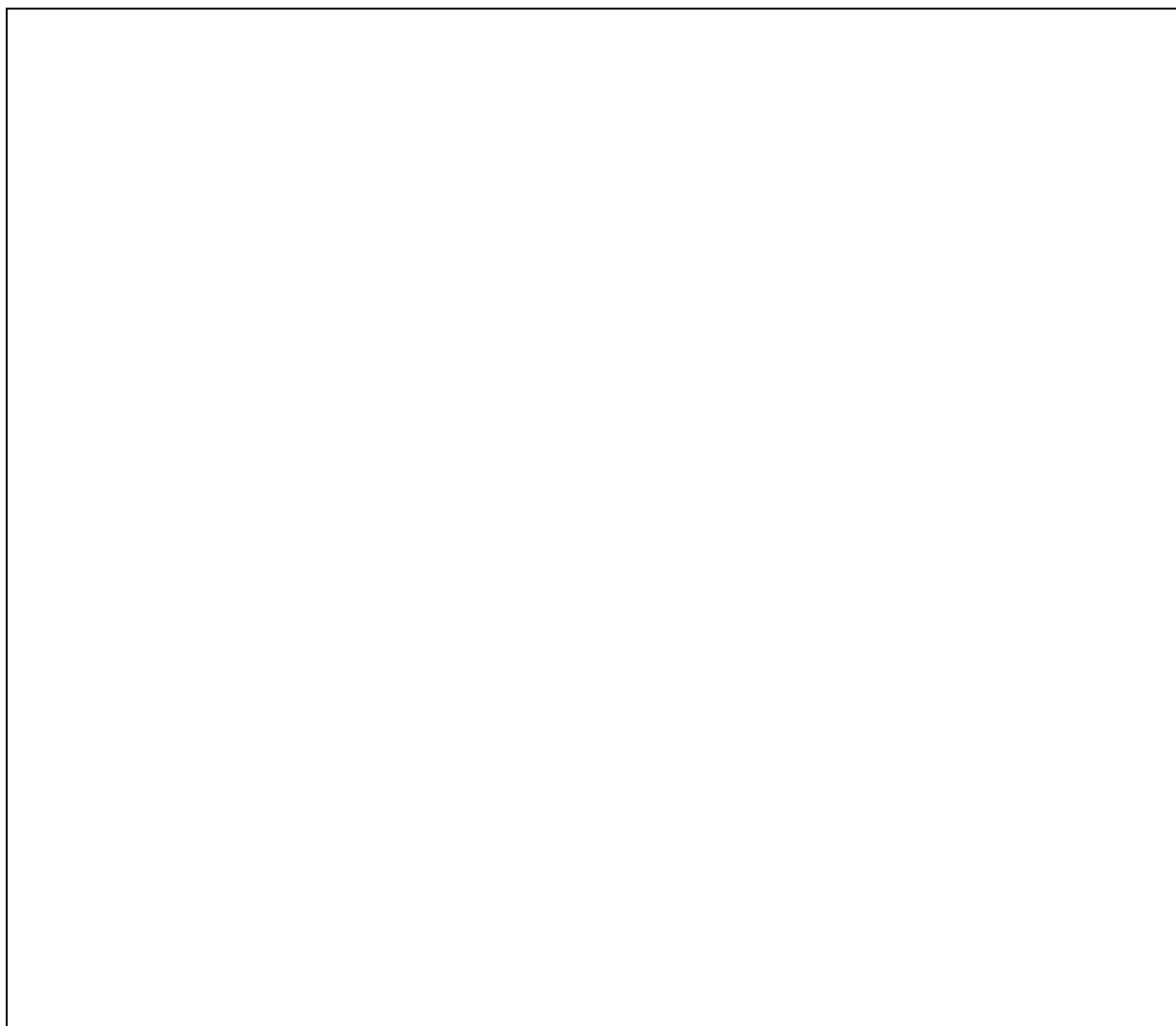


Figure 19: Mechanism of eIF2B inhibition by means of eIF2 phosphorylation. “(A) Close-up view of the interface for eIF2 α in the eIF2•eIF2B complex. Ser⁵¹ of eIF2 α and Glu¹³⁹ of eIF2B β are shown in stick models. The residues with mutations that partially mimic eIF2 α phosphorylation in *S. cerevisiae* eIF2B are shown as purple sticks. (B) The structures of the eIF2•eIF2B and eIF2(α P)•eIF2B complexes are superimposed so that the two α subunits of eIF2 are bound on the opposite sides of the central cavity of eIF2B. eIF2(α P) is shown in gray. (C) Close-up view of the interface between eIF2 γ and eIF2B ϵ -HEAT of the eIF2•eIF2B complex in the superimposed model. eIF2 γ of the eIF2(α P)•eIF2B complex clashes with eIF2B ϵ -HEAT and slightly with eIF2 γ of the eIF2•eIF2B complex. (D and E) Proposed mechanism of eIF2B inhibition by eIF2 phosphorylation. (D) The unphosphorylated eIF2 can bind to eIF2B in the productive or nonproductive mode and then shifts toward the more stable productive mode. A GDP molecule (cyan dot) bound to eIF2 γ dissociates in this productive mode. GTP (red dot) binds, and then Met-tRNA_i binding induces the dissociation from eIF2B as eIF2-TC. (E) The mode of eIF2(α P) binding to eIF2B is limited to the nonproductive mode because of the repulsion at the productive interface for eIF2 α , and nucleotide exchange is inhibited in this binding mode. The bound eIF2(α P) molecule also blocks the productive binding of eIF2 on the opposite side of eIF2B (Kashiwagi et al., 2019)”.

Following stress signals, the subsequent pathways known as Integrative stress response (ISR) are activated comprising four kinases as regulators, namely GCN2 (general control nonderepressible 2), PKR (protein kinase RNA activated), PERK (PKR-like endoplasmic reticulum kinase) and HRI (heme-regulated inhibitor kinase). Each of these kinases activation results from a different type of stress: amino acid deprivation, viral infection, ER stress and heme deprivation respectively (Wortham and Proud., 2015; Pakos-Zebrucka et al., 2016; Pavitt 2018) (Figure 20).

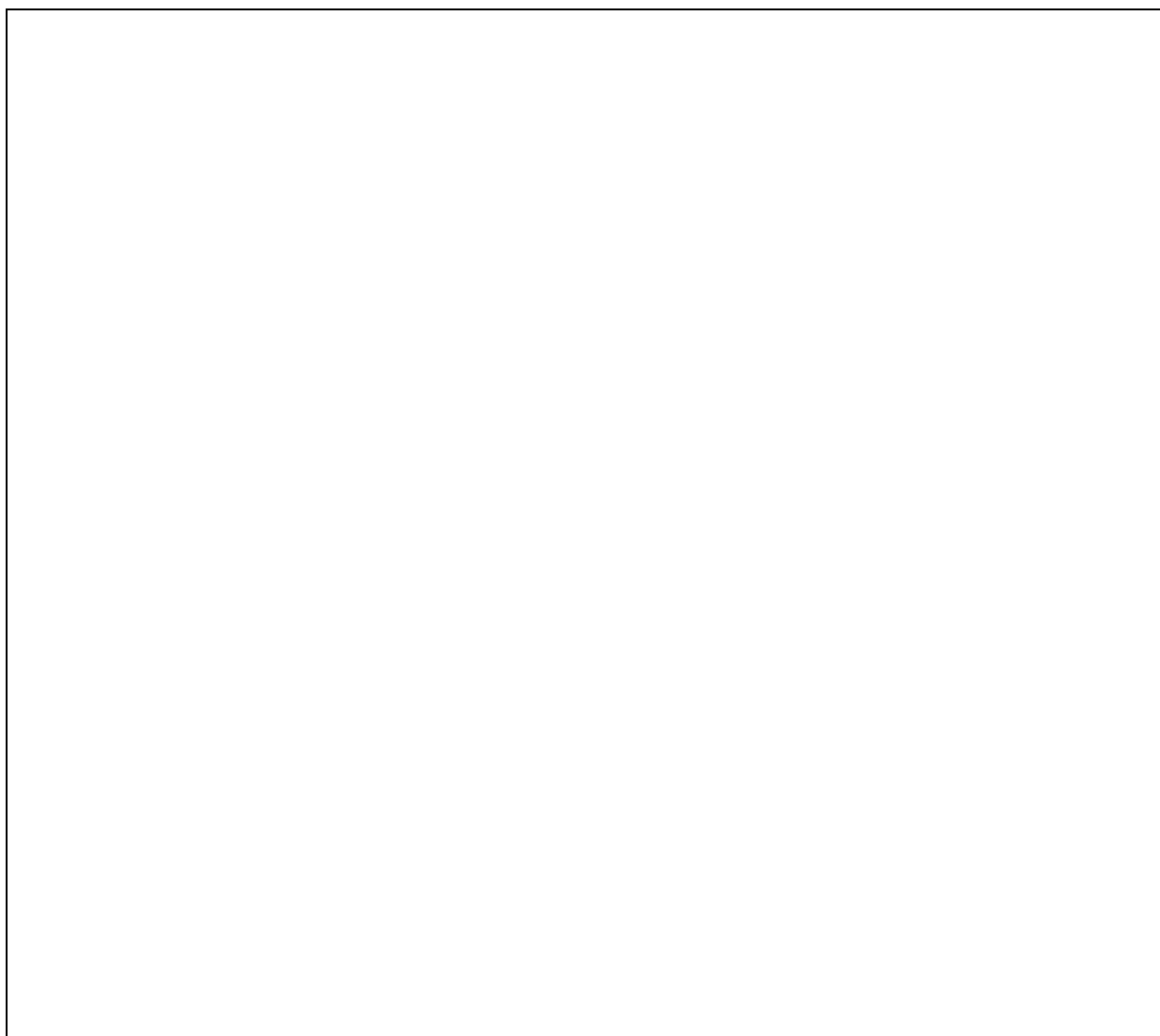


Figure 20: Integrated stress response signaling. “ER stress, viral infection, and other cellular stress signals activate PERK, PKR, HRI, and GCN2 kinases that converge on phosphorylation of eIF2 α , the core of ISR. This leads to global attenuation of Cap-dependent translation while concomitantly initiates the preferential translation of ISR-specific mRNAs, such as ATF4. ATF4

is the main effector of the ISR. It forms homo- and heterodimers that bind to DNA targets to control the expression of genes involved in cellular adaptation. Termination of the ISR is regulated by the constitutively expressed CREP and stress-inducible phosphatase GADD34 that dephosphorylate eIF2 α . Arrows denote activation or induction, while blunt lines indicate inhibition” (Pakos-Zebrucka et al., 2016).

This response to stress leads to the transcription of certain specific genes responsible for reestablishing normal physiological conditions of the cell or its apoptosis. One such gene is ATF4 (Activating Transcription Factor 4) whose expression is promoted by stress factors that lead to the phosphorylation of eIF2 α . Its 5' UTR has 2 uORF (upstream Open Reading Frame), one of which overlaps with the major ORF thus inhibiting the translation of ATF4. Under normal conditions, ternary complex is abundant, translation starts at uORF2 and ATF4, whose major ORF hasn't been read by the ribosome, is not translated. However, when under stress conditions, ternary complex is restricted, the ribosome scans through uORF2 and begins translation at the ATF4 major ORF leading to the translation of ATF4 (Figure 21) (Young and Wek., 2016).



Figure 21: Depiction of the ATF4 mechanism of preferential translation (Young and Wek., 2016).

In addition to ATF4, there are other genes that are preferentially expressed under stress conditions. Some help alleviate stress effects by promoting transcription of certain factors (ATF4, C/EBP α , and C/EBP β), while others promote apoptosis when the stress is too great (CHOP and ATF5). Feedback control and dephosphorylation is dependent on the GADD34 gene, and SLC35A4, CAT1, as well and the glutamyl-prolyl tRNA synthetase EPRS help

prepare the cell to resume global protein synthesis. Finally, IBTK α is a fate regulator for the cell (Young and Wek., 2016) (Figure 22).

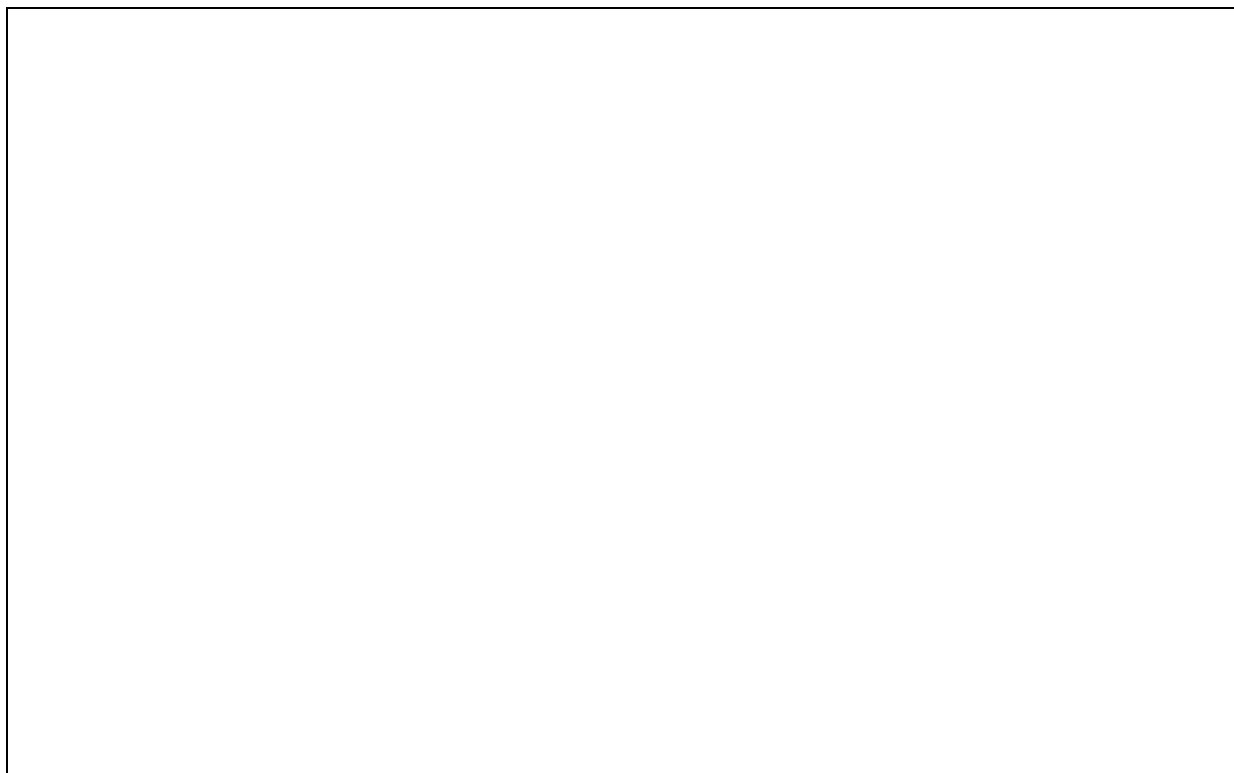


Figure 22: Depiction of the preferentially translated mRNAs and their function in stress remediation (Young and Wek., 2016).

4.4.3 ER stress and UPR

Proteins destined to be secreted and transmembrane ones are formed and folded in the endoplasmic reticulum (ER) which is also necessary to other processes such as synthesis of certain molecules (like cholesterol). This role of the ER is very energy-demanding and its disruption slows its folding activity causing stress to the cell and may cause the accumulation of unfolded proteins leading to cell death in some cases.

To cope with the effects of ER stress, new proteins are sometimes needed and their synthesis is thus activated while lowering global protein synthesis levels. This is known as the unfolded protein response (UPR). Another method consists of the autophagy of the unfolded proteins.

Three proteins act as sensors for the UPR and engage specific downstream pathways to reestablish homeostasis or cause apoptosis. Inositol-requiring enzyme 1 (IRE1) is an RNase which is also responsible for promoting the transcription of the X box-binding protein 1 (XBP1) transcription factor involved in restoring ER folding capacity and cell survival. Another sensor is the protein kinase RNA-like endoplasmic reticulum kinase (PERK), which is part of the ISR with its downstream pathways involving ATF4 and which also promotes the transcription of Nuclear factor erythroid 2-related factor 2 (NRF2) responsible for regulating antioxidant protein synthesis. The third sensor protein is the activating transcription factor 6 (ATF6) which, under stress conditions, is translocated to the Golgi and cleaved to become a transcription factor acting on chaperons or even inducing CHOP and XBP1 (Figure 23) (Lurlaro and Munoz-Pinedo., 2016).

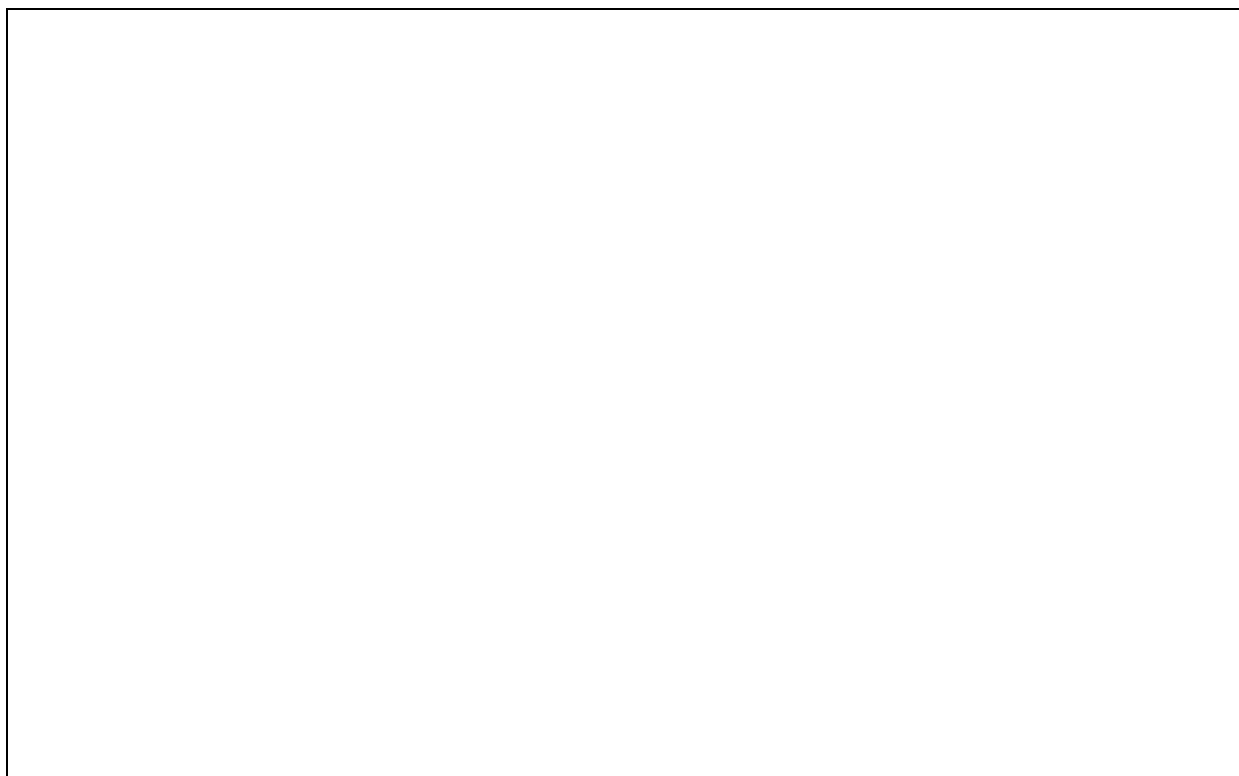


Figure 23: “The unfolded protein response. The three main sensors of the UPR are PERK, IRE1 and ATF6. PERK phosphorylates eIF2α attenuating mRNA translation, but it specifically induces the transcription factors ATF4 and CHOP, which will regulate the expression of genes involved in the restoration of the homeostasis and GADD34, an inhibitor of eIF2α, attenuating the response. PERK phosphorylates and also activates the transcription factor NRF2, which induces antioxidant responses. This eIF2α/ATF4/CHOP response is also known as the integrated stress response and other stimuli, such as nutrient deprivation, can engage it through activation of other kinases. IRE1 is a kinase and an endonuclease that regulates the

splicing of the transcription factor XBP1, resulting in the transcription of genes involved in restoring the ER folding capacity. ATF6 is translocated into the Golgi where it is cleaved to release the transcription factor that regulates chaperones expression and ER-associated degradation genes". (Lurlaro and Munoz-Pinedo., 2016)

5. EIF2B mutants Models

5.1 The Yeast model

One of the models used to study CACH/VWM was a yeast model.

Going from the fact that yeast represents a very good tool to studying eif2b function, structure and regulation in stress response, and the fact that a large number of mutations have previously been studied in yeast, Graham D. Pavitt's lab wanted to assess the effects that human mutations responsible for CACH/VWM equivalents would have on yeast growth ability and its capacity to cope with cellular stresses that usually alter the function of eif2b.

In their model they show the viability of their created yeast strains which led them to the conclusion that these "human mutations induced in yeast" were not severe enough to induce lethality, suggesting a partial subsistence of eif2b functions.

Despite the fact that all strains were viable, they all did not have the same effects. While most mutations caused deregulation in gene specific translational control and their downstream cascades when subjected to amino acid starvation, only eIF2B-alpha and eIF2B-epsilon mutations caused a decrease in protein levels (Richardson et al, 2004).

When taking the yeast model a little further, De Almeida et al introduced human vectors to yeast strain with a deletion for the corresponding vectors and showed that these vectors incorporate and complement the function of the mutated yeast even when going as far as using triple yeast eif2 gene deletion strains (De Almeida et al, 2013).

5.2 Mouse Models

5.2.1 The G2723A mutation KI mouse model

This mouse model was generated by inducing a missense mutation that replaces guanine by adenine at the 2723 position. This mutation resulted in changing the arginine to histidine at the 132 position on the protein level, which corresponds with the human R136H (Geva et al., 2010). The R136H mutation is related to the classical form of CACH/VWM disease (Kantor et al., 2005).

This resulted in a viable and fertile homozygous mouse for the R132H mutation.

The early assessments of this mouse didn't show any significant difference in Eif2b5 protein level in the cerebrum or cerebellum of the mutant mouse while a 23% decrease of the enzymatic activity of eif2b was detected in the cerebrum with no effect on global protein synthesis in total brain (Geva et al., 2010).

This mouse developed normally with no severe apparent symptoms outside some impaired motor functions, while in-depth analysis showed an affected white matter and hippocampus.

The white matter anomaly consisted of an increased proportion of small-caliber axons with late onset myelin degeneration, an increase in MBP levels with a decrease in PLP/DM20 levels which remained low at an older age contrary to the MBP levels that managed to normalize, while the remyelination process following cuprizone-induced demyelination was also affected.

In addition, an abnormal abundance of oligodendrocytes and astrocytes was noted, where oligodendrocytes were increased and astrocytes were decreased in the young mouse but not the older one that showed the normalization of the density of these cells (Geva et al., 2010).

The gene expression analysis of the brain of these mice showed a lower level of expression of cell-cycle specific genes in early postnatal brain development with a lower level of oligodendrocyte specific genes during the apex period of myelination (Marom et al., 2011).

The astrogliosis being impaired in this model, the astrocytes were dysmorphic with an overexpression of GFAP-delta. Adding to that, the reaction of these mice to the induction of

systemic stress (by introduction of LPS) was deficient and failed to induce sufficient secretion of certain cytokines like the pro-survival cytokines IL-6 and IL-1b while there was an increase at the RNA level. This deficiency was reported in both astrocytes and microglia hinting at the fact that incomplete astrocyte and microglia activation coupled with a defective inflammatory response might be the results of the eif2b5 mutation (Cabilly et al., 2012).

Another study, related to this model, which assessed the proteomics of myelin formation and regeneration revealed an alteration in the expression of nervous system essential pathways caused by the eif2b5 mutation. It also showed a dysregulation of the equilibrium between degradation and synthesis of proteins, and of the mitochondrial oxidative phosphorylation (Gat-Viks et al., 2015), which in turn was accompanied by an increased mitochondrial abundance (in MEFs, brain and astrocytes isolated from mutant mice), a decrease in the mitochondria-encoded oxidative phosphorylation protein synthesis and a decreased mitochondrial translation (Raini et al., 2017).

The mitochondrial abundance and defective oxidation phosphorylation was also present in the oligodendrocytes isolated from mutant mice and was, in contrast, accompanied by a lower level of basal oxidative respiration rate per cell which meant that the function of these mitochondria was defective and unable to supply enough energy to OPCs to allow them to reach maturity. So the OPCs were unable to differentiate and had an abnormal morphology (Herrero et al., 2019).

5.2.2 The 572G>A and the 1450C>T mutations KI mouse models

Two single mutant mouse models were generated by inserting a homozygous point mutation that replaces guanine by adenine at the 572 position of the Eif2b5 cDNA in the first and a homozygous point mutation that replaces cytosine by thymine at 1450 position of the Eif2b4 cDNA in the second. These mutations resulted in changing the arginine to histidine at the 191 position and the arginine to tryptophan at the 484 position respectively, on the protein level.

This resulted in two homozygous mice, the *Eif2b5*^{Arg191His/Arg191His} and *Eif2b4*^{Arg484Trp/Arg484Trp} also called the *2b5*^{ho} and the *2b4*^{ho} mice respectively (Dooves et al., 2016).

Double mutants, heterozygous for one mutation and homozygous for the other ($2b42b5^{he/ho}$ mice), and homozygous for both mutations ($2b4^{ho}2b5^{ho}$ mice) were also generated (Dooves et al., 2016).

The neurological phenotypes developed by these mice gave way to a classification according to the order of increasing level of severity observed: $2b4^{ho}$ with symptoms onset at 7 months and survival up to 20 months, $2b5^{ho}$ with symptoms onset at 5 months and survival up to 10 months, $2b42b5^{he/ho}$ with symptoms onset at 6 weeks and survival up to 5 months, and $2b4^{ho}2b5^{ho}$ with symptoms onset starting at P10 and survival for less than 3 weeks (Dooves et al., 2016).

Compared to their wildtype (WT) littermates, all these mice weighed less and exhibited ataxia and sporadic epileptic seizures (Dooves et al., 2016).

Symptoms also included longer arrests and reduced activity, motor deficits, loss of grip strength, increased latency and number of foot slips when traversing the narrow beam (Dooves et al., 2016).

In depth analysis of the four mouse lineages revealed certain specificities related to each one of them when compared to their WT littermates.

The $2b4^{ho}$ mice at 19 months of age revealed a slightly lower MBP protein level and a decrease in PLP mRNA levels (which started at 7 months) without the presence of vacuoles (Dooves et al., 2016), while also having normal myelin but smaller axonal diameters and a normal G-ratio (Klok et al., 2018).

The 1- to -7 month-old $2b5^{ho}$ mice showed increase in vacuolization starting at 5 month of age in addition to a decrease in Mbp and Mog protein amounts, and a decrease of Mbp, Plp and Mog mRNA levels compared to age matched controls. The Mbp protein level, which was already low, did not decrease further over time and neither did the mRNA levels or the numbers of immature oligodendrocytes in contrast with a decrease of mature oligodendrocytes' number, noting that the oligodendrocytes kept a normal morphology. These mice also presented immature white matter astrocytes, which have abnormal morphology, didn't show any signs of microglial activation, but had a prevalence of small-caliber axons (Dooves et al., 2016) accompanied with slightly thinner myelin sheaths and a lower G-ratio. Interestingly, the axonal diameter increased normally between 2 and 4 months but reverted to the size of 2-month-old axons at 7 months of age in what seemed like a secondary axonal atrophy (Klok et al., 2018).

The $2b42b5^{he/ho}$ mice at 4-month of age presented a decrease in myelin with an increase in vacuolization, accompanied by a decrease in Mbp protein and Mbp, Plp and Mog mRNA levels (Dooves et al., 2016). The axonal diameter was smaller and the myelin sheaths thicker with a lower G-ratio (Klok et al., 2018).

The P21 $2b4^{ho}2b5^{ho}$ mice were the most severely affected, presenting the highest level of vacuolization and the lowest level of Mbp with a decrease in the mature oligodendrocytes' number which was also present in $2b42b5^{he/ho}$ mice (Dooves et al., 2016).

There were also evidences showing that astrocytes from mutant $2b4^{ho}$ mice blocked the maturation of OPCs by secreted factors in co-cultures (Dooves et al., 2016).

Interestingly, the Bergmann glia in the mutant mice cerebellar cortex were more mislocalized to the molecular layer (instead of the Purkinje cell layer) with a more intense GFAP-delta immunoreactivity (Dooves et al., 2016).

These Bergmann glia were also characterized by markers of immaturity such as RC2 and Nestin at 7 months of age while lacking markers of proliferation such as CyclinD1.

Interestingly, the abnormal mislocalization of Bergmann glia was rescued by guanabenz treatment. Guanabenz is an alpha-2 adrenergic receptor agonist and is being used for arterial hypertension treatment. Recent studies credit it for an indirect eIF2B activity regulation and delaying recovery under stress conditions by extending eIF2 phosphorylation time, thus allowing to keep the rate of protein synthesis under control and in so doing, having a protective effect (Dooves et al., 2017).

Studying the white matter in the spinal cord of 7.5-month $2b5^{ho}$ mutant mice showed abnormalities including loss of organization of radial glial cells, an increased level of nestin expression and dysmorphic GFAP-positive cells while no defects were detected in the embryonic spinal cord (Leferink et al., 2017).

On the proteomic level, astrocytes from $2b5^{ho}$ mice showed the presence of 80 proteins regulated by the introduced mutation and that these proteins mainly localized to the plasma membrane, with evidence pointing to the fact that the observed changes in the protein levels was not caused by alterations in mRNA levels but at the translational level (Wisse et al., 2017).

When primary astrocytes isolated from $2b5^{ho}$ mutant mice and cultured were tested for their reaction to integrated stress response and the unfolded protein response, they were

found to react no differently from WT astrocytes at both the short and long term induction even at the level of cell viability (Wisse et al., 2018).

Interestingly, when 2b5^{ho} mice were injected with glial progenitor cells at P0, the injected cells managed to survive and incorporate into the host mice which showed an improved time while crossing the beam balance but not in the number of slips or the grip strength (Dooves et al., 2019).

Recently the *Eif2b5*^{Arg191His/Arg191His} mice were used for preclinical therapeutical trials using an EIF2B activator (ActEIF2B). They confirmed that the neurological defect is related to a chronic integrated stress respond and can be prevent by the tested molecule. Other than preventing ISR, this molecule also managed to rescue weight loss, motor deficits and myelin loss, in addition to normalizing profiles of transcriptome and proteome without rescuing eIF2B protein levels. Finally, Wong and colleagues suggest the possibility of ISR being upregulated in cell types other than astrocytes that could possibly contribute to the VWM disease in their mice (Wong et al., 2019).

Theses rodent models demonstrated that, in mice, homozygous mutations in both the catalytic (gamma) and regulating (delta) subunit are needed in order to obtain a neurological phenotype closed to what we observed in the human EIF2B related disorders However none of these models reproduce the acute neurological phases we frequently observed as the onset as well as during the evolution of the diseases in the different forms of EIF2B related disorders

5.2.3 The *Plp/Fv2E-PERK* mouse model

This mouse model is characterized by the fact that it expresses, specifically in oligodendrocytes, the Fv2E-PERK which is an artificial PERK derivative that can be activated independently from the ER stress cascade by injection of the compound AP20187. This activation didn't have negative effects on oligodendrocytes, myelin integrity or inflammatory response in the adult mice (Lin et al., 2013, Lin et al., 2014, Lin., 2015).

However, the Fv2E-PERK activation and the subsequent impaired eif2b activity in young myelinating mice, especially during the active phase of myelination, caused tremors and early death (Lin et al., 2014, Lin., 2015).

This was also coupled with foamy oligodendrocytes which were occasionally apoptotic, less CNS white matter myelination with thinner myelin sheaths, normal axonal diameter, a lower myelinated axons' percentage (Lin et al., 2014, Lin., 2015).

This conditioning mouse model demonstrated that the oligodendrocytes are particularly sensitive to the ER stress induced by PERK activation during their active maturation from premyelinating to myelinating oligodendrocytes.

5.3 Cellular models:

5.3.1 Lymphocytes / lymphoblasts

Lymphocytes from controls, heterozygous carriers and patients with different eif2b mutations were immortalized and the GEF assessed. The patients' lymphocytes showed a significant loss of GEF activity compared to the other groups, correlated with age and disease onset (Fogli et al., 2004).

This significant decrease in GEF activity was also observed when CACH/VWM patients' immortalized lymphocytes were compared with those from controls, patients presenting other eif2b-unrelated leukodystrophies and CACH/VWM-like patients while noting that the last 3 groups had no differences in GEF activity. The decrease was once again correlated with age at the onset of disease with lymphocytes from only a few patients having high GEF activity level but with evidence showing that the high level was not specific to a type of mutated gene or to a degree of clinical severity (Horzinski et al., 2009).

Although the GEF activity was decreased in immortalized patients' lymphocytes, there was no significant difference in the degree of reaction in the presence of an ER-stress agent, albeit an increase in ATF4 protein level that was present in all the groups treated with the ER-stress agent and not only those from patients, which was also not related to the immortalization process of the lymphocytes (Horzinski et al., 2010).

5.3.2 Fibroblasts

Skin fibroblasts from CACH/VWM patients were cultured and compared to their control counterparts. The GEF activity was found only slightly decreased in patient fibroblasts and the global protein synthesis regulation was the same in both groups, whereas the ATF4 levels in the presence of ER-stress agent were increased in patient fibroblasts compared to control ones but not in the transformed patient fibroblast when compared to their control counterparts (Kantor et al., 2005).

Transcriptomic analysis was performed in which fibroblasts from eif2b-mutated patients, eif2b-unrelated leukodystrophies and controls were compared. There was no effect of ER-stress on the expression of genes of the different groups. It also revealed 70 genes, which were specifically differentially expressed in eif2b-patients' fibroblasts with 67 being down-regulated and 3 being slightly upregulated. The downregulated genes were involved in (a) transcription or mRNA stabilization and splicing (25%), (b) mitochondria metabolism (15%), (c) development (12%), (d) cell cycle (10%), (e) DNA compaction or repair (8%), (f) cytoskeleton (5%), (g) protein synthesis (4%), and (h) other metabolic pathways (21%) with the highest number of genes being related to RNA process (Huyghe et al., 2012).

5.3.3 Embryonic stem cells

Mouse CGR8 embryonic stem cells (mESC) were transfected with either control vector (mock cells), WT human *EIF2B5* cDNA vector or CREE-mutated EIF2B5 cDNA vector, and mESCs constitutively overexpressing either vector were generated while inducible shRNA systems were used to create underexpressing mESC.

The EIF2B5-underexpressing cells displayed a 55-60% decrease in *Eif2b5* gene expression with no changes to cell morphology, in addition to a decreased GEF activity. However these cells failed to differentiate into the ectodermic neural lineage or the mesodermal lineage and the cells died.

The EIF2B5-overexpressing cells presented an 8 to 10 fold higher EIF2B5 expression level and managed to differentiate while keeping this rate with evidence showing that the

overexpression of EIF2B5 in the ES cells deregulates the neuroectodermal precursor cells at an early stage when compared with mock cells and that the neuronal differentiation profile was altered.

The EIF2B5-overexpressing cells also presented an altered glial differentiation especially in the CREE-mutated cells that showed a decrease in olig2 expression compared to the other groups, in contrast to the GFAP expression level increase observed in all the groups. This meant that CREE-mutated cells prioritized astroglial differentiation and not oligodendroglial one (Huyghe et al., unpublished data).

5.3.4 Induced pluripotent stem cells (iPSCs)

iPSCs are widely used as models for several diseases.

2 VWM iPSCs models were generated from human dermal fibroblasts belonging to 2 patients presenting EIF2B5 (VWM1-iPSCs) and EIF2B3 (VWM2-iPSCs) mutations respectively and compared with control iPSCs.

All groups managed to differentiate into neural stem cells (NSCs) which were then successfully differentiated into neurons and oligodendrocytes with no differences in markers or apoptosis in these cells between the control and the VWM cells.

The NSCs of all groups also differentiated into astrocytes with relatively the same timing. However the VWM-1 and VWM-2 derived astrocytes were dysmorphic, overexpressed GFAP-delta and presented an increase in apoptosis (Zhou et al., 2019).

II. Objectives

The objectives of my thesis were to study the consequences of inactivating eIF2B specifically in the macroglial cells.

For this reason we choose to use inducible conditional Knock-out mouse models respectively in the oligodendrocytes and the astrocytes in the adult mice.

In the material and methods chapter, I will present the general principal of the mouse models we used in addition to the main analysis techniques which will be detailed in the two articles of my thesis.

A summary of the obtained experimental results and their discussion will precede each article.

III- Materials and methods (summary)

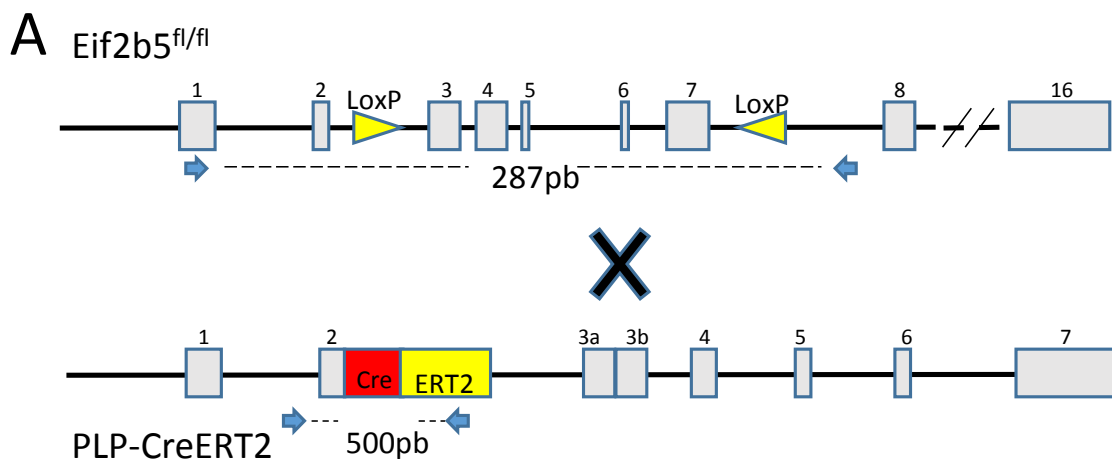
1. Mouse models: inducible eIF2B5 conditional Knock-out

The work was started with the generation of *Eif2b5* conditional Knock-out mice by introducing two flox sites in respectively before exon 3 and after exon 7 of the *Eif2b5* gene (*Eif2b5*^{fl/fl}) in collaboration with the Institut Clinique de la Souris (ICS) in Strasbourg-France (Grant supported by Fondation Maladies Rares -A Fogli).

In order to induce the *Eif2b5* conditional Knock-out in oligodendrocytes or in astrocytes we backcrossed the *Eif2b5*^{fl/fl} mice respectively with the Plp-Cre-ERT2 (Leone et al., 2003) and the Glast-Cre-ERT2 (Mori et al., 2006) mice resulting in the Plp-Cre-ERT2/*Eif2b5*^{fl/fl} and the Glast-Cre-ERT2/*Eif2b5*^{fl/fl} mice.

Mice backcross was done by Anne Fogli (ANR-A. Fogli) at the mice facility of the Clermont Auvergne University under the supervision of Melina Begou (Figure 24).

During all my thesis, the mice were reproduced in the CDTA-TAAM Orleans research center and transferred for experiments in the animal facilities of our INSERM U1141 (Robert Debré, Paris) or of the institute du cerveau et de la moelle épinière (ICM), Pitié salpêtrière, Paris for behavioural analysis



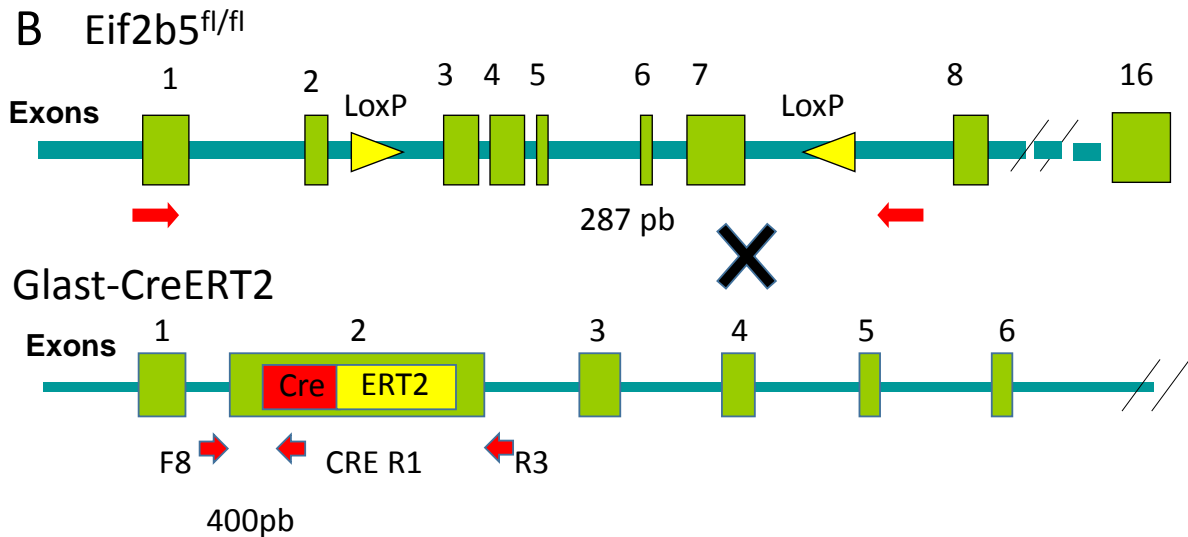


Figure 24: Generation of Plp -Cre-ERT2/ $Eif2b5^{fl/fl}$ and $Glax$ -Cre-ERT2/ $Eif2b5^{fl/fl}$ mice: A, for Plp -Cre-ERT2/ $Eif2b5^{fl/fl}$, 2 LoxP sites were inserted around exons 3 and 7 of the $eif2b5$ gene giving birth to the $Eif2b5^{fl/fl}$ mice which were then cross-bred with PLP -CreERT2 mice generated by fusing the CreERT2 cDNA to exon 2 of the plp gene to generate the Plp -Cre-ERT2/ $Eif2b5^{fl/fl}$ mice. B, For $Glax$ -Cre-ERT2/ $Eif2b5^{fl/fl}$, 2 LoxP sites were inserted around exons 3 and 7 of the $eif2b5$ gene giving birth to the $Eif2b5^{fl/fl}$ mice which were then cross-bred with PLP -CreERT2 mice generated by inserting the CreERT2 cDNA in the exon 2 of the $glax$ gene to generate the $Glax$ -Cre-ERT2/ $Eif2b5^{fl/fl}$.

In the Plp -Cre-ERT2/ $Eif2b5^{fl/fl}$, the Plp -Cre-ERT2 construction drives the expression of the Cre-ERT2 under the $Plp1$ promoter. The $Plp1$ is the gene encoding for the main specific myelin protein PLP and DM20. It is expressed in the oligodendrocytes lineage in the NG2+ OPC (Leone et al., 2003).

In the $Glax$ -Cre-ERT2/ $Eif2b5^{fl/fl}$ mice, the $Glax$ Cre-ERT2 construction drives the expression of the Cre-ERT2 under the $Glax$ promoter. The $Glax$ gene encode the glutamate transporter present in the astrocytes lineage as early as the radial glial cell (Mori et al., 2006).

$Eif2b5$ Knock-out was induced specifically in oligodendrocytes or astrocytes by injecting 2-month-old adult Plp -Cre-ERT2/ $Eif2b5^{fl/fl}$ or $Glax$ -Cre-ERT2/ $Eif2b5^{fl/fl}$ mice respectively by tamoxifen (TMX) at the dose of 1 milligram twice a day for five days. The tamoxifen, which is a ligand to the Cre-ERT2, has the capacity to promote the dissociation of the Cre-ERT2/HSP90 complex located in the cytoplasm, thus allowing the Cre-ERT2 translocation into the nucleus and the recombination at the loxP sites.

In the case of the $Glax$ -Cre-ERT2/ $Eif2b5^{fl/fl}$, we used 2 different genotypes, the mice heterozygote for $Glax$ -Cre-ERT2 ($Glax$ -Cre-ERT2^{+/+}/ $Eif2b5^{fl/fl}$) and the mice homozygote for

Glast-Cre-ERT2 (Glast-Cre-ERT2^{-/-}/Eif2b5^{fl/fl}.) Due to the insertion of the Cre-ERT2 in exon 2 of the *Glast* gene, the Glast-Cre-ERT2^{-/-}/Eif2b5^{fl/fl} mice did not express the Glast protein after Tamoxifen induction whereas the Glast-Cre-ERT2^{+/-}/Eif2b5^{fl/fl} do it normally.

At the time the mice was generated no tags able to follow the efficacy of the inducible ko was available as it is the case presently by using the Rosa marker (Abe et al., 2011).

At resting state Eif2b5 antibodies are detected by immunofluorescence mainly in neuronal cells (cytoplasmic localization) and poorly in glial cells. Western blot or RT-PCR technics of the whole brain extract are not able to demonstrate the decrease of Eif2b5 induced by the Tamoxifen. Therefore we decided to isolate by MACS the different glial cells (astrocytes, oligodendrocytes, microglial cells) from the same total brain hemisphere extracts in order to quantify the Eif2b5 mRNA in the different cell lines 10 days after the initiation of tamoxifen injections (see the chapter transcriptomic analysis: RNAseq).

2. Immunohistochemistry markers of astrocytes, microglial cells, neurons and oligodendrocytes

Immunohistochemistry was used to visualize and asses, under confocal microscopy (Leica SP8), the changes at the cellular levels. I used several cell-specific markers in order to analyze the consequences of Eif2b5 inactivation in the different cells of the CNS. See table (Cell type markers). The conditions used for each marker are mentioned in the joined articles.

Cell type markers

	OPC	Pre-OL	Mature-OL	Immature astrocytes	Mature astrocytes	Microglia	Neurons
NG2	+	-	-	-	-	-	-
Olig2	-	+	+	-	-	-	-
CC1	-	-	+	-	-	-	-
Nestin	-	-	-	+	-	-	-
GFAP	-	-	-	-	+	-	-
Iba1	-	-	-	-	-	+	-
NeuN	-	-	-	-	-	-	+

Double staining (Olig2 and CC1) was used in order to differentiate between premyelinating (Olig2⁺/CC1⁻) and myelinating (Olig2⁺/CC1⁺) oligodendrocytes.

We evaluate the effect of the Eif2b ko in different brain regions by choosing area rich in myelinated tracts (corpus callosum), in neuronal cells (cortex) and in CNS progenitors (Dentate Gyrus of the hippocampus)

Data are presented as the mean \pm standard error of the mean (SEM) for 5 different mice. Statistical analysis was performed with Prism 5 software, and the statistical significance of differences between the tamoxifen treated mice in comparison with the corn oil injected control was determined by 2-tailed t-test with values of $p < 0.05$.

Electron microscopy was used (in collaboration with Dr Brahim NAIT OUMESMAR at the Institut du Cerveau et de la moelle épinière (ICM, Pitié Salpêtrière, Paris) to assess the density of myelinated axons. More complex analysis has not been done at this point.

3. Behavioural tests: motor and cognitive functions

Different behavior tests were performed in the mice facility of the ICM under the supervision of Nadege Sarrazin. We assess different functions: motor coordination, locomotor activity, muscle strength, anxiety and functional memory.

The following table depicts the several tests used in addition to the aspects they classically assess:

Behavior tests

	Motor coordination	Locomotor activity	Muscle strength	Anxiety	Functional memory
Rotarod	+	-	-	-	-
Locotronic	+	-	-	-	-
Beam balance	+	-	-	-	-
Open field	-	+	-	+	-
Actimeter	-	+	-	-	-
Grip test	-	-	+	-	-
Elevated plus maze	-	+	-	+	-
Y maze	-	+	-	-	+

Data are presented as the mean \pm standard error of the mean (SEM) of 10 different mice. Statistical analysis was performed with Prism 5 software, and the statistical significance of differences between the tamoxifen treated mice in comparison with the corn oil injected control was determined by 2-tailed t-test with values of $p < 0.05$.

4. Transcriptomic analysis of isolated glial cells

4-1 MACS isolation of glial cells

We isolated from the mice total brain hemispheres astrocytes, oligodendrocytes and microglia cells using the Magnetic-Activated Cell Sorting (MACS) technique with different cell specific cell surface markers: the anti-ASCA2 antibody that recognizes the astrocyte cell surface antigen-2 which is expressed on Glast positive astrocytes, the anti-O4 antibody that recognize the O4 antigen which is expressed by late A2B5⁺ oligodendrocyte progenitors, persisting even after A2B5 is no longer expressed and finally the anti-CD11b antibody that recognizes the cell-surface CD11b which is expressed on monocytes, macrophages, and microglia.

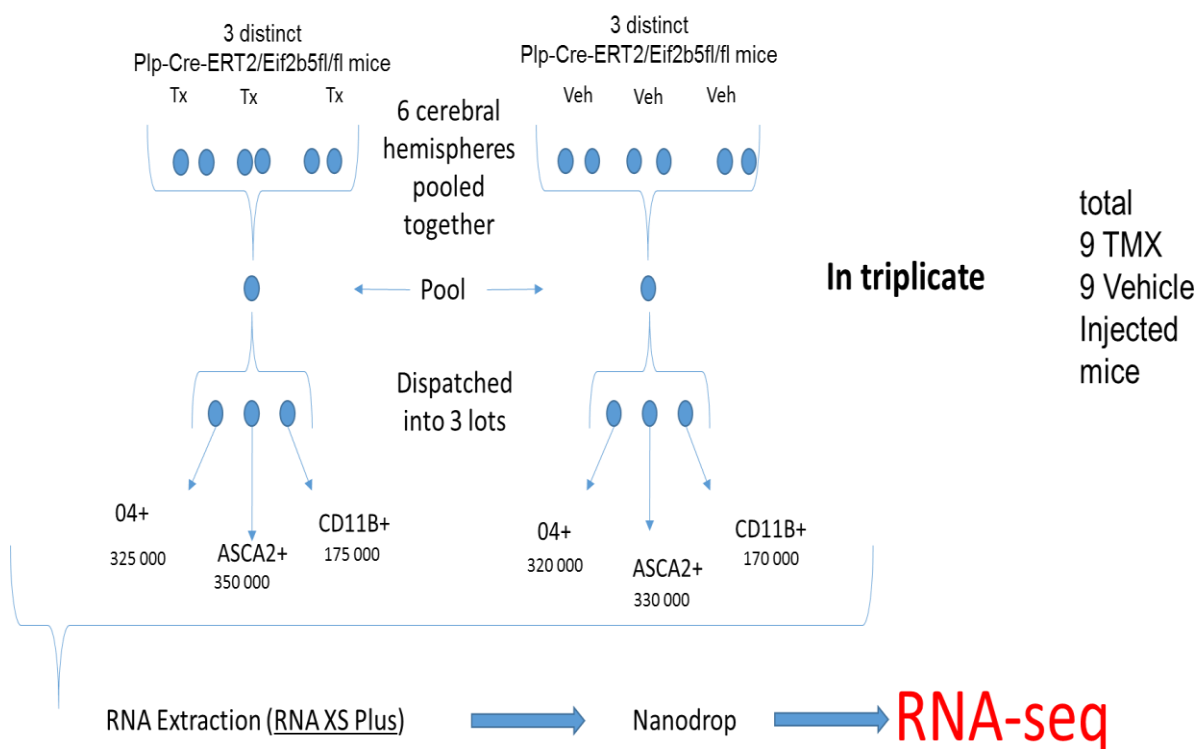


Diagram describing the MACS procedure (Tx=Tamoxifen, Veh=Vehicle)

The values represent the number of cells sorted using each antibody and resulting from pooling 6 hemispheres, then separating them into 3 lots each destined to a different

antibody). The whole procedure was repeated 3 times (triplicate) thus using a total of 9 TMX treated and 9 Vehicle treated mice.

These values seem within the range of sorted ACSA2⁺ cells' number reported by Kantzer and colleagues when first describing the anti-ACSA2 antibody in 2017 (Kantzer et al., 2017).

4-2. Transcriptomic analysis: RNAseq

RNA extraction was done using the The NucleoSpin® RNA Plus XS kit. Quantification was done using NanoDrop™ Spectrophotometer technology and the purity/integrity of the RNA were assessed using an 2200 TapeStation (Agilent Technologies). RNAseq was performed on the Plateforme de Genotypage et Séquençage at Institut du cerveau et de la moelle épinière (ICM-Hopital Pitié-Salpêtrière-PARIS where mRNA library preparation were done following manufacturer's recommendations (Kapa mRNA hyperprep from ROCHE) and Samples pooled library prep were sequenced on Nextseq 500 ILLUMINA to obtain 2*30Millions of 75bases reads for each sample. Bioinformatic data analysis was performed by iCONICS platform (ICM-Hopital Pitié-Salpêtrière-PARIS and quality of raw data has been evaluated with FastQC. Quantification of gene and isoform abundances has been done with rsem 1.2.28, prior to normalisation on library size. Finally, differential analysis has been conducted with edgeR and multiple hypothesis adjusted p-values were calculated with the Benjamini-Hochberg procedure to control FDR.

Epigenetic Dissection of Intra-Sample Heterogeneity (EpiDISH) was used to estimate the proportions of a priori known cell subtypes present in a sample representing a mixture of such cell-types and the ingenuity pathway analysis (IPA®, QIAGEN Redwood City, www.qiagen.com/ingenuity) was used to investigate the different involved pathways and to perform upstream regulator analysis, to predict the transcription factors upstream regulators.

IV: Results and discussion of the consequences of eIF2B5 inactivation in oligodendrocytes (summary)

1. Severe decrease of Eif2b5 transcripts in the premyelinating oligodendrocytes O4+ sorted cells

In light of the lack of ROSA markers in our model and since eIF2B5 is usually not highly expressed in glial cells thus making it difficult to quantify by immunohistochemistry/western blot, we opted to validate the inactivation of eIF2B5 in our model using the transcriptomic analysis in the sorted O4+ oligodendrocytes cells in comparison with the other ACSA2 + and CD11B+ sorted cells.

We first determined the transcriptomic profile of the different MACS isolated cells at 10 days post injection. We analyzed the expression of the mRNA corresponding to the cell specific antibodies used for the MACS (figure 25).

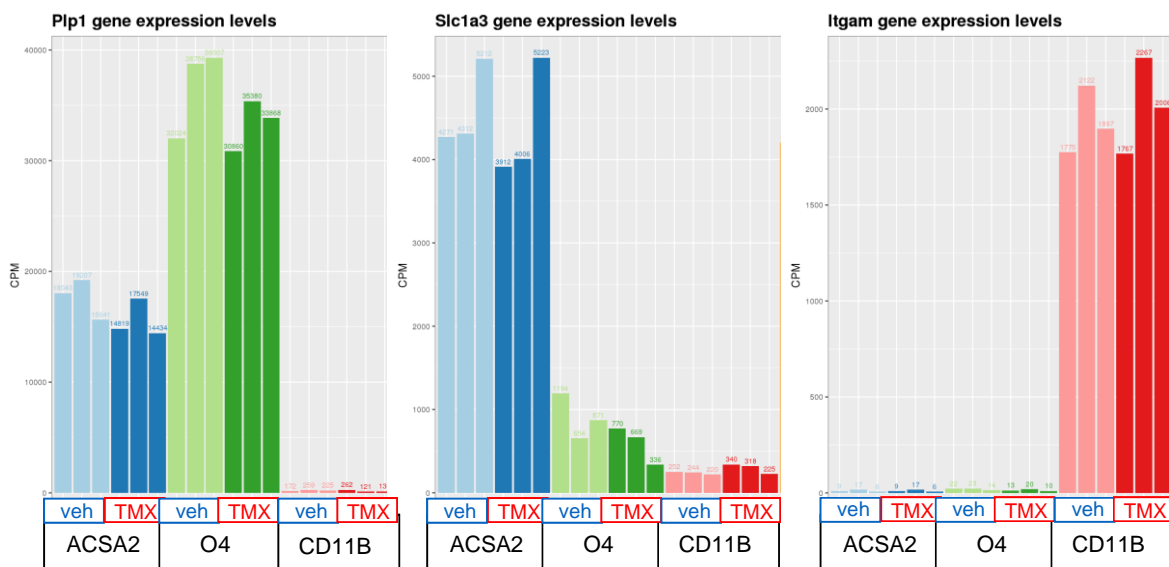


Figure 25: Enrichment analysis at D10 PI using Plp1 expression for O4+ cells enrichment, Slc1a3 for ACSA2+ cells enrichment and Itgam for CD11B+ cells enrichment. Veh=Vehicle, TMX=Tamoxifen

The **plp1** transcripts were almost exclusively found at a high level in O4+ isolated cells whereas the ACSA2+ sorted cells expressed, at a high level the *Slc1a3* transcripts encoding the GLAST protein present in the radial glial cells and astrocytes. Identically the *Itgam* transcripts encoding the CD11B+ marker of microglia cells was exclusively found in the CD11B+ sorted cells.

Using the EPIDISH software which allows to estimate the proportion of cell types using genes' expression profile, we better defined the respective cell types isolated with the different antibodies (figure 26).

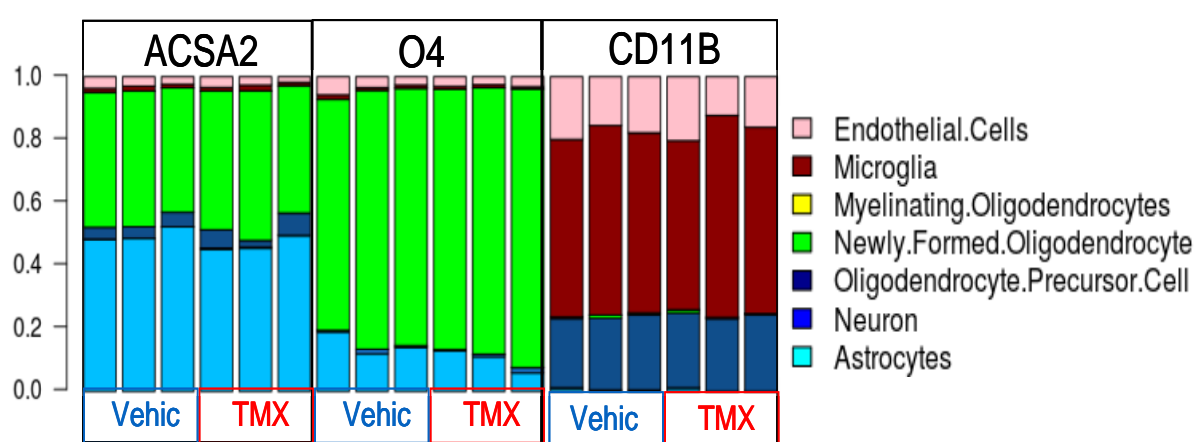


Figure 26: Gene expression profiles at D10 dissected by EPIDISH. Vehic=Vehicle, TMX=Tamoxifen

The cells isolated with the O4 antibodies have, for the large majority, the profile of newly formed oligodendrocytes (80 to 95%), O4 being the classical marker of this cell type (Zhang 2001).

Identically, the cells sorted with the CD11B antibodies expressed mainly microglia specific transcripts (60%) without cells having neuronal or astrocytes genes expression profile. Almost 30% of cells expressed transcripts characterizing OPC.

Cells sorted with the ACSA2 antibody are more heterogeneous, expressing genes classically found in astrocytes (50%) but also in newly formed oligodendrocytes (40%) and oligodendrocyte precursor cells (10%). The glutamate transporter Glast recognized by the ACSA2 antibody is the classical marker for the radial glial cells which give rise to the

astrocytes as well as oligodendrocytes precursor cells even in the maturing brain (Jungblut et al., 2012; Kantzer et al., 2017).

In conclusion we confirmed both the homogeneity of the triplicate obtained from the pool of 6 hemispheric brains and the cell specificity of our MACS sorting.

We then determined the relative eIF2B5 RNA expression at 10 days post induction (PI) in the TMX treated mice and compared it with the controls mice and with the RNA expression of the 4 other Eif2b transcripts (Eif2b1, 2, 3, 4). We found that the relative mRNA expression of the five Eif2B transcripts (1,2,3,4,5) encoding respectively the five Eif2B subunit α , β , δ , ϵ , γ are similar in the different glial cells. However the expression of the Eif2b5 transcripts in the different glial cells was the highest (40 CPM) and the Eif2b3 the lowest (15 CPM). In comparison, the Eif2b1, 2 and 4 transcripts were around 25-30 CPM (Figure 27). Interestingly, the Eif2b5 mRNA encodes the γ subunit which carries the GEF catalytic domain and is associated with the epsilon subunit.

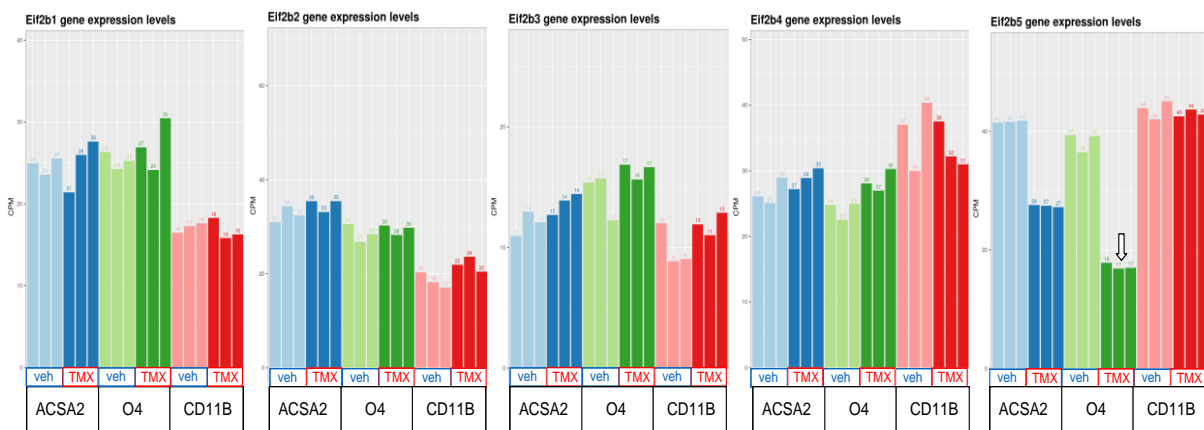


Figure 27: mRNA expression levels for each of the five genes (eIF2B1-5) coding for the five subunits of the eIF2B complex at D10

When we analyzed the effect of the TMX in the Plp-Cre-ERT2/Eif2b5^{fl/fl} mice in comparison with the vehicle (corn oil), we found a specific decrease of Eif2b5 transcripts (57%) specifically in the O4+ sorting cells (Figure 27). The more limited decrease (36%) observed in the ACSA2+ sorted cells is related to the proportion of newly formed cells (40%) observed by EPIDISH in the ACSA2+ population.

These results validated the effectiveness of our Eif2b5 ko specifically in the oligodendrocytes lineage particularly the preoligodendrocytes.

2. TMX treated Plp-Cre-ERT2/Eif2b5^{fl/fl} mice expressed, with a 2-months delay, an acute and severe neurological degradation

This work was initiated in our research group by Aurelia Huyghe and Melina Begou in the mice facility of Clermont University and Lyon INSERM (B Pain). During my thesis I confirmed their observations using the TMX induction versus corn oil in 94 females and 4 males from 9 distinct experiments.

In all experiments we observed between 7 and 9 weeks after the TMX injections a severe and sudden weight loss related to an acute lower limbs paralysis leading to sacrificing the mice at 9 weeks PI (see figure 1 article). No differences were observed between males and females however we used for the rest of the experiments only females.

In addition, the behavior analysis performed at 10 days, 4 and 8 weeks post injections showed no significant differences between the TMX and vehicle groups until 8 weeks PI when all motor performances (locomotor activity, motor coordination and muscle strength) were severely altered whereas the cognitive performances were less affected and limited to significant differences in spatial learning and memory.

In conclusion Eif2b inactivation in the oligodendrocyte lineage of adult mice induces an acute paralysis only 2 months after the induction with the TMX.

3. TMX treated Plp-Cre-ERT2/Eif2b5^{fl/fl} mice have a decrease in mature oligodendrocytes at the time of the acute neurological distress (W8 PI)

In the TMX treated versus vehicle Plp-Cre-ERT2/Eif2b5^{fl/fl} mice, the immunohistochemistry revealed:

- A decrease in the number of mature oligodendrocytes (Olig2-/CC1+) in the 3 brain areas analyzed (corpus callosum, cortex, dentate gyrus) associated with a significant decrease in the MBP staining only in the corpus callosum (see figure 3 in article 1). In contrast the immature pool of oligodendrocytes (olig2 +/CC1-) is maintained (Figure 3 in article 1) and is

even significantly increased in the dentate gyrus where the NG2+ progenitor pool is also increased (Figure 5 in article 1).

- An increase in the GFAP staining and branching of astrocytes with a 20% increase of the GFAP expression in the cortex and to a lesser extent (5%) in the corpus callosum. The number of immature astrocytes (Nestin positive) was increased in the 3 brain areas particularly in the cortex and dentate gyrus.

- An increase in the number and branching of microglial cells (IBA1+ cells) was observed in the 3 brain areas particularly in the cortex

- Finally, a moderate neuronal loss (NeuN + cells) was present in the cortex as well as the dentate gyrus but to a higher extent in the cortex.

Electron microscopy showed a non-significant tendency to decrease the number of myelinated axons in the TMX treated Plp-Cre-ERT2/Eif2b5^{fl/fl} mice. However the analysis was limited to the corpus callosum in only 3 distinct animals with large variation in the vehicle treated (control) animals.

In conclusion, two months after the Eif2b inactivation of the oligodendrocyte lineage, the brain of adult mice with acute paralysis showed a decrease in the number of mature myelinating oligodendrocytes associated with a limited number of myelin staining in the corpus callosum, contrasting with the maintenance or even increase of the immature and progenitor pool. Reactive astrocytes expressing the Nestin and reactive IBA1 positive microglia were particularly present in the neuron enriched area (cortex, dentate gyrus) where a neuronal loss is clearly present.

4. Eif2b5 inactivation induced a chronic integrated stress response in the O4+ sorted cells

When studying the transcriptomic profiles of our sorted cells, we started by looking at the differentially expressed genes in all three sorted cell types at D10 and W8 PI while comparing TMX treated to vehicle treated ones. Only a small number of genes were up and down regulated at D10 while the number of differentially regulated genes at W8 was several times higher in all three cell types (Figure 28).

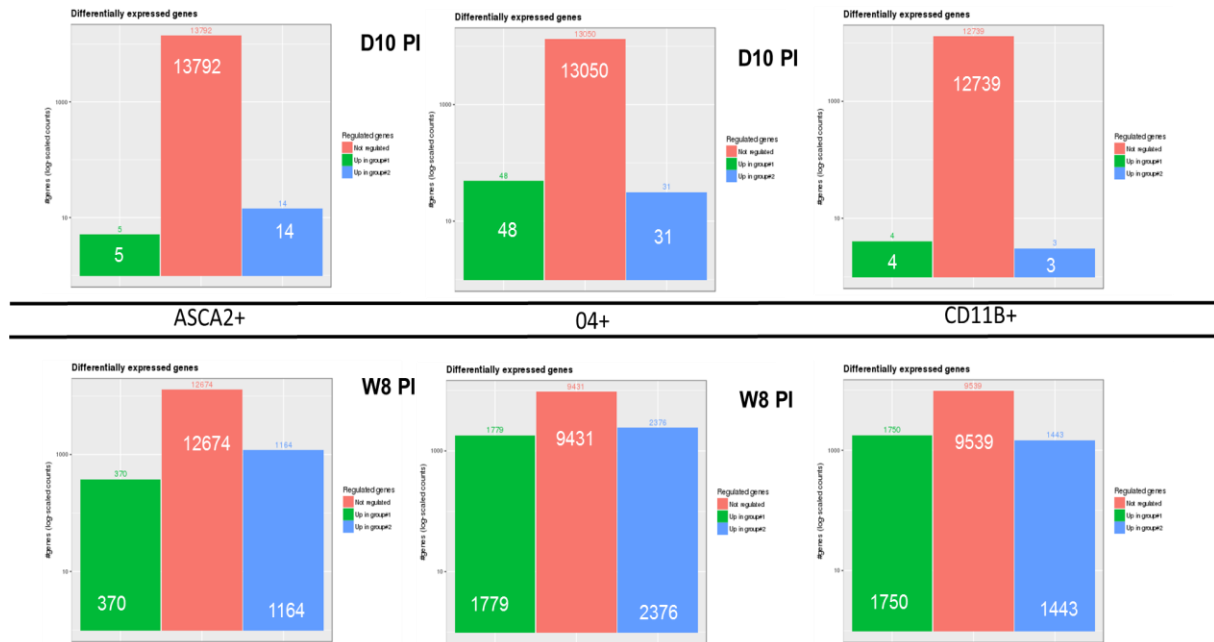


Figure 28: Transcriptomic analysis: differentially expressed genes in TMX versus vehicle injected mice

We then concentrated our RNA-seq analysis on the O4 sorted cells which are the target of the Eif2b5 inactivation. At D10 PI, 79 genes were differentially expressed genes (DEGs) (31 up and 48 downregulated) with a dramatic increase at the time of the neurological distress (W8 PI) reaching 4155 DEGs (2376 up and 1779 downregulated genes). (see the heatmap and volcano plot Figure 10 in article 1).

Among the 79 genes significantly upregulated in D10 PI O4+ sorted cells, we identified mainly genes reported in the endoplasmic reticulum (ER) stress response: Chac1; Asns; Nupr1; Atf5; Trib3; Cdkn1a (Table 1 in article 1). When we performed with IPA an upstream regulator analysis in order to predict the transcription factors upstream regulators, the most significant at D10 PI was ATF4. These results confirmed that the Eif2b5 inactivation in the O4+ cells induced a stress response (Table 2 A) .

When we analyzed the fold change expression of the 15 mRNA involved in the Integrated stress response (ISR) in the O4+ sorted cells of the hemispheric brain at the time of the neurological distress (W8 PI), we observed the persistence of a severe ISR (Figure 29).

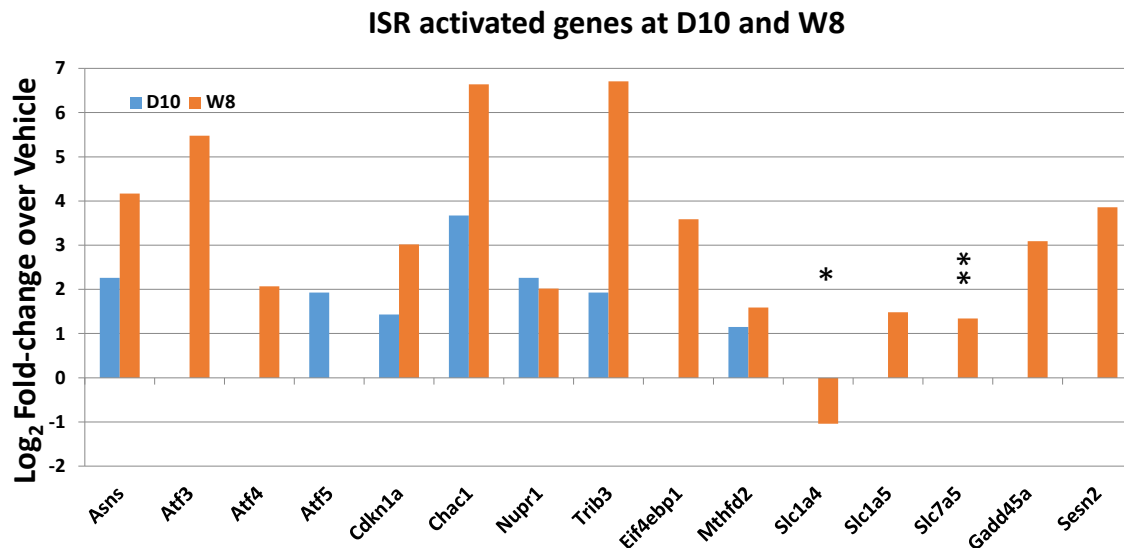


Figure 29: Activated genes. A, ISR activated genes at D10 and W8 expressed as Log₂ Fold-change in O4+ sorted cells. Data are shown normalized to Vehicle expression levels. Bars, mean of 3 samples. * $p<0.01$; ** $p<10^{-3}$; by Student's t-test (TMX compared to Vehicle). Transcripts without symbols were highly significant with $p<10^{-4}$

5. Eif2b5 inactivation induced severe changes in the gene profile expression of the O4+ sorted cells between D10 and W8 PI toward microglial gene expression and cytokines production

AT W8 PI, we saw a loss of specificity of certain mRNA such as TMX treated O4+ cells expressing Itgam, a microglia specific marker, at W8 PI.

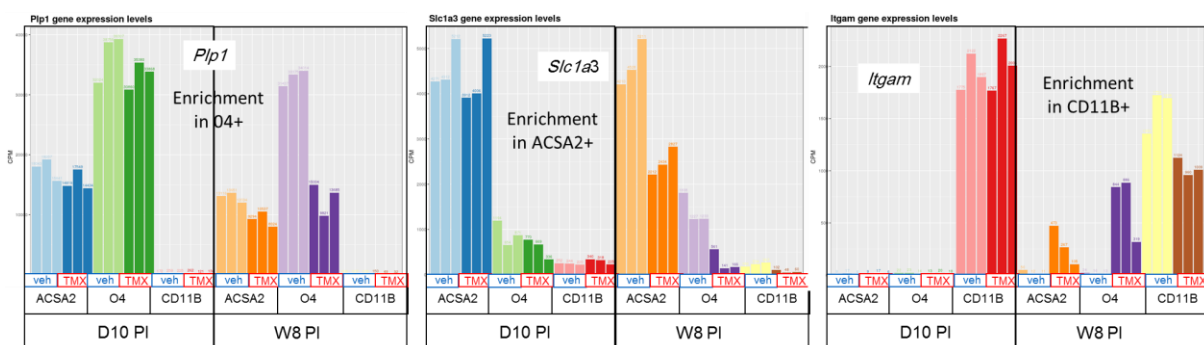


Figure 30: Cell type specific enrichment

To clarify this point we ran our data set through the EPIDISH process and found that the W8 PI TMX treated O4+ cells ended up with increased genes found in OPC and microglia, confirming a loss of cell specific gene expression (Figure 31).

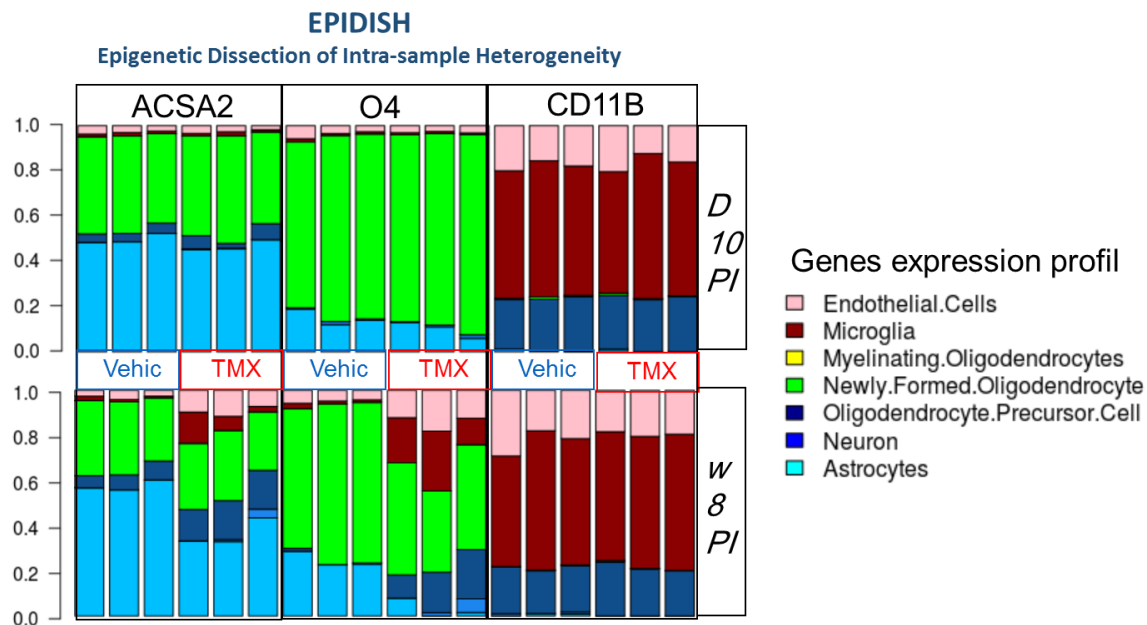


Figure 31: Transcriptomic analysis: Proportion of different cellular types

We further pushed our analysis on the O4+ cells to look for groups of genes and pathways that are differentially affected and found an upregulation of genes with established roles in inflammatory processes. That in addition to, at W8 PI, the upregulation of pathways implicated in inflammation and the repression of pathways such as cell cycle and synaptogenesis signaling pathways. Finally, an upstream analysis revealed the implication of activation of cytokines at W8 PI, which further supports the idea of inflammatory events at this stage.

At the transcriptomic analysis level, and for various reasons, only results pertaining to the O4+ cells will be further detailed in the article, while the same analysis strategy for the other two cell types (ACSA2+ and CD11B+ cells) is still underway in addition to other validation processes such as qRTPCR for the stress pathways and cytokines dosage in all three cell types.

In conclusion, in this work we prove the importance and efficiency of our models. As a matter of fact, constitutive Knock-out models are not viable, which led us to use induced conditional knock-out targeting oligodendrocytes. By using the MACS cell isolation technique from brain homogenates we were able to demonstrate a 53% decrease in the eif2b5 expression specifically in the immature premyelinating oligodendrocytes (O4+ cells) 10 days after TMX induction. A sudden severe weight loss with neurological degradation is observed two months after the eIF2B inactivation in oligodendrocytes. The neurological degradation is mainly related to motor coordination, locomotor activity and muscle strength problems with mild signs of spatial learning or memory deficits. No abnormalities have been found in the presymptomatic phase at 1 month after the TMX induction confirming the acute /subacute motor degradation observed.

Our model targeting eif2b5 in oligodendrocytes presents a decrease of mature oligodendrocytes' number and an increase of immature ones in addition to loss of myelin, which is in agreement with what was previously described in patients. This suggests a maturation problem where oligodendrocytes fail to reach maturity to generate myelin and are instead stuck at the immature stage. Increase of reactive astrocytes and microglia cells occurred particularly in the cortex where a mild neuronal loss is observed.

An important part of this work is the transcriptomic analysis of the three glial cell lines (oligodendrocytes, astrocytes and microglia) which were MACS sorted respectively with the O4, ACSA2, CD11B antibodies, at the same time from the same animals in order to better understand the consequences of eif2b5 knock-out in oligodendrocytes on all three of these cell lines. While analysis is still underway, we already demonstrated the activation of the ISR specifically in O4+ cells 10 days after the TMX induction as expected with an induced eif2b defect. However, this ISR activation remains chronic and increased in the O4+ sorted cells at W8 post TMX induction, when the acute symptomatic phase started.

In parallel the transcriptomic analysis of O4 + sorted cells showed changes in their programmed gene expression toward immature OPC and microglial cells. Both changes have been demonstrated in chronic stress situations in order to decrease ER stress and maintain cell survival. This process involved eIF2B independant gene translation which seems to maintain the cells in a less undifferentiated state.

Interestingly, one of the consequences of this chronic ER stress, in the O4+ cells, is inducing the upregulation of immune system related genes in addition to the activation of pathways involved in inflammation. These findings demonstrated for the first time that a primary stress event in O4+ cells can induce reprogramming events that activate inflammatory pathways. CACH/VWM patients, identically to patients with multiple sclerosis (MS), can present acute relapsing phases with a secondary progressive relapsing or non relapsing course, particularly in the classical childhood onset form (2-5 y) of the disease, whereas the infantile forms have a severe subacute evolution without recovery and the juvenile/adult forms a primary progressive relapsing or non relapsing form. Identically to MS, in CACH/VWM the neurological signs observed at the acute phases are very sensitive to high dose of corticosteroids which are anti inflammatory and anti stress molecules. Our findings suggest that a primary stress event in the O4+ cells, largely before the first acute neurological event would be able, by activating a chronic ISR, to trigger changes in the O4+ cells leading to the activation of inflammatory pathways responsible for cytokines' production and the repression of oligodendrocytes maturation leading to remyelination impairment. The development of molecules able to reverse the chronic ISR activation in CACH/VWM such as Guanabenz, sigma 1 receptor agonist and 2Bact could have potential effect on the remyelination capacity of the MS O4+ cells. On the opposite side, immunomodulators able to decrease the inflammatory O4 pathway activated by the chronic ISR could decrease the consequences of the chronic ISR by limiting astrocytes /microglial activation and neuronal loss. The present model is of great interest to specifically address the efficacy of drugs specifically on the chronic ISR of the oligodendrocytes at presymptomatic and symptomatic stages.

To further validate our transcriptomic results, proteomic/metabolomic analysis including ER stress protein and cytokines quantification will be important. However, the quantity of cells needed push towards avoiding the use of MACS cell isolation. The quantification of these proteins at the level of a whole brain extract would perhaps be not significant. The results obtained during my thesis using the cerebral hemispheres will be interesting to compare by using the cerebellum and the spinal cord.

Consequences of EIF2B inactivation during the active phase of the developmental myelination program will also be of great importance. TMX treatment of the mother would be an option in order to induce inactivation in the O4+ cells during the second week of life.

Article 1

Impaired *EIF2B5* specifically in adult oligodendrocytes induced, with delay, an acute neurological degradation related to chronic stress response and inflammation activation of the OPC

Impaired *EIF2B5* specifically in adult oligodendrocytes induced, with delay, an acute neurological degradation related to chronic stress response and inflammation activation of the OPC

Abed El Rahim BARK¹, Imen DORBOZ², Ronza ABDEL RASSOUL³, Nadège SARRAZIN⁴, Aurélia HUYGHE⁵, Bertrand PAIN⁵, Julie BONHEUR², Flavien LAMMENS¹, Brahim NAIT OUMESMAR⁴, Mélina BEGOU⁶, Odile BOESPFLUG-TANGUY^{1, 2}

1-Université de Paris UMR1141, NeuroDiderot, Inserm, PARIS, France,

2-Neurologie Pédiatrique, LEUKOFRANCE, Hôpital Robert Debré, AP-HP, PARIS, France,

3-Lebanese University, Masters of neuroscience department, Neuroscience research center, Faculty of medical sciences, Rafic Hariri campus, HADATH, Lebanon,

4-Institut du Cerveau et de la Moelle, ICM, UPMC 06 UM 75, INSERM U 1127, CNRS UMR 7225, PARIS, France

5-Université Lyon 1, Stem Cell and Brain Research Institute, U1208, INSERM, USC1361, INRA, LYON, France,

6-Université Clermont Auvergne, Inserm, U 1107, Neuro-Dol, Pharmacologie Fondamentale et Clinique de la Douleur, F-63000, Clermont-Ferrand, France

Keywords

EIF2B, oligodendrocytes, chronic ISR, neuroinflammation

Corresponding author: Odile BOESPFLUG-TANGUY, Neurologie Pédiatrique, LEUKOFRANCE, Hôpital Robert Debré, AP-HP and Université de Paris UMR1141, NeuroDiderot, Inserm, 48 boulevard Sérurier, 75019 Paris-France; Phone : +33 1 40 03 53 91, Fax: +33 1 40 03 47 74 ; E-mail: odile.boespflug-tanguy@aphp.fr

Running title: Impaired EIF2B5 in oligodendrocytes

Manuscript word count: 7423

ABSTRACT:

Mutations in the ubiquitous eukaryotic translation initiation factor 2B (*eIF2B*), which is involved in regulating global protein synthesis particularly in stress conditions, induced a recessive form of vacuolating leukodystrophy named childhood ataxia with central nervous system hypomyelination (CACH) or vanishing white matter disorder (VWM). We developed an inducible knock-out (cKO) mouse model for *eif2b5* specifically in the oligodendrocytes lineage by using a Plp1-promoter. Tamoxifen (TMX) Eif2b5 inactivation in 2-month-old female Plp-Cre-ERT2/*Eif2b5*^{fl/fl} mice induced at 8 weeks post-injection (PI) an acute motor degradation leading to death in 1 week. Decrease in myelinating oligodendrocytes' number with mild myelin loss contrasting with an increase in oligodendrocytes progenitors, reproduce what has been reported in the brain of CACH/VWM patients. Astrocytes and microglial activation is also observed mainly in the cortex. RNAseq analysis of O4+ sorted cells from the TMX treated mice brain 10 days PI show a 50% defect in *eif2b* expression associated with upregulation of the chronic integrative stress response (ISR). This chronic ISR is higher in the O4+ cells isolated at the time of the acute neurological phase. The gene expression profile of the stressed O4+cells change towards gene expressed in immature NG2+ OPC and microglial cells. Moreover, upregulation of the neuroinflammatory NFkB pathway with TNF α and IFN γ -dependent genes activation is seen. These results underlined the key role of oligodendrocytes in the pathophysiology of the CACH/VWMD particularly the exacerbating episodes frequently observed. This model could help testing new therapeutic strategies in order to prevent the neurological degradation observed in white matter diseases.

1- INTRODUCTION

Eukaryotic translation initiation factor 2B (EIF2B) is a 5 subunit complex (EIF2B α , EIF2B β , EIF2B γ , EIF2B δ , EIF2B ϵ), which is a major regulator of protein synthesis under normal and stress conditions (Pavitt 2005). At each round of translation, eIF2B serves as guanine exchange factor (GEF) for the GTPase and initiation factor eIF2. GTP-bound eIF2 binds to the initiator methionyl tRNA. The resulting ternary complex (eIF2.GTP.Met-tRNAⁱ) delivers the amino acid to the ribosome with hydrolysis of the GTP. The GDP-eIF2 is released. eIF2B activity allows the reactivation of eIF2 for a new round of protein synthesis. Therefore by controlling the level of ternary complexes, eIF2B governs the rate of global translation. In stress conditions, the four stress response kinases (PERK, HRI, GCN2 and PKR) phosphorylate eIF2. This phosphorylated eIF2 (eIF2-P) becomes a competitive inhibitor of eIF2B, triggering endoplasmic reticulum (ER) stress with an integrated stress response (ISR). ISR reduces translation initiation events and decreases global protein synthesis but increases, in parallel, translation of a subset of mRNA with inhibitory upstream reading frame (uORF) in their 5'UTRs including mRNA encoding stress response regulators such as ATF4. In acute /transient stress, a second ISR program induced GADD34 which dephosphorylates eIF2-P, restores eIF2B GEF activity and the translation program. In contrast to acute ER stress, the chronic stress triggers new ISR mechanisms. This chronic ISR is characterized by persistently elevated uORF mRNA translation and concurrent gene expression reprogramming which permits stress sensing and partial recovery of protein synthesis (Guan et al., 2017). This particularly permits translation of the unfolded protein response (UPR)–induced transcriptome which prevents ER dysfunction and promotes cell survival. This chronic ISR operates via PERK dependent orchestration of translational and transcriptional reprogramming. Translational initiation in this chronic stress situation is eIF2B independent and involves eIF3d-dependant mechanisms. Translational recovery during chronic ER-stress may differ depending on cell/type lineage.

Dysfunctions related to chronic ER-stress have been suggested as the main pathological mechanisms of a large number of human diseases particularly of the central nervous system (CNS), the CNS and the highly differentiated cells being the most sensitive (Zhang et al., 2008).

The discovery of eIF2B mutations in patients with a disorder affecting only the CNS has opened new insights into the sensitivity of CNS cells to chronic ER stress.

EIF2B mutations affecting one the 5 genes (*EIF2B1-5*) encoding the 5 subunits of the complex, have been described in a recessive neurodegenerative disease. Disease characteristic is the association of progressive ataxia, spasticity, cognitive deterioration to a cystic degeneration of the cerebral WM which continues to be vanished. For this reason, the disease has been successively named Ataxia with CNS Hypomyelination (CACH) and Vanishing white matter (VWM) (Hanefeld et al., 1993; Schiffmann et al., 1994; van der Knaap et al., 1997). However, a large clinical spectrum exists and is related to age of onset which is also predictive of disease progression (Fogli et al., 2004). Different groups of severity have been proposed from antenatal/congenital forms leading to death in few months to slow progressive adult forms (Fogli et al., 2004; Hamilton et al., 2018). In all cases, acute/subacute neurological dysfunctions are observed at the onset or during the evolution of the disease with frequently provoking factors (head trauma, infection, psychoaffective stress...). There are at least 160 mutations, most of which are missense mutations, the majority of these mutations affecting EIF2B5 (66.5%) (Fogli et al., 2004; Abbink et al., 2018; Van Der Knaap et al., 2019). Frameshift mutations and nonsense mutations can only be heterozygous, confirming that total loss of function of this initiation factor is non-viable even at the embryonic stage of development.

Studies of cellular and rodent mutants proposed that eIF2B mutations induced neurodevelopmental abnormalities. Impaired maturation of the white matter astrocyte cells and particularly the highly specialized Bergmann glia and Muller cells have been demonstrated in the homozygous double *knock in* (KI) mutant mice, Eif2b5Arg191His/Arg191His and Eif2b4Arg484Trp/Arg484Trp (*2b4^{ho}2b5^{ho}* mice) and in the human cerebellum (Dooves et al., 2016 and 2018). The inhibition of the oligodendrocyte maturation with hypomyelination and impaired remyelination observed in different homozygous KI mice (Geva et al., 2010; Gat-Viks et al., 2015; Klok et al., 2018) as well as in human CACH/VWM brains (Bugiani et al., 2011; Rodriguez et al., 1999; Klok et al., 2018) is

considered as secondary to abnormal astrocytes secreting factors (Dooves et al., 2018). On the other hand, strong PERK activation specifically in oligodendrocytes by using the conditional homozygous Plp/FvE-PERK transgenic mice suppressed eIF2B activity and reproduced the characteristic features of eIF2B related disorders such as hypomyelination, foamy oligodendrocytes and myelin loss (Lin et al., 2014). This result suggests a cell autonomous role of impaired eIF2B activity in myelinating oligodendrocytes in the pathogenesis of CACH/VWM.

Dysregulations of the mitochondrial functions related to the abnormal balance between mitochondrial proteins encoded by the nuclear versus mitochondrial DNA in the eIF2B mutants could explain the particular sensitivity of the glial cells which have high glycolytic activity for myelinating oligodendrocytes and supplying energy to neurons (Raini et al., 2017).

In order to further delineate the consequences of eIF2B dysfunction in the oligodendrocytes, we generated a transgenic mouse allowing temporally controlled eIF2B5 inactivation in oligodendrocytes (Plp-Cre-ERT2/Eif2b5^{fl/fl}). Tamoxifen induced eIF2B5 inactivation in oligodendrocytes of adult mice is responsible for an acute neurological degradation leading to death two months after the injection.

Transcriptomic analysis of the isolated O4 positive cells from the cerebral hemispheres of Tamoxifen treated (TMX) and control mice at 10 days (D10) and 8 weeks (8W) after the induction demonstrated the persistence of a chronic integrated stress response (ISR) in the premyelinating eIF2B induced ko oligodendrocytes. However at the time of the neurological degradation (8 weeks), the O4 positive cells had a severe change in their gene expression profile leading to inflammatory pathway activation and particularly of the tumor necrosis factor (TNF). Our findings indicate, for the first time, a direct link between chronic ER stress and inflammatory response in the premyelinating O4+ oligodendrocytes, opening new insights into the pathogenesis and treatment of inflammatory disorders of the white matter such as the multiple sclerosis.

2- MATERIALS AND METHODS

Mice

Eif2b5 gene being the most frequently mutated gene in the CACH/VWM human pathology, Eif2b5^{fl/fl} transgenic mice were generated at the “Institut Clinique de la Souris” (ICS, Illkirch-graffenstaden, Strasbourg) from a C57BL/6 strain by inserting gene lox P sites in introns 2-3 and introns 7-8 of the *eif2b5* gene (Fig.1). These animals have been cross bred with Plp-Cre-ERT2 transgenic mice (Leone et al., 2002) to obtain the Plp-Cre-ERT2/Eif2b5^{fl/fl} transgenic mice. Plp-Cre-ERT2/Eif2b5^{fl/fl} is an inducible Knock-out (KO) mouse in which the expression of the Cre recombinase excising the exon 3 to 7 of the *eif2b5* gene is driven by the *Plp1* promoter specifically in the oligodendrocytes lineage (mainly in the premyelinating and myelinating cells).

All experiments were carried out in compliance with INSERM ethical rules and approved by the institutional review board (Bichat-Robert Debre ethics committee, Paris, France, approval number APAFIS#1682-2015090819249420 v4).

Mice Genotype control

DNA was extracted by lysing tail samples using Kapa Mouse Genotyping kit (Clinisciences). Polymerase Chain Reaction (PCR) was realized in a total volume of 15 µL containing 2 µL of DNA, 7,5 µL of genotyping mix, 1,5 µL of H₂O and 1 µL of each of the following four primers solutions (10 µM) PLP-Cre Forward (Fw): 5'-CACTCTGTGCTTGGTAACATGG-3', PLP-Cre Reverse (R): 5'-TCGGATCCGCCGCATAACC-3', 4251 (Fw): 5'-GGAGCCAGTGACCTCTTCTG-3' and 4253 (R): 5'-TTAATCCCAGCACTCGGTCT-3'. The PCR was performed using Applied Biosystem 2720 Thermocycler using the following cycling parameters: 1 cycle of 5 minutes at 95°C followed by 35 cycles each of 30 seconds at 95°C, 30 seconds at 63°C and 30 seconds at 72°C, finishing with final extension for 10 minutes at 72°C.

DNA migration was done in 2% agarose gel in UltraPure™ TBE Buffer at 120 V, 10X (Invitrogen, 15581-028) diluted 1/10. DNA bands were expected at 500pb for Plp-Cre and 287pb for Eif2b5^{fl/fl} (Figure 1.B).

Knock-out induction/treatment Protocol

Two month old female Plp-Cre-ERT2/Eif2b5^{fl/fl} mice were injected intraperitoneally (IP) with 50 microliters of corn oil (Sigma Aldrich C8267-500mL) or Tamoxifen (Sigma Aldrich T5648-1G) (1 milligram Tamoxifen dissolved in 50 microliters of corn oil) twice a day for five days. The mice were weighed weekly and sacrificed at 10 days or 8 weeks after the first day of injection for cell sorting and/or immunohistochemistry. Other groups were intended for behavioral test, and they were studied at 10 days, 4 and 8 weeks after the first day of injection.

Behavioral evaluation

For the behavioral evaluation, 2 groups of ten mice each were injected either with Tamoxifen or Corn Oil at 2 month of age. Each of the tests were done at three time points for the 2 groups of mice: 10 days, 4 weeks and 8 weeks after the initiation of the treatment.

Rotarod test (Bioseb, Vitrolles, France) assesses motor coordination and equilibrium on an accelerating rod. Mice were placed on the rod with their head directed against the direction of the rotation so that the animal had to progress forward to maintain its balance. Mice were tested during three consecutive days and three trials each day (intertrial interval, time spent on rotarod before the fall). During these trials, the mice had to stay in balance on the rotating rod that accelerated from 4 to 40 r.p.m within 5 min. The latency until the mice fell from the rotating rod was recorded, up to a maximum of 5 min.

Beam balance This test assesses fine motor coordination and balance in rodents. Performance on the beam is quantified by the speed at which the beam is traversed and the number of times that the mouse slides on the beam. The time of fall of the bar is measured with a cut off of 3 min during the 5 successive tests.

Open-field allows the study of exploratory test. Locomotor activity was evaluated by placing the mice into the center of an open field arena (50×50×50 cm) for 10 min. Rodents typically prefer to stay in periphery. Movements were recorded using Top scan video tracking software (Cleversys, Reston, USA) in 3 sub-zones: apparatus, center and hyper-center. The distance traveled, the time spent and the velocity were evaluated in each sub-zone. Total path length was measured as an index of mouse locomotion.

Actimeter (Bioseb, Vitrolles, France) allows the study of spontaneous locomotor activity and rearings. The system is composed by a 2 dimensional (X and Y-axes) square frame. Each frame counts with 16 x 16 infrared beams for optimal subject detection. Horizontal and vertical locomotor activities were measured in apparatus (45x45x45 cm) by beam breaks every 3 min during 15 min. We measured: SM (slow movements, number of displacements below the threshold), FM (fast movements, number of displacements above the threshold), SS (slow stereotype, number of movements without displacement below the threshold), FS (fast stereotype, number of movements without displacement above the threshold), SR (slow rearing, number of times the animal stands up below the threshold), FR (fast rearing, number of times the animal stands up above the threshold).

Locotronic test objectively detects walking disorders and abnormalities of motor coordination by recording the number, position and duration of errors (fore and hind limbs as well as tail errors). Two compartments (a departure and an arrival box) are located on each side of a long horizontal ladder encased in an opaque corridor (124 x 28 x 20 cm, corridor 6 cm, 78 bars). The arrival box is a black compartment that attracts the animal, which walks towards the end of the ladder. On each side of the rungs, infrared beams and sensors detect the rodent's movements and are used to recognize and record the exact position and duration of the errors.

Grip strength test (Bioseb, Vitrolles, France) was done for both forelimbs and fore + hind limbs, and recorded the grasping force in grams. The test is performed successively three times for the forelimbs and the four legs. The mouse was held by the first third of the tail and was pulled horizontally slightly backwards by the tail while the 2 paws (forelimbs) grasped the bar or 4 paws grasped the grid.

Y-maze. Spontaneous Alternation is a behavioral test for measuring the willingness of rodents to explore new environments. Rodents typically prefer to investigate a new arm of the maze rather than returning to one that was previously visited. Testing occurs in a Y-shaped maze with three transparent plastic arms at a 120° angle from each other (30x30x30cm). After introduction to the center of the maze, the animal is allowed to freely explore the three arms. Over the course of multiple arm entries, the subject should show a tendency to enter a less recently visited arm. An entry occurs when all four limbs are within the arm. The number of arm entries and the number of trials are recorded in order to calculate the percentage of alternation via anymaze software (Dublin, Ireland).

Elevated plus maze. The elevated plus maze was used to investigate anxiety related behavior. Movements were recorded using Top scan video tracking software (Cleversys, Reston, USA). The apparatus consisted of a plus-shaped maze with two closed and two open arms (35x15x5 cm wide; height 50cm). Mice were placed at the center of the maze with their face in the direction of an opened arm, and were allowed to explore freely for 5 min. We used the time spent and number of entries into the open arms as a measure of anxiety and into closed arms as a measure of locomotor activity. Percentage of time spent in the open arms was calculated.

Immunohistochemistry

For Immunohistochemistry, the mice were anesthetized with 90 mg/kg pentobarbital (CEVA Santé Animale 54,7mg/mL) and sacrificed by intracardiac perfusion-fixation with 20 ml of normal saline solution (NaCl 0.9%), followed by 100 ml of 4% paraformaldehyde solution in PBS (Santa Cruz sc-281692). Brains were removed and post-fixed in the same fixative overnight at 4°C, and were then cryoprotected by immersion in 30% sucrose in PBS during 72 hours and then frozen using Isopentane at – (45-55) °C. Coronal sections of the brain were cut with cryostat (12 µm thick; Leica 3500 at -22°C). For each experimental condition, we used five mice.

Sections on slides were subjected to an antigen retrieval step using Target Retrieval Solution (DAKO S1700) following the manufacturer's protocol, allowed to cool down for 20 min at room temperature, washed 3 times for 5 min in PBS and then blocked for 1 hour at room temperature. Next, slides were incubated overnight at 4°C the same blocking solution containing 10% horse serum (Sigma-Aldrich), 0.2% Triton X-100 in PBS with primary antibodies against Olig2 (1:400, CHEMICON/Millipore AB9610), CC1 (1:400, Abcam ab16794), MBP (1/400, CHEMICON MAB384-1ML), NG2 (1:250, Millipore AB5320), GFAP ALEXA FLUOR 488 (1:400, CHEMICON/Millipore MAB3402X), Nestin (1/400, CHEMICON/Millipore MAB353), Iba1 (1:400, WAKO 019-19741) and NeuN (1:250, Millipore MAB377) . Sections were then washed three times in PBS/0.1% Triton and incubated with corresponding secondary antibodies Cy3-conjugated anti-mouse (1:1000, Jackson ImmunoResearch), Cy3-conjugated anti-rabbit (1:1000, Jackson ImmunoResearch), Alexa 488-conjugated anti-rabbit (1:1000, Jackson ImmunoResearch) or Cy5-conjugated anti-mouse (1:1000, Jackson ImmunoResearch) for one hour at room temperature. The sections

were washed 3 times in PBS for 5 minutes, mounted on slides with DAPI Fluoromount-G (SouthernBiotech) for nuclear counterstaining, coverslipped, and viewed under a Leica confocal microscope (TCS SP8 –DMI6000B-CS).

Quantification and cell counting were done using Fiji software , ImageJ.

Electron microscopy

Electron microscopy was performed as previously described (Fauveau et al. 2018). Briefly, after lethal anesthesia, mice were perfused with 4% PFA/2.5% glutaraldehyde in 0.2N phosphate buffer. Brains were dissected and cut into 100 μ m sections on a vibratome. Sections were post-fixed in 2% Osmium tetroxide solution, contrasted in 5% uranyl acetate and embedded in Epon after dehydration. Ultra-thin sections were visualized using a transmission electron microscope (Hitachi 120kV HT 7700, Krefeld, Germany).

The density of myelinated axons was evaluated in the corpus callosum and cortex. Three TMX and three Vehicle injected mice were used. Quantification was performed using ImageJ. Unpaired student t-test was used for statistical analysis.

Neural Tissue Dissociation and Magnetic-Activated Cell Sorting (MACS)

For cell sorting, the mice were also anesthetized with 90 mg/kg pentobarbital and intracardially perfused only with 20 ml of PBS and immediately processed for brain collection.

A total of the cerebral hemispheres of 9 animals for each experimental condition (TMX versus control mice at respectively 10 days and 8 weeks after the first injection) were collected for cell dissociation and glial cells enrichment using a magnetic-bead-coupled antibody extraction technique (MACS), as previously described and according to the manufacturer's protocol (Jungblut et al., 2012; Miltenyi Biotec, Bergisch Gladbach, Germany). In brief, after removing the cerebellum and olfactory bulbs, six cerebral hemispheres of 3 TMX mice were pooled versus the six cerebral hemispheres of 3 control mice . Brain tissues were dissociated using the Adult Neural Tissue Dissociation Kit. The resulting brain pool homogenates of respectively the 3 TMX and 3 control mice were, in turn, each divided into 3 samples. Each of these 3 samples, were used for one of the 3 types of glial cell specific MACS isolation. For this purpose the dissociated cells were incubated

with magnetic beads conjugated with antibodies specific of one of the glial cell surface markers respectively anti-ACSA2 antibody for the astrocytes; anti-O4 antibody for oligodendrocytes and anti-CD11B antibody for microglial cells. The enriched cell population was eluted from the column after successive washes that removed non-target cell populations, centrifuged for 10 min at 300g and conserved at -80°C. Therefore for the TMX versus control condition, each type of sorting cells (respectively ACSA2+, O4+ and CD11B+) were extracted from the same pool of six cerebral hemispheres homogenates in order to obtain enough cells from each cell type and were done in triplicate from 3 distinct pools of six cerebral hemispheres.

RNA extraction and Sequencing (RNAseq) and bioinformatic data analysis

RNA extraction was done using The NucleoSpin® RNA Plus XS kit. Cells were lysed by incubation with LB1 and LB2 buffers to inactivate RNases and genomic DNA was removed. RNA was bound to the column by adding BSXS buffer then washed using MDB and WB2 buffers and finally eluted in 16 µL RNase-free H₂O at 11000g.

Purified RNA was quantified using NanoDrop™ Spectrophotometer technology (Thermo Fischer Scientific, Wilmington, DE).

RNAseq was performed on the Plateforme de Genotypage et Séquençage at Institut du cerveau et de la moelle épinière (ICM-Hopital Pitié-Salpêtrière-PARIS).

The purity/integrity of the RNA were assessed using an 2200 TapeStation (Agilent Technologies). mRNA library preparations were done following manufacturer's recommendations (Kapa mRNA hyperprep from ROCHE) including PolyA selection, fragmentation, reverse transcription with hexamer primer, end repair, A-tailing and adapters ligation. Samples pooled library prep were sequenced on Nextseq 500 ILLUMINA to obtain 2*30Millions of 75bases reads for each sample.

Bioinformatic data analysis was performed by iCONICS platform (ICM-Hopital Pitié-Salpêtrière-PARIS). Quality of raw data has been evaluated with FastQC. Poor quality sequences and adaptors have been trimmed or removed with Fasp software to retain only good quality paired reads. Star v2.5.3a (Dobin et al., 2013) has been used to align reads on mm10 reference genome using standard options. Quantification of gene and isoform abundances has been done with rsem 1.2.28, prior to normalisation on library size. Finally, differential analysis has been conducted with edgeR (Robinson et al., 2010) bioconductor

package. Multiple hypothesis adjusted p-values were calculated with the Benjamini-Hochberg procedure to control FDR.

Cell-type deconvolution: we used the EpiDISH algorithm (Epigenetic Dissection of Intra-Sample Heterogeneity) (Teschendorff AE et al., 2017), to estimate the proportions of a priori known cell subtypes present in a sample representing a mixture of such cell-types.

Ingenuity pathway analysis (IPA)

The ingenuity pathway analysis (IPA[®], QIAGEN Redwood City, www.qiagen.com/ingenuity) was used to investigate the different involved pathways. IPA was also used to perform upstream regulator analysis, to predict the transcription factors upstream regulators.

Statistical analyses

Data are presented as the mean \pm standard error of the mean (SEM). Statistical analysis was performed with Prism 5 software, and the statistical significance of differences was determined by 2-tailed t-test with values of $p < 0.05$ considered significant for immunohistochemistry and by a Repeated ANOVA with Bonferroni's test, and values of <0.05 were considered significant for behavioral tests.

3- RESULTS

Induction of severe decrease of Eif2b5 transcripts in the oligodendrocytes of the Plp-CreERT2/Eif2b5^{fl/fl} mice treated by tamoxifen

We generated the conditional **Plp-CreERT2/Eif2b5^{fl/fl}** mouse model (Figure 1.A) in order to analyze the consequences of Eif2b5 loss preferentially in oligodendrocytes.

Our first objective was to confirm that intraperitoneal injection of 1mg of TMX, two times per day during 5 days, in 2-month-old **Plp-CreERT2/Eif2b5^{fl/fl}** females, induces a severe decrease in the expression of eif2b5 specifically in the oligodendrocytes' lineage in comparison with the control group injected with the corn oil (TMX vs Vehicle).

For this purpose we analyzed the gene expression profile of the O4+ sorted cells isolated from cerebral hemisphere homogenates of TMX versus control mice ten days after the

beginning of TMX induction (D10 PI). Using the EPIDISH software which allows to estimate the proportion of cell types using gene expression profiles, we found that the O4+ sorted cells have, for the large majority, the profile of newly formed oligodendrocytes (80 to 95%), O4 being the classical marker of this cell type (suppl figure 1 D10 PI). Identically, the cells sorted with the anti-CD11B antibodies expressed mainly microglia specific transcripts (60%) without cells having neuronal or astrocytes genes expression profiles. Almost 30% of the cells expressed transcripts characterizing OPCs. Cells sorted with the anti-ACSA2 antibody are more heterogeneous, expressing genes classically found in astrocytes (50%) but also in newly formed oligodendrocytes (40%) and oligodendrocyte precursor cells (10%). The glutamate transporter (Glast) recognized by the anti-ACSA2 antibody is the classical marker for the radial glial cells which give rise to astrocytes as well as oligodendrocyte precursor cells even in the maturing brain. When we analyzed, at 10D post induction, the expression of the mRNA corresponding to the cell specific antibodies used for the MACS in the TMX and Vehicle treated, sorted cells, no differences were found (suppl figure 2 D10 PI). The mild *plp1* expression in ACSA2+ cells is in relation with the presence of newly formed oligodendrocytes found with EPIDISH analysis. Similarly O4+ sorted cells expressed, at a low level, the *Slc1a3* mRNA encoding the GLAST transporter (ACSA2+).

We next evaluated *Eif2b5* RNA expression in O4 + cells at D10 PI (Figure 1.C, D). We found a 53% decrease in the TMX treated versus control cells (Figure 1.D). Again a limited decrease (36%) was observed in the ACSA2+ sorted cells probably related to the proportion of newly forming cells (40%) observed by EPIDISH in the ACSA2+ population. None of the other *Eif2b* RNA expression levels were modified (suppl figure 3).

In conclusion, TMX treatment induced a severe decrease in *eif2b5* expression specifically in the oligodendrocyte' lineage and particularly the newly formed premyelinating oligodendrocytes (O4+).

***Eif2b5* inactivation in the oligodendrocytes is associated with an acute motor degradation 2 months after the tamoxifen induction in the *Plp-CreERT2/Eif2b5^{fl/fl}* mice**

Nine weeks (w9) after injection, TMX treated *Plp-CreERT2/Eif2b5^{fl/fl}* mice showed an acute neurological degradation leading to death after a severe loss of weight starting from the eighth week after injection (loss of 9% of their weight compared to vehicle) to reach about 24% at w9 (8w: Vehicle=24.54±0.41, TMX=22.34±0.33, 9w: Vehicle=25.15±0.38,

TMX=19.13±0.21) compared to the vehicle group (Figure 1.E). We next evaluated *Eif2b5* RNA expression in O4 positive cells obtained by brain dissociation and magnetic-activated cell sorting, from mice 10 days after the last injection (Figure 1.C, D).

We subsequently assessed the effects of *Eif2b5* decrease on animal behavior at different times (10 days, 4 weeks and 8 weeks after TMX induction (Figure 1.C). At D10 and W4 after injection, TMX treated **Plp-CreERT2/*Eif2b5*^{fl/fl}** mice didn't show any significant difference in motor coordination compared to vehicle treated mice. In contrast, at W8 after injection, TMX treated mice showed an increased balance and motor coordination deficit compared to vehicle treated ones. The rod fall-off latencies drop at W8 PI to 30,8 ± 16,3 seconds in TMX compared to 138,6 ± 15,6 seconds in control animals (p-value=0.00001) (Figure 2.A, left graph). In addition, only at W8 PI the speed for which the mice stay in balance on the rotating rod is severely decreased in TMX treated mice compared to vehicle (Figure 2.A, right graph). Similarly, the beam balance test showed a severe deficit in the time spent on the beam, only at W8 PI, in the TMX compared to the control group (TMX =28,8 ± 3,81 seconds versus vehicle =90 ± 7.86 seconds, (p-value<0.00001)) (Figure 2.B).

Locomotor activity and muscle strength have also been assessed, and results showed respectively a decrease of the distance covered in the open field test (but not in the time spent nor the speed in the different sections of the open field) by the mice and the strength of the grip, assessed using the grip test, only at W8 after TMX injection compared to vehicle (OF distance in apparatus: TMX= 11403.05mm±2602.64, versus vehicle= 26369.82mm±2592.84, p=0.0005; 4 limbs grip strength: TMX=157.11 ±4.75g versus Vehicle= 197.08± 6.52g, p=0,00001) (Figure 2.C,E).

The spatial learning and memory of our mice model have also been tested. We observed a significant decrease –more than 50%- of the number of entries into the different arms of the Y maze in the TMX treated mice at W8 PI (TMX=15,6± 3,4 versus vehicle=28,5±2, p-value=0.015). A non-significant decrease was also observed at W4 PI in the TMX treated group. In contrast no difference was noted concerning the percentage of alternation between the three arms of the Y maze. (Figure 2.D, left and right). Moreover, we did not observe any effect of *eif2b5* decrease on anxiety in mice at the different time points of testing since no difference in speed (data not shown) nor time spent in the different sections of the elevated plus maze (EPM) was recorded, while the only significant difference was a decrease in the distance covered by the TMX treated mice compared to the vehicle ones in

the closed arms of the EPM at 8w only (TMX=3538,66±601,23 mm; versus Vehicle=6546,31±436,42 mm, p-value<0.00001) (Figure 2.F EPM left and right).

In conclusion, induced *Eif2b5* decrease in oligodendrocytes of adult mice results in a delayed (8 weeks) and acute neurological dysfunction mainly on the motor performances (locomotor activity, coordination, muscle strength) and, to a lesser extent on spatial learning and memory performances.

The observation of behavioral problems at W8 in OF, GT and Y maze and not before (at W4 or D10) could be associated to an important loss of weight and absence of anxiety, suggesting motor problems similar to what we observe in patients carrying *eif2b* mutations.

The acute motor degradation is associated, in the brain of Plp-CreERT2/*Eif2b5*^{fl/fl} treated mice, to a loss of mature oligodendrocytes with hypomyelination contrasting with the maintenance of the immature pool

We first investigated the effect of the *eif2b5* ko on the oligodendrocytes lineages in different regions of the mouse brain. At the moment of neurological degradation, W8 after injection, we found an important decrease of mature oligodendrocytes' numbers (Olig2+/CC1+ cells) in TMX treated mice in the cortex (TMX=5,47±0,22 versus Vehicle=21,35±1,67; p-value<0,0001) (Figure 3.A, B), the corpus callosum (CC) (TMX=19,68±1,32; Vehicle=75,87±1,54, p-value<0,0001) (Figure 3.C, D) and the dentate gyrus (DG) (TMX=8,98±0,54 versus Vehicle=14,31±0,42, p-value<0,0001) (Figure 3.E, F). In parallel, the level of myelin basic protein (MBP) expression by mature myelinating oligodendrocytes was significantly decreased only in the CC area (TMX=40,18±2,05; Vehicle=54,05±4,72, p-value=0,0273), (Figure 4). This finding tends to be confirmed by the slight decrease in the number of myelinated axons in the CC of the TMX treated mice compared to the control which was not significant due to the variations observed in the control group and the low number of mice (3 mice per group). Myelin structure was also clearly abnormal in the TMX treated group (Figure 4.G).

In contrast, no differences were observed in the number of immature oligodendrocytes (Olig2+/CC1-), with even a slight significant increase observed in the DG (TMX=7,98±0,37 versus Vehicle=6,40±0,55, p-value=0,0444) (Figure 3.E). In the DG, the number of

oligodendrocyte precursor cells (OPC) labeled by the neural/glial antigen 2 (NG2) were also significantly increase (TMX=7,91±0,69;versus Vehicle=5,36±0,53, p-value=0,0184) (Fig. 5E, F). In conclusion, at the time of the neurological degradation, the pool of mature myelinating oligodendrocytes is clearly decreased in the grey as well as white matter structures associated with a mild myelin loss and myelinated axons in the corpus callosum. In contrast the immature pool is maintained or even increased in the DG where neural stem cells are still present and active in the adult brain.

The acute motor degradation is associated in the brain of Plp-CreERT2/Eif2b5^{fl/fl} treated mice, to activation of astrocytes and microglial cells and mild loss of neuronal cells

We next evaluated the expression level of the astrocyte marker glial fibrillary acidic protein (GFAP). The mean GFAP+ area showed in the TMX treated brain an impressive increase (+21%) in the cortex (TMX= 17,27±1,24% versus Vehicle=0,82±0,11%, p-value < 0.0001) (Figure 6.A, B), and to a lesser extent (+2.5%) in the CC (TMX=31,04±2,86%; Vehicle=12,96±1,65%, p-value < 0.0001) (Figure 6.C, D) but not in the DG (Figure 6.E and F). In addition, these astrocytes have the morphology of reactive astrocytes. The increase in the expression level of the immature astrocytes marker, nestin in the TMX treated brain was even more extended in the CC (+5%) (TMX=2,53±0,83% versus vehicle=0,51±0,05%, p-value=0,0419) and in the DG (+1.5%) (TMX=1,75±0,10% versus vehicle=1,20±0,12%, p-value=0,0089) but not in the cortex (+2%) (TMX=1,57±0,20%; versus vehicle=0,71±0,12%,p-value=0,0062) (Figure 7).

When we used the Iba1 marker to evaluate the microglial cells we observed an increased number of positive cells in the 3 tested regions of the brain: higher in the cortex (+4.5%) (TMX=16,16±0,74 versus vehicle=3,49±0,25, p-value< 0.0001), than in the CC (+3.5%) (TMX=9,1±1,75, versus vehicle=2,6±0,16 p-value=0,0059), or in the DG (+1.8%), (TMX=10,85±0,50 versus vehicle=5,86±0,53, p-value=0,0001) (Figure 8.B, D and F). In the treated brain, the Iba1+ cells appeared with larger cell bodies and longer processes, characteristic of activated microglial cells (Figure 8.A and C).

Finally, in the TMX treated brains, the number of neurons quantified by the number of NeuN (neuronal nuclear marker) positive cells was decreased in the cortex (8%) (TMX=47,78±0,74,

versus vehicle= $55,48 \pm 0,84$, $p\text{-value} < 0,0001$) and to the same extent in the DG (7%)($TMX=41,85 \pm 0,75$, versus vehicle= $47,36 \pm 1,51$, $p\text{-value} < 0,0001$) of (Figure 9.B, D F).

In conclusion, at the time of the acute motor degradation, a large activation of mature as well as immature astrocytes and of the microglial cells is observed particularly in the cortex where a neuronal loss is observed.

Eif2b5 inactivation in the oligodendrocytes of TMX treated Plp-CreERT2/Eif2b5^{fl/fl} mice induced a chronic stress response (ISR) of the O4+ sorted cells, increasing between D10 and W8 PI

We performed RNAseq analysis of the O4+ sorted cells, isolated from the brain homogenates of TMX or vehicle treated **Plp-CreERT2/Eif2b5^{fl/fl}** mice at D10 and W8 PI and in triplicate. Then we analyzed the global differentially expressed genes (DEGs) defined as those with a fold change (FC) > 2 . At D10 79 DEGs (31 up and 48 downregulated) (Suppl table 1) were identified in the O4+ sorted cells whereas this number increases at W8 to 4155 DEGs (2376 up and 1779 downregulated genes) (Suppl table 2) (figure 10 volcano plot and Heatmap representation). In comparison, at D10 only 19 DEG (14 up and 5 down regulated) and 7 DEG (4 up and 3 down regulated) were respectively observed in the ACSA2+ and the CD11B+ sorted cells, confirming that changes related to the TMX induced eif2b5 inactivation were specifically in the oligodendrocyte lineage (suppl figure 4).

Among the genes significantly upregulated in the D10 PI O4+ sorted cells, the large majority were involved in the integrated stress response (ISR). The most significant were Chac1; Asns; Nupr1; Atf5; Trib3; Cdkn1a (Figure 11.A and table 1). Then we used Ingenuity® Pathway Analysis (IPA®) for upstream regulator analysis in order to predict the transcription factors' upstream regulators. At D10 PI the most significant was ATF4 confirming the major involvement of the endoplasmic reticulum stress response (Table 2.A and suppl table 3). None of these genes involved in the ISR were DEG in the ACSA2+ nor the CD11B+ sorted cells confirming that ISR resulting of the eIF2B decrease is specifically in the O4+ premyelinating or immature oligodendrocytes.

When we analyzed the 15 ISR genes among the 4155 DEG in the W8 PI O4+ sorted cells we found that all of them were present and upregulated (except one) (Figure 11.A). Chac1 and Trib3 remain the two genes with the highest \log_2 fold change. Interestingly Atf3 and Atf4

were differentially expressed at W8 and not at D10 PI whereas Atf5 was upregulated at D10 PI but not at W8 PI.

In conclusion, in our model eIF2B inactivation induced early gene expression changes specifically of the O4+ sorted cells related, as expected, to ISR activation. Subsequently ISR becomes chronic and is largely increased in the O4+ at the time of the acute motor degradation.

Eif2b5 inactivation in the oligodendrocytes of TMX treated Plp-CreERT2/Eif2b5^{fl/fl} mice induced change in the cell type gene expression profile of the O4+ sorted cells toward microglial cells with activation of genes involved in inflammations

In order to analyze the gene expression reprogramming related to the increasing ISR, we compared the cell type gene expression profile of the O4+ sorted cells between D10 and W8 PI using the EPIDISH software (Suppl figure 1). Gene expression profile of the O4+ sorted cells isolated at W8 PI from the mice brain demonstrated severe changes in TMX treated samples with 15% of cells expressing a microglial gene expression profile never observed in the control samples, 10% of cells with an OPC and 10% with an endothelial cells gene expression profile rarely observed in the control cells (suppl figure 1). These findings were confirmed by the low plp1 expression and the high Itgam expression observed in the O4+ sorted cells from TMX versus control brain at W8 PI but not at D10 PI (suppl figure 2).

Finally the list of the top 20 up regulated genes in O4+ sorted cells of TMX versus control mice at W8 PI (Table 1) revealed a number of genes with established roles in inflammatory processes such: Spp1, Bpifc, Pdcd1, Fosl1, Cd5l, and Atp6v0d2. A large number of cytokines are differentially expressed in the TMX treated O4 pool in comparison with the control group (Figure 11 B). Among them, TNF alpha is largely upregulated as well as its receptors, the Tnfrsf1b with a higher fold change than the Tnfrsf1a. Genes encoding the receptors for Interferon gamma (IFN γ) (Ifngr1 and Ifngr2) and for CSF2 (Csf2ra, Csf2rb, Csf2rb2) are also activated.

To investigate the pathways involved in the acute neurological degradation, we applied IPA[®] tool to the DEGs found in the O4+ sorted cells by taking $-\log(p\text{-value})$ threshold at 1.3 and z-score at 2 (Figure 12.B and Suppl table 4). The significant canonical activated pathways with a z-score ≥ 2 were involved in (i) inflammation (Neuroinflammation Signaling Pathway (NF- κ B Signaling)), (ii) Production of Nitric Oxide and Reactive Oxygen Species in Macrophages

(STAT3 Pathway) (Figure 12.B). On the other hand the significant canonical suppressed pathways with a z-score ≤ 2 involved (i) Cell Cycle (G2/M DNA Damage Checkpoint Regulation), (ii) Synaptogenesis Signaling Pathway, (iii) Fcγ Receptor-mediated Phagocytosis in Macrophages and Monocytes (Figure 12.B).

The IPA® for upstream regulator analysis revealed, among the most significant pathways, IFN γ , TNF and CSF2 (Table 2.B and suppl table 5).

In conclusion, eIF2B inactivation induced inflammatory response (TNF, IFN γ , NF- κ B Signaling) in the O4+ sorted cells at the time of the acute motor degradation.

4- DISCUSSION

In this work we prove the importance and the efficiency of our model to induce Eif2b5 inactivation in the oligodendrocytes lineage. We found a specific and severe decrease of the eif2b5 expression as well as an activation of the ISR including ATF4 dependent genes in the O4 premyelinating oligodendrocytes isolated from the brain homogenates of the TMX treated mice. Interestingly, motor as well as cognitive tests of the mice were normal until the 8 week post induction where an acute motor degradation with severe weight loss is observed, sacrificing of the animal in one week. The time course of this acute degradation was remarkably constant in female as well as males. Motor difficulties are frequently the first clinical symptoms of CACH/VWM during childhood with an acute onset in 50% of cases occurring frequently after head trauma or banal viral infection (Fogli et al., 2004). Acute neurological distress with coma is even observed. Acute inflammatory disorder of the white matter is frequently the differential diagnosis in children when the MRI characteristics of CACH/VWM are not noticed. In the juvenile/adult onset forms acute onset with paralysis is more rarely found (14%). Exacerbating disease course was described in 82% of patients (median number of episodes 3). In 99% of patients, episodes involved motor problems, most often gait problems (Hamilton et al., 2018). In the juvenile/adult forms, the relapsing remitting episodes with a progressive course could suggest a multiple sclerosis (MS) (Labauge et al., 2015). These acute, sometimes stress-induced, episodes which represent one of the clinical characteristics of CACH/VWMD have never been observed in the different eIF2B KI rodent mutants reported until now including in the most severe progressive form

observed in the double homozygous mutants $Eif2b5^{Arg191His/Arg191His}/Eif2b4^{Arg484Trp/Arg484Trp}$ (Dooves et al 2016).

Moreover, at the time of this acute degradation, we found in the brain of the TMX treated mice a decrease in the number of myelinating oligodendrocytes associated with a mild hypomyelination but with the persistence or even the increase number of immature oligodendrocytes including OPC. This contrast suggests a blockade in the maturation of the oligodendrocytes which is one of the neuropathological characteristic of the less affected white matter lesions of CACH/VWM brains (Rodriguez et al 1999, Brück et al., 2001, Bugiani 2011, Huyghe et al 2012).

The paucity of astrogliosis despite severe global white matter degeneration and the abnormal morphology of astrocytes in affected white matter areas are exquisitely typical of VWM (Bugiani 2018). At the opposite, in our model with a restricted eIF2B inactivation to oligodendrocytes, we observed an astrogliosis particularly in the cortex. This observation confirms that the astrocytes are also a target of the eIF2B dysfunction with abnormal astrocytes maturation leading to the mislocalization of Bergmann glia in the cerebellum (Dooves 2018, Bugiani 2018).

Therefore our results clearly demonstrated that the impaired EIF2B activity of oligodendrocytes plays also a major role in the neurological distress observed in the majority of CACH/VWM patients. This is in accordance with the myelin loss and abnormal oligodendrocytes reported in the Plp/Fv2E-PERK transgenic mice with a PERK activation specifically in oligodendrocytes (Lin et al., 2014).

We performed glial cell specific transcriptomic analysis in order to determine the cellular pathways' changes at the time of the acute neurological deterioration. For this purpose, we used MACS cell sorting with different antibodies: anti-ACSA2+ antibodies recognizing the Glutamate transporter specific of astrocytes and radial glia cells, anti-O4 antibodies a glycoprotein present at the surface of the premyelinating oligodendrocytes and anti-CD11B antibodies present at the surface of the microglial cells. We pooled 6 cerebral hemispheres in order to obtain the 3 types of cell sorting from the same brain homogenates. For each group of mice (TMX treated versus vehicle) three distinct pools of brain homogenates were used in order to obtain transcriptomic analysis in triplicate for each glial cell types. This protocol allowed a robust reproducibility in the gene expression profile of the same cell type, the O4+ sorted cells being mainly premyelinating oligodendrocytes, the CD11B+ sorted

cells being microglial cells and ACSA2+ sorted cells with astrocytes or premyelinating oligodendrocytes gene expression profile. We then confirmed that the O4+ sorted cells were the target of the eif2b5 inactivation with a 50% decrease in the eif2b5 expression only in the O4+ cells isolated from the mice brain, 10 days after the TMX induction. The cellular effect of this impaired eIF2B activity was assessed by the up regulation of the genes involved in the ISR and ATF4 dependent specifically in the D10 PI O4+ sorted cells. Eight weeks after the TMX induction, when the sudden neurological deterioration occurs, the intensity and number of the up regulated ISR genes has specifically increased in the O4+ sorted cells demonstrating that the impaired eIF2B activity has induced, in the O4+ premyelinating oligodendrocytes, a chronic ISR (Guan et al., 2017); Our results are in agreement with the chronic ISR response recently reported in the homozygous KI mice $Eif2b5^{R132H/R132H}$ (Wong et al., 2019). This strain of mice developed a spontaneous progressive motor deficit between 3 and 5 months of age. A severe myelin loss (33 to 50%) with a significant increase in the number of Olig2+ cells, an astrogliosis and microglial activation are observed in the spinal cord and brain at the sacrifice (5-8 months). ISR up regulation is observed in the cerebellum as early as 2 months and increases at 5 -7 months particularly the Trb3 and Chac1 transcripts identically to our mice model. Trb3 is considered as a negative feedback regulator of the ATF4 dependent transcription and participates in the fine regulation of the ISR (Jousse et al., 2007). When they performed single cells RNAseq in the forebrain and cerebellum of 2 month old mice, they found that the ISR signature was restricted to astrocytes (Bergman glia) but also in cells with myelinating oligodendrocytes and endothelial cells' signatures.

In our model, the high chronic ISR specifically observed in the O4+ cells obtained from TMX treated mice brains were associated with changes in the gene expression profile of the cells, confirming the transcriptional reprogramming under chronic stress conditions (Guan et al., 2017). Interestingly these changes tend to push the cell program toward the expression of genes found in more immature oligodendrocytes such as OPC and in microglia cells. No changes are observed in the CD11B+ sorted cells and to a minor extend in the ACSA2+ sorted cells.

Confirming the “microglial” gene expression profile changes of the ER stressed O4+ cells, we found a large activation of the genes involved in the neuroinflammation signaling pathway (NF- κ B), particularly the genes under the control of the TNF alpha, the IFN gamma and the SC2. These results clearly demonstrated, for the first time, a direct link between chronic ER

stress and inflammatory response in the immature oligodendrocytes. When we compare the DEG of our stressed O4+ cells with those obtained in the MOG model of EAE (Raddatz et al., 2014), our stressed O4+ cells share only 43 upregulated genes observed during the acute phase of the MOG-induced EAE (suppl figure 5), 21 being involved in the immune system, 18 in the cytokines signaling pathway and 10 in the cell homeostasis.

Premyelinating and oligodendrocyte progenitor cells are increasingly being recognized for their roles other than differentiating into oligodendrocytes during remyelination. OPCs morphologically respond to injury in a way comparable to microglia, they secrete cytokines and they regulate scar formation. In these capacities, OPC are considered as an alternative CNS-innate immune cell. (Baaklini et al., 2019). Our findings emphasized the key role of the chronic stress in this “microglial” transformation of the premyelinating cells leading to a defect in their myelination program as observed in the CACH/VWM brains. The acute neurological impairment and the relapsing remitting episodes observed in CACH/VWMD as well as in MS could result of this adaptive mechanism. The great adaptability of the OPC would permit an excellent tolerability until a threshold is reached leading the apparent on/off effect observed. The provocative effect of various stress situations including emotional stress is in favor of this threshold effect.

Many situations can induce a decrease in the EIF2 activity. The severity of this defect as well as the capacity of the OPC to switch from an acute to a chronic ISR could be the trigger for a chronic neuroinflammation. Major environmental (geographic latitude , tobacco exposure, obesity, and virus...) and genetic (mainly immune-pathway genes) risk factors have been associated with an enhanced risk of multiple sclerosis. All risk factors could be the trigger of chronic ISR.

Further analyses are need in order to confirm this stress trigger hypothesis. These would open new avenues in the treatment of both CACH/VWM and MS. Our model is a unique model to test the therapeutic effect of molecules targeting this chronic ISR-inflammatory pathway.

5- CONCLUSION

Our work emphasized the key role of the oligodendrocytes in the pathophysiological mechanisms of CACH/VWMM. Impaired EIF2B activity specifically in oligodendrocytes induced a chronic ISR able to provoke an acute neurological distress when reaching a certain level. One trigger seems to involve an adaptive immune transformation of the non myelinating O4+ oligodendrocytes with a secondary block in their myelinating capacity. This opens new insights in the understanding and treatment of chronic inflammatory white matter diseases.

6- ACKNOWLEDGMENTS

We thank Zsolt CSABA, Justine GUEGUIN, Radmila PANIC for excellent technical support. We acknowledge grant support of Association RHAGENE.

7- Compliance with ethical standards

The authors declare that they followed the ethical standards for all studies

8- Conflict of interest

The authors have no conflict of interest to declare

References

- Abbink, T.E.M., Wisse, L.E., Wang, X., Proud, C.G., 2018. Role of Eukaryotic Initiation Factor eIF2B in Vanishing White Matter Disease, in: Sossin, W. (Ed.), *The Oxford Handbook of Neuronal Protein Synthesis*. Oxford University Press
- Baaklini, C. S., Rawji, K. S., Duncan, G. J., Ho, M. F. S., & Plemel, J. R. (2019). Central Nervous System Remyelination: Roles of Glia and Innate Immune Cells. *Frontiers in Molecular Neuroscience*, 12, 225. <https://doi.org/10.3389/fnmol.2019.00225>
- Brück, W., Herms, J., Brockmann, K., Schulz-Schaeffer, W., & Hanefeld, F. (2001). Myelinopathia centralis diffusa (vanishing white matter disease): Evidence of apoptotic oligodendrocyte degeneration in early lesion development: Oligodendrocyte Apoptosis in Leukoencephalopathy. *Annals of Neurology*, 50(4), 532–536. <https://doi.org/10.1002/ana.1227>

Bugiani, M., Boor, I., van Kollenburg, B., Postma, N., Polder, E., van Berkel, C., ... van der Knaap, M. S. (2011). Defective Glial Maturation in Vanishing White Matter Disease. *Journal of Neuropathology & Experimental Neurology*, 70(1), 69–82. <https://doi.org/10.1097/NEN.0b013e318203ae74>

Bugiani, M., Vuong, C., Breur, M., & van der Knaap, M. S. (2018). Vanishing white matter: A leukodystrophy due to astrocytic dysfunction: Vanishing White Matter. *Brain Pathology*, 28(3), 408–421. <https://doi.org/10.1111/bpa.12606>

Dobin, Alexander, et al. "STAR: ultrafast universal RNA-seq aligner." *Bioinformatics* 29.1 (2013): 15-21.

Dooves, S., Bugiani, M., Postma, N.L., Polder, E., Land, N., Horan, S.T., van Deijk, A.-L.F., van de Kreeke, A., Jacobs, G., Vuong, C., Klooster, J., Kamermans, M., Wortel, J., Loos, M., Wisse, L.E., Scheper, G.C., Abbink, T.E.M., Heine, V.M., van der Knaap, M.S., 2016. Astrocytes are central in the pathomechanisms of vanishing white matter. *Journal of Clinical Investigation* 126, 1512–1524.

Dooves, S., Bugiani, M., Wisse, L.E., Abbink, T.E.M., van der Knaap, M.S., Heine, V.M., 2018. Bergmann glia translocation: a new disease marker for vanishing white matter identifies therapeutic effects of Guanabenz treatment. *Neuropathol Appl Neurobiol* 44, 391–403.

Dooves, S., Leferink, P.S., Krabbenborg, S., Breeuwsma, N., Bots, S., Hillen, A.E.J., Jacobs, G., van der Knaap, M.S., Heine, V.M., 2019. Cell Replacement Therapy Improves Pathological Hallmarks in a Mouse Model of Leukodystrophy Vanishing White Matter. *Stem Cell Reports* 12, 441–450.

Fogli, A., Schiffmann, R., Bertini, E., Ughetto, S., Combes, P., Eymard-Pierre, E., Kaneski, C.R., Pineda, M., Troncoso, M., Uziel, G., Surtees, R., Pugin, D., Chaunu, M.-P., Rodriguez, D., Boespflug-Tanguy, O., 2004. The effect of genotype on the natural history of eIF2B-related leukodystrophies. *Neurology* 62, 1509–1517

Gat-Viks, I., Geiger, T., Barbi, M., Raini, G., Elroy-Stein, O., 2015. Proteomics-level analysis of myelin formation and regeneration in a mouse model for Vanishing White Matter disease. *J. Neurochem.* 134, 513–526.

Geva, M., Cabilly, Y., Assaf, Y., Mindroul, N., Marom, L., Raini, G., Pinchasi, D., Elroy-Stein, O., 2010. A mouse model for eukaryotic translation initiation factor 2B-leucodystrophy reveals abnormal development of brain white matter. *Brain* 133, 2448–2461.

Guan BJ, van Hoef V, Jobava R, Elroy-Stein O, Valasek LS, Cargnello M, Gao XH, Krokowski D, Merrick WC, Kimball SR, Komar AA, Koromilas AE, Wynshaw-Boris A, Topisirovic I, Larsson O, Hatzoglou M. *Mol Cell.* 2017 Dec 7;68(5):885-900.e6. A Unique ISR Program Determines Cellular Responses to Chronic Stress.

Hamilton, E.M.C., van der Lei, H.D.W., Vermeulen, G., Gerver, J.A.M., Lourenço, C.M., Naidu, S., Mierzewska, H., Gemke, R.J.B.J., de Vet, H.C.W., Uitdehaag, B.M.J., Lissenberg-Witte, B.I., VWM Research Group, van der Knaap, M.S., 2018. Natural History of Vanishing White Matter: Natural History of VWM. *Ann Neurol.* 84, 274–288.

Hanefeld, F., Holzbach, U., Kruse, B., Wilichowski, E., Christen, H., Frahm, J., 1993. Diffuse White Matter Disease in Three Children: An Encephalopathy with Unique Features on Magnetic Resonance Imaging and Proton Magnetic Resonance Spectroscopy.

Huyghe, A., Horzinski, L., Hénaut, A., Gaillard, M., Bertini, E., Schiffmann, R., ... Fogli, A. (2012). Developmental Splicing Deregulation in Leukodystrophies Related to EIF2B Mutations. *PLoS ONE*, 7(6), e38264. <https://doi.org/10.1371/journal.pone.0038264>

Jousse, C., Deval, C., Maurin, A.-C., Parry, L., Chérasse, Y., Chaveroux, C., ... Fafournoux, P. (2007). TRB3 Inhibits the Transcriptional Activation of Stress-regulated Genes by a Negative Feedback on the ATF4 Pathway. *Journal of Biological Chemistry*, 282(21), 15851–15861. <https://doi.org/10.1074/jbc.M611723200>

Jungblut, M., Tiveron, M. C., Barral, S., Abrahamsen, B., Knöbel, S., Pennartz, S., Bosio, A. (2012). Isolation and characterization of living primary astroglial cells using the new GLAST-specific monoclonal antibody ACSA-1. *Glia*, 60(6), 894–907. <https://doi.org/10.1002/glia.22322>

Klok, M.D., Bugiani, M., de Vries, S.I., Gerritsen, W., Breur, M., van der Sluis, S., Heine, V.M., Kole, M.H.P., Baron, W., van der Knaap, M.S., 2018. Axonal abnormalities in vanishing white matter. *Ann Clin Transl Neurol* 5, 429–444.

Lin, Y., Pang, X., Huang, G., Jamison, S., Fang, J., Harding, H.P., Ron, D., Lin, W., 2014. Impaired Eukaryotic Translation Initiation Factor 2B Activity Specifically in Oligodendrocytes Reproduces the Pathology of Vanishing White Matter Disease in Mice. *Journal of Neuroscience* 34, 12182–12191.

Pavitt, G. D. (2005). EIF2B, a mediator of general and gene-specific translational control. *Biochemical Society Transactions*, 33, 6.

Raddatz, B. B. R., Hansmann, F., Spitzbarth, I., Kalkuhl, A., Deschl, U., Baumgärtner, W., & Ulrich, R. (2014). Transcriptomic Meta-Analysis of Multiple Sclerosis and Its Experimental Models. *PLoS ONE*, 9(1), e86643. <https://doi.org/10.1371/journal.pone.0086643>

Raini, G., Sharet, R., Herrero, M., Atzmon, A., Shenoy, A., Geiger, T., Elroy-Stein, O., 2017. Mutant eIF2B leads to impaired mitochondrial oxidative phosphorylation in vanishing white matter disease. *J. Neurochem.* 141, 694–707.

Rodriguez, D., Gelot, A., della Gaspera, B., Robain, O., Ponsot, G., Sarliève, L.L., Ghandour, S., Pompidou, A., Dautigny, A., Aubourg, P., Pham-Dinh, D., 1999. Increased density of oligodendrocytes in childhood ataxia with diffuse central hypomyelination (CACH) syndrome: neuropathological and biochemical study of two cases. *Acta Neuropathologica* 97, 469–480.

Schiffmann, R., Moller, J.R., Trapp, B.D., Shih, H.H.-L., Farrer, R.G., Katz, D.A., Alger, J.R., Parker, C.C., Hauer, P.E., Kaneski, C.R., Heiss, J.D., Kaye, E.M., Quarles, R.H., Brady, R.O., Barton, N.W., 1994. Childhood ataxia with diffuse central nervous system hypomyelination. *Ann Neurol.* 35, 331–340.

Teschendorff AE, Breeze CE, Zheng SC, Beck S (2017). "A comparison of reference-based algorithms for correcting cell-type heterogeneity in Epigenome-Wide Association Studies." *BMC bioinformatics*, 18(1), 105.

van der Knaap, M.S., Barth, P.G., Gabreels, F.J.M., Franzoni, E., Begeer, J.H., Stroink, H., Rotteveel, J.J., Valk, J., 1997. A new leukoencephalopathy with vanishing white matter. *Neurology* 48, 845–854.

Van der Knaap, M.S., Fogli, A., Boespflug-Tanguy, O., Abbink, T.E., 2019. Childhood Ataxia with Central Nervous System Hypomyelination / Vanishing White Matter.

Zhang X, Zhang G, Zhang H, Karin M, Bai H, Cai D. Hypothalamic IKKbeta/NF-kappaB and ER stress link overnutrition to energy imbalance and obesity. *Cell*. 2008;135:61–73.

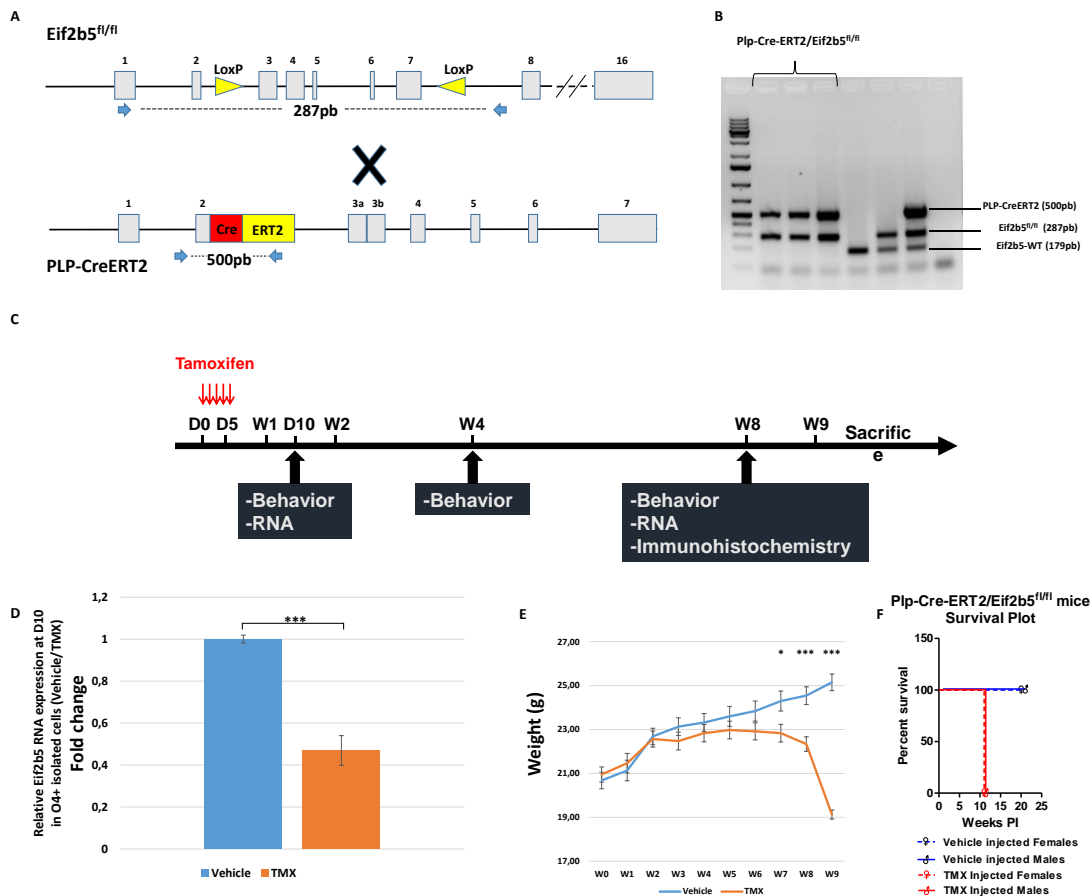


Figure 1: Generation of *Plp-Cre-ERT2/Eif2b5*^{fl/fl} mice: A, 2 *LoxP* sites were inserted around exons 3 and 7 of the *eif2b5* gene giving birth to the *Eif2b5*^{fl/fl} mice which were then cross-bred with *PLP-CreERT2* mice generated by fusing the *CreERT2* cDNA to exon 2 of the *plp* gene to generate the *Plp-Cre-ERT2/Eif2b5*^{fl/fl} mice. B, expected PCR products for *Plp-Cre-ERT2/Eif2b5*^{fl/fl} mice genotyping are 500pb for *PLP-CreERT2* and 287pb for *Eif2b5*^{fl/fl}. C, Tamoxifen treatment protocol 1mgx2/day for 5 days IP showing time-points corresponding to each analysis done. D, RNA-seq analysis showed a 53% decrease of *Eif2b5* mRNA at D10 in Tamoxifen treated mice (Fc=0,47) compared to Vehicle treated ones (Fc=1) with $p < 0.0001$. E, Weight plot following 28 tamoxifen injected and 27 vehicle injected *Plp-Cre-ERT2/Eif2b5*^{fl/fl} mice over 9 weeks. W0 represents the beginning of treatment at 2 months of age. The plot shows a sudden weight loss at W8-W9 with $p < 0,0001$. F, Survival plot for the *Plp-Cre-ERT2/Eif2b5*^{fl/fl} mice including males and females for both vehicle and TMX injected mice. TMX injected female and male mice all die at week 11 post injection (PI), while Vehicle injected ones survive normally until sacrificed at week 20 PI.

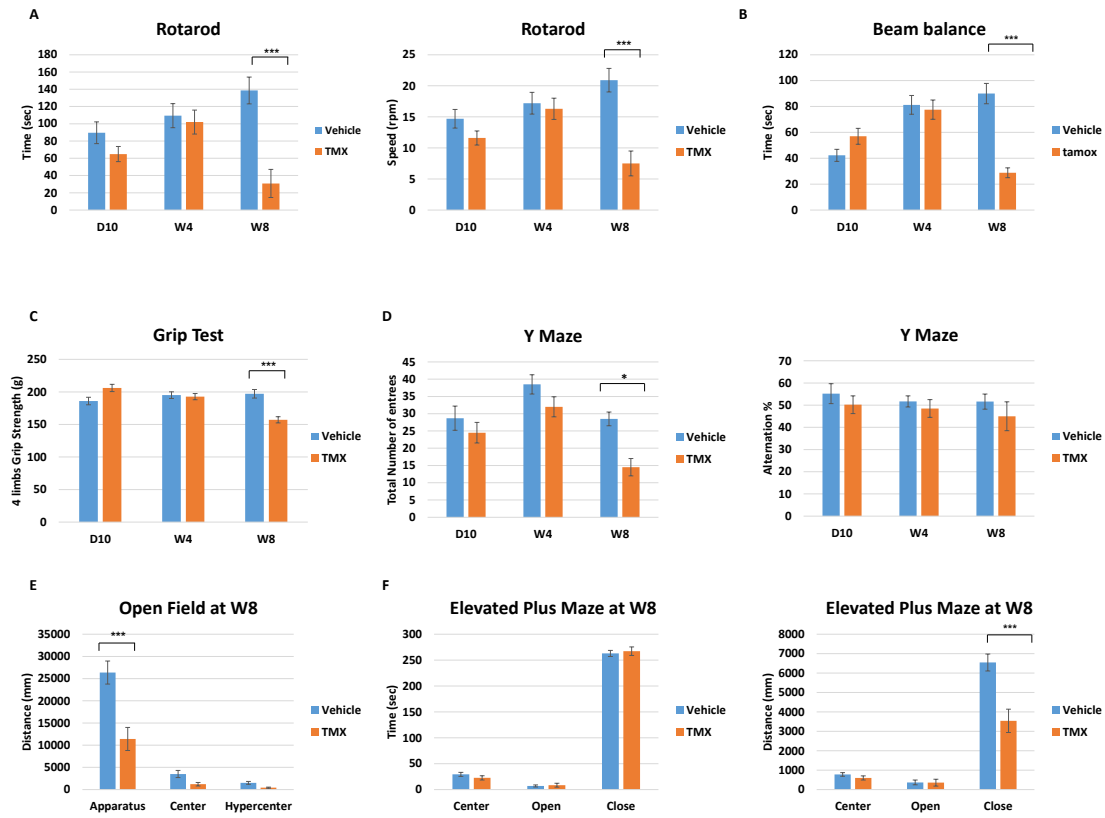


Figure 2: Behavior assessment

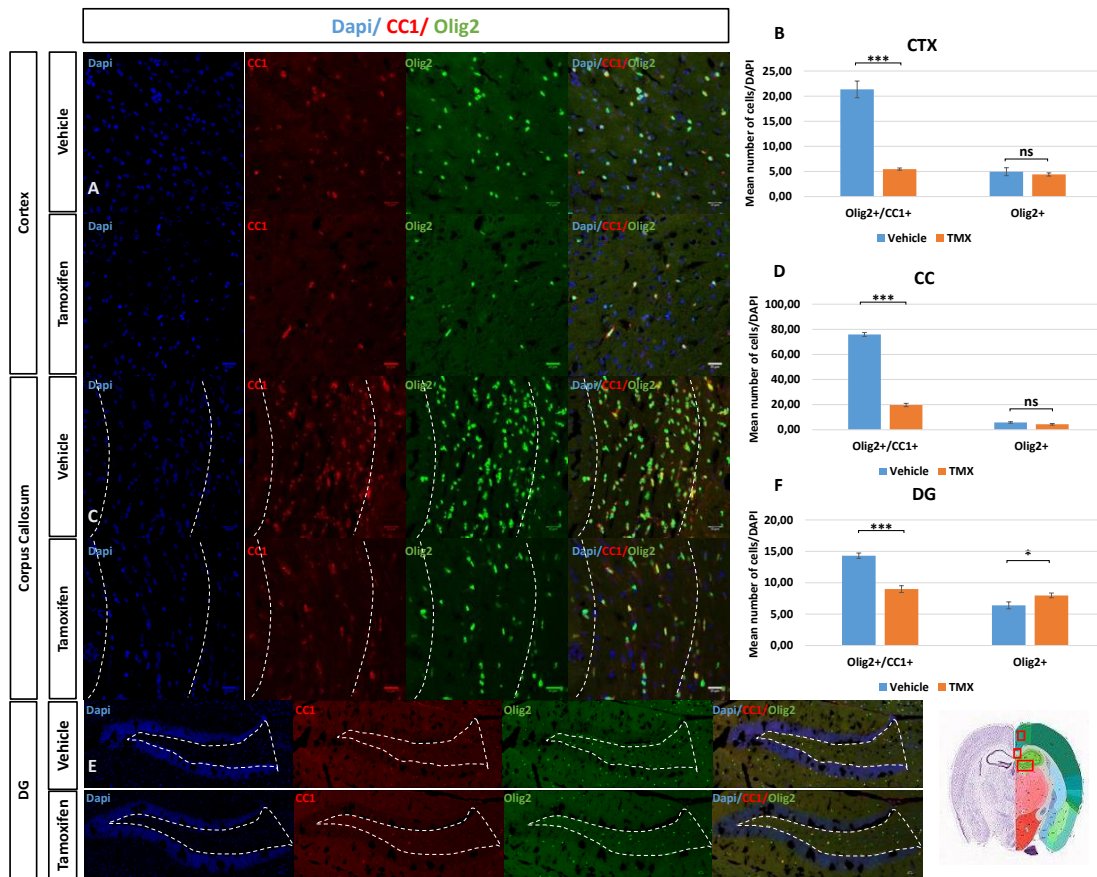


Figure 3: Alterations in percentage of mature and immature oligodendrocytes in tamoxifen injected *Plp-Cre-ERT2/Eif2b5^{fl/fl}* mice. Olig2 and CC1 double-labelling showed a strong decrease in mature oligodendrocytes (Olig2+/CC1+ cells) percentage in Cortex area with $p < 0.0001$ (A, B), Corpus Callosum area with $p < 0.0001$ (C, D), and Dentate Gyrus Area with $p < 0.0001$ (E, F), while an increase in immature oligodendrocytes (Olig2+/CC1- cells) percentage was observed only in the Dentate Gyrus area with $p = 0.04$ (E, F). Number of oligodendrocyte cells was normalized over total number of cells (Dapi+ cells). $N = 5$ animals. TMX = Tamoxifen. Error bars represent Standard Error of the Mean (SEM). * = $P < 0.05$, *** = $P < 0.001$, ns = non significant. Scalebar = 25 μm .

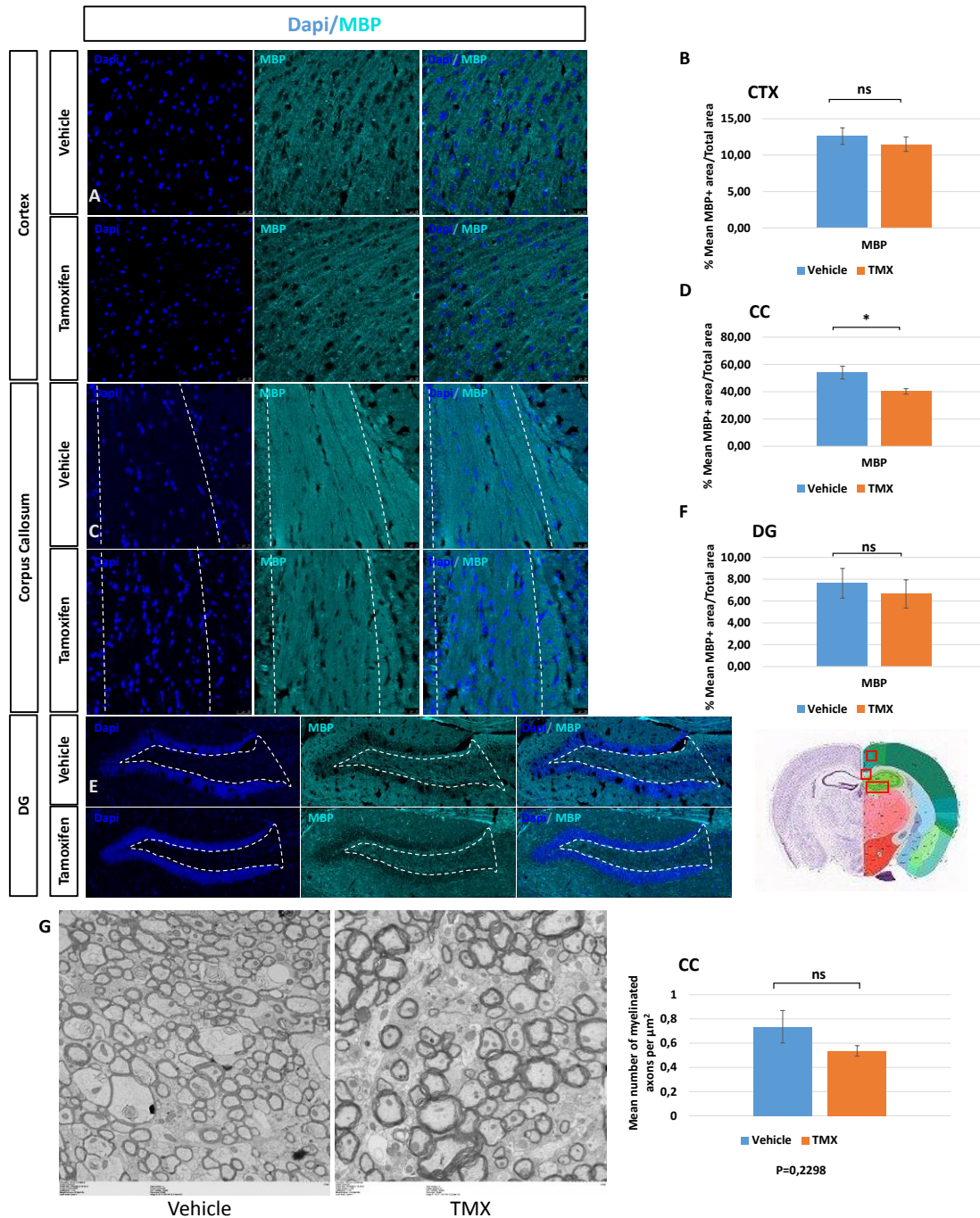
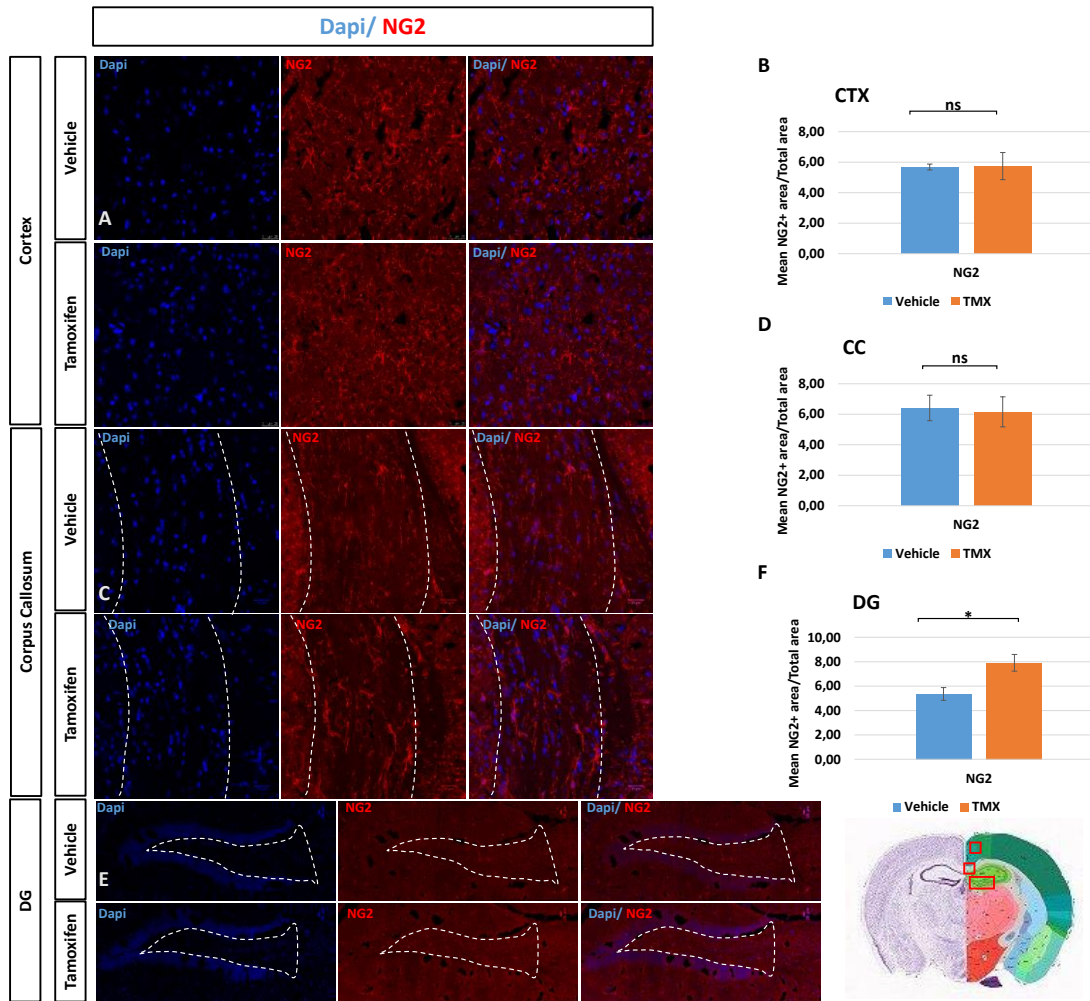


Figure 4: Alterations in Myelin Basic Protein (MBP) expression in tamoxifen injected *Plp-Cre-ERT2/Eif2b5^{fl/fl}* mice. MBP-labelling showed a decrease of the expression level only in the Corpus Callosum area ($p=0,027$) (C, D), while no difference was noted in the Cortex area ($p=0,48$) (A, B) nor the Dentate Gyrus area ($p=0,62$) (E, F). (G), Electron microscopy showing axons and myelin sheaths in Corpus callosum area of *Plp-Cre-ERT2/Eif2b5^{fl/fl}* mice in addition to myelinated axons quantification (Mean number of myelinated axons/ μm^2). Expression level of MBP was normalized over total area scanned. $N=5$ animals. TMX=Tamoxifen. Error bars represent Standard Error of the Mean (SEM). * = $P < 0.05$, ns= non significant. Scalebar = 25 μm .



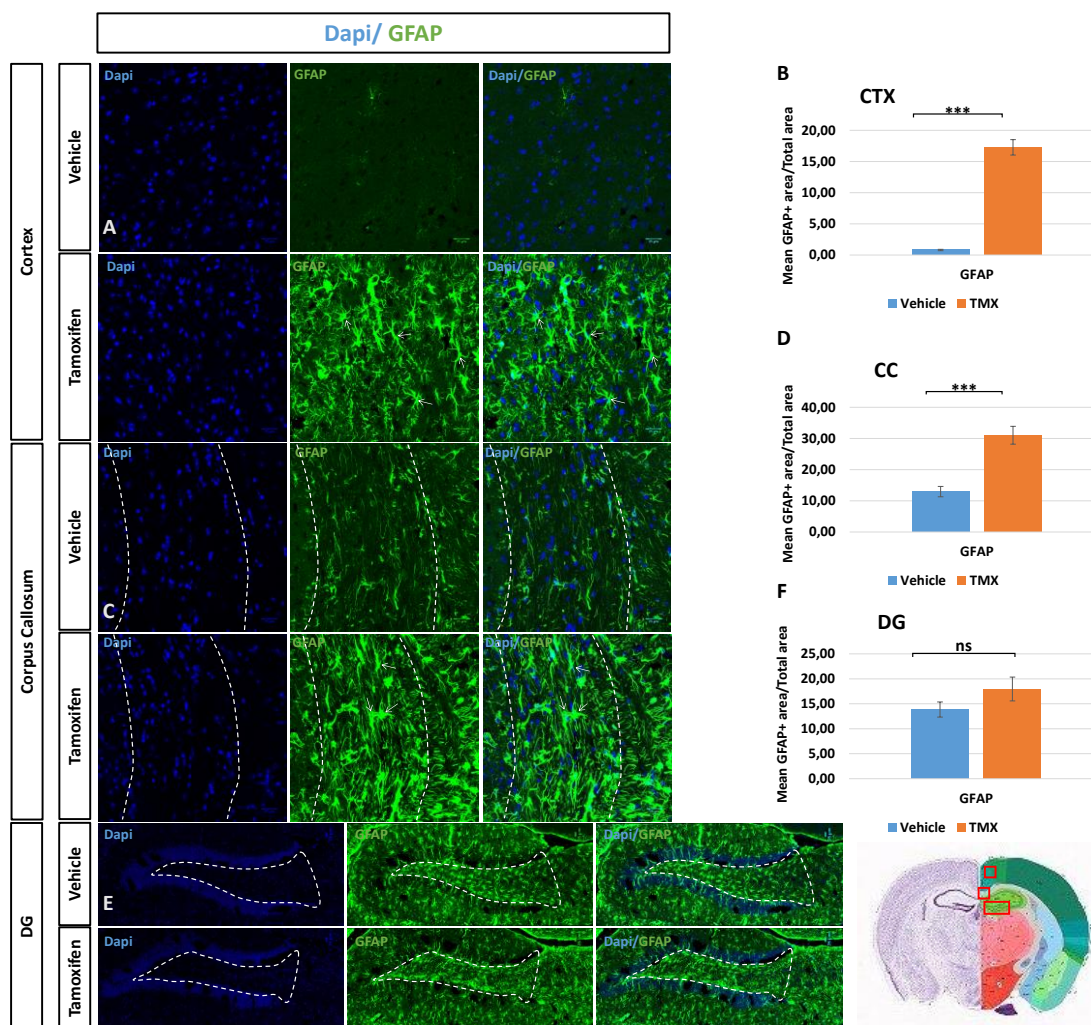


Figure 6: Alterations in astrocyte cell marker's expression in tamoxifen injected Plp-Cre-ERT2/Eif2b5^{fl/fl} mice. GFAP-labelling showed a strong increase in GFAP expression in Cortex area ($p < 0.0001$) (A, B) and Corpus Callosum area ($p = 0.0006$) (C, D), but not in Dentate Gyrus Area ($p = 0.1842$) (E, F). Expression level of GFAP was normalized over total area scanned. N=5 animals. TMX=Tamoxifen. Error bars represent Standard Error of the Mean (SEM). *** = $P < 0.001$, ns= non significant. Scalebar = 25 μm .

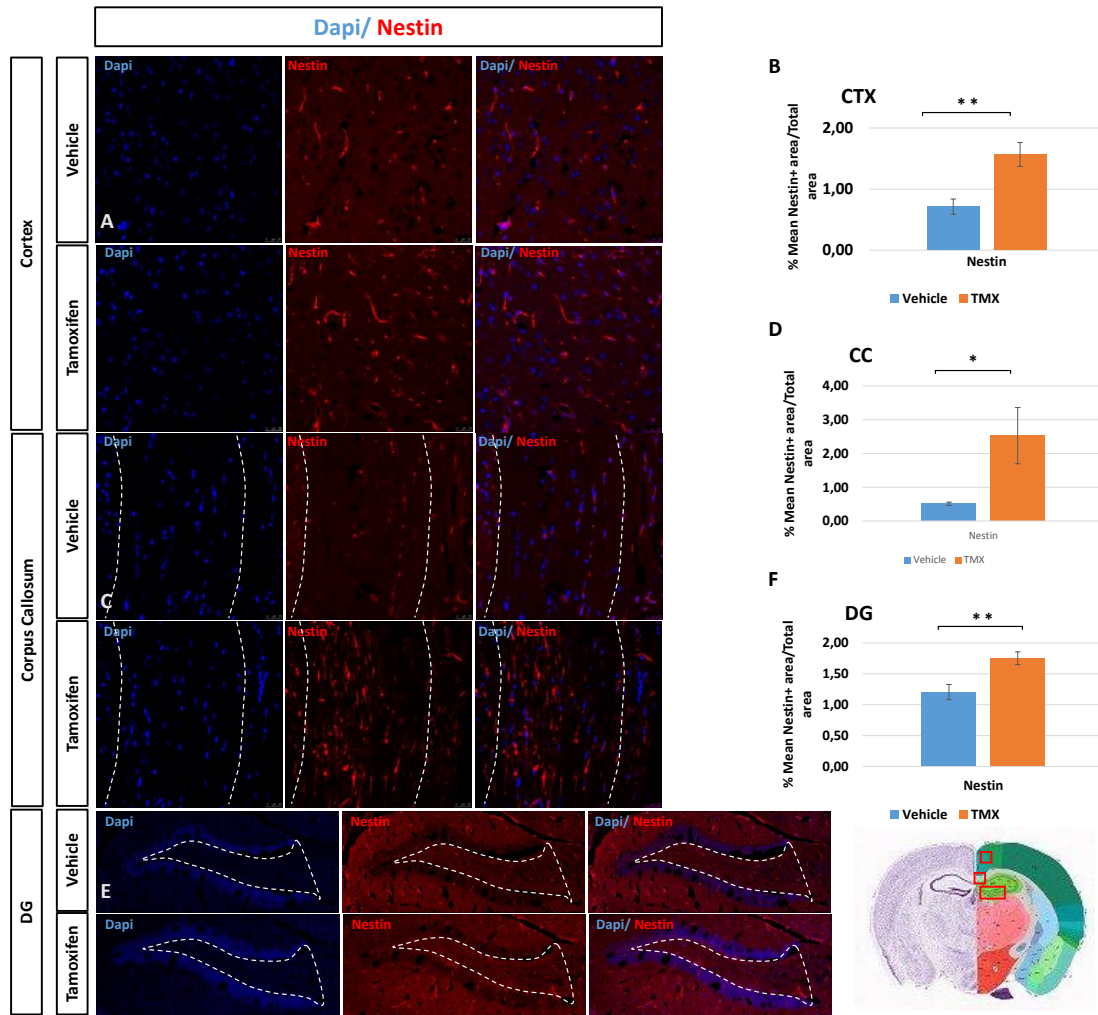


Figure 7: Alterations in Nestin expression in tamoxifen injected *Plp-Cre-ERT2/Eif2b5^{fl/fl}* mice. Nestin-labelling showed a strong increase in Nestin expression in the Cortex area ($p=0,006$) (A, B), the Corpus Callosum area ($p=0,042$) (C, D), and the Dentate Gyrus area ($p=0,009$) (E, F). Expression level of Nestin was normalized over total area scanned. $N=5$ animals. TMX=Tamoxifen. Error bars represent Standard Error of the Mean (SEM). * = $P < 0.05$, **= $P < 0.01$. Scalebar = 25 μm .

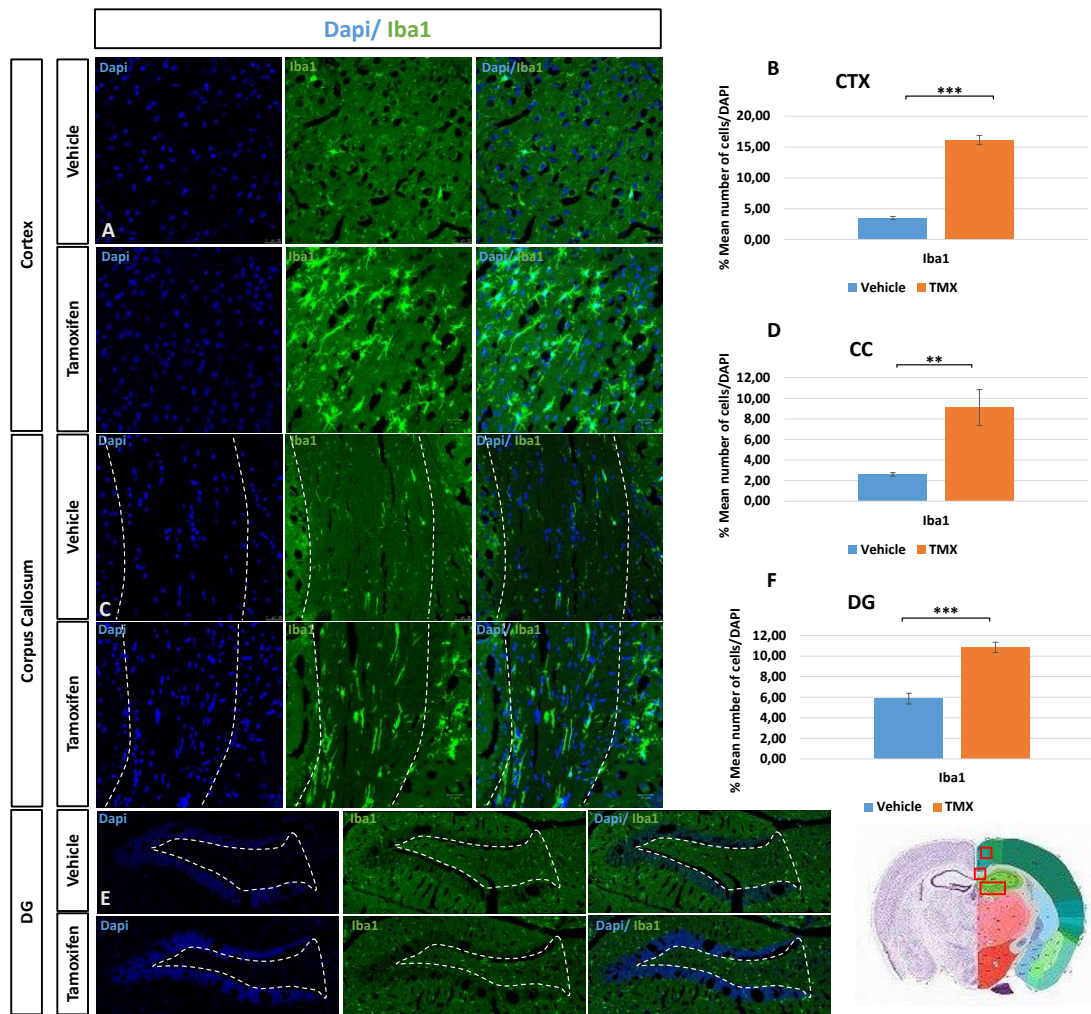
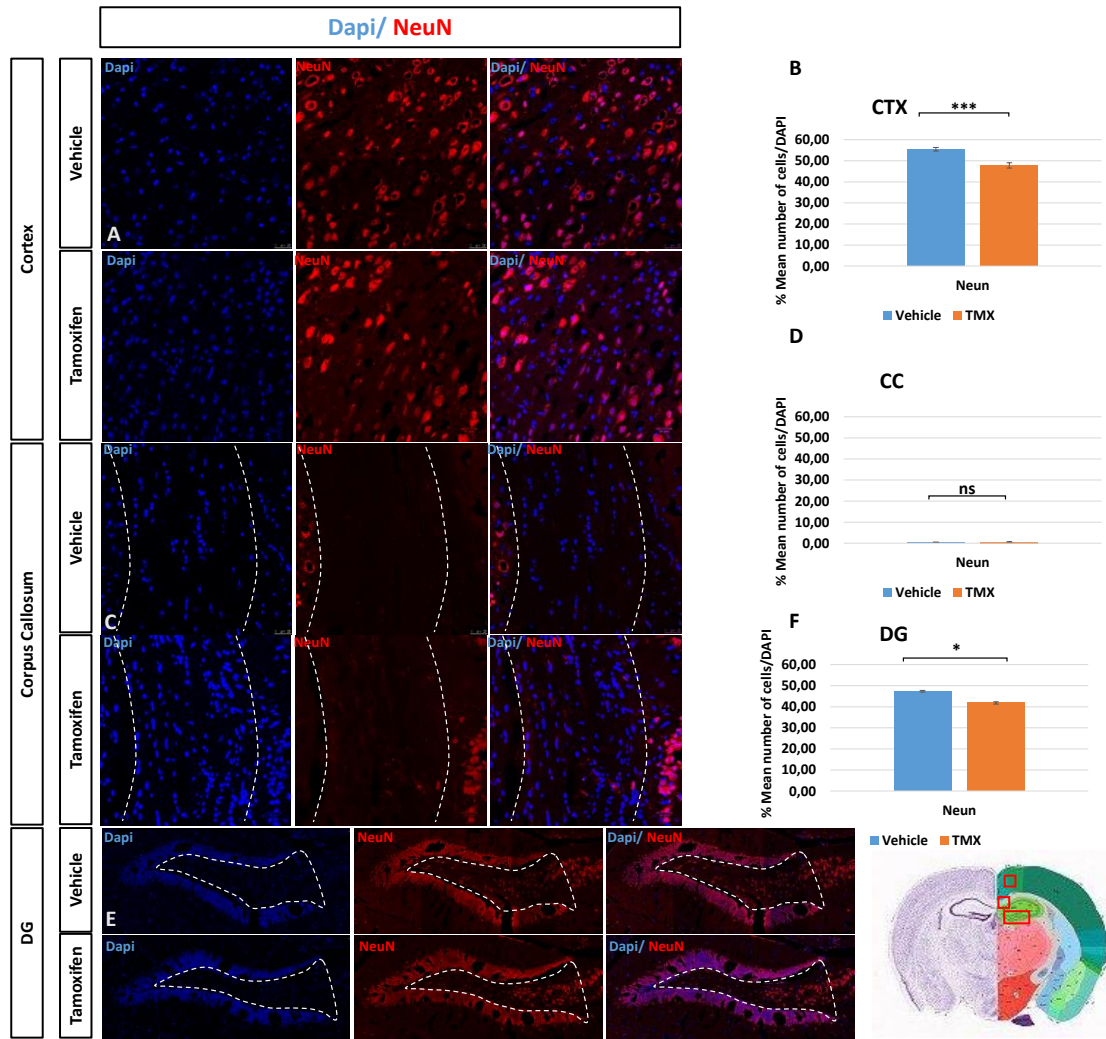


Figure 8: Alterations in percentage of microglial cell numbers in tamoxifen injected *Plp-Cre-ERT2/Eif2b5^{fl/fl}* mice. *Iba1*-labelling showed a strong increase in microglial cell numbers (*Iba1*+ cells) percentage in Cortex area ($p < 0.0001$) (A, B), Corpus Callosum area ($p = 0.0059$) (C, D), and Dentate Gyrus Area ($p = 0.0001$) (E, F). Number of microglial cells was normalized over total number of cells (*Dapi*+ cells). $N = 5$ animals. TMX=Tamoxifen. Error bars represent Standard Error of the Mean (SEM). * = $P < 0.05$, ** = $P < 0.01$, *** = $P < 0.001$. Scalebar = 25 μm .



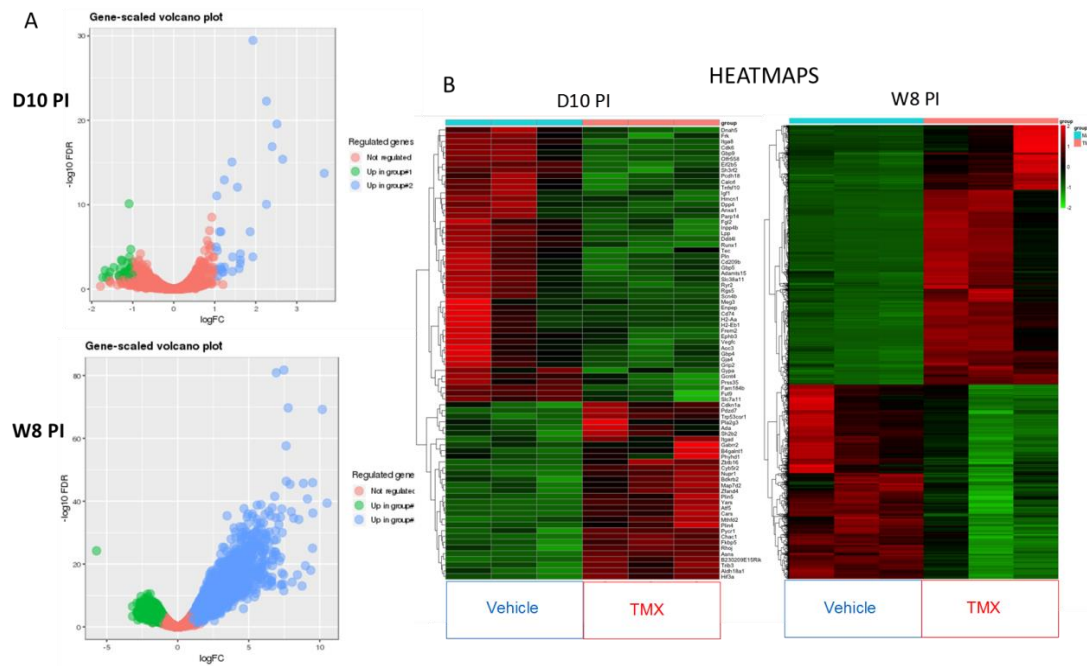


Figure 10: Visualization of DEGs in control (Vehicle) and Tamoxifen (TMX) at 10 days and 8w. (A) The volcano plot showed significantly changed mRNAs with $\log_2 \text{FC} \geq 1$. The blue color represents up-regulated genes, the green color represents down-regulated genes, and the red showed no significance. (B) Hierarchical clustering analysis of DEG. Red represent increased expression and green indicates decreased expression

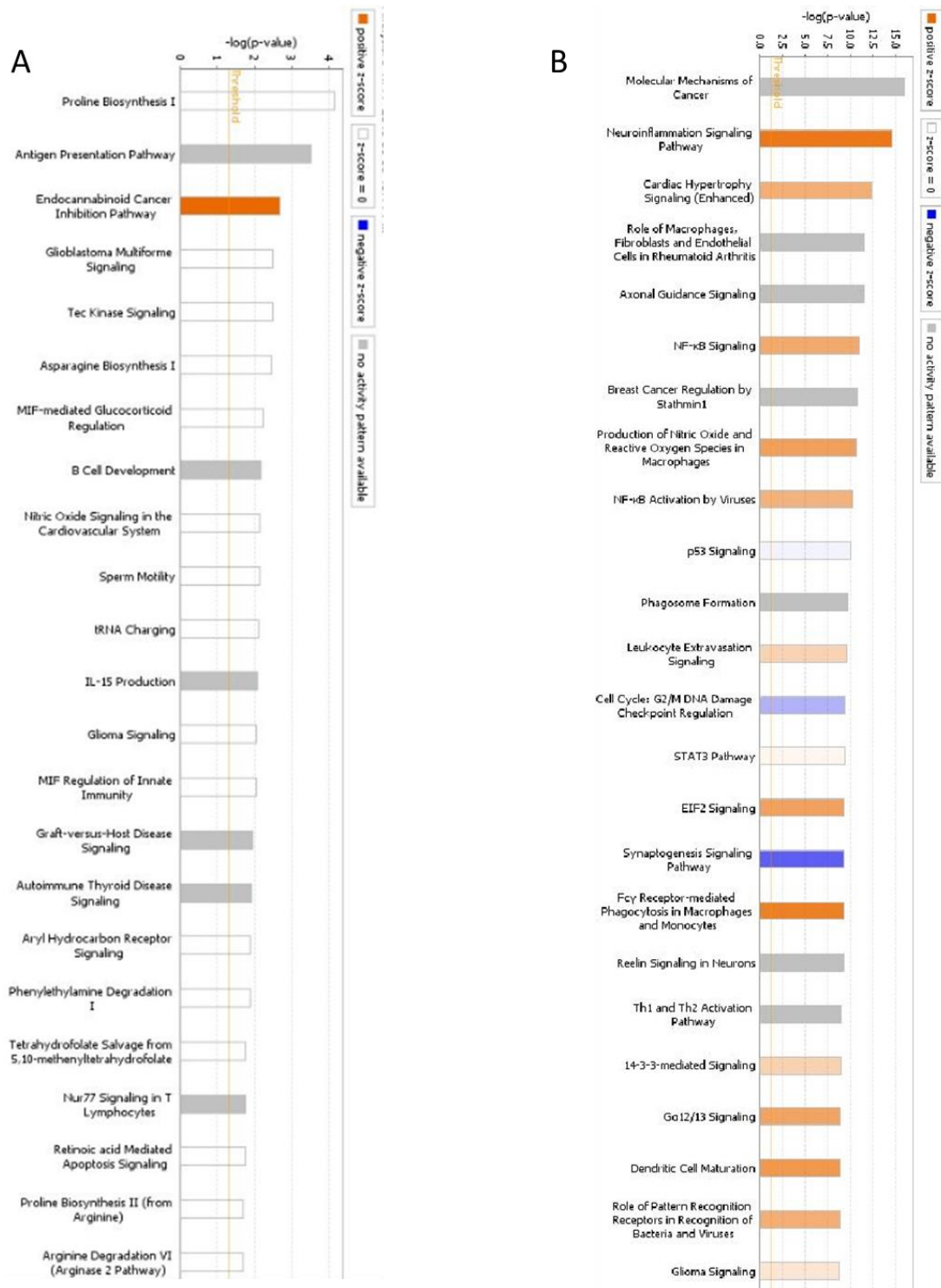


Figure 11: Pathways identified by IPA: The bars reflect the p value for each pathway calculated in IPA by right-tailed Fischer's exact t -test. The Zscore reflects how much the pathway or function is activated. The orange colored bars represent predicted pathway activation, the blue colored bars represent predicted inhibition, white bars are those with a z-score at or very close to 0. Gray bars indicate pathways where no prediction can currently be made. (A) pathways identified at D10. (B) pathways at W8

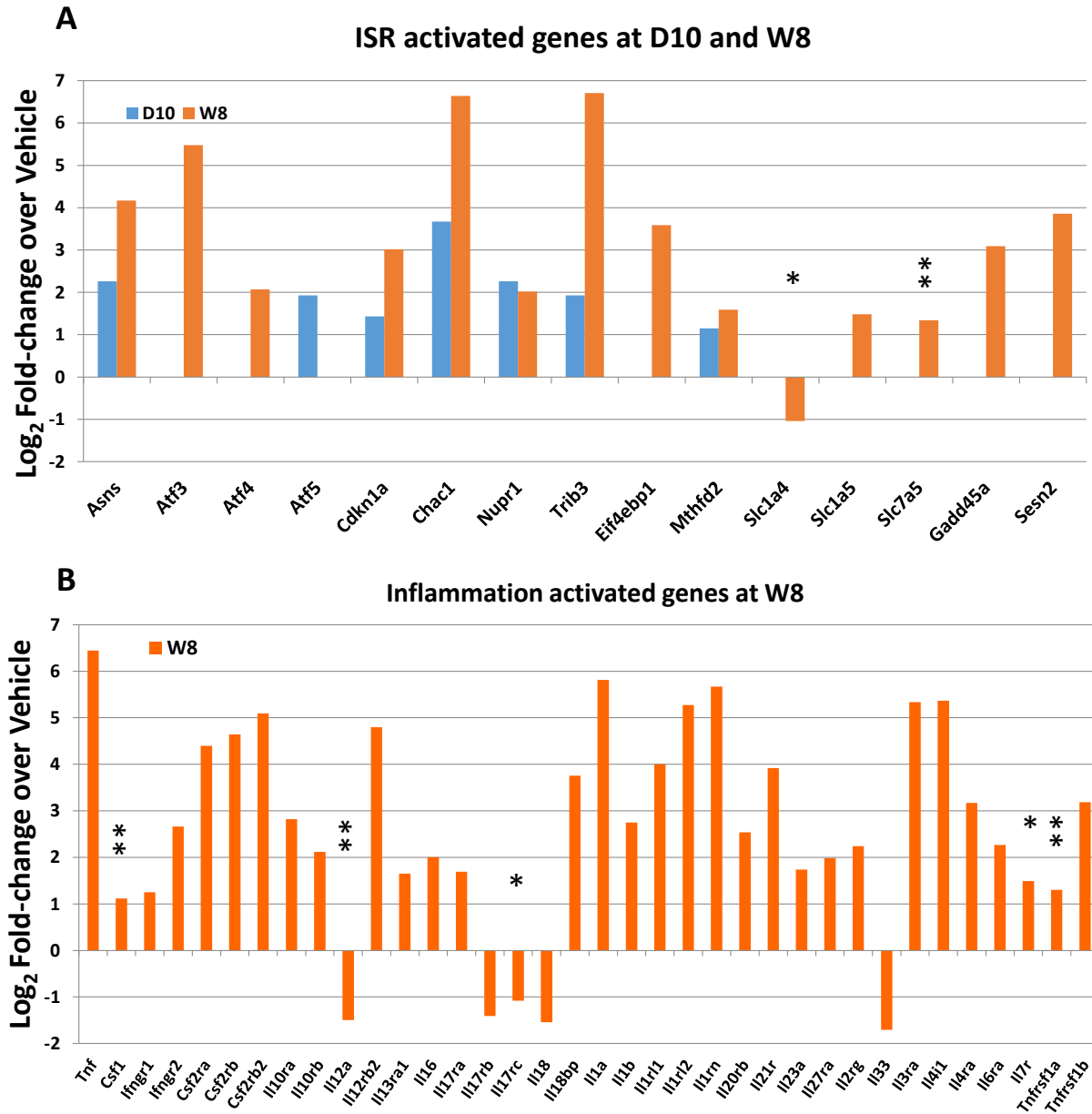


Figure 12: Activated genes. A, ISR activated genes at D10 and W8 expressed as Log₂ Fold-change in O4+ sorted cells. B, Inflammation activated genes at W8 expressed as Log₂ Fold-change in O4+ sorted cells. Data are shown normalized to Vehicle expression levels. Bars, mean of 3 samples. * $p < 0.01$; ** $p < 10^{-3}$; by Student's t-test (TMX compared to Vehicle). Transcripts without symbols were highly significant with $p < 10^{-4}$

Top 20 upregulated genes at 10 days				
FeatureID	Description	logFC	PValue	FDR
Chac1	ChaC, cation transport regulator 1	3.67183224867424	1.01092903057663e-14	1.89606960606293e-14
Cyb5r2	cytochrome b5 reductase 2	2.65804382634389	1.55021057799663e-16	4.07054293570355e-16
Plin4	perilipin 4	2.51756496952743	6.17960208627855e-20	2.7043998596917e-20
Zbtb16	zinc finger and BTB domain containing 16	2.40132674288944	4.01991772943806e-17	1.31943749674481e-17
Asns	asparagine synthetase	2.2623979445836	8.21768665902847e-23	5.39450040731924e-23
Nupr1	nuclear protein transcription regulator 1	2.2620844941664	8.18239313782004e-11	8.95221995886995e-11
Atf5	activating transcription factor 5	1.93302445807377	2.56927046760468e-30	3.37319519691818e-30
Trib3	tribbles pseudokinase 3	1.92987500169522	3.33992086077101e-00	0.000151206279245044
Zfand4	zinc finger, AN1-type domain 4	1.86415467604471	2.06751890933314e-07	1.59673269180204e-07
Trp53cor1	tumor protein p53 pathway corepressor 1	1.62857689002221	9.26140172408822e-00	0.000352205695341131
Itgad	integrin, alpha D	1.62513209247025	1.32751503290328e-05	6.48953146501884e-05
Sh2b2	SH2B adaptor protein 2	1.62194356052172	3.36397307336419e-00	0.00088331204960397
Pla2g3	phospholipase A2, group III	1.59739415853163	2.41692100131692e-00	0.00373314774426939
Fkbp5	FK506 binding protein 5	1.55402497430294	5.77740687190219e-13	8.42795275791154e-13
Cdkn1a	cyclin-dependent kinase inhibitor 1A	1.43493711082957	3.64198610062807e-00	0.000155111521611678
Plin5	PILR alpha associated neural protein	1.43027028454459	7.56872029426276e-00	0.00801368780188514
Hif3a	hypoxia inducible factor 3, alpha subunit	1.42051776503434	4.05420249081143e-16	8.87127075031054e-16
Gabbr2	gamma-aminobutyric acid (GABA) C receptor	1.23943580684751	1.15120401579053e-00	0.00241912291551495
Cars	serine (or cysteine) peptidase inhibitor, cl. 1	1.23362814783902	7.04442313825075e-13	1.15607789227618e-13
Pycr1	pyrroline-5-carboxylate reductase 1	1.21166824586908	0.0001043750721094	0.0100171405472608
Top 20 downregulated genes at 10 days				
FeatureID	Description	logFC	PValue	FDR
Dpp4	dipeptidylpeptidase 4	-1.6761793834649	4.88424583314615e-00	0.00599301528442765
Fam184b	family with sequence similarity 184, member 1	-1.56095902331274	9.6294575241382e-00	0.00950565021311356
Fgl2	fibrinogen-like protein 2	-1.33898498666164	0.0004144445465387	0.0246210065679073
Anxa1	annexin A1	-1.22575015411318	0.0006444842808565	0.0331820946014351
Dnah5	dynein, axonemal, heavy chain 5	-1.20685021673822	0.0003682338066813	0.0231455688559639
Frk	fyn-related kinase	-1.17548625705255	0.0008559467762119	0.0401560558706929
Cd74	CD74 antigen	-1.15061899966661	0.0001510965244118	0.0131373925099542
Fut9	fucosyltransferase 9	-1.14741476092841	0.0001745045850916	0.01478110127528
Gbp4	guanylate binding protein 4	-1.14677755216647	0.0002630173701252	0.0189733794086524
Enpep	glutamyl aminopeptidase	-1.1389217492052	0.0003829051787905	0.0233821492667034
Cd209b	CD209b antigen	-1.12560411934334	0.0009165084462495	0.0415533504241177
Cdk6	cyclin-dependent kinase 6	-1.12132906735429	7.47327468318109e-00	0.00799557906874731
Ephb3	Eph receptor B3	-1.11125586282014	7.11242125679769e-00	0.00778158155670807
Eif2b5	eukaryotic translation initiation factor 2B subunit 5	-1.08992786713996	6.45523327652638e-00	7.70461433522862e-11
Adamts15	ADAM metalloproteinase with thrombospondin type 1 motifs 15	-1.08863650127781	0.0007250068087284	0.0360089628952263
Gbp5	guanylate binding protein 5	-1.04062470973561	0.0005608489786772	0.0298656640593123
Ddit4l	DNA-damage-inducible transcript 4-like	-1.03821254997783	1.31828799812159e-00	0.00262239441323309
Frem2	Fras1 related extracellular matrix protein 2	-1.03556580262226	0.0008773051661491	0.04055682931821
Aoc3	amine oxidase, copper containing 3	-1.02873791669826	4.65671862047298e-00	0.0057757627373405
Calcr1	calcitonin receptor-like	-1.01870340526737	1.22402717164846e-00	0.00251097699008947

Table 1: Top 20 up and down regulated genes at D10 and W8 PI (continued)

Top 20 upregulated genes at 8w				
FeatureID	Description	logFC	Pvalue	FDR
Apoc4	apolipoprotein C-IV	9.51815211882678	8.52121427543627e-40	5.78846085730386e-37
Spp1	secreted phosphoprotein 1	9.5037646994543	6.30390806225689e-50	1.2234984990546e-46
Oaz1-ps	ornithine decarboxylase antizyme 1, pseudogene	9.49195316323405	6.79201714453687e-28	9.2276344925678e-26
Bpifc	BPI fold containing family C	9.36628667901134	1.88757056570874e-20	9.22465241212913e-19
Cd200r4	CD200 receptor 4	9.13222699298405	1.52542662322248e-44	1.88404055482733e-41
Kynu	kynureninase	8.99118158597285	5.48453310715861e-22	3.31168296861586e-20
Stra6l	STRA6-like	8.85124314066583	1.22137873993997e-49	2.07420644510306e-46
Sphk1	sphingosine kinase 1	8.75045950495491	3.65855927283336e-15	9.07028946728358e-14
Pdcd1	programmed cell death 1	8.52925164106655	1.49527454445051e-37	6.3483749877827e-35
Fosl1	fos-like antigen 1	8.4324891857344	7.18347673581332e-19	2.7569128512079e-17
Cd5l	CD5 antigen-like	8.16834050518119	5.55830823572544e-38	2.51717252301886e-35
Olfr110	olfactory receptor 110	8.05900081771457	1.98675406631273e-16	5.64687044872904e-15
Hcar2	hydroxycarboxylic acid receptor 2	7.99704237954107	2.89880961230379e-40	2.07280144172418e-37
Lpl	lipoprotein lipase	7.90999480050973	2.74814630306784e-49	4.14847951927552e-46
Mmp12	matrix metalloproteinase 12	7.77405751780899	4.48124253281507e-74	2.02940536836085e-70
Atp6v0d2	ATPase, H ⁺ transporting, lysosomal V0 subunit D2	7.64689771582735	1.96605726411844e-50	4.45180899838552e-47
Pianp	PILR alpha associated neural protein	7.63066365435005	8.7928899657072e-62	2.38920406148196e-58
Itgax	integrin alpha X	7.47536691336331	1.32052457937003e-86	1.79406469353212e-82
Ecel1	endothelin converting enzyme-like 1	7.46535953375698	1.46865031569666e-13	3.1031233575129e-12
Serpinb1c	serine (or cysteine) peptidase inhibitor, clade B, men	7.45088161969174	5.69121133685608e-19	2.20916563492933e-17
Top 20 downregulated genes at 8w				
FeatureID	Description	logFC	Pvalue	FDR
Gdf1	growth differentiation factor 1	-5.71571437366863	4.96157313680747e-27	5.91297654707599e-25
A330076C08Rik	RIKEN cDNA A330076C08 gene	-3.17776262398572	2.80765565226252e-08	3.02977042824771e-07
Nkx2-9	NK2 homeobox 9	-3.17556763220112	9.05046147646638e-05	0.000400259015687735
S100b	S100 protein, beta polypeptide, neural	-2.87269291699503	5.57909036258647e-06	3.46107404868035e-05
Fndc5	fibronectin type III domain containing 5	-2.86738116747619	1.76167552933044e-09	2.33731677162923e-08
Olfr287	olfactory receptor 287	-2.86073020289194	1.91981858803055e-06	1.35143291901467e-05
Btbd17	BTB (POZ) domain containing 17	-2.85791613322145	3.85262574427569e-06	2.49841400294652e-05
Gm11627	predicted gene 11627	-2.83332085956146	1.55632760726884e-06	1.11992938942555e-05
Spock3	sparc/osteonectin, cwcv and kazal-like domains prote	-2.82536788723567	1.14854984045431e-05	6.4855353837998e-05
9330199G10Rik	RIKEN cDNA 9330199G10 gene	-2.80120426284745	0.00176718950658471	0.00549783298293104
Ucp3	uncoupling protein 3 (mitochondrial, proton carrier)	-2.77303681606214	1.82199460814348e-05	9.71873527531892e-05
Col2a1	collagen, type II, alpha 1	-2.76426352063583	1.49770949726409e-06	1.08348675345207e-05
Slc34a3	solute carrier family 34 (sodium phosphate), member	-2.7452938505178	5.02767845002185e-07	4.15992931924463e-06
A730020M07Rik	RIKEN cDNA A730020M07 gene	-2.73220327690339	0.000109272214399284	0.000473095062086893
Egfl6	EGF-like-domain, multiple	-2.72307388662142	4.62306696704029e-06	2.93911969182075e-05
Smtnl2	smoothelin-like 2	-2.72233063365033	5.48865008946914e-07	4.47591837428138e-06
Dclk3	doublecortin-like kinase 3	-2.72058030014741	1.04819500167533e-05	5.99107164188517e-05
Kcng4	potassium voltage-gated channel, subfamily G, mem	-2.71186302888144	0.000162401509022101	0.000669616662086271
Cldn10	potassium voltage-gated channel, subfamily G, mem	-2.70840066660187	3.83637996271687e-06	2.49144637540495e-05
Ttpa	tocopherol (alpha) transfer protein	-2.70525265179945	7.05095032904228e-06	4.24243627858142e-05

Table 1 (continued); Top 20 up and down regulated genes at D10 and W8 PI

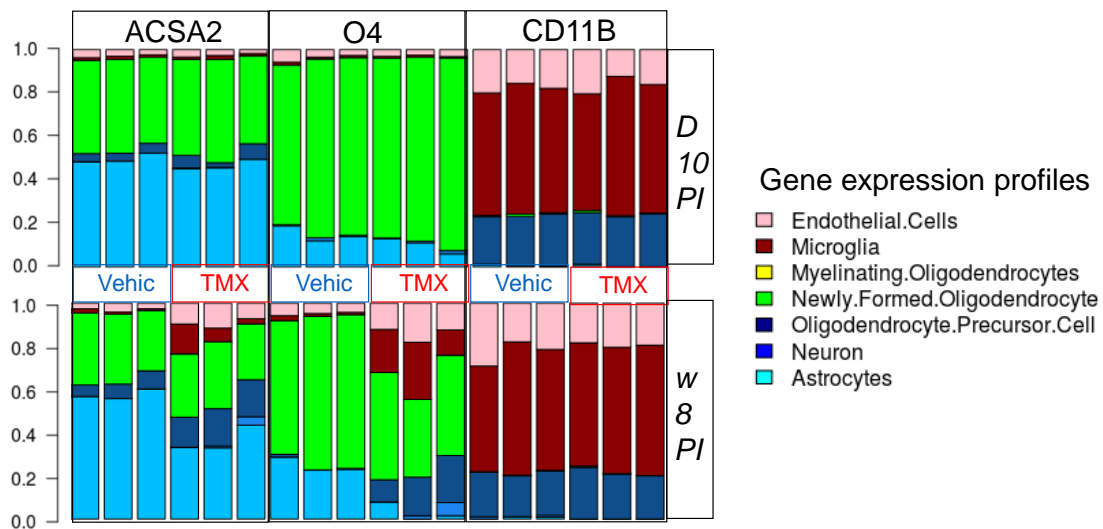
A D10

Upstream Regulator	Expr Log Ratio	Molecule Type	Predicted Activation State	Activation z-score	p-value of overlap	Target molecules in dataset	Mechanistic Network
ATF4		transcription regulator	Activated	2,42	2,06E-10	ASNS,ATF5,CARS,CDKN1A,CHAC1,MT HFD2,NUPR1,PYCR1,SLC7A11,TRIB3	10 (3)
UCP1		transporter	Activated	2,768	1,07E-07	ALDH18A1,ASNS,ATF5,MTHFD2,NUPR 1,PHYHD1,PYCR1,TRIB3	
PRDM1		transcription regulator	Activated	2,63	0,0000172	ADA,CD74,CDK6,HLA-DQA1,MAP7D2,PCDH18,TNFSF10	15 (3)
STAT3		transcription regulator	Activated	2,504	0,0000354	CD74,CDKN1A,DPP4,FGL2,GBP5,GBP6 ,HLA-DQA1,HLA-DRB5,RUNX1,TNFSF10	24 (7)
JAK1/2		group	Inhibited	-2	0,000112	CD74,GBP5,HLA-DQA1,HLA-DRB5	16 (5)

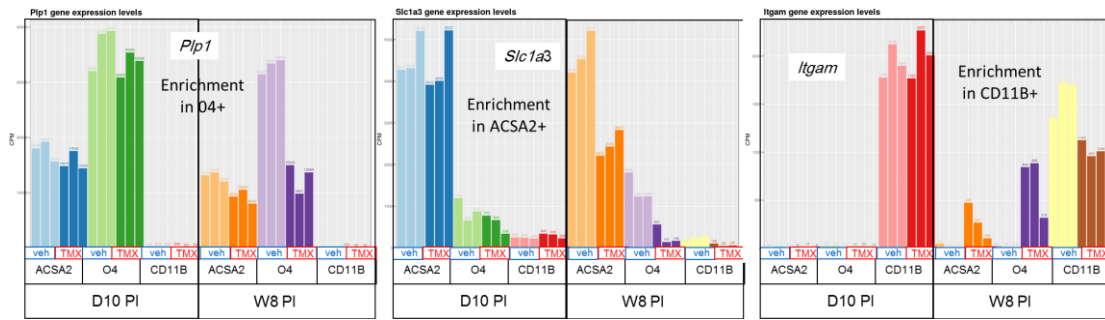
B W8

Upstream Regulator	Expr Log Ratio	Molecule Type	Predicted Activation State	Activation z-score	p-value of overlap	Target molecules in dataset	Mechanistic Network
IFNG		cytokine	Activated	10,468	3,03E-57	ABCA1,ABCA6,Acot1,ADAM17,ADAMTS9,ADC	1071 (15)
TGFB1	4,025	growth factor	Activated	4,427	2,51E-56	AASS,ABCA1,Acot1,Acp5,ACSL3,ADAM17,ADP	1783 (19)
TNF	6,444	cytokine	Activated	9,206	1,5E-50	AATK,ABCA1,Abcb1b,ABCC3,ABCD2,ACKR3,A	1459 (16)
ERBB2		kinase	Activated	5,759	1,48E-43	ABRACL,ACSL4,ACSS2,ADAM17,ADAM19,ADP	1330 (19)
CSF2		cytokine	Activated	10,125	1,26E-40	ABCA1,ADAM17,ADAM8,ADORA2B,AKR1A1,A	1554 (19)
Vegf		group	Activated	5,577	3,45E-38	ACKR3,ADAM15,ADAMTS1,ADORA2A,AKAP13	1465 (20)
HGF		growth factor	Activated	7,082	1,69E-35	ABCB4,ACKR3,ADAMTS1,ADORA2A,AKAP13,A	1116 (16)
CDKN1A	3,017	kinase	Inhibited	-2,817	1,47E-32	ANLN,APP,ASPM,ATAD2,AURKA,AURKB,BAX,E	933 (13)
IL4		cytokine	Activated	5,17	2,44E-32	ABCA1,ABCA2,Acp5,ACSL4,ADAM17,ADAM19	1177 (16)
IL1B	2,75	cytokine	Activated	6,415	3,44E-31	ABCC3,ACHE,ADAM8,ADAMTS1,ADAMTS4,AC	1142 (14)
APP	-1,101	other	Activated	2,553	5,4E-31	ABCA1,ACHE,ADAMTS4,ADAP1,ADORA3,AIF1	1460 (18)
IL6		cytokine	Activated	4,953	8,13E-31	ABCA1,ABCC3,Acp5,ADAMTS1,ADAMTS4,ADC	1226 (14)

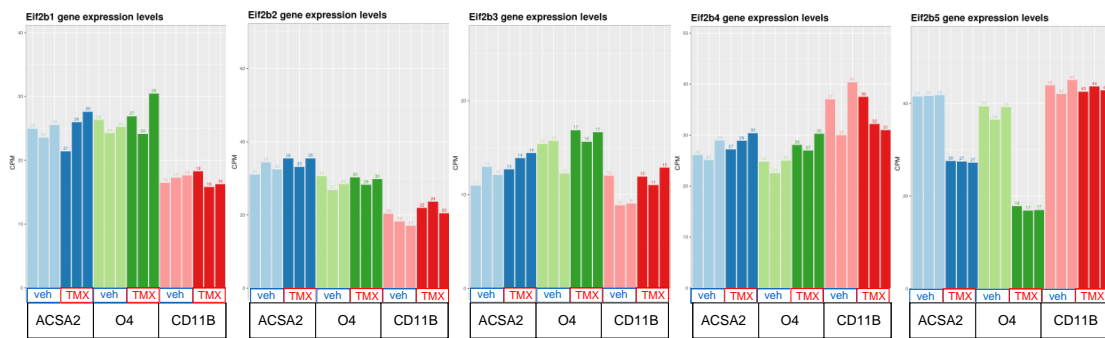
Table 2: Upstream regulators found at D10 (A) and W8 (B)



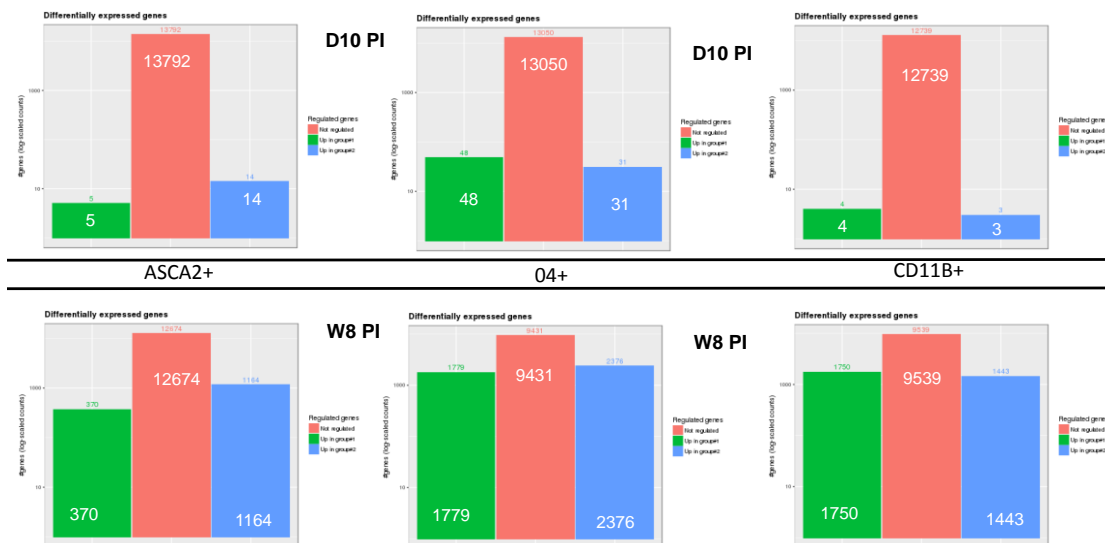
Supplemental figure 1: Gene expression profiles at D10 and W8 dissected by EPIDISH.
 Vehic=Vehicle, TMX=Tamoxifen, D10 PI=10days post induction, W8 PI=8weeks post induction



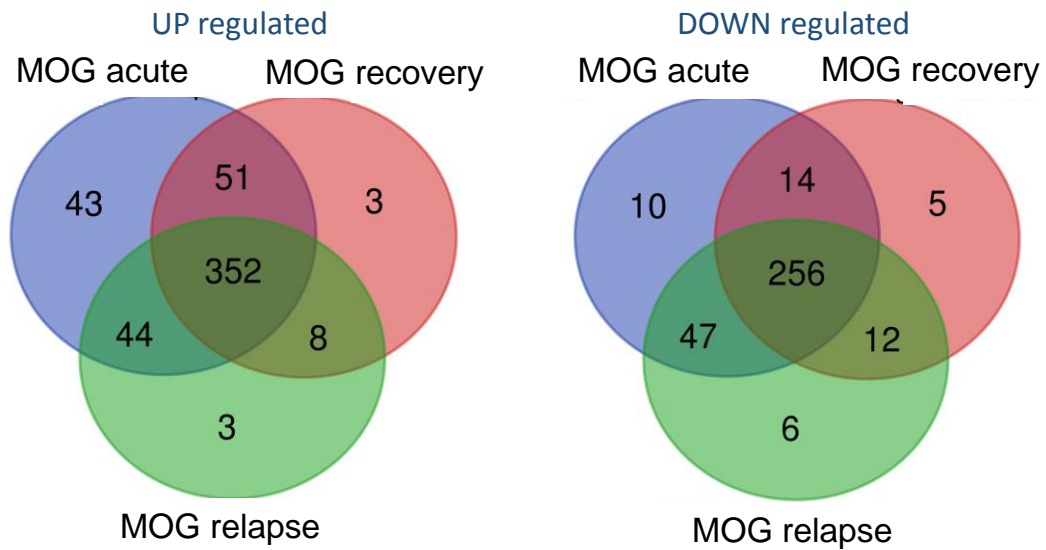
Supplemental figure 2: Enrichment analysis at D10 PI and W8 PI using *Plp1* expression for O4+ cells enrichment, *Slc1a3* for ACSA2+ cells enrichment and *Itgam* for CD11B+ cells enrichment. Veh=Vehicle, TMX=Tamoxifen, D10 PI=10days post induction, W8 PI=8weeks post induction.



Supplemental figure 3: mRNA expression levels for each of the five genes (*eIF2B1-5*) coding for the five subunits of the *eIF2B* complex



Supplemental figure 4: Transcriptomic analysis : differentially expressed genes in TMX versus vehicle injected mice



Supplemental figure 5: Comparaison of differentially expressed genes in the spinal cord at different phases of MOG-induced EAE and in the O4+ sorting cells of the Plp-Cre-ERT2/Eif2b5^{fl/fl} brains obtained at W8 PI by TMX

V. Results and discussion of the consequences of eIF2B5 inactivation in astrocytes

The mouse model used in this part of the work is the *Glast-Cre-ERT2/Eif2b5^{fl/fl}* in which we targeted the *eif2b5* gene in astrocytes using the same system with the Cre expressed in the locus of the Glutamate-Aspartate Transporter (*Glast*) protein that allows precisely timed gene deletion in adult astrocytes.

TMX induction resulted in two distinct phenotypes related to the presence or not of a copy of the *Glast* locus in the resulting mice:

- In the heterozygous *Glast-Cre-ERT2^{+/-}/Eif2b5^{fl/fl}*, treated male or female mice, developed no symptoms even after 1 year post injection. At the histological level, we observed an increase of number of GFAP+ astrocytes and Iba1+ microglia with an activated aspect of both cell types without oligodendrocyte nor neuronal changes.
- In the homozygous *Glast-Cre-ERT2^{-/-}/Eif2b5^{fl/fl}* the Cre-ERT2 cassette is included inside the exon 2 of *Glast*. Therefore, TMX by inducing the Cre recombinase expression is responsible for the absence of *Glast* expression (*Glast* null mice). In this mutant only the females expressed a severe phenotype characterized by an acute loss of weight and paraplegia observed at six weeks after TMX induction. An increase in the number of GFAP+ astrocytes and Iba1+ microglia with an activated aspect of both cell types is observed, in addition to mature oligodendrocyte and neuronal loss.

Details of the results, presently limited to the immunochemistry of the two strains of conditional eIF2B5 inactivation in astrocytes, is presented in the following article in preparation.

By investigating the consequences of eIF2B5 inactivation in astrocytes in adult mice, we found a large difference between mice heterozygous or homozygous for the *Glast* promoter and the female versus male.

What is the role of the *Glast* defect in the severity of the phenotype observed? The *Glast*-null animals show severe neurological deterioration symptoms and weight loss similar to the ones observed in the oligodendrocyte-targeting model, and at an even earlier time frame (6 weeks post-injection of tamoxifen instead of 9 weeks). These animals also show, identically

to the oligodendrocyte targeting model, a proliferation of reactive astrocytes, a decrease of mature oligodendrocytes suggesting an effect of astrocyte activation on oligodendrocyte maturation (which was previously described by Dooves et al., 2016), a proliferation of microglia and loss of neurons suggesting the presence of inflammation and a possible explanation of the neurological symptoms.. The defect in the glutamate transporter induced a persistent higher level of glutamate, which increased the oligodendrocyte and neuronal stress, both of the latter having highly regulated glutamate receptors. On the other hand we know that the ACSA2 sorted cells expressed, in 40% of cells, non myelinating immature gene expression profiles. Therefore, the *Glast* promoter is probably also active in the immature oligodendrocytes particularly in stress conditions related to *Glast* inactivation. The association of *eif2B5* induced stress and *Glast* defect in the astrocytes would be a trigger for O4 chronic ISR.

As a matter of fact, females in a number of species such as rodents and humans are more sensitive and responsive to potential threats in addition to having a more important response to stress. Among the influencers of such sex differences is the estrogen hormone (among other hormones) which plays a role in social recognition and social learning in addition to other effects. In addition, since TMX is an estrogen receptor antagonist, it might not be too farfetched to propose sex difference as an aggravating factor in the case of our model (Choleris et al., 2018).

The myelin sex difference of the brain is another complementary hypothesis. This sex difference emerges in the mice during the first 10 postnatal days, precisely at a stage when a late wave of oligodendrocyte progenitor cells arises and starts differentiating. Androgen levels, higher in males than in females during this period would be responsible for a higher density of oligodendrocytes (20±40% greater) with thicker myelin in adult males compared with females. This early myelin sex difference could account for female predominance in multiple sclerosis. Therefore, this sex myelin difference would be responsible for the greater sensitivity of the oligodendrocytes to chronic ISR.

Further experiments are needed in order to decipher the mechanisms of this *eif2b5* inactivation in astrocytes. Transcriptomic analysis of individual glial cells, identically to the *Plp-Cre-ERT2/Eif2b5^{fl/fl}* model performed during my thesis, would be of great interest comparing (i) TMX treated versus control female ***Glast-Cre-ERT2^{-/-}/Eif2b5^{fl/fl}*** and ***Glast-Cre-***

ERT2^{+/-}/Eif2b5^{fl/fl}, (ii) TMX treated versus control female versus male **Glast-Cre-ERT2^{-/-}/Eif2b5^{fl/fl}** and (iii) the TMX treated versus female Plp-Cre-ERT2/Eif2b5^{fl/fl}.

Article 2 (in preparation)

**Conditional inactivation of the translation
initiation factor *eif2b5* gene in astrocytes
induced a delayed acute neurological distress
only in the Glast null mouse but not in the Glast-
Cre-ERT2^{+/-}/Eif2b5^{fl/fl}**

Materials and methods

Mice

Eif2b5 gene being the most frequently mutated gene in the CACH/VWM human pathology, Eif2b5^{fl/fl} transgenic mice were generated at the “Institut Clinique de la Souris” (ICS, Illkirch-graffenstaden, Strasbourg) from a C57BL/6 strain by targeting exons 3 to 7 in eif2b5 gene, where the lox P sites were inserted in introns 2-3 and introns 7-8 (Fig.). These animals have been cross bred with Glast-Cre-ERT2 (Mori et al., 2006) transgenic mice to obtain 2 distinct mice lines namely the homozygous Glast-Cre-ERT2^{-/-}/Eif2b5^{fl/fl} (later referred to as GcKO Ho) and the heterozygous Glast-Cre-ERT2^{+/-}/Eif2b5^{fl/fl} (later referred to as GcKO Hz) (C57BL/6 strain) transgenic mice. Glast-Cre-ERT2/Eif2b5^{fl/fl} is an inducible Knock-out (KO) mouse in which the expression of the Cre recombinase excising the eif2b5 gene specifically in astrocytes and radial glial cells is under the control of the Glast promoter.

For this study, we injected 2-month-old female Glast-Cre-ERT2^{-/-}/Eif2b5^{fl/fl} and Glast-Cre-ERT2^{+/-}/Eif2b5^{fl/fl} mice with either Tamoxifen (Sigma Aldrich T5648-1G) or Corn oil (Sigma Aldrich C8267-500mL) and sacrificed them at 6 weeks after treatment.

All experiments were carried out in compliance with INSERM ethical rules and approved by the institutional review board (Bichat-Robert Debre ethics committee, Paris, France, approval number APAFIS#1682-2015090819249420 v4).

Mice Genotype control

DNA was extracted by lysing tail samples using Kapa Multiplex Genotyping kit (Clinisciences). Polymerase Chain Reaction (PCR) was realized in a total volume of 15 µL containing 2 µL of DNA, 7,5 µL of genotyping mix, 1,5 µL of H₂O and 1 µL of each of the following primers solutions (10 µM) Glast Forward (F8): 5'-GAGGCACTTGGCTAGGCTCTGAGGA-3', Glast Reverse (R3): 5'-GAGGAGATCCTGACCGATCAGTTGG-3', CRE-R1: 5'-GGTGTACGGTCAGTAAATTGGACAT to detect the Glast sequence and the primers 4251 (Fw): 5'-GGAGCCAGTGACCTCTTCTG-3' and 4253 (R): 5'-TTAATCCCAGCACTCGGTCT-3' to detect the Eif2b5 sequence. The PCR was performed using Applied Biosystem 2720 Thermocycler using

the following cycling parameters: 1 cycle of 5 minutes at 95°C followed by 35 cycles each of 30 seconds at 95°C, 30 seconds at 63°C and 30 seconds at 72°C, finishing with final extension for 10 minutes at 72°C.

DNA migration was done in 2% agarose gel in UltraPure™ TBE Buffer at 120 V, 10X (Invitrogen, 15581-028) diluted 1/10. DNA bands were expected at 400pb for Glax-Cre and 287pb for Eif2b5^{fl/fl}.

Knock-out induction/treatment Protocol

Two month old female Glax-Cre-ERT2^{-/-}/Eif2b5^{fl/fl} and Glax-Cre-ERT2^{+/-}/Eif2b5^{fl/fl} mice were injected intraperitoneally (IP) with 50 microliters of corn oil (Sigma Aldrich C8267-500mL) or Tamoxifen (Sigma Aldrich T5648-1G) (1 milligram Tamoxifen dissolved in 50 microliters of corn oil) twice a day for five days. The mice were weighed weekly and sacrificed at 6 weeks after injection for immunohistochemistry.

Brain Samples

For Immunohistochemistry, the mice were anesthetized with 90 mg/kg pentobarbital (CEVA Santé Animale 54,7mg/mL) and sacrificed by intracardiac perfusion-fixation with 20 ml of normal saline solution (NaCl 0.9%), followed by 100 ml of 4% paraformaldehyde solution in PBS (Santa Cruz sc-281692). Brains were removed and post-fixed in the same fixative overnight at 4°C, and were then cryoprotected by immersion in 30% sucrose in PBS during 72 hours and then frozen using Isopentane at – (45-55) °C. Coronal sections of the brain were cut with cryostat (12 µm thick; Leica 3500 at -22°C).

Immunohistochemistry

For each experimental condition, we used five mice. Sections on slides were subjected to an antigen retrieval step using Target Retrieval Solution (DAKO S1700) following the manufacturer's protocol, allowed to cool down for 20 min at room temperature, washed 3 times for 5 min in PBS and then blocked for 1 hour at room temperature. Next, slides were incubated overnight at 4°C the same blocking solution containing 10% horse serum (Sigma-Aldrich), 0.2% Triton X-100 in PBS with primary antibodies against Olig2 (1:400,

CHEMICON/Millipore AB9610), CC1 (1:400, Abcam ab16794), GFAP ALEXA FLUOR 488 (1:400, CHEMICON/Millipore MAB3402X), Iba1 (1:400, WAKO 019-19741) and NeuN (1:250, Millipore MAB377) . Sections were then washed three times in PBS/0.1% Triton and incubated with corresponding secondary antibodies Cy3-conjugated anti-mouse (1:1000, Jackson ImmunoResearch), Cy3-conjugated anti-rabbit (1:1000, Jackson ImmunoResearch), Alexa 488-conjugated anti-rabbit (1:1000, Jackson ImmunoResearch) or Cy5-conjugated anti-mouse (1:1000, Jackson ImmunoResearch) for one hour at room temperature. The sections were washed 3 times in PBS for 5 minutes, mounted on slides with DAPI Fluoromount-G (SouthernBiotech) for nuclear counterstaining, coverslipped, and viewed under a Leica confocal microscope (TCS SP8 –DMI6000B-CS).

Quantification and cell counting were done using Fiji software (Fiji is just ImageJ).

Statistical analyses

Data are presented as the mean \pm standard error of the mean (SEM). Statistical analysis was performed with Prism 5 software, and the statistical significance of differences was determined by 2-tailed t-test with values of $p < 0.05$ considered significant.

Results

Generation and Characterization of *Glast-Cre-ERT2^{+/-}/Eif2b5^{fl/fl}*:

We generated *Glast-Cre-ERT2^{+/-}/Eif2b5^{fl/fl}* mouse model in order to understand CACH/VWM disease. By intraperitoneal injection of 1mg of tamoxifen, two times per day during 5 days, we induce the excision of eif2b5 (exons 3 to 7) at two levels, where the lox P sites were inserted in introns 2-3 and introns 7-8. However, this excision is specifically in astrocytes, where the CreERT2 expression is under the control of *Glast* promotor (Figure 32). Two-month-old adult *Glast-Cre-ERT2^{+/-}/Eif2b5^{fl/fl}* female mice have been treated with 1mg of tamoxifen, 2 times per day during 5 days. Another group of female mice treated with the vehicle (Corn Oil) according to the same protocol has been considered as control. Five to six

weeks (w5-w6) after injection, **Glast-Cre-ERT2^{+/-}/Eif2b5^{fl/fl}** tamoxifen treated mice showed no apparent neurological deterioration nor weight loss compared to vehicle treated ones (w5: Vehicle=22.98±0.38, TMX=22.14±0.45 with p=0.1696, w6: Vehicle=23.33±0.38, TMX=22.43±0.28 with p=0.0618) (Figure 32). In addition, a survival study involving Vehicle and TMX treated male and female mice showed that all the mice survived for 20 weeks PI when they were sacrificed (Figure 32).

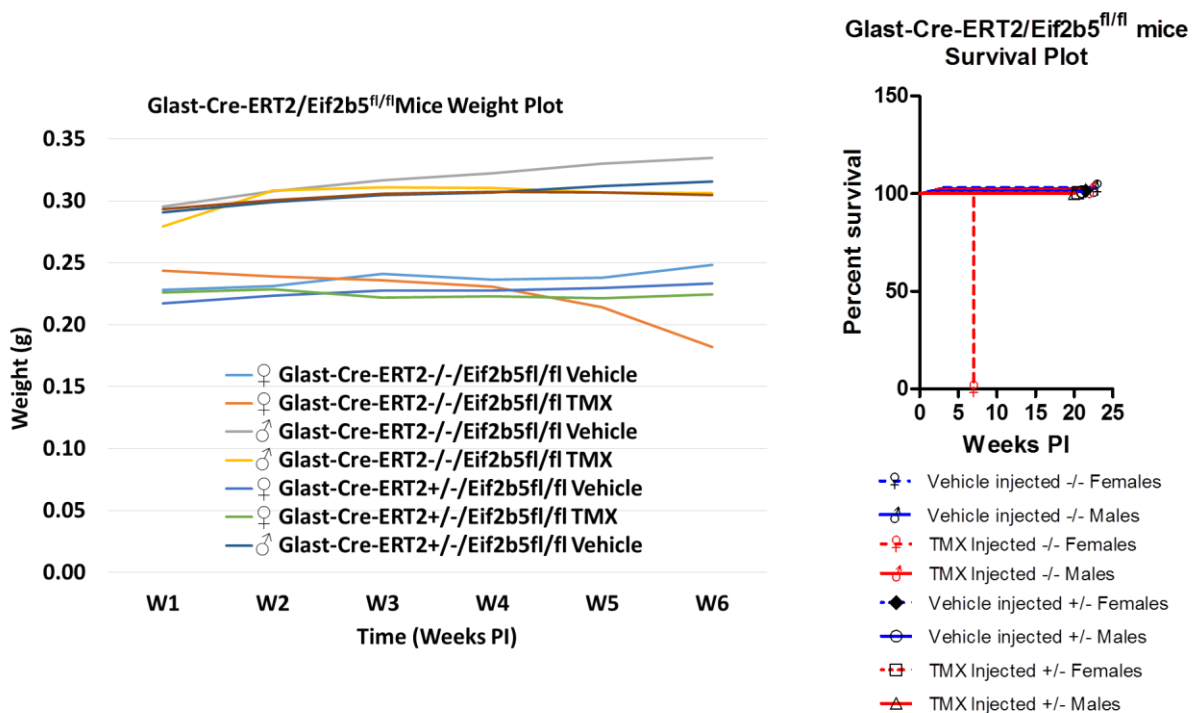
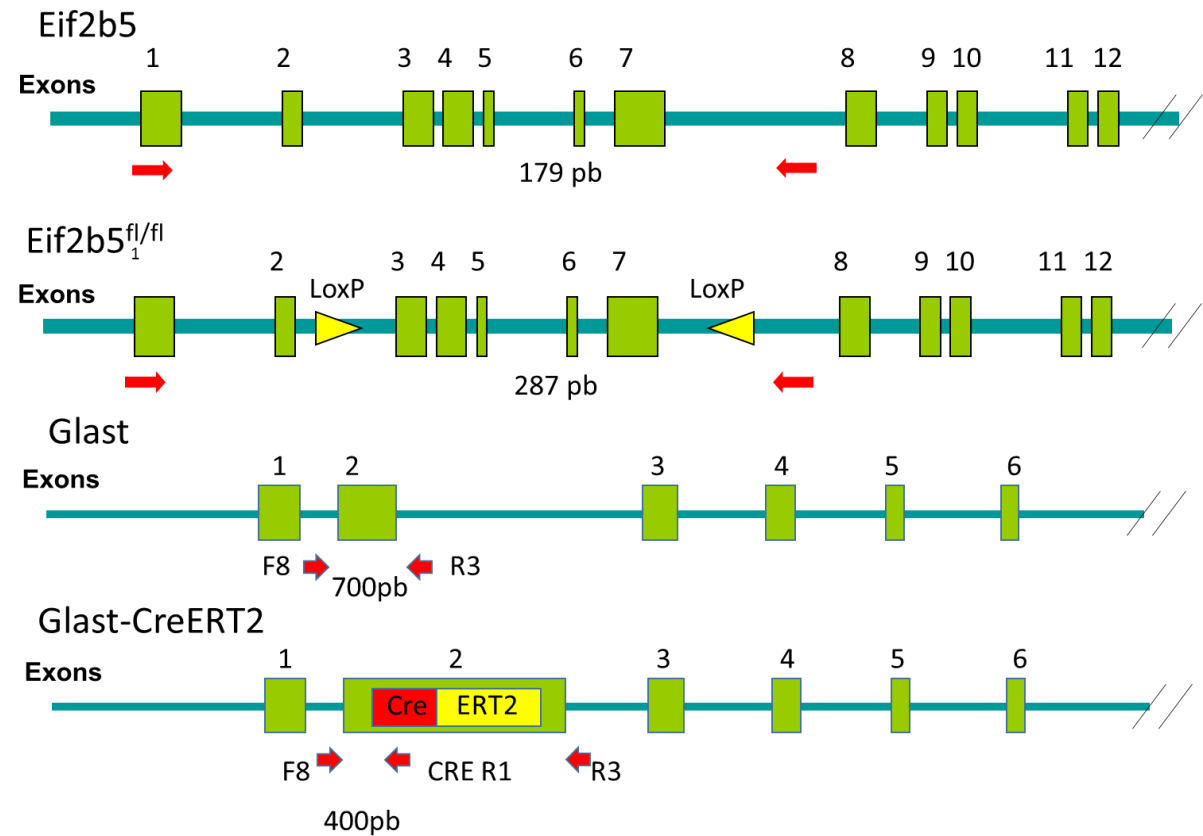
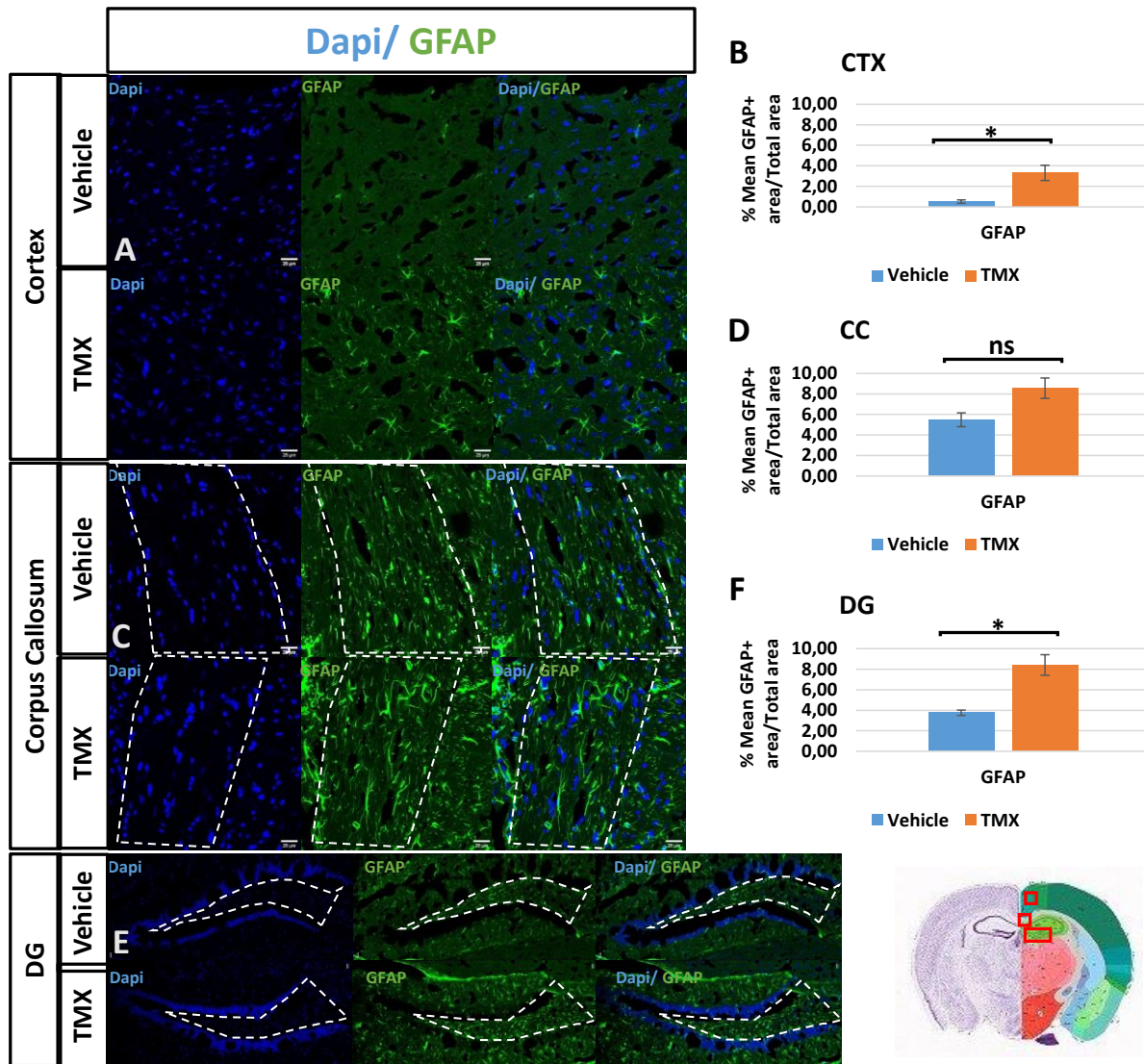


Figure 32: Construction (up), weight plot (bottom left) and survival plot (bottom right) of *Glast-Cre-ERT2/Eif2b5*^{fl/fl} mice

Eif2b5 knock-out induces activation of astrocytes and GFAP over expression in *Glast-Cre-ERT2*^{+/+}/*Eif2b5*^{fl/fl} treated mice

In CACH/VWMD, abnormal astrogliosis, astrocytic defective morphology and severe white matter devastations are the main features where astrocytes and oligodendrocytes are affected. In our model, *Eif2b5* knock-out is specifically induced in astrocytes by having CreERT2 expression under the control of the *Glast* promotor. For these reasons, we evaluated the expression level of the astrocyte marker Glial fibrillary acidic protein or GFAP. The mean GFAP+ area showed an increase of about 6 folds in the cortex (Vehicle=0,52±0,17%, TMX= 3,3±0,74%; p-value=0.022)) (Figure 33.A, B), as well as an increase in DG (Vehicle=3,76±0,26%, TMX=8,41±1,01%; p-value=0.0111) (Figure 33.E, F) 6w after tamoxifen treatment. In addition, these astrocytes seem to show signs of the reactive astrocytes' morphology especially in the cortex (Figure 33.A). However, no significant changes have been shown in the CC (Vehicle=5,47±0,68%, TMX=8,56±0,99%; p-value=0,0619) (Figure 33.C and D).

These results show an effect of *Eif2b5* knock-out on astrocytes' activation and reaction in the *Glast-Cre-ERT2*^{+/-}/*Eif2b5*^{fl/fl} treated mice.



No loss of mature oligodendrocytes in *Glast-Cre-ERT2^{+/-}/Eif2b5^{fl/fl}* treated mice

We next investigated the evaluation of oligodendrocytes, and their maturation in different regions of the mouse brain. At 6w after injection, we found no difference in the number of Olig2+/CC1+ cells mature oligodendrocytes percentage in Cortex area (Vehicle=15,64±0,88, TMX=20,46±1,74; p= 0.0690) (Figure 34.A, B), Corpus Callosum area (Vehicle=66,42±3,61, TMX=71,2±1,05; p= 0.2727) (Figure 34.C, D), and Dentate Gyrus Area (Vehicle=16,04±1,17, TMX=14,57±2,29; p= 0.5979) (Figure 34.E and F) or in Olig2-/CC1+ cells mature oligodendrocytes percentage in Cortex area (Vehicle=7,81±0,92, TMX=6,72±0,34; p= 0.3297) (Figure 34.A, B), Corpus Callosum area (Vehicle=5,37±0,53, TMX=52,33±0,33; p= 0.8339) (Figure 34.C, D), and Dentate Gyrus Area (Vehicle=6,42±0,97, TMX=5,9±0,27; p= 0.6304) (Figure 34.E, F). There was also no difference observed in immature oligodendrocytes (Olig2+/CC1- cells) percentage in Cortex area (Vehicle=7,73±1,01, TMX=5,22±0,81; p= 0.1239) (Figure 34.A, B), Corpus Callosum area (Vehicle=5,56±0,43, TMX=5,32±0,3; p= 0.6738) (Figure 34.C, D), and Dentate Gyrus Area (Vehicle=5,54±0,65, TMX=5,97±0,77; p= 0.6886) (Figure 34.E, F).

These results suggest that *Eif2b5* excision specifically in the astrocytes of our *Glast-Cre-ERT2^{+/-}/Eif2b5^{fl/fl}* mice might not have any effects on oligodendrocyte maturation.

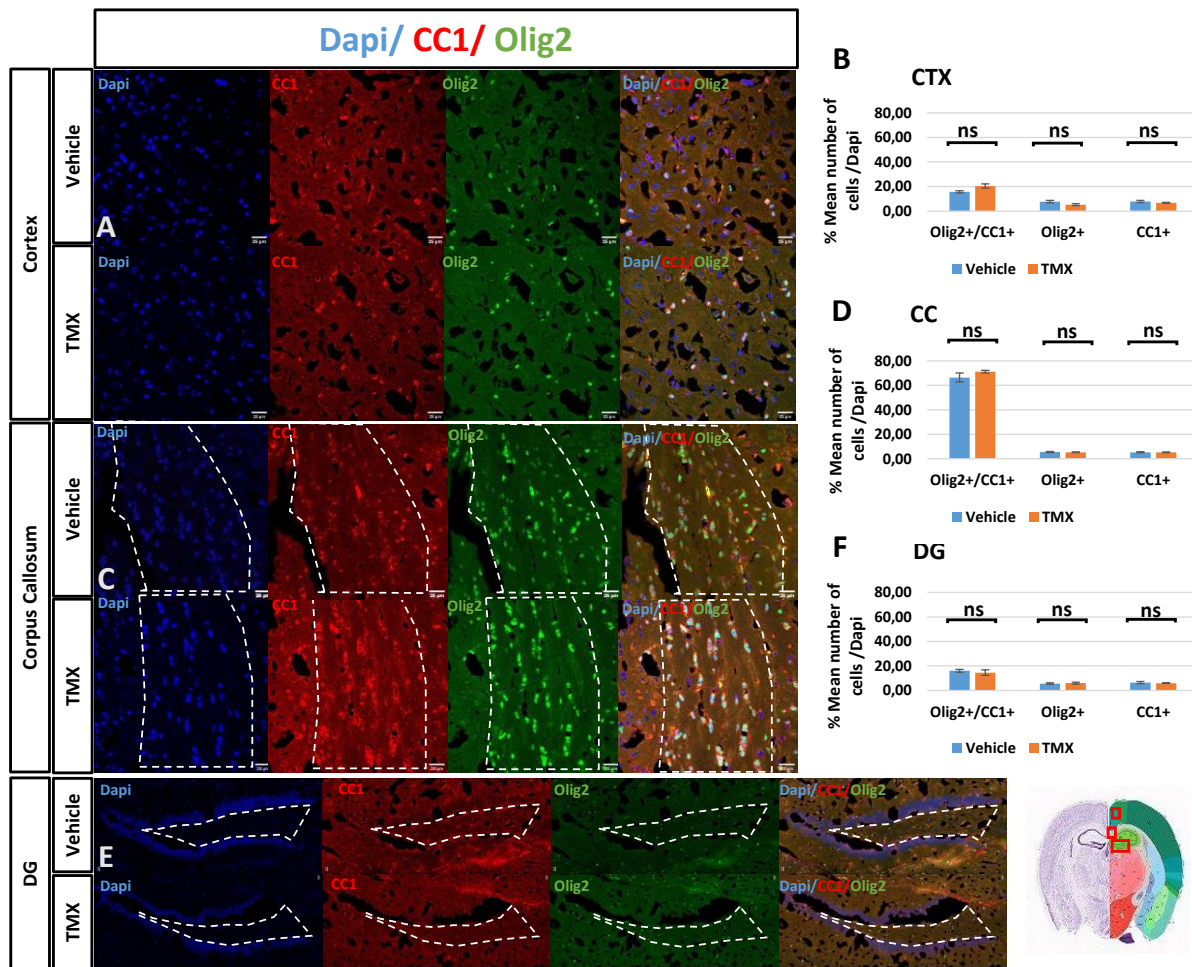
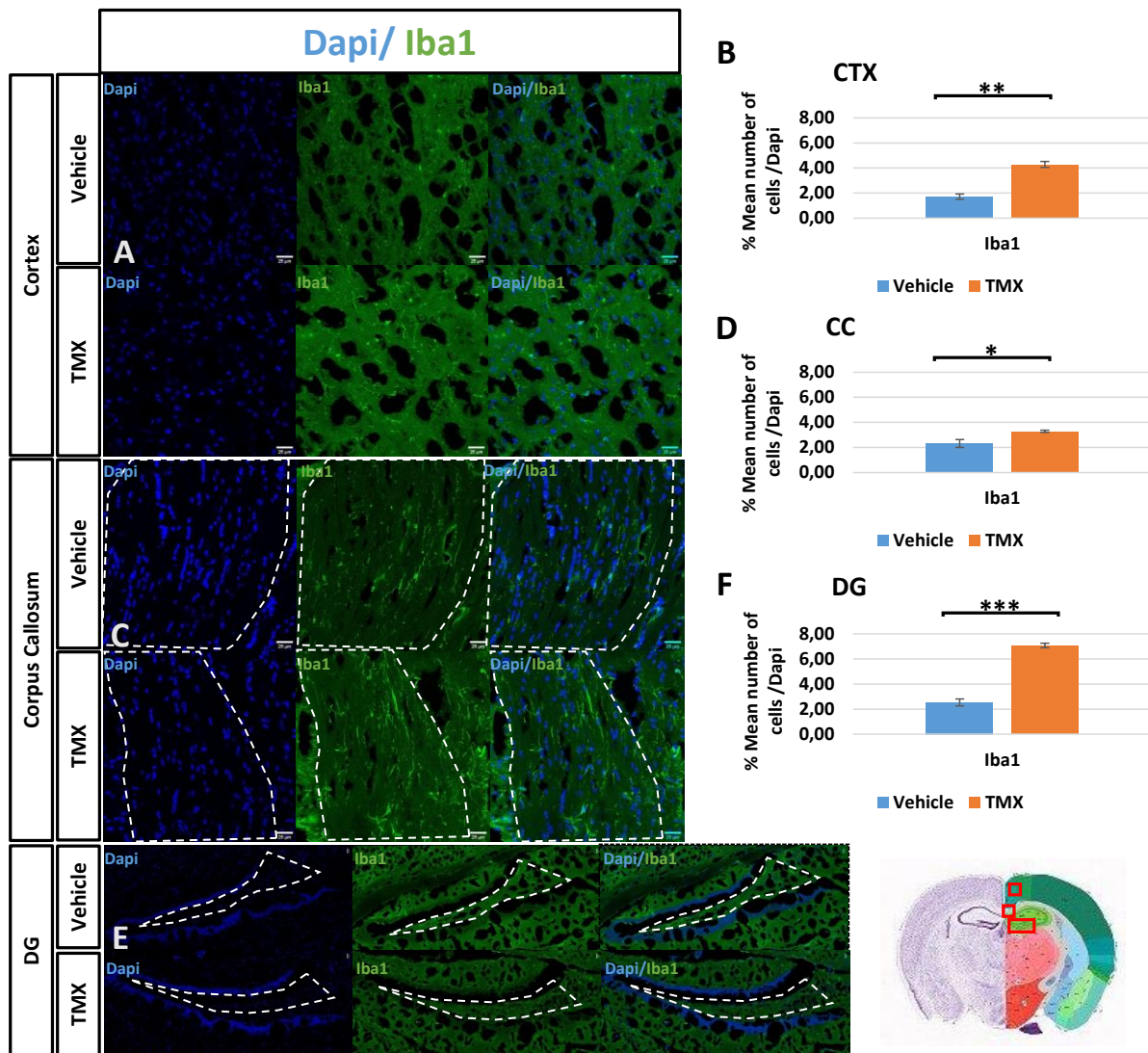


Figure 34: Alterations in percentage of mature and immature oligodendrocytes in tamoxifen injected *Glaxt-Cre-ERT2^{+/+}/Eif2b5^{fl/fl}* mice. Olig2 and CC1 double-labelling showed no difference in Olig2+/CC1+ cells mature oligodendrocytes percentage in Cortex area with $p=0.0690$ (A, B), Corpus Callosum area with $p=0.2727$ (C, D), and Dentate Gyrus Area with $p=0.5979$ or in Olig2-/CC1+ cells mature oligodendrocytes percentage in Cortex area with $p=0.3297$ (A, B), Corpus Callosum area with $p=0.8339$ (C, D), and Dentate Gyrus Area with $p=0.6304$ (E, F). There was also no difference observed in immature oligodendrocytes (Olig2+/CC1- cells) percentage in Cortex area with $p=0.1239$ (A, B), Corpus Callosum area with $p=0.6738$ (C, D), and Dentate Gyrus Area with $p=0.6886$ (E, F). Number of oligodendrocyte cells was normalized over total number of cells (Dapi+ cells). $N=3$ animals. TMX=Tamoxifen. Error bars represent Standard Error of the Mean (SEM). ns= non significant. Scalebar = 25 μm .

Activation of microglia in *Glast-Cre-ERT2^{+/-}/Eif2b5^{fl/fl}* treated mice

In addition, we investigated whether *Eif2b5* knock-out induced an inflammatory effect in the brain. For that, we looked for microglial cells in different regions of the brain using Iba1, a microglial cell marker. Interestingly, we observe morphological changes in 6w tamoxifen treated mice compared to vehicle treated ones. These changes are characterized by a larger cell body of microglia and longer processes that define the activated form of this cell type in the brain (Figure 35.A and C). In addition, cell number quantification of Iba1+ cells showed an increase for the TMX treated mice in the three tested regions of the brain, where in the cortex we observe an increase of about 2.5% (Cortex: Vehicle=1,72±0,21, TMX=4,29±0,24, p-value=0.0013), about 1% in the CC (Vehicle=2,31±0,32, TMX=3,29±0,08, p-value=0,0412), and also an increase of 4.5% in DG, (Vehicle=2,54±0,28, TMX=7,07±0,18, p-value=0,0002) (Figure 35).

The increased number of microglial cells in the brain has been associated to inflammation; this suggests that the *Eif2b5* knock-out triggered an inflammatory process determined by the elevated number of Iba1+ cells in different brain regions. In contrast, in VWM animal models, Iba+ cells did not show any significant changes in two point mutations in *eif2b5* gene (Dooves S. et al., 2016 JCI). However, the inflammation in VWM/CACH patients has not yet been investigated and described. Interestingly, our model is the first showing an inflammation in VWM/CACH disease (Figure 35).



Eif2b5 knock-out does not affect the neurons' number in the brain of Glast-Cre-ERT2^{+/-}/Eif2b5^{fl/fl} treated mice

Since Eif2b5 knock-out in the astrocytes of Glast-Cre-ERT2^{+/-}/Eif2b5^{fl/fl} treated mice had no apparent effect on oligodendrocyte maturation, we wanted to see if the neurons are still affected somehow. For this reason, neurons' numbers detected by the neuronal nuclear antigen NeuN have been assessed, and results showed no difference in Neurones (NeuN+ cells) percentage in Cortex area (Vehicle=42,34±1,33, TMX=41,72±1,05, p-value=0,7354) (Figure 36.A and B), nor Dentate Gyrus Area (Vehicle=35,58±1,87, TMX=36,4±1,86, p-value=0,7732) (Figure 36.E and F).

These results suggest that eif2b5 knock out in the Glast-Cre-ERT2^{+/-}/Eif2b5^{fl/fl} mice has no effect on neurons' numbers, which might explain the absence of neurological deteriorations in these mice.

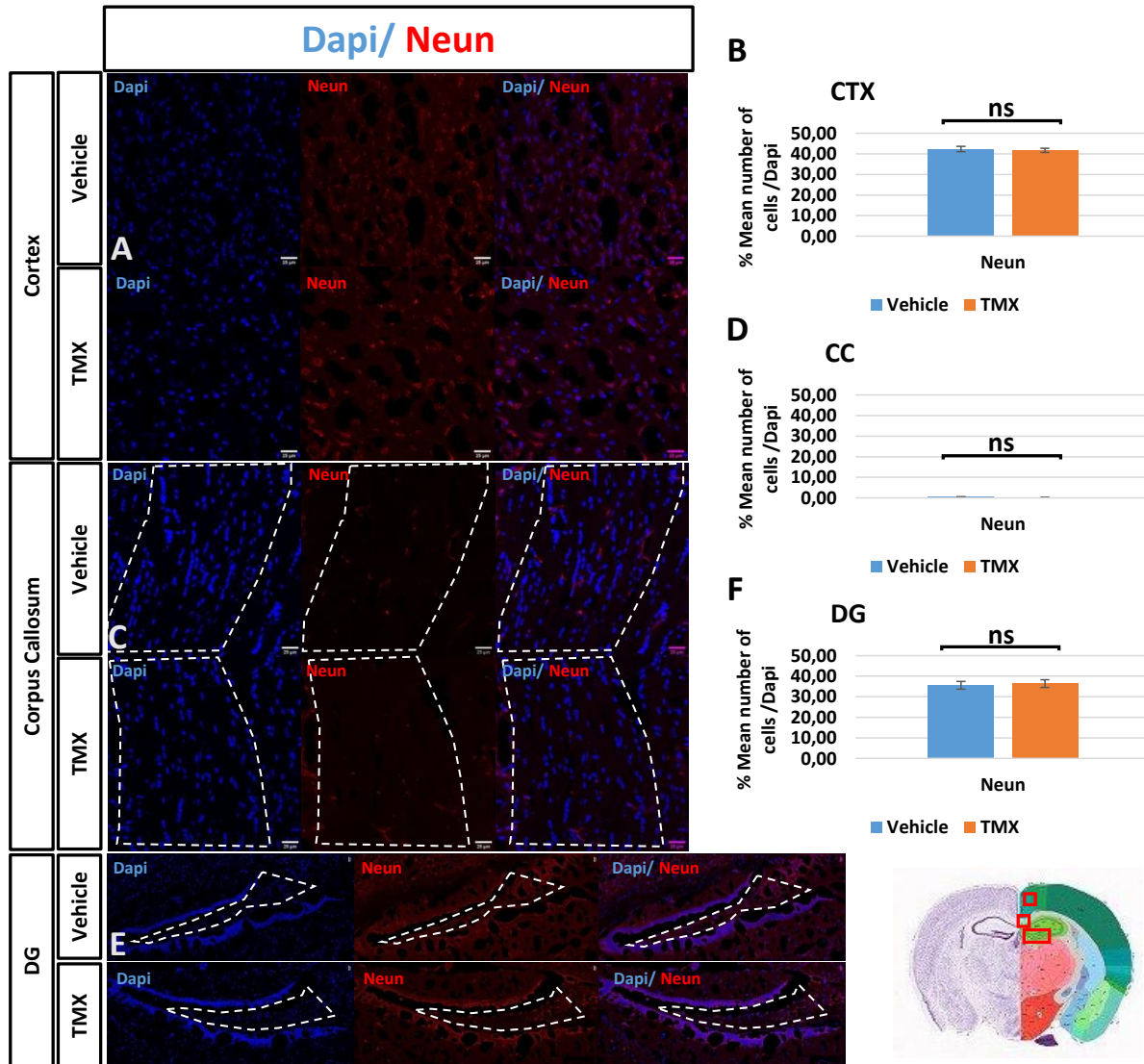


Figure 36: Alterations in percentage of microglial cell numbers in tamoxifen injected *Glax-Cre-ERT2^{+/-}/Eif2b5^{fl/fl}* mice. NeuN-labelling showed no difference in Neurones (Neun+ cells) percentage in Cortex area ($p= 0.7354$) (A, B), Corpus Callosum area ($p=0,2144$) (C, D), and Dentate Gyrus Area ($p=0,7732$) (E, F). Number of Neurones was normalized over total number of cells (Dapi+ cells). $N=3$ animals. TMX=Tamoxifen. Error bars represent Standard Error of the Mean (SEM). ns= non significant. Scalebar = 25 μ m.

Generation and Characterization of *Glast-Cre-ERT2^{-/-}/Eif2b5^{fl/fl}*

We generated *Glast-Cre-ERT2^{-/-}/Eif2b5^{fl/fl}* mouse model in order to understand CACH/VWM disease. By intraperitoneal injection of 1mg of tamoxifen, two times per day during 5 days, we induce the excision of *eif2b5* (exons 3 to 7) at two levels, where the lox P sites were inserted in introns 2-3 and introns 7-8. However, this excision is specifically in astrocytes, where the CreERT2 expression is under the control of *Glast* promotor (Figure 33). Two-month-old adult *Glast-Cre-ERT2^{-/-}/Eif2b5^{fl/fl}* mice have been treated with 1mg of tamoxifen, 2 times per day during 5 days. Another group of mice treated with the vehicle (Corn Oil) according to the same protocol has been considered as control. Five to six weeks (w5-w6) after injection, tamoxifen treated mice showed a neurological degradation leading to death after a severe loss of weight starting from the fifth week after injection (loss of 10% of their weight compared to vehicle) to reach about 27% at w6 (w5: Vehicle=23.82±0.18, TMX=21.43±0.31, w6: Vehicle=24.85±0.61, TMX=18.22±0.27) compared to the vehicle group (Figure 32).

In addition the survival study involving Vehicle and TMX treated male and female mice showed that all the female TMX treated mice died at week 7 PI whereas the vehicle treated females and all the males (irrelevant of the treatment) survived for 20 weeks PI when they were sacrificed (Figure 32 bottom right).

This neurological degradation observed at w6 in tamoxifen treated female mice mimics the symptoms observed in CACH patients carrying *eif2b5* mutation.

Eif2b5 knock-out induces activation of astrocytes and GFAP over expression in *Glast-Cre-ERT2^{-/-}/Eif2b5^{fl/fl}* treated mice

In CACH/VWMD, abnormal astrogliosis, astrocytic defective morphology and severe white matter devastations are the main features where astrocytes and oligodendrocytes are affected. In our model, *Eif2b5* knock-out is specifically induced in astrocytes by having CreERT2 expression under the control of the *Glast* promotor. For these reasons, we first evaluated the expression level of the astrocyte marker Glial fibrillary acidic protein or GFAP. The mean GFAP+ area showed an increase of about 15 fold in the cortex

(Vehicle=0,23±0,08%, TMX= 3,63±0,24%; p-value < 0.0001)) (Figure 37.A, B), as well as an increase in DG (Vehicle=5,79±0,21%, TMX=8,79±1,18%; p-value=0.0363) (Figure 37.E, F) 6w after tamoxifen treatment. In addition, these astrocytes seem to show signs of the reactive astrocytes' morphology especially in the cortex (Figure 37.A). However, no significant changes have been shown in the CC (Vehicle=5,78±0,68%, TMX=4,71±1,28%; p-value=0,4589) (Figure 37.C and D).

These results show an effect of *Eif2b5* knock-out on astrocytes' activation and reaction.

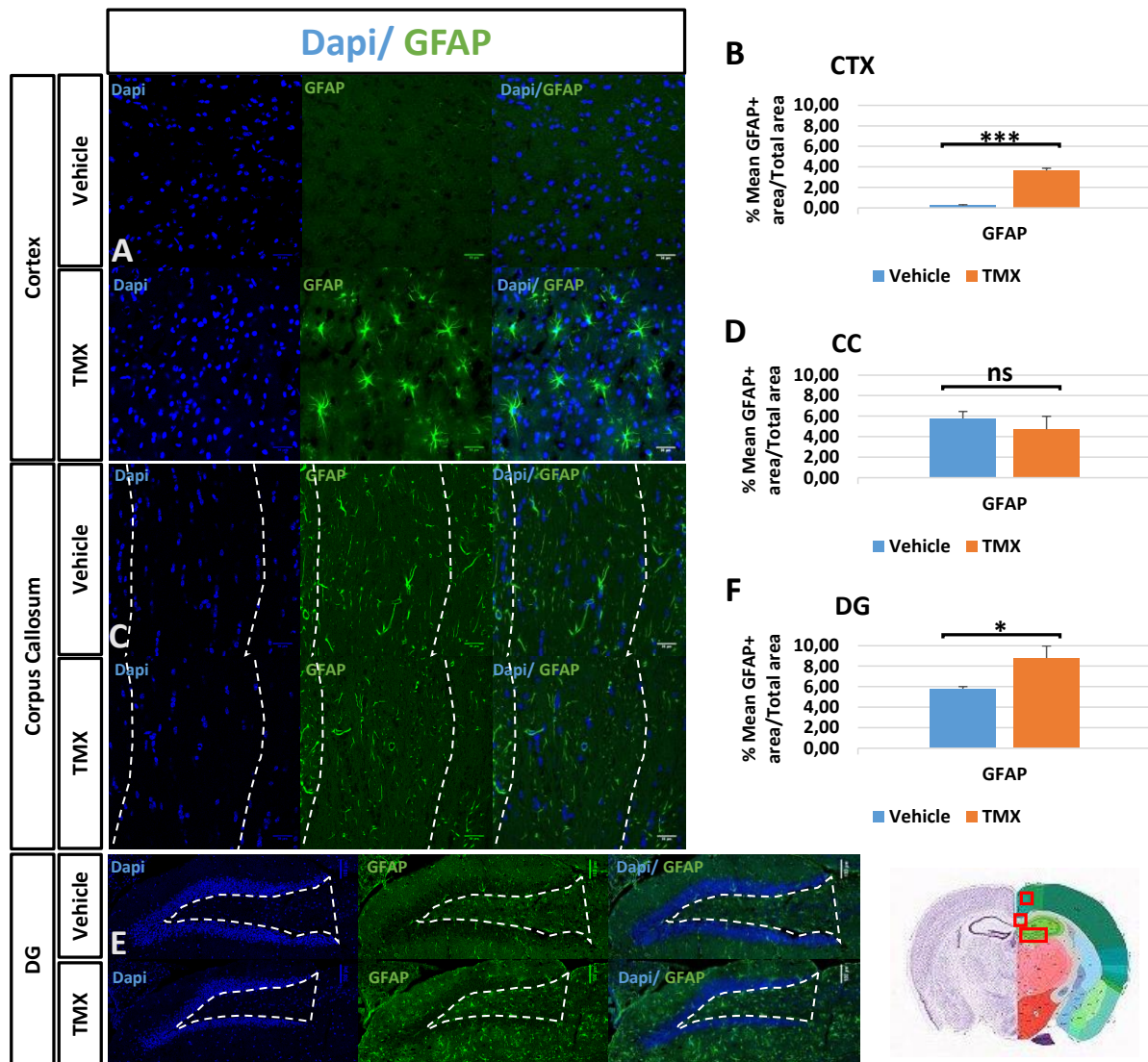


Figure 37: Alterations in astrocyte cell marker's expression in tamoxifen injected *Glax-Cre-ERT2^{-/-}/Eif2b5^{fl/fl}* mice. GFAP-labelling showed an increase in GFAP expression in Cortex area ($p < 0.0001$) (A, B) and area Dentate Gyrus ($p = 0.0363$) (E, F), but not in Corpus Callosum Area

($p=0,4589$) (C, D). Expression level of GFAP was normalized over total area scanned. $N=5$ animals. TMX=Tamoxifen. Error bars represent Standard Error of the Mean (SEM). * = $P < 0.05$, *** = $P < 0.001$, ns= non significant. Scalebar = 25 μm .

Loss of mature oligodendrocytes in $\text{Glast-Cre-ERT2}^{-/-}/\text{Eif2b5}^{\text{fl/fl}}$ treated mice

We next investigated the evaluation of oligodendrocytes, and their maturation in different regions of the mouse brain. At the moment of neurological degradation, 6w after injection, we found an important decrease of mature oligodendrocytes' numbers (Olig2+/CC1+ cells) in tamoxifen treated mice in the cortex area (Vehicle=29,6 \pm 5,33, TMX=13,98 \pm 1,46; $p= 0.0475$) (Figure 38.A, B), Corpus Callosum area (Vehicle=82,11 \pm 1,14, TMX=64,20 \pm 1,99; $p= 0.0014$) (Figure 38.C, D), but not in Dentate Gyrus Area (Vehicle=41,26 \pm 2,34, TMX=30,54 \pm 7,62; $p= 0.2499$) (Figure 38 E, F). Quantification of Olig2-/CC1+ cells mature oligodendrocytes percentage showed a significant increase in Corpus Callosum area (Vehicle=7,63 \pm 0,41, TMX=12,33 \pm 0,72; $p= 0.0047$) (Figure 38.C, D), but not in Cortex area (Vehicle=11,83 \pm 2,05, TMX=7,52 \pm 2,51; $p= 0.2642$) (Figure 38.A, B), or Dentate Gyrus Area (Vehicle=8,9 \pm 0,08, TMX=9,4 \pm 2,59; $p= 0.8583$) (Figure 38.E, F). There was also no difference observed in immature oligodendrocytes (Olig2+/CC1- cells) percentage in Cortex area (Vehicle=7,67 \pm 1,23, TMX=5,33 \pm 0,62; $p=0.1237$) (Figure 38.A, B), Corpus Callosum area (Vehicle=1,77 \pm 0,62, TMX=6,16 \pm 2,44; $p=0.1557$) (Figure 38.C, D), and Dentate Gyrus Area (Vehicle=2,91 \pm 0,62, TMX=7,02 \pm 3,79; $p=0.3445$) (Figure 38.E, F). The decrease of mature oligodendrocytes and the absence of any changes of immature form in different brain regions, especially in CC suggest an effect of *Eif2b5* excision on cell maturation of oligodendrocytes.

These results taken together suggest an effect of *Eif2b5* excision on astrocyte activation, which in turn affects oligodendrocyte maturation where we observe a decreased number of mature oligodendrocytes in different brain region in the mutant mice. Recently, it has been shown that in co-culture of VWM astrocyte and OPCs, these last, failed to mature and express myelinating cells such as MBP+ cells (Dooves S. et al., JCI,2016).

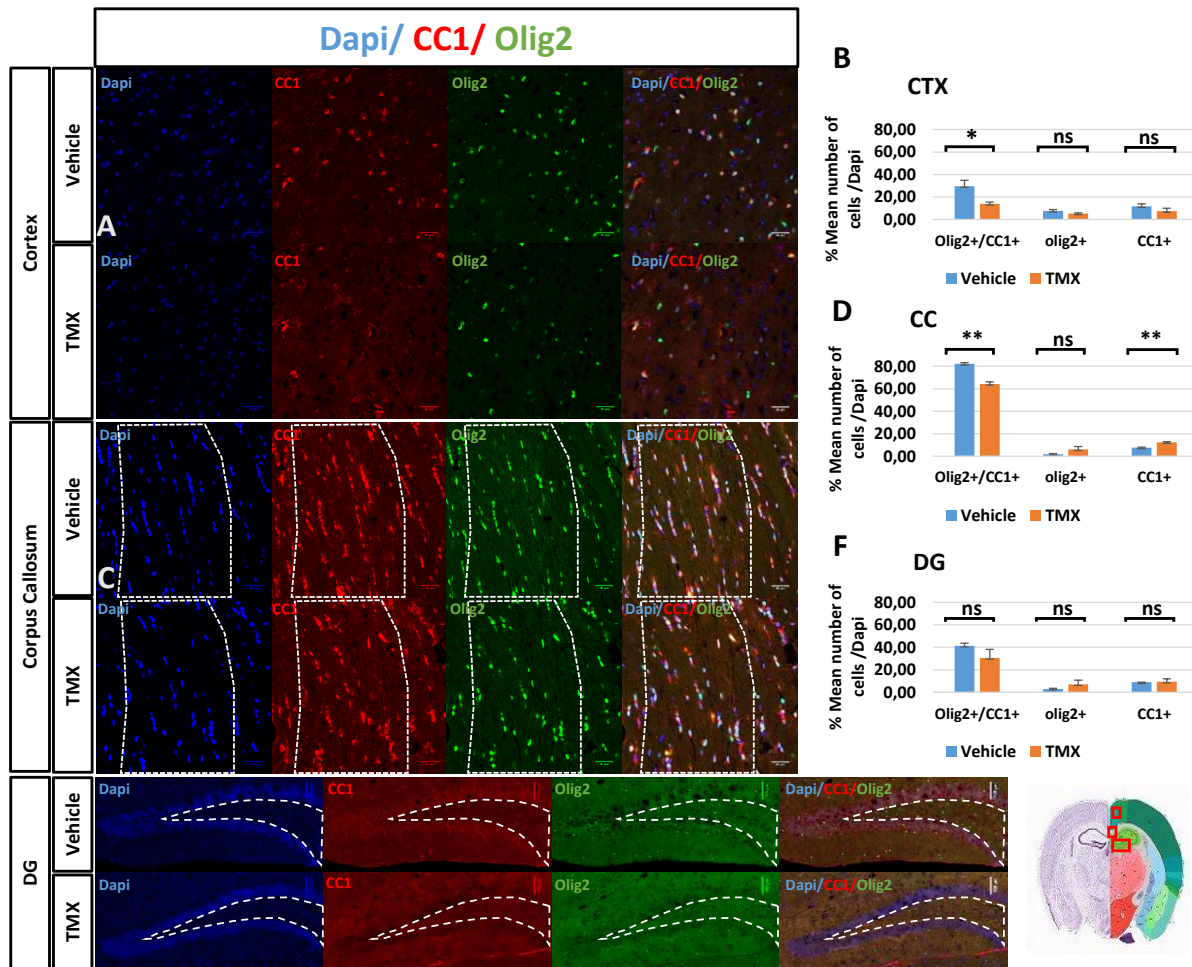


Figure 38: Alterations in percentage of mature and immature oligodendrocytes in tamoxifen injected *Glax-Cre-ERT2^{-/-}/Eif2b5^{fl/fl}* mice. Olig2 and CC1 double-labelling showed a decrease in mature oligodendrocytes (Olig2+/CC1+ cells) percentage in Cortex area with $p = 0.0475$ (A, B), Corpus Callosum area with $p = 0.0014$ (C, D), but not in Dentate Gyrus Area with $p = 0.2499$. Quantification of Olig2-/CC1+ cells mature oligodendrocytes percentage showed a significant increase in Corpus Callosum area with $p = 0.0047$ (C, D), but not in Cortex area with $p = 0.2642$ (A, B), or Dentate Gyrus Area with $p = 0.8583$ (E, F). There was also no difference observed in immature oligodendrocytes (Olig2+/CC1- cells) percentage in Cortex area with $p = 0.1237$ (A, B), Corpus Callosum area with $p = 0.1557$ (C, D), and Dentate Gyrus Area with $p = 0.3445$ (E, F). Number of oligodendrocyte cells was normalized over total number of cells (Dapi+ cells). $N=3$ animals. TMX=Tamoxifen. Error bars represent Standard Error of the Mean (SEM). * = $P < 0.05$, ** = $P < 0.01$, ns= non significant. Scalebar = 25 μm .

Activation of microglia in *Glast-Cre-ERT2^{-/-}/Eif2b5^{fl/fl}* treated mice

In addition, we investigated whether *Eif2b5* knock-out induced an inflammatory effect in the brain. For that, we looked for microglial cells in different regions of the brain using Iba1, a microglial cell marker. Interestingly, we observe morphological changes in 6w tamoxifen treated mice compared to vehicle treated ones. These changes are characterized by a larger cell body of microglia and longer processes that define the activated form of this cell type in the brain (Figure 39.A and C). In addition, cell number quantification of Iba1+ cells showed an increase for the TMX treated mice of about 8% in the CC (Vehicle=8,26±0,92, TMX=16,53±2,96, p-value=0,0214) (Figure 39.C and D), and an increase of 6% in DG (Vehicle=18,38±0,94, TMX=24,68±2,05, p-value=0,0196) (Figure 39.E and F), but no difference was found in the cortex area (Cortex: Vehicle=10,26±0,96, TMX=11,5±1,41, p-value=0.4758). The increased number of microglial cells in the brain has been associated to inflammation; this suggests that the *Eif2b5* knock-out triggered an inflammatory process determined by the elevated number of Iba1+ cells in different brain regions. In contrast, in VWM animal models, Iba+ cells did not show any significant changes in two point mutations in *eif2b5* gene (Dooves S. et al., 2016 JCI). However, the inflammation in VWM/CACH patients has not yet been investigated and described. Interestingly, our model is the first showing an inflammation in VWM/CACH disease (Figure 39).

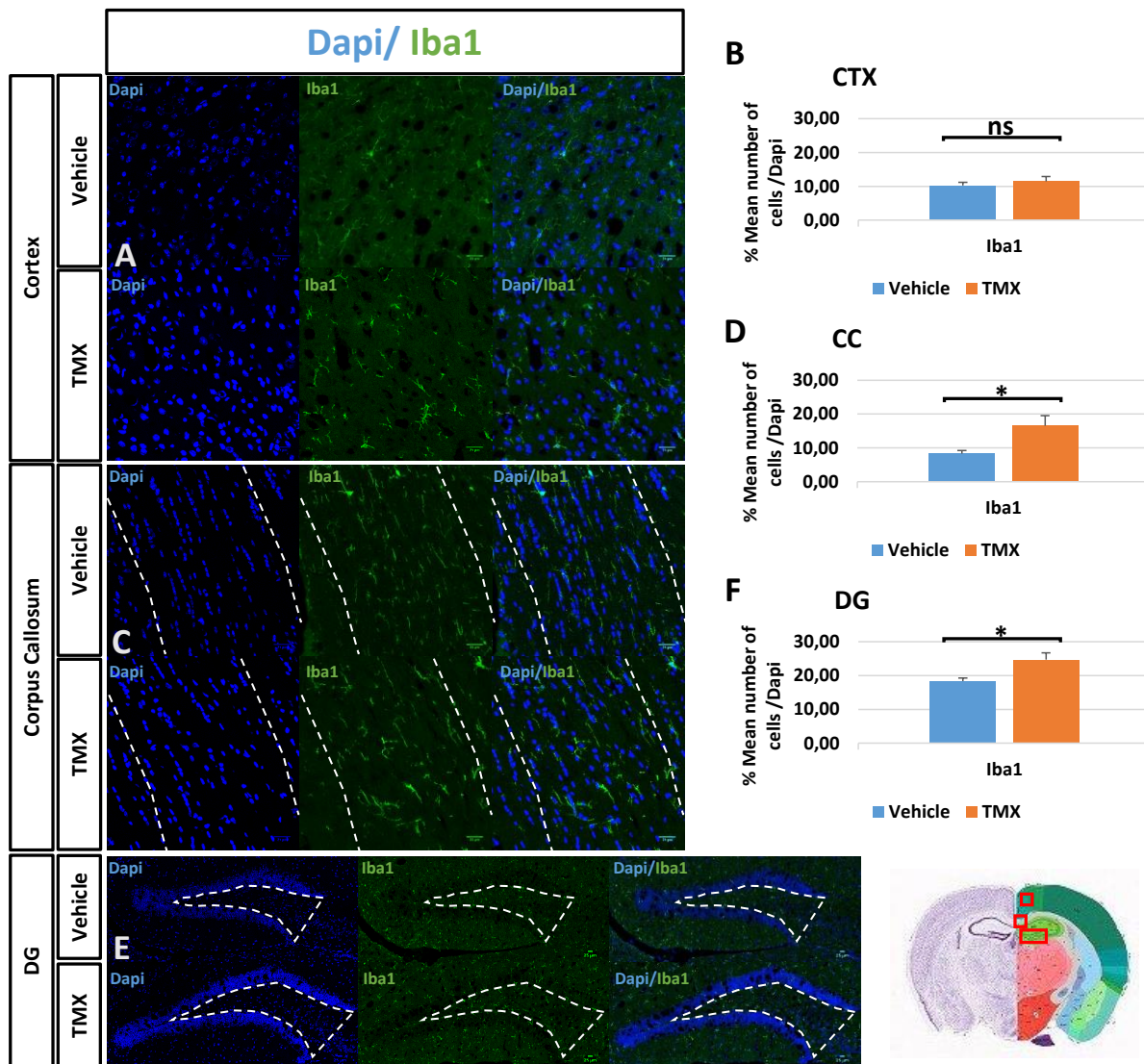


Figure 39: Alterations in percentage of microglial cell numbers in tamoxifen injected *Glax-Cre-ERT2^{-/-}/Eif2b5^{fl/fl}* mice. Iba1-labelling showed an increase in microglial cell numbers (Iba1+ cells) percentage in Corpus Callosum area ($p=0,0214$) (C, D), and Dentate Gyrus Area ($p=0,0196$) (E, F), but not in Cortex area ($p=0,4758$) (A, B). Number of microglial cells was normalized over total number of cells (Dapi+ cells). $N=5$ animals. TMX=Tamoxifen. Error bars represent Standard Error of the Mean (SEM). * = $P < 0.05$, ns= non significant. Scalebar = 25 μm .

Eif2b5 knock-out induces a decrease of neurons' number in cortex and dentate gyrus in *Glax-Cre-ERT2^{-/-}/Eif2b5^{fl/fl}* treated mice

Since loss of mature oligodendrocyte-the myelinating type of oligodendrocytes- is significantly shown in eif2b5 knock-out mice, neuronal variation can also be a consequence of this loss. In addition, a paucity of myelin and thin vacuolated sheaths of myelin formation

observed in CACH/VWMD patients renders neuronal axons to be surrounded with uncompacted myelin around their membranes. Moreover, the axonal loss is obvious in areas with cavitation in WM whereas they are still preserved in spared WM with a thinned structure. For this reason, neurons' numbers have been assessed, and results showed a decrease of neurons' number detected by the neuronal nuclear antigen NeuN in tamoxifen treated mice compared to vehicle ones (Figure 40.A, C and E). This decrease was about 7% in the cortex (Vehicle=62,02±1,01, TMX=55,83±0,33, p-value=0,0044) (Figure 40.A and B). Interestingly this decrease was also significant in DG (9%) (Vehicle=58,36±0,94, TMX=49,19±2,08, p-value=0,0158) (Figure 40.E and F). These results suggest that eif2b5 knock out induce a loss of neurons, moreover, it can explain the neurological deterioration observed in observed in these mice.

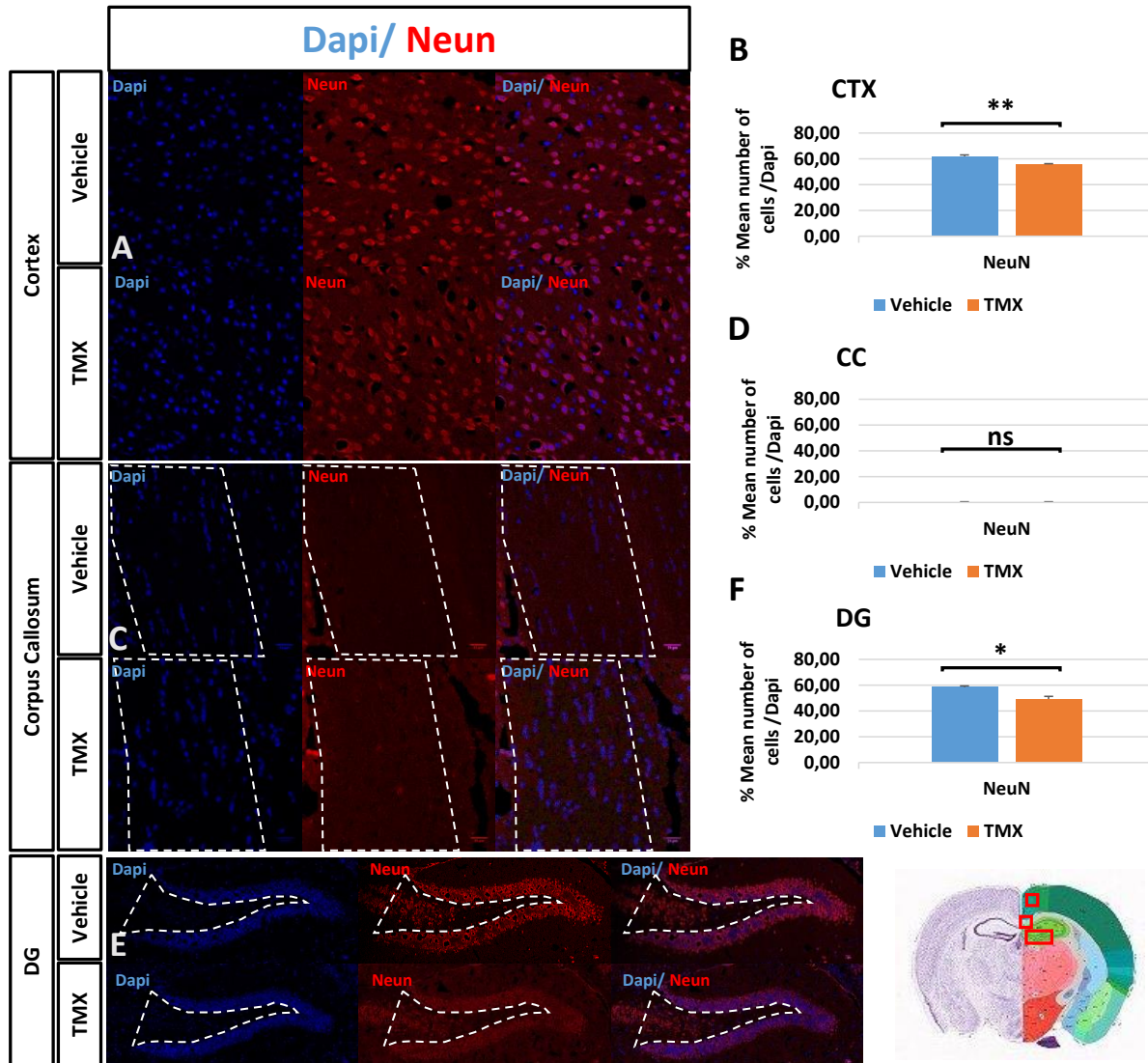


Figure 40: Alterations in percentage of Neurones in tamoxifen injected *Glax-Cre-ERT2^{-/-}/Eif2b5^{fl/fl}* mice. NeuN-labelling showed a decrease in Neurones (NeuN+ cells) percentage in Cortex area ($p=0.0044$) (A, B) and Dentate Gyrus Area ($p=0.0158$) (E, F) while no difference was found in the Corpus Callosum area ($p=0.183$) (C, D). Number of Neurones was normalized over total number of cells (Dapi+ cells). $N=3$ animals. TMX=Tamoxifen. Error bars represent Standard Error of the Mean (SEM). * = $P < 0.05$, ** = $P < 0.01$, ns= non significant. Scalebar = 25 μm .

VI. General discussion and perspectives

Here we investigate the consequences of eIF2B5 inactivation in oligodendrocytes and in astrocytes in adult mice in order to decipher the glial cell sensitivity to ER stress.

For this purpose, the **eIF2B models are of great interest because eIF2B is the major regulator of protein synthesis under normal and stress conditions**. By controlling the level of ternary complexes, eIF2B governs the rate of global translation. In stress condition, the four stress response kinases (PERK, HRI, GCN2, PKR) phosphorylate eIF2. This phosphorylated eIF2 (eIF2-P) becomes a competitive inhibitor of eIF2B triggering endoplasmic reticulum (ER) stress with an integrated stress response (ISR). ISR reduces translation initiation events and decrease global protein synthesis but increases, in parallel, translation of a subset of mRNA with inhibitory upstream reading frame (uORF) in their 5'UTRs including mRNA encoding stress response regulators such as ATF4. In acute /transient stress, a second ISR program induced GADD34, which dephosphorylates eIF2-P, restores eIF2B GEF activity and the translation program. In contrast to acute ER stress, the chronic stress triggers new ISR mechanisms. This chronic ISR is characterized by persistently elevated uORF mRNA translation and concurrent gene expression reprogramming which permits stress sensing and partial recovery of protein synthesis (Guan et al 2017). Translational initiation in this chronic stress situation is eIF2B independent and involved other mechanisms. Dysfunctions related to chronic ER-stress has been suggested as the main pathological mechanisms of a large number of human diseases particularly of the central nervous system (CNS), the CNS and the highly differentiated cells being the most sensitive (Zhang et al 2008).

Our results clearly demonstrated that during adult life, eIF2B inactivation in astrocytes is less deleterious than in oligodendrocytes, underlining the greater sensitivity of the oligodendrocytes to ER stress. These results seems not in agreement with the general assessment that astrocytes are the target of CACH/VWM disease. The main arguments are coming from the aberrant Bergmann glia found in the cerebellum of CACH/VWM patient as

well as from the double KI Eif2b4/eIF2b5. This observation seems more related to the neurodevelopmental impairment observed in CACH/VWM. The vacuolating aspect of the white matter on MRI is present even in presymptomatic patient. This aspect is observed in other leukodystrophies in which the genetic target is the astrocytes such as the MLC1 and GFAP mutations suggesting that the MRI white matter aspect in CACH/VWM is probably related to the abnormal astrocytes development particularly at the blood vessels-brain parenchyma interface. In addition, the co-culture experiments of astrocytes and oligodendrocytes have demonstrated the inhibiting effect of the supernatant of eIF2b mutated astrocytes on the oligodendrocytes maturation and not the opposite. Our results suggest that the oligodendrocytes would play a key role in the hypomyelination observed in CACH/VWM as well as in the acute neurological deterioration and progressive neurodegenerative associated process leading to the severe prognostic of eIF2B related disorders.

During adult life, eIF2B inactivation in oligodendrocytes is independant of the sex whereas in astrocytes (or at least the Glast expressing cells) sex difference with female sensitivity seems to trigger acute neurological distress particularly when associated with other proactive factors.

These results could be related to astrocytes or oligodendrocytes sex differences. However, different arguments are in favor of oligodendrocytes sex dependence: (i) higher sensitivity of oligodendrocytes to glutamate increase, (ii) myelin sex difference related to a larger number of myelinating oligodendrocytes with a thick myelin in males, (iii) similarity in the cellular consequences of eIF2B5 inactivation in either oligodendrocytes or astrocytes when an acute neurological distress is observed.

We found that **the chronic ER stress induced by eIF2B defect in O4+ immature oligodendrocytes changes the gene expression profile toward immaturity and inflammatory response.** It has been extensively reported in the literature that OPCs and oligodendrocytes of the adult brain can express key players of immune and inflammatory processes, in pathological conditions. This includes studies of patients affected by multiple sclerosis (MS) or in in-vivo models of experimental autoimmune encephalomyelitis (EAE;

reviewed in Zeis et al 2016). However, the direct consequences of ER stress on the expression of immune and inflammatory processes of OPCs and oligodendrocytes of the adult brain have not been clearly demonstrated. Recently single cell transcriptomic analysis of OL lineage cells from spinal cord of mice induced by EAE as well from MS patients demonstrated that specific OL lineage populations are active immunomodulators (Falcao et al., 2018). OPC may be co-opted by the immune system in MS to perpetuate the autoimmune response (Kirby et al., 2019). Our results suggested that the activation of the immunomodulating capacity of the oligodendrocytes could be not related to the immune system but an autonomous dysregulation of the O4+ immature oligodendrocytes by chronic ISR leading to remodeling of the gene expression causing impairment of the remyelination program. Other metabolic factors described in CACH/VWM as well as in MS particularly of the mitochondrial functions could also be the result of this reprogramming.

The conditional ko models have the advantage to address the physiopathological mechanisms to a specific cell type without lethality. However, the specificity of the promoter used is never perfect. We choose the Glast promoter in order to target the whole astrocyte lineage. However, the Glast expression is probably larger, including immature oligodendrocytes. Single cell MACS isolation is a powerful tool with excellent reproducibility for comparative cell specific RNAseq studies. The disadvantage of these techniques is avoiding to take in account the effect of different affected cell types with large interactions as it is the case for the ubiquitously expressed eIF2B factor. None of the KI eIF2B mice reproduces the human pathology with acute phase. A chronic neurodegenerative process similar to the slow progressive form of CACH/VWM is observed only in a homozygous double KI suggesting that the mice is more resistant to ER stress. Translation from mice to human remains a challenge in terms of cellular stress and glial cells functions.

Additional studies particularly proteomics/metabolic of the transgenic mice brains are needed in order to evaluate the proteins involved.

VII. Conclusions

All of the work we have done underlines the susceptibility of the oligodendrocyte cells, particularly the immature ones, to chronic ER stress induced by a deficit in EIF2B leading to a delayed fast and brutal neurological degradation as observed during the phases of acute decompensation of the CACH/VWM disease and even in the MS.

The astrocytes, which were until now considered as the target of the pathology in the KI eIF2B mouse models, require the association of several factors to the acute neurological distress in our conditional KO model.

They might be more involved in in the developmental phase of cohesion of the white matter and the more chronic dysfunction of the white matter homeostasy.

VIII. References

- Abbink, T.E.M., Wisse, L.E., Jaku, E., Thiecke, M.J., Voltolini-González, D., Fritsen, H., Bobeldijk, S., Braak, T.J., Polder, E., Postma, N.L., Bugiani, M., Struijs, E.A., Verheijen, M., Straat, N., Sluis, S., Thomas, A.A.M., Molenaar, D., Knaap, M.S., 2019. Vanishing white matter: deregulated integrated stress response as therapy target. *Ann Clin Transl Neurol* acn3.50826. <https://doi.org/10.1002/acn3.50826>
- Abbink, T.E.M., Wisse, L.E., Wang, X., Proud, C.G., 2018. Role of Eukaryotic Initiation Factor eIF2B in Vanishing White Matter Disease, in: Sossin, W. (Ed.), *The Oxford Handbook of Neuronal Protein Synthesis*. Oxford University Press. <https://doi.org/10.1093/oxfordhb/9780190686307.013.7>
- Alamri, H., Al Mutairi, F., Alothman, J., Alothaim, A., Alfadhel, M., Alfares, A., 2016. Diabetic ketoacidosis in vanishing white matter. *Clin Case Rep* 4, 717–720. <https://doi.org/10.1002/ccr3.597>
- Allen, N.J., Lyons, D.A., 2018. Glia as architects of central nervous system formation and function. *Science* 362, 181–185. <https://doi.org/10.1126/science.aat0473>
- Atzmon, A., Herrero, M., Sharet-Eshed, R., Gilad, Y., Senderowitz, H., Elroy-Stein, O., 2018. Drug Screening Identifies Sigma-1-Receptor as a Target for the Therapy of VWM Leukodystrophy. *Front. Mol. Neurosci.* 11, 336. <https://doi.org/10.3389/fnmol.2018.00336>
- Aviner, R., Hofmann, S., Elman, T., Shenoy, A., Geiger, T., Elkon, R., Ehrlich, M., Elroy-Stein, O., 2017. Proteomic analysis of polyribosomes identifies splicing factors as potential regulators of translation during mitosis. *Nucleic Acids Research* 45, 5945–5957. <https://doi.org/10.1093/nar/gkx326>
- Baaklini, C. S., Rawji, K. S., Duncan, G. J., Ho, M. F. S., & Plemel, J. R. (2019). Central Nervous System Remyelination: Roles of Glia and Innate Immune Cells. *Frontiers in Molecular Neuroscience*, 12, 225. <https://doi.org/10.3389/fnmol.2019.00225>
- Baumann, N., Turpin, J.-C., 2000. Adult-onset leukodystrophies. *Journal of Neurology* 247, 751–759. <https://doi.org/10.1007/s004150070088>
- Bayraktar, O.A., Fuentealba, L.C., Alvarez-Buylla, A., Rowitch, D.H., 2015. Astrocyte Development and Heterogeneity. *Cold Spring Harb Perspect Biol* 7, a020362. <https://doi.org/10.1101/cshperspect.a020362>
- Bergles, D.E., Richardson, W.D., 2016. Oligodendrocyte Development and Plasticity. *Cold Spring Harb Perspect Biol* 8, a020453. <https://doi.org/10.1101/cshperspect.a020453>
- Bergström, T., Forsberg-Nilsson, K., 2012. Neural stem cells: Brain building blocks and beyond. *Upsala Journal of Medical Sciences* 117, 132–142. <https://doi.org/10.3109/03009734.2012.665096>

- Black, D.N., Watters, G.V., Andermann, E., Dumont, C., Kabay, M.E., Kaplan, P., Meagher-Villemure, K., Michaud, J., O'gorman, G., Reece, E., Tsoukas, C., Wainberg, M.A., 1988. Encephalitis among cree children in northern Quebec. *Ann Neurol.* 24, 483–489. <https://doi.org/10.1002/ana.410240402>
- Bluml, S., Philippart, M., Schiffmann, R., Seymour, K., Ross, B.D., 2003. Membrane phospholipids and high-energy metabolites in childhood ataxia with CNS hypomyelination. *Neurology* 61, 648–654. <https://doi.org/10.1212/WNL.61.5.648>
- Boespflug-Tanguy, O., Labauge, P., Fogli, A., Vauris-Barriere, C., 2008. Genes involved in leukodystrophies: A glance at glial functions. *Curr Neurol Neurosci Rep* 8, 217–229. <https://doi.org/10.1007/s11910-008-0034-x>
- Bogorad, A.M., Lin, K.Y., Marintchev, A., 2018. eIF2B Mechanisms of Action and Regulation: A Thermodynamic View. *Biochemistry* 57, 1426–1435. <https://doi.org/10.1021/acs.biochem.7b00957>
- Bonkowsky, J.L., Nelson, C., Kingston, J.L., Filloux, F.M., Mundorff, M.B., Srivastava, R., 2010. The burden of inherited leukodystrophies in children. *Neurology* 75, 718–725. <https://doi.org/10.1212/WNL.0b013e3181eee46b>
- Brück, W., Herms, J., Brockmann, K., Schulz-Schaeffer, W., Hanefeld, F., 2001. Myelinopathia centralis diffusa (vanishing white matter disease): Evidence of apoptotic oligodendrocyte degeneration in early lesion development: Oligodendrocyte Apoptosis in Leukoencephalopathy. *Ann Neurol.* 50, 532–536. <https://doi.org/10.1002/ana.1227>
- Buck, M.L., Gurka, M.J., Goodkin, H.P., 2007. POSTMARKETING MODIFICATIONS IN THE SAFETY LABELING OF THE NEW ANTIEPILEPTICS. *Neurology* 68, 1536–1537. <https://doi.org/10.1212/01.wnl.0000260700.58495.f6>
- Bugiani, M., Boor, I., Powers, J.M., Scheper, G.C., van der Knaap, M.S., 2010. Leukoencephalopathy With Vanishing White Matter: A Review. *J Neuropathol Exp Neurol* 69, 987–996. <https://doi.org/10.1097/NEN.0b013e3181f2eafa>
- Bugiani, M., Boor, I., van Kollenburg, B., Postma, N., Polder, E., van Berkel, C., van Kesteren, R.E., Windrem, M.S., Hol, E.M., Scheper, G.C., Goldman, S.A., van der Knaap, M.S., 2011. Defective Glial Maturation in Vanishing White Matter Disease. *J Neuropathol Exp Neurol* 70, 69–82. <https://doi.org/10.1097/NEN.0b013e318203ae74>
- Bugiani, M., Vuong, C., Breur, M., van der Knaap, M.S., 2018. Vanishing white matter: a leukodystrophy due to astrocytic dysfunction: Vanishing White Matter. *Brain Pathology* 28, 408–421. <https://doi.org/10.1111/bpa.12606>
- Cabilly, Y., Barbi, M., Geva, M., Marom, L., Chetrit, D., Ehrlich, M., Elroy-Stein, O., 2012. Poor Cerebral Inflammatory Response in eIF2B Knock-In Mice: Implications for the Aetiology of Vanishing White Matter Disease. *PLoS ONE* 7, e46715. <https://doi.org/10.1371/journal.pone.0046715>

- Chabriat, H., Joutel, A., Dichgans, M., Tournier-Lasserre, E., Bousser, M.-G., 2009. CADASIL. [https://doi.org/10.1016/S1474-4422\(09\)70127-9](https://doi.org/10.1016/S1474-4422(09)70127-9)
- Chen, V.S., Morrison, J.P., Southwell, M.F., Foley, J.F., Bolon, B., Elmore, S.A., 2017. Histology Atlas of the Developing Prenatal and Postnatal Mouse Central Nervous System, with Emphasis on Prenatal Days E7.5 to E18.5. *Toxicol Pathol* 45, 705–744. <https://doi.org/10.1177/0192623317728134>
- Choleris, E., Galea, L.A.M., Sohrabji, F., Frick, K.M., 2018. Sex differences in the brain: Implications for behavioral and biomedical research. *Neuroscience & Biobehavioral Reviews* 85, 126–145. <https://doi.org/10.1016/j.neubiorev.2017.07.005>
- Clinical European Network on Brain Dysmyelinating Disease†, Cailloux, F., Gauthier-Barichard, F., Mimault, C., Isabelle, V., Courtois, V., Giraud, G., Dastugue, B., Boespflug-Tanguy, O., 2000. Genotype–phenotype correlation in inherited brain myelination defects due to proteolipid protein gene mutations. *Eur J Hum Genet* 8, 837–845. <https://doi.org/10.1038/sj.ejhg.5200537>
- Colonna, M., Butovsky, O., 2017. Microglia Function in the Central Nervous System During Health and Neurodegeneration. *Annu. Rev. Immunol.* 35, 441–468. <https://doi.org/10.1146/annurev-immunol-051116-052358>
- Crow, Y.J., Vanderver, A., Orcesi, S., Kuijpers, T.W., Rice, G.I., 2014. Therapies in Aicardi-Goutières syndrome: Therapies in AGS. *Clin Exp Immunol* 175, 1–8. <https://doi.org/10.1111/cei.12115>
- Damon-Perriere, N., Menegon, P., Olivier, A., Boespflug-Tanguy, O., Niel, F., Creveaux, I., Dousset, V., Brochet, B., Goizet, C., 2008. Intra-familial phenotypic heterogeneity in adult onset vanishing white matter disease. *Clinical Neurology and Neurosurgery* 110, 1068–1071. <https://doi.org/10.1016/j.clineuro.2008.08.003>
- de Almeida, R.A., Fogli, A., Gaillard, M., Scheper, G.C., Boespflug-Tanguy, O., Pavitt, G.D., 2013. A Yeast Purification System for Human Translation Initiation Factors eIF2 and eIF2Bε and Their Use in the Diagnosis of CACH/VWM Disease. *PLoS ONE* 8, e53958. <https://doi.org/10.1371/journal.pone.0053958>
- Delhay-Bouchaud, N., 2001. Développement du système nerveux central chez les mammifères. *Neurophysiologie Clinique/Clinical Neurophysiology* 31, 63–82. [https://doi.org/10.1016/S0987-7053\(01\)00249-0](https://doi.org/10.1016/S0987-7053(01)00249-0)
- Dietrich, J., Lacagnina, M., Gass, D., Richfield, E., Mayer-Pröschel, M., Noble, M., Torres, C., Pröschel, C., 2005. EIF2B5 mutations compromise GFAP+ astrocyte generation in vanishing white matter leukodystrophy. *Nat Med* 11, 277–283. <https://doi.org/10.1038/nm1195>
- Dimou, L., Gallo, V., 2015. NG2-glia and their functions in the central nervous system: NG2-Glia in the CNS. *Glia* 63, 1429–1451. <https://doi.org/10.1002/glia.22859>

- Dobin, Alexander, et al. "STAR: ultrafast universal RNA-seq aligner." *Bioinformatics* 29.1 (2013): 15-21.
- Dooves, S., Bugiani, M., Postma, N.L., Polder, E., Land, N., Horan, S.T., van Deijk, A.-L.F., van de Kreeke, A., Jacobs, G., Vuong, C., Klooster, J., Kamermans, M., Wortel, J., Loos, M., Wisse, L.E., Scheper, G.C., Abbink, T.E.M., Heine, V.M., van der Knaap, M.S., 2016. Astrocytes are central in the pathomechanisms of vanishing white matter. *Journal of Clinical Investigation* 126, 1512–1524. <https://doi.org/10.1172/JCI83908>
- Dooves, S., Bugiani, M., Wisse, L.E., Abbink, T.E.M., van der Knaap, M.S., Heine, V.M., 2018. Bergmann glia translocation: a new disease marker for vanishing white matter identifies therapeutic effects of Guanabenz treatment. *Neuropathol Appl Neurobiol* 44, 391–403. <https://doi.org/10.1111/nan.12411>
- Dooves, S., Leferink, P.S., Krabbenborg, S., Breeuwsma, N., Bots, S., Hillen, A.E.J., Jacobs, G., van der Knaap, M.S., Heine, V.M., 2019. Cell Replacement Therapy Improves Pathological Hallmarks in a Mouse Model of Leukodystrophy Vanishing White Matter. *Stem Cell Reports* 12, 441–450. <https://doi.org/10.1016/j.stemcr.2019.01.018>
- Dreha-Kulaczewski, S.F., Dechent, P., Finsterbusch, J., Brockmann, K., Gärtner, J., Frahm, J., Hanefeld, F.A., 2008. Early Reduction of Total N-Acetyl-Aspartate-Compounds in Patients With Classical Vanishing White Matter Disease. A Long-Term Follow-Up MRS Study. *Pediatr Res* 63, 444–449. <https://doi.org/10.1203/01.pdr.0000304934.90198.25>
- Duncan, I.D., Bugiani, M., Radcliff, A.B., Moran, J.J., Lopez-Anido, C., Duong, P., August, B.K., Wolf, N.I., van der Knaap, M.S., Svaren, J., 2017. A mutation in the *Tubb4a* gene leads to microtubule accumulation with hypomyelination and demyelination: *Tubb4a* Mutation. *Ann Neurol* 81, 690–702. <https://doi.org/10.1002/ana.24930>
- Falcão, A. M., van Bruggen, D., Marques, S., Meijer, M., Jäkel, S., Agirre, E., ... Castelo-Branco, G. (2018). Disease-specific oligodendrocyte lineage cells arise in multiple sclerosis. *Nature Medicine*, 24(12), 1837–1844. <https://doi.org/10.1038/s41591-018-0236-y>
- Federico, A., Scali, O., Stromillo, M.L., Di Perri, C., Bianchi, S., Sicurelli, F., De Stephano, N., Malandrini, A., Dotti, M.T., 2006. Peripheral neuropathy in vanishing white matter disease with a novel EIF2B5 mutation. <https://doi.org/10.1212/01.wnl.0000225077.40532.a5>
- Fields, R.D., 2015. A new mechanism of nervous system plasticity: activity-dependent myelination. *Nat Rev Neurosci* 16, 756–767. <https://doi.org/10.1038/nrn4023>
- Fogli, A., Dionisi-Vici, C., Deodato, F., Bartuli, A., Boespflug-Tanguy, O., Bertini, E., 2002. A severe variant of childhood ataxia with central hypomyelination/vanishing white matter leukoencephalopathy related to EIF2B5 mutation. *Neurology* 59, 1966–1968. <https://doi.org/10.1212/01.WNL.0000041666.76863.47>
- Fogli, A., Merle, C., Roussel, V., Schiffmann, R., Ughetto, S., Theisen, M., Boespflug-Tanguy, O., 2012. CSF N-Glycan Profiles to Investigate Biomarkers in Brain Developmental Disorders:

- Application to Leukodystrophies Related to eIF2B Mutations. PLoS ONE 7, e42688. <https://doi.org/10.1371/journal.pone.0042688>
- Fogli, A., Rodriguez, D., Eymard-Pierre, É., Boespflug-Tanguy, O., 2003a. eIF2B et la leucodystrophie des Indiens Cree. Med Sci (Paris) 19, 283–285. <https://doi.org/10.1051/medsci/2003193283>
- Fogli, A., Rodriguez, D., Eymard-Pierre, E., Bouhour, F., Labauge, P., Meaney, B.F., Zeeman, S., Kaneski, C.R., Schiffmann, R., Boespflug-Tanguy, O., 2003b. Ovarian Failure Related to Eukaryotic Initiation Factor 2B Mutations. The American Journal of Human Genetics 72, 1544–1550. <https://doi.org/10.1086/375404>
- Fogli, A., Schiffmann, R., Bertini, E., Ughetto, S., Combes, P., Eymard-Pierre, E., Kaneski, C.R., Pineda, M., Troncoso, M., Uziel, G., Surtees, R., Pugin, D., Chaunu, M.-P., Rodriguez, D., Boespflug-Tanguy, O., 2004. The effect of genotype on the natural history of eIF2B-related leukodystrophies. Neurology 62, 1509–1517. <https://doi.org/10.1212/01.WNL.0000123259.67815.DB>
- Fogli, Anne, Schiffmann, R., Hugendubler, L., Combes, P., Bertini, E., Rodriguez, D., Kimball, S.R., Boespflug-Tanguy, O., 2004. Decreased guanine nucleotide exchange factor activity in eIF2B-mutated patients. Eur J Hum Genet 12, 561–566. <https://doi.org/10.1038/sj.ejhg.5201189>
- Fogli, Anne, Wong, K., Eymard-Pierre, E., Wenger, J., Bouffard, J.-P., Goldin, E., Black, D.N., Boespflug-Tanguy, O., Schiffmann, R., 2002. Cree leukoencephalopathy and CACH/VWM disease are allelic at the EIF2B5 locus. Ann Neurol. 52, 506–510. <https://doi.org/10.1002/ana.10339>
- Francalanci, P., Eymard, E., Dionisi, C., Boldrini, R., Piemonte, F., Virgili, R., Fariello, G., Bosman, C., Santorelli, F.M., Boespflug, O., Bertini, E., n.d. Fatal infantile leukodystrophy 6.
- Gat-Viks, I., Geiger, T., Barbi, M., Raini, G., Elroy-Stein, O., 2015. Proteomics-level analysis of myelin formation and regeneration in a mouse model for Vanishing White Matter disease. J. Neurochem. 134, 513–526. <https://doi.org/10.1111/jnc.13142>
- Gebauer, F., Hentze, M.W., 2004. Molecular mechanisms of translational control. Nat Rev Mol Cell Biol 5, 827–835. <https://doi.org/10.1038/nrm1488>
- Geva, M., Cabilly, Y., Assaf, Y., Mindroul, N., Marom, L., Raini, G., Pinchasi, D., Elroy-Stein, O., 2010. A mouse model for eukaryotic translation initiation factor 2B-leucodystrophy reveals abnormal development of brain white matter. Brain 133, 2448–2461. <https://doi.org/10.1093/brain/awq180>
- Ginhoux, F., Prinz, M., 2015. Origin of Microglia: Current Concepts and Past Controversies. Cold Spring Harb Perspect Biol 7, a020537. <https://doi.org/10.1101/cshperspect.a020537>
- Gordon, N., 2007. Sjögren-Larsson syndrome. Developmental Medicine & Child Neurology 49, 152–154. <https://doi.org/10.1111/j.1469-8749.2007.00152.x>

- Gotz, M., 2001. Cerebral Cortex Development 7. <https://doi.org/10.1038/npg.els.0000787>
- Guan BJ, van Hoef V, Jobava R, Elroy-Stein O, Valasek LS, Cargnello M, Gao XH, Krokowski D, Merrick WC, Kimball SR, Komar AA, Koromilas AE, Wynshaw-Boris A, Topisirovic I, Larsson O, Hatzoglou M. Mol Cell. 2017 Dec 7;68(5):885-900.e6. A Unique ISR Program Determines Cellular Responses to Chronic Stress.
- Hamilton, E.M.C., van der Lei, H.D.W., Vermeulen, G., Gerver, J.A.M., Lourenço, C.M., Naidu, S., Mierzewska, H., Gemke, R.J.B.J., de Vet, H.C.W., Uitdehaag, B.M.J., Lissenberg-Witte, B.I., VWM Research Group, van der Knaap, M.S., 2018. Natural History of Vanishing White Matter: Natural History of VWM. Ann Neurol. 84, 274–288. <https://doi.org/10.1002/ana.25287>
- Han, J., Back, S.H., Hur, J., Lin, Y.-H., Gildersleeve, R., Shan, J., Yuan, C.L., Krokowski, D., Wang, S., Hatzoglou, M., Kilberg, M.S., Sartor, M.A., Kaufman, R.J., 2013. ER-stress-induced transcriptional regulation increases protein synthesis leading to cell death. Nat Cell Biol 15, 481–490. <https://doi.org/10.1038/ncb2738>
- Hanefeld, F., Holzbach, U., Kruse, B., Wilichowski, E., Christen, H., Frahm, J., 1993. Diffuse White Matter Disease in Three Children: An Encephalopathy with Unique Features on Magnetic Resonance Imaging and Proton Magnetic Resonance Spectroscopy. Neuropediatrics 24, 244–248. <https://doi.org/10.1055/s-2008-1071551>
- Hellen, C.U.T., 2001. Internal ribosome entry sites in eukaryotic mRNA molecules. Genes & Development 15, 1593–1612. <https://doi.org/10.1101/gad.891101>
- Henneke, M., Diekmann, S., Ohlenbusch, A., Kaiser, J., Engelbrecht, V., Kohlschütter, A., Krätzner, R., Madruga-Garrido, M., Mayer, M., Opitz, L., Rodriguez, D., Rüschenhoff, F., Schumacher, J., Thiele, H., Thoms, S., Steinfeld, R., Nürnberg, P., Gärtner, J., 2009. RNASET2-deficient cystic leukoencephalopathy resembles congenital cytomegalovirus brain infection. Nat Genet 41, 773–775. <https://doi.org/10.1038/ng.398>
- Herrero, M., Mandelbaum, S., Elroy-Stein, O., 2019. eIF2B Mutations Cause Mitochondrial Malfunction in Oligodendrocytes. Neuromol Med 21, 303–313. <https://doi.org/10.1007/s12017-019-08551-9>
- Hinnebusch, A.G., Lorsch, J.R., 2012. The Mechanism of Eukaryotic Translation Initiation: New Insights and Challenges. Cold Spring Harbor Perspectives in Biology 4, a011544–a011544. <https://doi.org/10.1101/cshperspect.a011544>
- Horzinski, L., Huyghe, A., Cardoso, M.-C., Gonthier, C., Ouchchane, L., Schiffmann, R., Blanc, P., Boespflug-Tanguy, O., Fogli, A., 2009. Eukaryotic Initiation Factor 2B (eIF2B) GEF Activity as a Diagnostic Tool for EIF2B-Related Disorders. PLoS ONE 4, e8318. <https://doi.org/10.1371/journal.pone.0008318>

- Horzinski, L., Kantor, L., Huyghe, A., Schiffmann, R., Elroy-Stein, O., Boespflug-Tanguy, O., Fogli, A., 2010. Evaluation of the endoplasmic reticulum-stress response in eIF2B-mutated lymphocytes and lymphoblasts from CACH/VWM patients. *BMC Neurol* 10, 94. <https://doi.org/10.1186/1471-2377-10-94>
- Huntsman, R.J., Seshia, S., Lowry, N., Lemire, E.G., Harder, S.L., 2007. Peripheral Neuropathy in a Child With Cree Leukodystrophy. *J Child Neurol* 22, 766–768. <https://doi.org/10.1177/0883073807304010>
- Huyghe, A., Horzinski, L., Hénaut, A., Gaillard, M., Bertini, E., Schiffmann, R., Rodriguez, D., Dantal, Y., Boespflug-Tanguy, O., Fogli, A., 2012. Developmental Splicing Deregulation in Leukodystrophies Related to EIF2B Mutations. *PLoS ONE* 7, e38264. <https://doi.org/10.1371/journal.pone.0038264>
- Inoue, K., 2005. PLP1-related inherited dysmyelinating disorders: Pelizaeus-Merzbacher disease and spastic paraplegia type 2. *Neurogenetics* 6, 1–16. <https://doi.org/10.1007/s10048-004-0207-y>
- Iurlaro, R., Muñoz-Pinedo, C., 2016. Cell death induced by endoplasmic reticulum stress. *FEBS J* 283, 2640–2652. <https://doi.org/10.1111/febs.13598>
- James, C.C., Smyth, J.W., 2018. Alternative mechanisms of translation initiation: An emerging dynamic regulator of the proteome in health and disease. *Life Sciences* 212, 138–144. <https://doi.org/10.1016/j.lfs.2018.09.054>
- Jansen, A.C., Andermann, E., Niel, F., Creveaux, I., Boespflug-Tanguy, O., Andermann, F., 2008. Leucoencephalopathy with vanishing white matter may cause progressive myoclonus epilepsy. *Epilepsia* 49, 910–913. <https://doi.org/10.1111/j.1528-1167.2008.01542.x>
- Jenkinson, E.M., Rodero, M.P., Kasher, P.R., Ugenti, C., Oojageer, A., Goosey, L.C., Rose, Y., Kershaw, C.J., Urquhart, J.E., Williams, S.G., Bhaskar, S.S., O’Sullivan, J., Baerlocher, G.M., Haubitz, M., Aubert, G., Barañano, K.W., Barnicoat, A.J., Battini, R., Berger, A., Blair, E.M., Brunstrom-Hernandez, J.E., Buckard, J.A., Cassiman, D.M., Caumes, R., Cordelli, D.M., De Waele, L.M., Fay, A.J., Ferreira, P., Fletcher, N.A., Fryer, A.E., Goel, H., Hemingway, C.A., Henneke, M., Hughes, I., Jefferson, R.J., Kumar, R., Lagae, L., Landrieu, P.G., Lourenço, C.M., Malpas, T.J., Mehta, S.G., Metz, I., Naidu, S., Öunap, K., Panzer, A., Prabhakar, P., Quaghebeur, G., Schiffmann, R., Sherr, E.H., Sinnathuray, K.R., Soh, C., Stewart, H.S., Stone, J., Van Esch, H., Van Mol, C.E.G., Vanderver, A., Wakeling, E.L., Whitney, A., Pavitt, G.D., Griffiths-Jones, S., Rice, G.I., Revy, P., van der Knaap, M.S., Livingston, J.H., O’Keefe, R.T., Crow, Y.J., 2016. Mutations in SNORD118 cause the cerebral microangiopathy leukoencephalopathy with calcifications and cysts. *Nat Genet* 48, 1185–1192. <https://doi.org/10.1038/ng.3661>
- Jin, X., 2016. The role of neurogenesis during development and in the adult brain. *Eur J Neurosci* 44, 2291–2299. <https://doi.org/10.1111/ejn.13251>

- Jousse, C., Deval, C., Maurin, A.-C., Parry, L., Chérasse, Y., Chaveroux, C., ... Fafournoux, P. (2007). TRB3 Inhibits the Transcriptional Activation of Stress-regulated Genes by a Negative Feedback on the ATF4 Pathway. *Journal of Biological Chemistry*, 282(21), 15851–15861. <https://doi.org/10.1074/jbc.M611723200>
- Jungblut, M., Tiveron, M. C., Barral, S., Abrahamsen, B., Knöbel, S., Pennartz, S., Bosio, A. (2012). Isolation and characterization of living primary astroglial cells using the new GLAST-specific monoclonal antibody ACSA-1. *Glia*, 60(6), 894–907. <https://doi.org/10.1002/glia.22322>
- Kabba, J.A., Xu, Y., Christian, H., Ruan, W., Chenai, K., Xiang, Y., Zhang, L., Saavedra, J.M., Pang, T., 2018. Microglia: Housekeeper of the Central Nervous System. *Cell Mol Neurobiol* 38, 53–71. <https://doi.org/10.1007/s10571-017-0504-2>
- Kameneva, P., Adameyko, I., 2019. Recent advances in our understanding of central and peripheral nervous system progenitors. *Current Opinion in Cell Biology* 61, 24–30. <https://doi.org/10.1016/j.ceb.2019.07.003>
- Kamphuis, W., Mamber, C., Moeton, M., Kooijman, L., Sluijs, J.A., Jansen, A.H.P., Verveer, M., de Groot, L.R., Smith, V.D., Rangarajan, S., Rodriguez, J.J., Orre, M., Hol, E.M., 2012. GFAP Isoforms in Adult Mouse Brain with a Focus on Neurogenic Astrocytes and Reactive Astroglisis in Mouse Models of Alzheimer Disease. *PLoS ONE* 7, e42823. <https://doi.org/10.1371/journal.pone.0042823>
- Kantor, L., Harding, H.P., Ron, D., Schiffmann, R., Kaneski, C.R., Kimball, S.R., Elroy-Stein, O., 2005. Heightened stress response in primary fibroblasts expressing mutant eIF2B genes from CACH/VWM leukodystrophy patients. *Hum Genet* 118, 99–106. <https://doi.org/10.1007/s00439-005-0024-x>
- Kantor, L., Pinchasi, D., Mintz, M., Hathout, Y., Vanderver, A., Elroy-Stein, O., 2008. A Point Mutation in Translation Initiation Factor 2B Leads to a Continuous Hyper Stress State in Oligodendroglial-Derived Cells. *PLoS ONE* 3, e3783. <https://doi.org/10.1371/journal.pone.0003783>
- Karinch, A.M., Kimball, S.R., Vary, T.C., Jefferson, L.S., 1993. Regulation of eukaryotic initiation factor-2B activity in muscle of diabetic rats. *American Journal of Physiology-Endocrinology and Metabolism* 264, E101–E108. <https://doi.org/10.1152/ajpendo.1993.264.1.E101>
- Kasai, S., Yamazaki, H., Tanji, K., Engler, M., Matsumiya, T., Itoh, K., 2019. Role of the ISR-ATF4 pathway and its cross talk with Nrf2 in mitochondrial quality control. <https://doi.org/10.3164/jcbn.18-37>
- Kashiwagi, K., Yokoyama, T., Nishimoto, M., Takahashi, M., Sakamoto, A., Yonemochi, M., Shirouzu, M., Ito, T., 2019. Structural basis for eIF2B inhibition in integrated stress response 5. <https://doi.org/10.1126/science.aaw4104>
- Kaye, E.M., 2001. Update on genetic disorders affecting white matter. *Pediatric Neurology* 24, 11–24. [https://doi.org/10.1016/S0887-8994\(00\)00232-0](https://doi.org/10.1016/S0887-8994(00)00232-0)

- Kelava, I., Huttner, W.B., 2012. Neurogenesis in the Developing Mammalian Neocortex, in: John Wiley & Sons, Ltd (Ed.), *ELS. John Wiley & Sons, Ltd, Chichester, UK*, p. a0022541. <https://doi.org/10.1002/9780470015902.a0022541>
- Kimball, S.R., Jefferson, L.S., 1995. Allosteric Regulation of Eukaryotic Initiation Factor eIF-2B by Adenine Nucleotides. <https://doi.org/10.1006/bbrc.1995.2079>
- Kirby, L., Jin, J., Cardona, J. G., Smith, M. D., Martin, K. A., Wang, J., ... Calabresi, P. A. (2019). Oligodendrocyte precursor cells present antigen and are cytotoxic targets in inflammatory demyelination. *Nature Communications*, 10(1), 3887. <https://doi.org/10.1038/s41467-019-11638-3>
- Klingelhoefer, L., Misbahuddin, A., Jawad, T., Mellers, J., Jarosz, J., Weeks, R., Ray Chaudhuri, K., 2014. Vanishing White Matter Disease Presenting as Opsoclonus Myoclonus Syndrome in Childhood—A Case Report and Review of the Literature. *Pediatric Neurology* 51, 157–164. <https://doi.org/10.1016/j.pediatrneurol.2014.03.008>
- Klok, M.D., Bugiani, M., de Vries, S.I., Gerritsen, W., Breur, M., van der Sluis, S., Heine, V.M., Kole, M.H.P., Baron, W., van der Knaap, M.S., 2018. Axonal abnormalities in vanishing white matter. *Ann Clin Transl Neurol* 5, 429–444. <https://doi.org/10.1002/acn3.540>
- Knott, G., Molnar, Z., 2001. Cells of the Nervous System, in: John Wiley & Sons, Ltd (Ed.), *Encyclopedia of Life Sciences*. John Wiley & Sons, Ltd, Chichester, p. a0000031. <https://doi.org/10.1038/npg.els.0000031>
- Kohlschütter, A., Bley, A., Brockmann, K., Gärtner, J., Krägeloh-Mann, I., Rolfs, A., Schöls, L., 2010. Leukodystrophies and other genetic metabolic leukoencephalopathies in children and adults. *Brain and Development* 32, 82–89. <https://doi.org/10.1016/j.braindev.2009.03.014>
- Labauge, P., Boespflug-Tanguy, O., 2010. Maladies démyélinisantes d'origine génétique. *La Presse Médicale* 39, 363–370. <https://doi.org/10.1016/j.lpm.2009.11.011>
- Labauge, P., Fogli, A., Niel, F., Rodriguez, D., Boespflug-Tanguy, O., 2007. Le syndrome CACH/VWM et les leucodystrophies liées à des mutations EIF2B. *Revue Neurologique* 163, 793–799. [https://doi.org/10.1016/S0035-3787\(07\)91461-7](https://doi.org/10.1016/S0035-3787(07)91461-7)
- Labauge, P., Horzinski, L., Ayrignac, X., Blanc, P., Vukusic, S., Rodriguez, D., Mauguier, F., Peter, L., Goizet, C., Bouhour, F., Denier, C., Confavreux, C., Obadia, M., Blanc, F., Seze, J. d., Fogli, A., Boespflug-Tanguy, O., 2009. Natural history of adult-onset eIF2B-related disorders: a multi-centric survey of 16 cases. *Brain* 132, 2161–2169. <https://doi.org/10.1093/brain/awp171>
- Lacerda, R., Menezes, J., Romão, L., 2017. More than just scanning: the importance of cap-independent mRNA translation initiation for cellular stress response and cancer. *Cell. Mol. Life Sci.* 74, 1659–1680. <https://doi.org/10.1007/s00018-016-2428-2>

- Leegwater, P.A.J., Könst, A.A.M., Kuyt, B., Sandkuijl, L.A., Naidu, S., Oudejans, C.B.M., Schutgens, R.B.H., Pronk, J.C., van der Knaap, M.S., 1999. The Gene for Leukoencephalopathy with Vanishing White Matter Is Located on Chromosome 3q27. *The American Journal of Human Genetics* 65, 728–734. <https://doi.org/10.1086/302548>
- Leegwater, P.A.J., Vermeulen, G., Könst, A.A.M., Naidu, S., Mulders, J., Visser, A., Kersbergen, P., Mobach, D., Fonds, D., van Berkel, C.G.M., Lemmers, R.J.L.F., Frants, R.R., Oudejans, C.B.M., Schutgens, R.B.H., Pronk, J.C., van der Knaap, M.S., 2001. Subunits of the translation initiation factor eIF2B are mutant in leukoencephalopathy with vanishing white matter. *Nat Genet* 29, 383–388. <https://doi.org/10.1038/ng764>
- Leferink, P.S., Breeuwsma, N., Bugiani, M., van der Knaap, M.S., Heine, V.M., 2018. Affected astrocytes in the spinal cord of the leukodystrophy vanishing white matter. *Glia* 66, 862–873. <https://doi.org/10.1002/glia.23289>
- Leone, D.P., Genoud, S. téphane, Atanasoski, S., Grausenburger, R., Berger, P., Metzger, D., Macklin, W.B., Chambon, P., Suter, U., 2003. Tamoxifen-inducible glia-specific Cre mice for somatic mutagenesis in oligodendrocytes and Schwann cells. *Molecular and Cellular Neuroscience* 22, 430–440. [https://doi.org/10.1016/S1044-7431\(03\)00029-0](https://doi.org/10.1016/S1044-7431(03)00029-0)
- Liddelow, S.A., Barres, B.A., 2017. Reactive Astrocytes: Production, Function, and Therapeutic Potential. *Immunity* 46, 957–967. <https://doi.org/10.1016/j.immuni.2017.06.006>
- Lin, W., 2015. Impaired eIF2B activity in ligodendrocytes contributes to VWMD pathogenesis. *Neural Regen Res* 10, 195. <https://doi.org/10.4103/1673-5374.152366>
- Lin, W., Lin, Y., Li, J., Fenstermaker, A.G., Way, S.W., Clayton, B., Jamison, S., Harding, H.P., Ron, D., Popko, B., 2013. Oligodendrocyte-Specific Activation of PERK Signaling Protects Mice against Experimental Autoimmune Encephalomyelitis. *Journal of Neuroscience* 33, 5980–5991. <https://doi.org/10.1523/JNEUROSCI.1636-12.2013>
- Lin, Y., Pang, X., Huang, G., Jamison, S., Fang, J., Harding, H.P., Ron, D., Lin, W., 2014. Impaired Eukaryotic Translation Initiation Factor 2B Activity Specifically in Oligodendrocytes Reproduces the Pathology of Vanishing White Matter Disease in Mice. *Journal of Neuroscience* 34, 12182–12191. <https://doi.org/10.1523/JNEUROSCI.1373-14.2014>
- Losada-Perez, M., 2018. Glia: from ‘just glue’ to essential players in complex nervous systems: a comparative view from flies to mammals. *Journal of Neurogenetics* 32, 78–91. <https://doi.org/10.1080/01677063.2018.1464568>
- Marom, L., Ulitsky, I., Cabilly, Y., Shamir, R., Elroy-Stein, O., 2011. A Point Mutation in Translation Initiation Factor eIF2B Leads to Function- and Time-Specific Changes in Brain Gene Expression. *PLoS ONE* 6, e26992. <https://doi.org/10.1371/journal.pone.0026992>
- Mathis, S., Scheper, G.C., Baumann, N., Petit, E., Gil, R., van der Knaap, M.S., Neu, J.-P., 2008. The ovarioleukodystrophy. *Clinical Neurology and Neurosurgery* 110, 1035–1037. <https://doi.org/10.1016/j.clineuro.2008.06.002>

- Merrick, W.C., Pavitt, G.D., 2018. Protein Synthesis Initiation in Eukaryotic Cells. Cold Spring Harb Perspect Biol 10, a033092. <https://doi.org/10.1101/cshperspect.a033092>
- Mignot, C., Boespflug-Tanguy, O., Gelot, A., Dautigny, A., Pham-Dinh, D., Rodriguez, D., 2004. Alexander disease: putative mechanisms of an astrocytic encephalopathy. Cellular and Molecular Life Sciences (CMLS) 61, 369–385. <https://doi.org/10.1007/s00018-003-3143-3>
- Moffett, J.R., Arun, P., Ariyannur, P.S., Namboodiri, A.M.A., 2013. N-Acetylaspartate reductions in brain injury: impact on post-injury neuroenergetics, lipid synthesis, and protein acetylation. Front. Neuroenergetics 5. <https://doi.org/10.3389/fnene.2013.00011>
- Monje, M., 2018. Myelin Plasticity and Nervous System Function. Annu. Rev. Neurosci. 41, 61–76. <https://doi.org/10.1146/annurev-neuro-080317-061853>
- Mori, T., Tanaka, K., Buffo, A., Wurst, W., Kühn, R., Götz, M., 2006. Inducible gene deletion in astroglia and radial glia-A valuable tool for functional and lineage analysis. Glia 54, 21–34. <https://doi.org/10.1002/glia.20350>
- Morrison, B.M., Lee, Y., Rothstein, J.D., 2013. Oligodendroglia: metabolic supporters of axons. Trends in Cell Biology 23, 644–651. <https://doi.org/10.1016/j.tcb.2013.07.007>
- Ohno, N., Ikenaka, K., 2019. Axonal and neuronal degeneration in myelin diseases. Neuroscience Research 139, 48–57. <https://doi.org/10.1016/j.neures.2018.08.013>
- Ohtake, H., Shimohata, T., Terajima, K., Kimura, T., Jo, R., Kaseda, R., Iizuka, O., Takano, M., Akaiwa, Y., Goto, H., Kobayashi, H., Sugai, T., Muratake, T., Hosoki, T., Shioiri, T., Okamoto, K., Onodera, O., Tanaka, K., Someya, T., Nakada, T., Tsuji, S., 2004. Adult-onset leukoencephalopathy with vanishing white matter with a missense mutation in *EIF2B5*. Neurology 62, 1601–1603. <https://doi.org/10.1212/01.WNL.0000123117.11264.0E>
- Ohtsuka, T., Kageyama, R., 2019. Regulation of temporal properties of neural stem cells and transition timing of neurogenesis and gliogenesis during mammalian neocortical development. Seminars in Cell & Developmental Biology S1084952118300624. <https://doi.org/10.1016/j.semcd.2019.01.007>
- Ohtsuka, T., Shimojo, H., Matsunaga, M., Watanabe, N., Kometani, K., Minato, N., Kageyama, R., 2011. Gene Expression Profiling of Neural Stem Cells and Identification of Regulators of Neural Differentiation During Cortical Development. STEM CELLS 29, 1817–1828. <https://doi.org/10.1002/stem.731>
- Pakos-Zebrucka, K., Koryga, I., Mnich, K., Lujic, M., Samali, A., Gorman, A.M., 2016. The integrated stress response. EMBO Rep 17, 1374–1395. <https://doi.org/10.15252/embr.201642195>
- Pant, D.C., Dorboz, I., Schluter, A., Fourcade, S., Launay, N., Joya, J., Aguilera-Albesa, S., Yoldi, M.E., Casanovas, C., Willis, M.J., Ruiz, M., Ville, D., Lesca, G., Siquier-Pernet, K., Desguerre, I., Yan, H., Wang, J., Burmeister, M., Brady, L., Tarnopolsky, M., Cornet, C., Rubbini, D.,

- Terriente, J., James, K.N., Musaev, D., Zaki, M.S., Patterson, M.C., Lanpher, B.C., Klee, E.W., Pinto e Vairo, F., Wohler, E., Sobreira, N.L. de M., Cohen, J.S., Maroofian, R., Galehdari, H., Mazaheri, N., Shariati, G., Colleaux, L., Rodriguez, D., Gleeson, J.G., Pujades, C., Fatemi, A., Boespflug-Tanguy, O., Pujol, A., 2019. Loss of the sphingolipid desaturase DEGS1 causes hypomyelinating leukodystrophy. *Journal of Clinical Investigation* 129, 1240–1256. <https://doi.org/10.1172/JCI123959>
- Pap, M., Cooper, G.M., 2002. Role of Translation Initiation Factor 2B in Control of Cell Survival by the Phosphatidylinositol 3-Kinase/Akt/Glycogen Synthase Kinase 3 Signaling Pathway. *Molecular and Cellular Biology* 22, 578–586. <https://doi.org/10.1128/MCB.22.2.578-586.2002>
- Pavitt, G. D. (2005). EIF2B, a mediator of general and gene-specific translational control. *Biochemical Society Transactions*, 33, 6.
- Pavitt, G.D., 2018. Regulation of translation initiation factor eIF2B at the hub of the integrated stress response. *WIREs RNA* 9, e1491. <https://doi.org/10.1002/wrna.1491>
- Payne, S.C., Bartlett, C.A., Savigni, D.L., Harvey, A.R., Dunlop, S.A., Fitzgerald, M., 2013. Early Proliferation Does Not Prevent the Loss of Oligodendrocyte Progenitor Cells during the Chronic Phase of Secondary Degeneration in a CNS White Matter Tract. *PLoS ONE* 8, e65710. <https://doi.org/10.1371/journal.pone.0065710>
- Perea, G., Navarrete, M., Araque, A., 2009. Tripartite synapses: astrocytes process and control synaptic information. *Trends in Neurosciences* 32, 421–431. <https://doi.org/10.1016/j.tins.2009.05.001>
- Peter, L., Niel, F., Catenoix, H., Jung, J., Demarquay, G., Petiot, P., Rudigoz, R.C., Boespflug-Tanguy, O., Ryvlin, P., Mauguère, F., 2007. Acute neurological deterioration in ovarioleukodystrophy related to EIF2B mutations: pregnancy with oocyte donation is a potentially precipitating factor. *Eur J Neurol* 0, 071116221701005-??? <https://doi.org/10.1111/j.1468-1331.2007.01999.x>
- Pitale, P.M., Gorbatyuk, O., Gorbatyuk, M., 2017. Neurodegeneration: Keeping ATF4 on a Tight Leash. *Front. Cell. Neurosci.* 11, 410. <https://doi.org/10.3389/fncel.2017.00410>
- Potic, A., Brais, B., Choquet, K., Schiffmann, R., Bernard, G., 2012. 4H Syndrome With Late-Onset Growth Hormone Deficiency Caused by POLR3A Mutations. *Arch Neurol* 69. <https://doi.org/10.1001/archneurol.2011.1963>
- Preston, A.N., Cervasio, D.A., Laughlin, S.T., 2019. Visualizing the brain's astrocytes, in: *Methods in Enzymology*. Elsevier, pp. 129–151. <https://doi.org/10.1016/bs.mie.2019.02.006>
- Price, N., Proud, C., n.d. The guanine nucleotide-exchange factor, eIF-2B 13.
- Proud, C.G., 2005. eIF2 and the control of cell physiology. *Seminars in Cell & Developmental Biology* 16, 3–12. <https://doi.org/10.1016/j.semcd.2004.11.004>

- Raddatz, B. B. R., Hansmann, F., Spitzbarth, I., Kalkuhl, A., Deschl, U., Baumgärtner, W., & Ulrich, R. (2014). Transcriptomic Meta-Analysis of Multiple Sclerosis and Its Experimental Models. *PLoS ONE*, 9(1), e86643. <https://doi.org/10.1371/journal.pone.0086643>
- Raini, G., Sharet, R., Herrero, M., Atzmon, A., Shenoy, A., Geiger, T., Elroy-Stein, O., 2017. Mutant eIF2B leads to impaired mitochondrial oxidative phosphorylation in vanishing white matter disease. *J. Neurochem.* 141, 694–707. <https://doi.org/10.1111/inc.14024>
- Richardson, J.P., Mohammad, S.S., Pavitt, G.D., 2004. Mutations Causing Childhood Ataxia with Central Nervous System Hypomyelination Reduce Eukaryotic Initiation Factor 2B Complex Formation and Activity. *Molecular and Cellular Biology* 24, 2352–2363. <https://doi.org/10.1128/MCB.24.6.2352-2363.2004>
- Rodriguez, D., Gelot, A., della Gaspera, B., Robain, O., Ponsot, G., Sarliève, L.L., Ghandour, S., Pompidou, A., Dautigny, A., Aubourg, P., Pham-Dinh, D., 1999. Increased density of oligodendrocytes in childhood ataxia with diffuse central hypomyelination (CACH) syndrome: neuropathological and biochemical study of two cases. *Acta Neuropathologica* 97, 469–480. <https://doi.org/10.1007/s004010051016>
- Rozpedek, W., Pytel, D., Mucha, B., Leszczynska, H., Diehl, J.A., Majsterek, I., 2016. The Role of the PERK/eIF2 α /ATF4/CHOP Signaling Pathway in Tumor Progression During Endoplasmic Reticulum Stress. *CMM* 16, 533–544. <https://doi.org/10.2174/1566524016666160523143937>
- Saab, A.S., Tzvetanova, I.D., Nave, K.-A., 2013. The role of myelin and oligodendrocytes in axonal energy metabolism. *Current Opinion in Neurobiology* 23, 1065–1072. <https://doi.org/10.1016/j.conb.2013.09.008>
- Scheper, G.C., Thomas, A.A.M., Wijk, van R., 1998. Inactivation of eukaryotic initiation factor 2B in vitro by heat shock. *Biochemical Journal* 334, 463–467. <https://doi.org/10.1042/bj3340463>
- Schiffmann, R., Boespflug-Tanguy, O., 2001. An update on the leukodystrophies. <https://doi.org/10.1097/00019052-200112000-00018>
- Schiffmann, R., Elroy-Stein, O., 2006. Childhood ataxia with CNS hypomyelination/vanishing white matter disease—A common leukodystrophy caused by abnormal control of protein synthesis. *Molecular Genetics and Metabolism* 88, 7–15. <https://doi.org/10.1016/j.ymgme.2005.10.019>
- Schiffmann, R., Moller, J.R., Trapp, B.D., Shih, H.H.-L., Farrer, R.G., Katz, D.A., Alger, J.R., Parker, C.C., Hauer, P.E., Kaneski, C.R., Heiss, J.D., Kaye, E.M., Quarles, R.H., Brady, R.O., Barton, N.W., 1994. Childhood ataxia with diffuse central nervous system hypomyelination. *Ann Neurol.* 35, 331–340. <https://doi.org/10.1002/ana.410350314>

- Schiffmann, R., Tedeschi, G., Kinkel, R.P., Trapp, B.D., Frank, J.A., Kaneski, C.R., Brady, R.O., Barton, N.W., Nelson, L., Yanovski, J.A., 1997. Leukodystrophy in patients with ovarian dysgenesis. *Ann Neurol.* 41, 654–661. <https://doi.org/10.1002/ana.410410515>
- Shirokikh, N.E., Preiss, T., 2018. Translation initiation by cap-dependent ribosome recruitment: Recent insights and open questions. *WIREs RNA* 9, e1473. <https://doi.org/10.1002/wrna.1473>
- Simonović, M., Steitz, T.A., 2009. A structural view on the mechanism of the ribosome-catalyzed peptide bond formation. *Biochimica et Biophysica Acta (BBA) - Gene Regulatory Mechanisms* 1789, 612–623. <https://doi.org/10.1016/j.bbagra.2009.06.006>
- Skaper, S.D., 2019. Oligodendrocyte precursor cells as a therapeutic target for demyelinating diseases, in: *Progress in Brain Research*. Elsevier, pp. 119–144. <https://doi.org/10.1016/bs.pbr.2019.03.013>
- Sofroniew, M.V., Vinters, H.V., 2010. Astrocytes: biology and pathology. *Acta Neuropathol* 119, 7–35. <https://doi.org/10.1007/s00401-009-0619-8>
- Song, H., Haeri, S., Vogel, H., van der Knaap, M., Van Haren, K., 2017. Postmortem Whole Exome Sequencing Identifies Novel EIF2B3 Mutation With Prenatal Phenotype in 2 Siblings. *J Child Neurol* 32, 867–870. <https://doi.org/10.1177/0883073817712588>
- Teschendorff AE, Breeze CE, Zheng SC, Beck S (2017). “A comparison of reference-based algorithms for correcting cell-type heterogeneity in Epigenome-Wide Association Studies.” *BMC bioinformatics*, 18(1), 105.
- Thiffault, I., Wolf, N.I., Forget, D., Guerrero, K., Tran, L.T., Choquet, K., Lavallée-Adam, M., Poitras, C., Brais, B., Yoon, G., Sztriha, L., Webster, R.I., Timmann, D., van de Warrenburg, B.P., Seeger, J., Zimmermann, A., Máté, A., Goizet, C., Fung, E., van der Knaap, M.S., Fribourg, S., Vanderver, A., Simons, C., Taft, R.J., Yates III, J.R., Coulombe, B., Bernard, G., 2015. Recessive mutations in POLR1C cause a leukodystrophy by impairing biogenesis of RNA polymerase III. *Nat Commun* 6, 7623. <https://doi.org/10.1038/ncomms8623>
- Van der Knaap, M., Pronk, J.C., Scheper, G.C., 2006. Vanishing white matter disease. [https://doi.org/10.1016/S1474-4422\(06\)70440-9](https://doi.org/10.1016/S1474-4422(06)70440-9)
- van der Knaap, M.S., Barth, P.G., Gabreels, F.J.M., Franzoni, E., Begeer, J.H., Stroink, H., Rotteveel, J.J., Valk, J., 1997. A new leukoencephalopathy with vanishing white matter. *Neurology* 48, 845–854. <https://doi.org/10.1212/WNL.48.4.845>
- Van der Knaap, M.S., Fogli, A., Boespflug-Tanguy, O., Abbink, T.E., 2019. Childhood Ataxia with Central Nervous System Hypomyelination / Vanishing White Matter. <https://www.ncbi.nlm.nih.gov/books/NBK1258/>
- van der Knaap, M.S., Leegwater, P.A.J., Könst, A.A.M., Visser, A., Naidu, S., Oudejans, C.B.M., Schutgens, R.B.H., Pronk, J.C., 2002. Mutations in each of the five subunits of translation

- initiation factor eIF2B can cause leukoencephalopathy with vanishing white matter: Five Genes for Vanishing White Matter. *Ann Neurol.* 51, 264–270. <https://doi.org/10.1002/ana.10112>
- van der Knaap, M.S., van Berkel, C.G.M., Herms, J., van Coster, R., Baethmann, M., Naidu, S., Boltshauser, E., Willemsen, M.A.A.P., Plecko, B., Hoffmann, G.F., Proud, C.G., Scheper, G.C., Pronk, J.C., 2003. eIF2B-Related Disorders: Antenatal Onset and Involvement of Multiple Organs. *The American Journal of Human Genetics* 73, 1199–1207. <https://doi.org/10.1086/379524>
- van der Lei, H.D.W., van Berkel, C.G.M., van Wieringen, W.N., Brenner, C., Feigenbaum, A., Mercimek-Mahmutoglu, S., Philippart, M., Tatli, B., Wassmer, E., Scheper, G.C., van der Knaap, M.S., 2010. Genotype-phenotype correlation in vanishing white matter disease. *Neurology* 75, 1555–1559. <https://doi.org/10.1212/WNL.0b013e3181f962ae>
- van Tilborg, E., de Theije, C.G.M., van Hal, M., Wagenaar, N., de Vries, L.S., Benders, M.J., Rowitch, D.H., Nijboer, C.H., 2018. Origin and dynamics of oligodendrocytes in the developing brain: Implications for perinatal white matter injury. *Glia* 66, 221–238. <https://doi.org/10.1002/glia.23256>
- Vanderver, A., 2005. Decreased Asialotransferrin in Cerebrospinal Fluid of Patients with Childhood-Onset Ataxia and Central Nervous System Hypomyelination/Vanishing White Matter Disease. *Clinical Chemistry* 51, 2031–2042. <https://doi.org/10.1373/clinchem.2005.055053>
- Vanderver, A., Hathout, Y., Maletkovic, J., Gordon, E.S., Mintz, M., Timmons, M., Hoffman, E.P., Horzinski, L., Niel, F., Fogli, A., Boespflug-Tanguy, O., Schiffmann, R., 2008. Sensitivity and specificity of decreased CSF asialotransferrin for eIF2B-related disorder. *Neurology* 70, 2226–2232. <https://doi.org/10.1212/01.wnl.0000313857.54398.0e>
- Vaurs-Barrière, C., Deville, M., Sarret, C., Giraud, G., Des Portes, V., Prats-Viñas, J.-M., De Michele, G., Dan, B., Brady, A.F., Boespflug-Tanguy, O., Touraine, R., 2009. Pelizaeus-Merzbacher-Like disease presentation of MCT8 mutated male subjects. *Ann Neurol.* 65, 114–118. <https://doi.org/10.1002/ana.21579>
- Vermeren, M., Keynes, R., 2010. Vertebrate Central Nervous System: Pattern Formation, in: John Wiley & Sons, Ltd (Ed.), *Encyclopedia of Life Sciences*. John Wiley & Sons, Ltd, Chichester, UK, p. a0000794.pub2. <https://doi.org/10.1002/9780470015902.a0000794.pub2>
- Vermeulen, G., Seidl, R., Mercimek-Mahmutoglu, S., Rotteveel, J.J., Scheper, G.C., van der Knaap, M.S., 2005. Fright is a provoking factor in vanishing white matter disease. *Ann Neurol.* 57, 560–563. <https://doi.org/10.1002/ana.20418>
- Viganò, F., Dimou, L., 2016. The heterogeneous nature of NG2-glia. *Brain Research* 1638, 129–137. <https://doi.org/10.1016/j.brainres.2015.09.012>

- Wang, X., Paulin, F.E.M., Campbell, L.E., Gomez, E., O'Brien, K., Morrice, N., Proud, C.G., 2001. Eukaryotic initiation factor 2B: identification of multiple phosphorylation sites in the e-subunit and their functions in vivo. <https://doi.org/10.1093/emboj/20.16.4349>
- Ward, R., 2001. Vertebrate Central Nervous System. <https://doi.org/10.1038/npg.els.0000785>
- Welsh, G.I., Miyamoto, S., Price, N.T., Safer, B., Proud, C.G., 1996. T-cell Activation Leads to Rapid Stimulation of Translation Initiation Factor eIF2B and Inactivation of Glycogen Synthase Kinase-3. *J. Biol. Chem.* 271, 11410–11413. <https://doi.org/10.1074/jbc.271.19.11410>
- Wisse, L.E., Penning, R., Zaal, E.A., van Berkel, C.G.M., ter Braak, T.J., Polder, E., Kenney, J.W., Proud, C.G., Berkers, C.R., Altelaar, M.A.F., Speijer, D., van der Knaap, M.S., Abbink, T.E.M., 2017. Proteomic and Metabolomic Analyses of Vanishing White Matter Mouse Astrocytes Reveal Deregulation of ER Functions. *Front. Cell. Neurosci.* 11, 411. <https://doi.org/10.3389/fncel.2017.00411>
- Wisse, L.E., ter Braak, T.J., van de Beek, M.-C., van Berkel, C.G.M., Wortel, J., Heine, V.M., Proud, C.G., van der Knaap, M.S., Abbink, T.E.M., 2018. Adult mouse eIF2B ϵ Arg191His astrocytes display a normal integrated stress response in vitro. *Sci Rep* 8, 3773. <https://doi.org/10.1038/s41598-018-21885-x>
- Wong, K., Armstrong, R.C., Gyure, K.A., Morrison, A.L., Rodriguez, D., Matalon, R., Johnson, A.B., Wollmann, R., Gilbert, E., Le, T.Q., Bradley, C.A., Crutchfield, K., Schiffmann, R., 2000. Foamy cells with oligodendroglial phenotype in childhood ataxia with diffuse central nervous system hypomyelination syndrome. *Acta Neuropathologica* 100, 635–646. <https://doi.org/10.1007/s004010000234>
- Woods, Y.L., Cohen, P., Becker, W., Jakes, R., Goedert, M., Wang, X., Proud, C.G., 2001. The kinase DYRK phosphorylates protein-synthesis initiation factor eIF2B ϵ at Ser539 and the microtubule-associated protein tau at Thr212 : potential role for DYRK as a glycogen synthase kinase 3-priming kinase. <https://doi.org/10.1042/bj3550609>
- Wortel, I.M.N., van der Meer, L.T., Kilberg, M.S., van Leeuwen, F.N., 2017. Surviving Stress: Modulation of ATF4-Mediated Stress Responses in Normal and Malignant Cells. *Trends in Endocrinology & Metabolism* 28, 794–806. <https://doi.org/10.1016/j.tem.2017.07.003>
- Wortham, N.C., Proud, C.G., 2015. eIF2B: recent structural and functional insights into a key regulator of translation. *Biochemical Society Transactions* 43, 1234–1240. <https://doi.org/10.1042/BST20150164>
- Yang, Y., Jackson, R., 2019. Astrocyte identity: evolutionary perspectives on astrocyte functions and heterogeneity. *Current Opinion in Neurobiology* 56, 40–46. <https://doi.org/10.1016/j.conb.2018.11.006>
- Yang, Q.-K., Xiong, J.-X., Yao, Z.-X., 2013. Neuron-NG2 Cell Synapses: Novel Functions for Regulating NG2 Cell Proliferation and Differentiation. *BioMed Research International* 2013, 1–14. <https://doi.org/10.1155/2013/402843>

- Young, S.K., Wek, R.C., 2016. Upstream Open Reading Frames Differentially Regulate Gene-specific Translation in the Integrated Stress Response. *J. Biol. Chem.* 291, 16927–16935. <https://doi.org/10.1074/jbc.R116.733899>
- Zara, F., Biancheri, R., Bruno, C., Bordo, L., Assereto, S., Gazzero, E., Sotgia, F., Wang, X.B., Gianotti, S., Stringara, S., Pedemonte, M., Uziel, G., Rossi, A., Schenone, A., Tortori-Donati, P., van der Knaap, M.S., Lisanti, M.P., Minetti, C., 2006. Deficiency of hyccin, a newly identified membrane protein, causes hypomyelination and congenital cataract. *Nat Genet* 38, 1111–1113. <https://doi.org/10.1038/ng1870>
- Zhang, K., & Kaufman, R. J. (2008). From endoplasmic-reticulum stress to the inflammatory response. *Nature*, 454(7203), 455–462. <https://doi.org/10.1038/nature07203>
- Zhang X, Zhang G, Zhang H, Karin M, Bai H, Cai D. Hypothalamic IKKbeta/NF-kappaB and ER stress link overnutrition to energy imbalance and obesity. *Cell*. 2008;135:61–73.
- Zhou, L., Li, P., Chen, N., Dai, L., Gao, K., Liu, Y., Shen, L., Wang, J., Jiang, Y., Wu, Y., 2019. Modeling vanishing white matter disease with patient-derived induced pluripotent stem cells reveals astrocytic dysfunction. *CNS Neurosci Ther* 25, 759–771. <https://doi.org/10.1111/cns.13107>
- Zuchero, J.B., Barres, B.A., 2015. Glia in mammalian development and disease. *Development* 142, 3805–3809. <https://doi.org/10.1242/dev.129304>